Contemporary Food Engineering Series

Da-Wen Sun, Series Editor

Ultraviolet Light in Food Technology

Principles and Applications

Tatiana N. Koutchma
Larry J. Forney
Carmen I. Moraru

CRC Press
Taylor & Francis Group

Ultraviolet Light in Food Technology

Principles and Applications

Contemporary Food Engineering

Series Editor

Professor Da-Wen Sun, Director
Food Refrigeration & Computerized Food Technology
National University of Ireland, Dublin
(University College Dublin)
Dublin, Ireland
http://www.ucd.ie/sun/

Ultraviolet Light in Food Technology: Principles and Applications, *Tatiana N. Koutchma, Larry J. Forney, and Carmen I. Moraru* (2009)

Advances in Deep-Fat Frying of Foods, *edited by Serpil Sahin and Servet Gülüm Sumnu* (2009)

Extracting Bioactive Compounds for Food Products: Theory and Applications, *edited by M. Angela A. Meireles* (2009)

Advances in Food Dehydration, *edited by Cristina Ratti* (2009)

Optimization in Food Engineering, *edited by Ferruh Erdoğdu* (2009)

Optical Monitoring of Fresh and Processed Agricultural Crops, *edited by Manuela Zude* (2009)

Food Engineering Aspects of Baking Sweet Goods, *edited by Servet Gülüm Sumnu and Serpil Sahin* (2008)

Computational Fluid Dynamics in Food Processing, *edited by Da-Wen Sun* (2007)

Contemporary Food Engineering Series
Da-Wen Sun, Series Editor

Ultraviolet Light in Food Technology

Principles and Applications

Tatiana N. Koutchma
Larry J. Forney
Carmen I. Moraru

CRC Press
Taylor & Francis Group
Boca Raton London New York

CRC Press is an imprint of the
Taylor & Francis Group, an **informa** business

CRC Press
Taylor & Francis Group
6000 Broken Sound Parkway NW, Suite 300
Boca Raton, FL 33487-2742

Printed in the United States of America on acid-free paper
10 9 8 7 6 5 4 3 2 1

International Standard Book Number-13: 978-1-4200-5950-2 (Hardcover)

Library of Congress Cataloging-in-Publication Data

Koutchma, Tatiana.
Ultraviolet light in food technology : principles and applications / Tatiana Koutchma, Larry J. Forney, and Carmen J. Moraru.
p. cm. -- (Contemporary food engineering ; 8)
Includes bibliographical references and index.
ISBN-13: 978-1-4200-5950-2 (alk. paper)
ISBN-10: 1-4200-5950-5 (alk. paper)
1. Radiation preservation of food. 2. Ultraviolet radiation. I. Forney, L. J. (Larry J.), 1944- II. Moraru, Carmen J. III. Title. IV. Series.

TP371.8.K67 2009
664'.0288--dc22 2008040758

Visit the Taylor & Francis Web site at
http://www.taylorandfrancis.com

and the CRC Press Web site at
http://www.crcpress.com

Contents

Preface to Contemporary Food Engineering Series

Food engineering is the multidisciplinary field of applied physical sciences combined with the knowledge of product properties. Food engineers provide technological knowledge essential to the cost-effective production and commercialization of food products and services. In particular, food engineers develop and design processes and equipment in order to convert raw agricultural materials and ingredients into safe, convenient, and nutritious consumer food products. However, food engineering topics are continuously undergoing changes to meet diverse consumer demands, and the subject is being rapidly developed to reflect the market needs.

In the development of food engineering, one of the many challenges is to employ modern tools and knowledge, such as computational materials science and nanotechnology, to develop new products and processes. Simultaneously, improving food quality, safety, and security remain critical issues in food engineering study. New packaging materials and techniques are being developed to provide a higher level of protection to foods and novel preservation technologies are emerging to enhance food security and defense. Additionally, process control and automation regularly appear among the top priorities identified in food engineering. Advanced monitoring and control systems are developed to facilitate automation and flexible food manufacturing. Furthermore, energy saving and minimization of environmental problems continue to be important food engineering issues and significant progress is being made in waste management, efficient utilization of energy, and the reduction of effluents and emissions in food production.

Consisting of edited books, the Contemporary Food Engineering book series attempts to address some of the recent developments in food engineering. Advances in classical unit operations in engineering applied to food manufacturing are covered as well as such topics as progress in the transport and storage of liquid and solid foods; heating, chilling, and freezing of foods; mass transfer in foods; chemical and biochemical aspects of food engineering and the use of kinetic analysis; dehydration, thermal processing, nonthermal processing, extrusion, liquid food concentration, membrane processes and applications of membranes in food processing; shelf-life, electronic indicators in inventory management, and sustainable technologies in food processing; and packaging, cleaning, and sanitation. These books are intended for use by professional food scientists, academics researching food engineering problems, and graduate level students.

The editors of the books are leading engineers and scientists from many parts of the world. All the editors were asked to present their books in a manner that will address the market's needs and pinpoint the cutting edge technologies in food engineering. Furthermore, all contributions are written by internationally renowned experts who

have both academic and professional credentials. All authors have attempted to provide critical, comprehensive, and readily accessible information on the art and science of a relevant topic in each chapter, with reference lists to be used by readers for further information. Therefore, each book can serve as an essential reference source to students and researchers at universities and research institutions.

Da-Wen Sun
Series Editor

Preface

Modern consumers demand tasty, safe, healthy, organic, natural, and fresh foods—"green" foods—produced in an environmentally friendly manner. Sustainable methods with small carbon footprints are also required. The negative public reaction over chemicals added to foods is also growing. To address the challenges and issues facing the food industry, alternative opportunities to current practices of food processing that are both more sophisticated and diverse are being investigated.

As a physical preservation method, ultraviolet (UV)-light irradiation has a positive consumer image and is of interest to the food industry as a nonthermal method of processing. Recent advances in the science and engineering of UV-light irradiation have demonstrated that UV treatment holds considerable promise in food processing as an alternative to traditional thermal treatment for liquid foods (fresh juices, soft drinks, and beverages), post-processing treatment for ready-to-eat (RTE) meats, and shelf-life extension of fresh produce.

The application of UV light to process food products is a relatively new and challenging area compared with the UV treatment of water and wastewater, air disinfection, and surface decontamination. In general, effective UV treatment for food applications requires the development of alternative approaches to those normally employed for water or air treatment, as the UV-absorption effects of food products are significantly higher than those of water or air.

UV light can be effective in treating transparent liquid foods such as clarified juices and soft drinks, but it is less effective in treating turbid liquids with particulates (e.g., apple cider and orange juice), where UV light is strongly absorbed, scattered, or reflected. A systematic approach to evaluating UV light as an alternative pasteurization method entails consideration of the properties and composition of the food product to be treated, characteristics of the UV radiation source, microbial effects, modeling considerations, and commercial aspects.

Numerous reports are available on particular aspects of UV applications for food treatment. However, no other books are available that integrate fundamental knowledge about UV light with current food applications and challenges, evaluation of UV system performance, practical recommendations for design of UV reactors, selection of commercial UV sources, and the outlook for future successful food applications. A few books are available on the subject of UV radiation and its industrial applications in water treatment and sanitation, and these contain general topics that can be related to food applications. However, as the first book in the area of UV-light application in food processing, *Ultraviolet Light in Food Technology: Principles and Applications* is a new resource that will greatly benefit the food industry. The goal of the book is to integrate fundamental knowledge of UV-light generation and propagation, bringing together available information on UV-light technologies and summarizing the findings of published studies that investigate the UV treatment of

foods. The book also analyzes the concerns and challenges associated with food applications of both continuous and pulsed applications of UV light.

One of the important goals of this book is to be a source of current information on the U.S. and international regulations for the use of UV-light irradiation for foods. The U.S. Food and Drug Administration (U.S. FDA) and U.S. Department of Agriculture (USDA) have concluded that the use of UV irradiation is safe. In 2000, the FDA approved the use of UV light as an alternative treatment to thermal pasteurization of fresh juice products. In addition, the U.S. FDA issued Code 21CFR179.41, which approved the use of pulsed UV light in the production, processing, and handling of food. Health Canada has conducted an assessment of UV-treated apple juice and cider, and it concluded that there are no human safety concerns. In Europe, UV light is already used for disinfection of water and air in the food industry. In addition, in 2004, the National Advisory Committee on Microbiological Criteria for Foods (NACMCF) of USDA revised its definition of "pasteurization" for foods. This term now includes any process, treatment, or combination thereof that is applied to food to reduce the highest level of microorganism(s) of significance to public health. The processes and technologies described in the NACMCF report included UV irradiation as an alternative to heat for use as a pasteurization treatment. The scientific parameters for establishing the equivalence of UV light as an alternative method of pasteurization are presented in this book.

Chapter 1 introduces the principles of UV technology, including essential terms and definitions. The chapter also reviews current applications of UV light in food processing. The efficacy and specific features of the application of UV light for the disinfection of liquid foods or the surfaces of solid foods such as fresh produce, fresh-cut fruits, cheeses, meats, eggs, or bakery items are summarized and discussed.

Chapter 2 reviews the sources of UV light that are commercially available or are under development. Mercury-emission lamps and special-technology UV lamps are discussed. Guidelines for the choice of UV lamps for specific applications are also included. Optical properties, along with the design of UV reactors, are the major factors affecting UV inactivation of microbes in liquid foods with high UV-absorptive properties. The discussion emphasizes the need to properly assess the physical and chemical properties that influence the effectiveness of UV treatment.

Chapter 3 discusses the characterization of UV-light absorbance of selected foods that are currently processed as well as the impact of absorbance and scattering on the performance of UV reactors. The UV sensitivity of microorganisms of concern is another key factor affecting the efficacy of UV treatment of foods. Knowledge of the UV decimal reduction dose is a requirement to design a preservation process. A clear understanding of how variations in product characteristics can affect UV inactivation must be established so that appropriate operating parameters can be developed. The discussion emphasizes the need to properly measure and assess the impact of physical and chemical properties in foods on inactivation kinetics.

Chapter 4 provides information regarding these important issues in UV treatment to inactivate microbes in liquid foods. Chapter 5 addresses the effects of UV processing on food quality.

In Chapters 6, 7, and 8, consideration is given to the engineering aspects of UV-light treatment. Transport phenomena of UV irradiation are discussed, including

the rate-limiting diffusion step for microbes and device power requirements. UV process calculations for establishing specification of product preservation and delivery of the scheduled process are presented. Finally, continuous-flow reactor geometries that approach ideal plug flow are presented. Microbe inactivation levels are presented for the latter geometries in terms of nondimensional coordinates, and comparisons are made between the important reactor designs for processing liquid foods and beverages.

Chapter 9, which describes the principles of validation of UV reactors, will be of special interest for food specialists working on new industrial implementations of UV-light processing.

Chapter 10, by Carmen Moraru and Aaron Uesugi, discusses the principles and applications of UV pulsed light (PL). The generation of PL light, PL sources, and parameters that should be used to characterize PL are reviewed. PL inactivation of food-related microorganisms and factors that can affect inactivation are also featured in this chapter. The chapter concludes with a discussion of food and nonfood applications of PL treatment and future prospects of PL treatment in the food industry.

All chapters were written by international authors from academia and government who have both academic and professional credentials as well as a vision for the future.

Ultraviolet Light in Food Technology: Principles and Applications is intended to provide food engineers and scientists as well as undergraduate and graduate students working in research, development, and operations with broad and readily accessible information on the science and applications of UV-light technology. This book currently represents the most comprehensive and ambitious undertaking on the subject of UV technology for foods.

Series Editor

Born in southern China, Professor **Da-Wen Sun** is a world authority in food engineering research and education. His main research activities include cooling, drying, and refrigeration processes and systems, quality and safety of food products, bioprocess simulation and optimization, and computer vision technology. Especially, his innovative studies on vacuum cooling of cooked meats, pizza quality inspection by computer vision, and edible films for shelf-life extension of fruits and vegetables have been widely reported in national and international media. Results of his work have been published in over 180 peer-reviewed journal papers and in more than 200 conference papers.

He received BSc honors and an MSc in mechanical engineering, and a PhD in chemical engineering in China before working at various universities in Europe. He became the first Chinese national to be permanently employed at an Irish university when he was appointed college lecturer at the National University of Ireland, Dublin (University College Dublin) in 1995, and was then continuously promoted in the shortest possible time to senior lecturer, associate professor, and full professor. Dr. Sun is now professor of Food and Biosystems Engineering and director of the Food Refrigeration and Computerized Food Technology Research Group at University College Dublin.

As a leading educator in food engineering, Professor Sun has significantly contributed to the field of food engineering. He has trained many PhD students, who have made their own contributions to the industry and academia. He has also given lectures on advances in food engineering on a regular basis at academic institutions internationally and delivered keynote speeches at international conferences. As a recognized authority in food engineering, he has been conferred adjunct/visiting/consulting professorships from ten top universities in China including Shanghai Jiaotong University, Zhejiang University, Harbin Institute of Technology, China Agricultural University, South China University of Technology, and Jiangnan University. In recognition of his significant contributions to food engineering worldwide and his outstanding leadership in the field, the International Commission of Agricultural Engineering (CIGR) awarded him the CIGR Merit Award in 2000 and again in 2006; the Institution of Mechanical Engineers (IMechE) based in the UK named him ''Food Engineer of the Year 2004''; in 2008, he was awarded the CIGR Recognition Award in honor of his distinguished achievements in the top one percent of agricultural engineering scientists in the world.

He is a fellow of the Institution of Agricultural Engineers. He has also received numerous awards for teaching and research excellence, including the President's Research Fellowship, and twice received the President's Research Award of University College Dublin. He is a member of the CIGR executive board and honorary

vice-president of CIGR, editor-in-chief of *Food and Bioprocess Technology—An International Journal* (Springer), series editor of the ''Contemporary Food Engineering'' book series (CRC Press/Taylor & Francis), former editor of *Journal of Food Engineering* (Elsevier), and an editorial board member for *Journal of Food Engineering (Elsevier), Journal of Food Process Engineering* (Blackwell), *Sensing and Instrumentation for Food Quality and Safety* (Springer), and the *Czech Journal of Food Sciences.* He is also a chartered engineer registered in the UK Engineering Council.

Authors

Tatiana Koutchma is a research scientist at Agriculture and Agri-Food Canada (AAFC). Before she joined the AAFC, she was a research associate professor at the National Center for Food Safety and Technology (NCFST) at the Illinois Institute of Technology in Chicago. She received her doctoral degree in food process engineering from Moscow State University of Food Production. Since 1990, she has worked internationally (Russia, the United States, and Canada) in academia and government research programs in emerging food-processing technologies. For the past 10 years, her main research focus and interest has been the application of such innovative technologies as UV light, microwave heating, and high hydrostatic pressure for improved food safety, security, shelf life, and product acceptability. She initiated a research program on UV light for food preservation and was actively involved in core functions associated with R&D, process design, and validation of this technology for the food industry. She is a member of the editorial board of the *Journal of Food Processing* and of *Food and Bioprocess Technology*, and she is a member of the Innovative Technologies Board of PepsiCo. Since 1998, she has published over 40 manuscripts and research papers on a wide range of topics related to food processing.

Larry Forney is on the professorial staff at the Georgia Institute of Technology, School of Chemical & Biomolecular Engineering. He received his undergraduate degree in engineering science from Case Western Reserve University, an MS degree in mechanical engineering from MIT, and a PhD in engineering science from Harvard University. The focus of his research has been the effects of fluid mixing in the petrochemical and pharmaceutical industries, in particular, the optimum mixing conditions to increase yield from mixing sensitive reactions in both plug-flow and stirred-tank reactors. Since 1998, the focus of his research has been the application of Taylor–Couette flow to increase mass transfer in emulsion liquid membrane applications and the disinfection of liquids with UV radiation. The latter work has resulted in one patent, several patent disclosures, and a license for the development of the technology in the food processing, water treatment, and biological fluid industries. He was nominated for the IChemE water Award for Innovation and Excellence in 2008 for his research on the disinfection of liquids with UV radiation in Taylor–Couette flow.

Carmen Moraru is a faculty member in the Department of Food Science at Cornell University. She received her doctoral degree in food engineering and equipment from the University of Galati, Romania, where she has also served as a faculty member for several years. Between 1999 and 2003 she worked as a postdoctoral associate

and then as an assistant research professor in the Department of Food Science at Rutgers University. She joined the Cornell faculty in 2003 and is currently carrying out research and teaching in the area of food processing and engineering. A central focus of her research is the development of novel intervention strategies for the removal or inactivation of pathogenic microorganisms from foods. In past years, her research group has explored some of the most important unknowns associated with microbial inactivation by pulsed-light treatment.

1 Principles and Applications of UV Technology

There is a growing negative public reaction over chemical preservatives added to foods to extend their shelf life and to protect against food-borne pathogens and spoilage microorganisms. To address the consumers' demands for healthier food, alternatives to current practices are being investigated. As a physical preservation method, ultraviolet (UV)-light irradiation has a positive consumer image and is of interest to the food industry as a nonthermal method of inactivation. Although the use of UV light is well established for water treatment, air disinfection, and surface decontamination, its use is still limited in food treatment. Recent advances in the science and engineering of UV-light irradiation have demonstrated that UV treatment holds considerable promise in food processing as an alternative to traditional thermal processing for liquid foods such as fresh juices, soft drinks, and beverages; for postlethality treatment for ready-to-eat (RTE) meats; and for shelf-life extension of fresh fruits and vegetables.

Considering its importance, surprisingly little is known about the interaction of UV light with matter, especially with a complex food matrix. Radiative transfer covers all processes in which light or other electromagnetic energy is emitted or radiated, with some of this energy transferred from one form to another, as occurs in scattering and absorption. The particular type of interaction taking place in a liquid matrix can often be referred to as radiative transfer in a semi-transparent or turbid medium. A turbid medium is defined as a substance that both scatters and absorbs part of the light falling on it. All translucent and opaque materials are, therefore, turbid media.

This chapter provides an overview of the fundamental scientific and technological principles of UV-light treatments for foods. As a starting point to understanding UV-light technology, recent information is provided on the nature of UV light, including the basic principles of UV-light generation and propagation. The applications of UV light for food processing—including pasteurization of fresh juices, postlethality treatment for meats, treatment of food-contact surfaces and packaging materials, and extension of the shelf-life of fresh produce—are reviewed. The current status of the U.S. and international regulations for the use of UV light for food treatments is also discussed.

1.1 BASIC PRINCIPLES OF UV-LIGHT TECHNOLOGY

Light is just one portion of the spectrum of various electromagnetic waves traveling through space. The electromagnetic spectrum covers a broad range from radio waves with wavelength of a meter or more, down to x-rays with wavelength of less

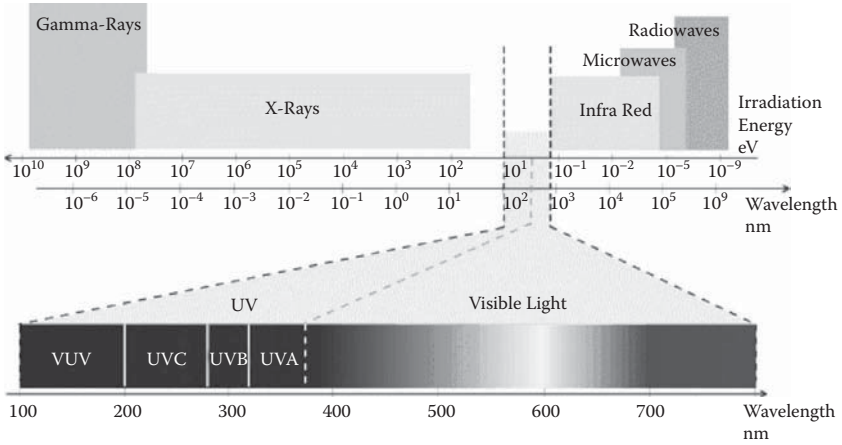

FIGURE 1.1 Electromagnetic radiation spectrum with a division of light spectrum on visible and UV light in the three different types. (From http://www.zontec.net/files/uvSpectrum.gif.)

than a billionth of a meter (Figure 1.1). Typically, the wavelength for UV processing ranges from 100 to 400 nm. This range may be further subdivided into UV-A (315–400 nm), normally responsible for changes in human skin called tanning; UV-B (280–315 nm), which can cause skin burning and eventually lead to skin cancer; UV-C (200–280 nm), called the germicidal range, since it effectively inactivates bacteria and viruses; and the vacuum UV range (100–200 nm), which can be absorbed by almost all substances and thus can be transmitted only in a vacuum. Short UV-C is almost completely absorbed in air within a few hundred meters. When UV-C photons collide with oxygen atoms, the energy exchange causes the formation of ozone. UV-C is almost never observed in nature, since it is absorbed so quickly.

1.1.1 Mechanisms of UV-Light Generation

Atoms and ions emit light when they change from a higher to a lower energy state. An atom and most ions consist of electrons orbiting a nucleus of protons and neutrons. The electrons in each orbital occupy a unique energy state, with the electrons closest to the nucleus having a lower energy and the electrons further away having a higher energy. When electrons make a transition from a higher energy, E2, to a lower energy, E1, a discrete amount of energy is released as photons of light. As first stated by Planck, each photon carries an energy E (J) described by equation (1.1).

$$E = E_2 - E_2 = hc/\lambda \tag{1.1}$$

where h is Planck's constant (6.23×10^{-34} J × s), c is the speed of light (2.998×10^{8} m × s^{-1}), and λ is the wavelength of radiation (m). Energy levels of a given atom or ion are unique, arising from the number of electrons, protons, and neutrons within that

atom or ion and their interaction with external force fields. As such, each element emits a unique spectrum of light. If the difference between energy levels is appropriate, the light emitted is UV.

A transition from a lower to a higher energy state requires an energy input. This energy may be derived from the collision of the atom with a photon of light of wavelength λ or by collision with other atoms, ions, or electrons. Energy transferred to the atom may result in an increase in the atom's kinetic energy, the transfer of an electron to a higher energy level, or the removal of an electron from the atom. Removal of an electron from the atom is termed ionization and results in a positively charged cation and a negatively charged free electron. Recombination of a free electron and a cation may result in the emission of light. Since the free electron and cation may have a range of kinetic energies, the wavelength of emitting light will vary over a continuum or range. This wavelength (equation 1.2) will be bound at one end by the ionization energy E_0 of the atom and peak at a wavelength dependent on the temperature of the electrons and cations

$$\lambda_{max} = hc/E_0 \tag{1.2}$$

For expressing the energy of a single photon, the unit of joules (J) is rather large. Conventionally, the electronvolt (eV) is used. One eV is defined as the energy gained by an electron in passing through a potential difference of 1 V, which equals 1.6×10^{-19} J. For photochemical purposes, the photon energy is often expressed in kilocalories per Einstein. Note that 1 Einstein is defined as being equal to Avogadro's number (N_A) of photons = 6.02×10^{23} photons. Absorption of 1 Einstein can excite 1 mole of the absorbing substance (equation 1.3)

$$E_E = h\frac{c}{\lambda}N_A \tag{1.3}$$

where E_E is energy per Einstein, and N_A is Avogadro's number.

The photon may be viewed as the smallest discrete unit of radiation energy. Corresponding photon energies exist across the electromagnetic spectrum in a wide range of wavelength, as shown in Table 1.1.

Radiation of UV light and the adjacent visible (VIS) spectral range as well as other less-energetic types are summarily called nonionizing radiation as opposed to ionizing radiation. The latter is represented in the electromagnetic spectrum by x-rays and gamma rays. Other kinds of ionizing radiation consist of ionizing particles (beta rays, alpha rays, protons). Ionizing radiation, in contrast to nonionizing radiation, is capable of ionizing many atoms and molecules. Absorption of nonionizing radiation, however, leads to electronic excitation of atoms and molecules.

1.1.2 Gas Discharge

A gas discharge is a mixture of nonexcited atoms, excited atoms, cations, and free electrons formed when a sufficiently high voltage is applied across a volume of gas. Light is emitted from the gas discharge at wavelengths dependent upon the elemental

TABLE 1.1
Spectrum of Electromagnetic Radiation and Corresponding Photon Energies

Radiation Type	Wavelength (nm)	Photon Energy (kJ/Einstein)
Gamma rays	<0.1	$>10^6$
X-rays	0.1–50	$\approx 10^6$–2,400
UV light	50–400	≈2,400–300
Vacuum	50–200	2400–600
UV-C	200–270	600–440
UV-B	270–330	440–360
UV-A	330–400	360–300
Visible	400–700	300–170
Infrared	700–10^7	170–0.01
Microwaves	10^7–10^8	0.01–0.001
Radio waves	10^8–10^{13}	0.001–10^{-8}

composition of the gas discharge as well as the excitation, ionization, and kinetic energy of those elements. Gas discharges are responsible for the light emitted from UV lamps. When a voltage is first applied, free electrons and ions present in the gas are accelerated by the electric field formed between two electrodes. With sufficient voltage, the electrons are accelerated to high kinetic energies. Collisions of the free electrons with atoms result in a transfer of energy to the atoms, and if the energy is sufficient, the atoms are ionized. This ionization results in a rapid increase in the number of electrons and cations, with a corresponding increase in lamp current and a drop in the voltage across the lamp.

Cations colliding with the electrodes cause electrons to be emitted. If sufficient electrons are emitted, a self-sustaining discharge occurs, termed a *glow discharge*. With an increase in current, the larger fraction of each electrode will emit electrons until the whole electrode is in use. To increase the current beyond that point, the voltage is increased to provide more kinetic energy to the cations. High-energy cations colliding with the electrode increase the electrode's temperature. At high enough temperatures, the electrode begins to emit electrons, and a further increase in current reduces the voltage requirement. At this point, the process is termed an *arc discharge*.

The voltage required to start the gas discharge is typically higher than the ionization potential of the gas unless a means is used to introduce electrons. Because voltage across the gas discharge is inversely related to current, the gas discharge has negative impedance and is intrinsically unstable. The ballast is therefore placed in series with the gas discharge to provide positive impedance to the power supply.

1.2 PROPAGATION OF UV LIGHT

UV light emitted from the atoms and ions within the gas discharge of a UV lamp will propagate away from those atoms and ions. As UV light propagates, it interacts with the materials it encounters through absorption, reflection, refraction, and scattering.

In a UV reactor, UV light emitted will interact with components of the UV reactor such as the lamp, the lamp sleeve, the reactor walls, as well as the liquid substance being treated. Each of these phenomena influences the intensity and wavelength of the UV light reaching the bacteria or chemical compound in the liquid.

1.2.1 Basic Principle of Photochemistry

Photochemical reactions proceed as a direct result of radiation energy (photons) being introduced to a system. In view of the wavelengths used in most UV-light treatments, the molecules (A) are primarily affected by energy absorption that results in photochemical reactions. In the general case, the process may be viewed as

$$A + h\nu \rightarrow A_{+}^{+} \rightarrow \text{Products} \tag{1.4}$$

The first step in this reaction is the absorbance of a photon by a reactant molecule (A), leading to the production of an electronically excited intermediate. The excited state can be for a period of 10^{-10} to 10^{-8} s, during which the energy of the electrons is increased by the amount of photon energy. Under some conditions, the intermediate may undergo a chemical change to yield products that are relatively stable. This basic model reveals two critical conditions that must be met for a photochemical reaction to proceed.

1. Photons must have sufficient energy to promote a reaction, i.e., to break or form a bond.
2. Photon energy must be absorbed to promote reactions.

The summary of representative values of the bond energies that characterize some of the common bonds of molecular groups relevant to biomolecules and organic molecules are given in Table 1.2. From this summary, it is evident that the bond

TABLE 1.2
Typical Bond Energies of Important Biological Moieties and Their Corresponding Wavelengths

Bond	Typical Bond Energy (kJ/mole)	Corresponding Wavelength (nm)
O–H	460	260
C–H	410	290
N–H	390	310
C–O	370	320
C=C	830	140
C=N	850	140
C=O	740	160
C=N	600	200

Source: Blatchley and Peel (2001).

energies of interest are generally coincident with photon energies in the UV portion of the spectrum. In particular, radiation with wavelength less than approximately 320 nm appears to be sufficiently energetic to promote photochemical reactions in biomolecules.

The excitation energy provided by UV photons is much higher than the energy of thermal motions of the molecules at physiological temperatures. The latter is on the order of Boltzmann's constant times the absolute temperature, which at 27°C amounts to 0.026 eV/molecule (0.60 kcal/mole), in contrast to the 3.3–6.5 eV/molecule (75–150 kcal/mole) available from UV absorption.

1.2.2 Terms and Definitions

Absorption of light is the transformation of energy of light photons to other forms of energy as they travel through a substance. When UV light (I) passes through a substance, its intensity is affected according to equation (1.5)

$$I_1/I_0 = 10^{-\sum \varepsilon cd} = 10^{-\alpha_{10} d} = 10^{-A} = e^{-\alpha_e d} \tag{1.5}$$

where I_1 and I_0 are the UV-light intensities (mW/cm^2) incident on the substance and transmitted through a length d (cm), respectively; d is distance traveled by light; ε is the extinction coefficient (molar absorptivity) of the absorbing species (L/mol/cm), which is a measure of the amount of light absorbed per unit concentration; c is concentration within the substance of the absorbing species (mol/L); α_{10} is the logarithmic absorption coefficient of the medium (cm^{-1}); α_e is the Napierian (base e) coefficient of the medium (cm^{-1}); and A is the logarithmic absorbance of a substance at a given wavelength defined by $A = \log_{10} (I_0/I_1)$. In practice, because of reflections at the quartz–air interfaces, I_0 is the spectrophotometer reading with pure solvent in the cell, and I_1 is the reading with the solution of interest in the cell.

When UV light is absorbed, it is no longer available for inactivating microorganisms. The remaining interactions, including reflection, refraction, and scattering, change the direction of UV light, but the light is still available for disinfection.

Reflection is the change in the direction of propagation experienced by light deflected by an interface. Reflection may be classified as specular or diffuse. Specular reflection occurs from smooth polished surfaces where the roughness of the surface is smaller than the wavelength of light. Diffuse reflection occurs from rough surfaces, where light is scattered in all directions with little dependence on the incidence angle.

Scattering is the phenomenon that includes any process that deflects electromagnetic radiation from a straight path through an absorber when light interacts with a particle. Rayleigh scattering is the scattering of light by particles that are much smaller than the wavelength of the light. With larger particles, more light is scattered in the forward direction, and interference causes intensity minima and maxima to form as a function of scattering angle. UV light scattered from particles is capable of killing microbes. Much of the scattered light is in the forward direction and is a significant portion of the transmitted UV light. The scattering phenomenon plays an important role in disinfecting food liquids with particles.

Refraction of light is the change in the direction of propagation experienced by light as it passes from one medium to another. In UV reactors, refraction occurs when light passes from air to quartz or from quartz to liquid. Refraction is governed by Snell's law, which states

$$n_1 \sin\Theta_1 = n_2 \sin\Theta_2 \tag{1.6}$$

where n_1 is the index of refraction of the first medium, n_2 is the index of refraction of the second medium, Θ_1 is the incident angle onto the interface, and Θ_2 is the exit angle from the interface.

1.2.3 UV Radiation Energy

Evaluation of the UV-light-induced effects based on dose-effects statistics is one of the practical approaches toward the understanding of UV-light phenomena. Therefore, accurate determination of the radiation quantities is vital in any UV-light experiment. The most common measured quantity of UV radiation is the energy *incident* per unit area normal to the beam. The terms for the quantity are energy fluence and fluence rate.

Fluence rate or irradiance (E') is the total radiant power incident from all directions onto an infinitesimally small sphere of cross-sectional area dA, divided by dA in units of W/m^2 or mW/cm^2. Fluence (UV dose) (H') is the total amount of radiant energy from all directions incident on an infinitesimally small sphere of cross-sectional area dA, divided by dA in units of J/m^2 or mJ/cm^2. To determine the energy fluence, the fluence rate should be measured and multiplied by the time of exposure. In the common case of irradiation with a germicidal lamp, a calibrated radiometer is used for this purpose. The fluence rate should always be determined exactly at the location of exposed sample. However, the determination of the energy fluence applied to the sample does not indicate how much of the radiation energy is actually absorbed by the material or, more specifically, by particular components of it.

1.2.4 Absorbed Energy

The amount of energy absorbed by the materials depends on the nature of the material and the manner of radiation exposure. According to Harm (1980), several materials can be considered as typical examples. They can be characterized as homogeneous solutions (transparent, semitransparent, and opaque) and particulate samples or suspensions. If the sample is a homogeneous liquid, light absorption in homogeneous solutions follows relatively simple laws. However, very often the suspensions of whole cells are irradiated, and these can be considered as dense packages of absorbing molecules separated from each other by the suspension liquid.

The suspension liquid itself may not absorb UV radiation, as is the case if the liquid is water, an inorganic buffer solution, or a glucose–salts medium. In homogeneous solutions, if a uniform layer is exposed to a parallel beam of monochromatic UV radiation at a fluence rate E_0, the fluence rate of the unabsorbed radiation emerging after passage through the layer is expressed by equation (1.7)

$$E = E_0 \cdot 10^{-A} \text{ or } E = E_0 e^{-A\ln 10} \tag{1.7}$$

If the broadside area of the solution, S, is exposed to the fluence, F, which is the product of fluence rate and the time, E_0t, the equation to calculate absorbed energy can be obtained from equation (1.8)

$$H_{abs} = (E_0 - E)tS = E_0t(1 - e^{-A \ln 10})S = H_0(1 - e^{-A \ln 10})S \tag{1.8}$$

The calculation of H_{abs} is the easiest for solutions that are either nearly transparent or virtually opaque. In the nearly transparent case, where $A << 1$, the expression $(1-e^{-A \ln 10})$ can be approximated by A ln 10 or $2.3A$ to obtain equation (1.9)

$$H_{abs} = 2.3H_0AS = 2.3H_0\varepsilon cdS \tag{1.9}$$

Since the product of cdS equals the total quantity of absorbing material (q, mole), the energy absorbed per unit quantity of absorbing material is expressed by H_{abs}/q and called the absorbed dose D (J/mole), expressed by equation (1.10)

$$D = 2.3H_0\varepsilon \tag{1.10}$$

In the nearly opaque case, where virtually all UV energy entering the solution is absorbed ($A > 2$), it follows from equation (1.11)

$$H_{abs} = H_0S \tag{1.11}$$

If the solution consists of a single absorbing component and it is well stirred to expose all molecules equally, the absorbed dose can be estimated using equation (1.12)

$$D = H_{abs}/q = H_0q/cdq = H_0/cd \tag{1.12}$$

The energy absorbed per unit quantity of material depends on its concentration and the thickness of the irradiated layer, but it is independent of ε.

The intermediate or semitransparent case is represented by a solution that absorbs a measurable fraction of the incident photons but lets the remainder pass. If the solution is well stirred so that all molecules are statistically equally exposed to the radiation, such a case can be treated for the purpose of the calculations as a near-transparent solution receiving a lower fluence, as seen in equation (1.13)

$$D = H_{abs}/q = \left[\frac{1 - e^{-A \ln 10}}{A}\right]\varepsilon H_0 \text{ (J/mol)} \tag{1.13}$$

However, the situation encountered in actual UV experiments with food liquids can be generally more complex. In addition to the homogeneous solution of liquid foods or its ingredients, the solution can contain suspended solids. The suspended solids often contain other absorbing molecules that can harbor bacterial cells. The degree of transparency of the particles in the solution can be determined from the measured absorption of a suspension of randomly distributed particles at known concentration, provided that light scattering is also taken into consideration.

Volume-averaged fluence (absorbed dose) in the flow-through UV reactor can be determined as a volume-averaged fluence rate (mW/cm^2) multiplied by the hydraulic residence time (s). The Beer–Lambert law (equation 1.14) serves as the main mathematical basis for computation of UV irradiance distribution in a medium within the annulus.

$$E_r = E_0 \frac{r_0}{r} \exp[-\alpha_e (r - r_0)] \tag{1.14}$$

where E_r is UV fluence at a distance r from center (W/cm^2); E_0 is UV fluence at the surface of the UV source (W/cm^2); r is the radial distance between the center of the source to the point at which irradiance is measured (cm); r_0 is a radius of the UV lamp (cm); and α_e is the absorption coefficient of the medium (cm^{-1}).

1.3 APPLICATION GUIDANCE IN FOOD PROCESSING

1.3.1 Disinfection of Surfaces

UV light is used in the food industry for different purposes. Applications include decontamination of surfaces of equipment in bakeries and cheese and meat plants, as an adjunct to usual cleaning and sanitizing practices, and for decontamination of conveyor surfaces and packaging containers such as boxes, caps, bottles, cartons, tubes, films, and foils. Despite the efficacy of UV light to disinfect smooth surfaces, there are relatively few applications of this technology in the food processing industry. The restricted range of commercially available equipment for disinfecting solids may contribute to its limited use. In addition, most kinetic data of microbial inactivation have been obtained in suspension in aqueous media or air. These data are of limited use in predicting the surface disinfection rate. Since complex interactions may occur between microorganisms and surface materials, such as shielding effects from incident UV, the efficacy of UV light depends on surface structure or topography. For example, Gardner and Shama (2000) presented a model to account for inactivation by UV light of microorganisms on the surfaces of solid materials. In the model, the surface was divided into a discrete number of zones with a characteristic exposure factor, which is a ratio of the UV fluence rate actually seen by the microorganism to that incident on the surface. Application of the model requires inactivation data obtained under conditions where the surface microorganisms are fully exposed to incident UV as well as inactivation kinetics data for the tested microorganism. The model was applied to UV inactivation of *Bacillus subtilis* spores on filter paper. Good representation of the data was observed by the authors.

However, despite these limitations, the research on the application of UV light to reduce microbial contamination on the surfaces of solid foods is growing. The main groups of food that were studied include RTE meats, bread, in-shell eggs, fish, whole and fresh-cut fruits and vegetables, and powders.

1.3.1.1 RTE Meats

The recent outbreaks of *Listeria* in ready-to-eat (RTE) meats prompted the USDA to implement a regulation to control *Listeria* in facilities producing RTE

products (FSIS 2003). Alternatives 1 and 2 of this regulation include the use of a postlethality treatment and an antimicrobial agent together or separately to reduce or eliminate the bacterium on the product. The ability of UV light to disinfect surfaces of meat products has been reported in the literature. A few studies have evaluated the use of UV irradiation to reduce levels of *Escherichia coli* and *Salmonella* on pork skin and muscle (Wong et al. 1998), *Listeria monocytogenes* on chicken meat (Kim et al. 2002), and *Salmonella typhimurium* on poultry carcasses (Wallner-Pendleton et al. 1994). Despite the known limited ability of UV light to penetrate rough food surfaces such as meats, these studies demonstrated that UV light has the potential to reduce bacterial contamination on food surfaces and therefore has the potential to be used as a postlethality treatment to control *L. monocytogenes* and other pathogens of concern in meat and poultry processing facilities.

An example of a commercially available system to decontaminate surfaces of foods is the UV tumbling process that was developed by C&S Equipment Co. (Chapman 2003). The company incorporated either a rotating drum or screw conveyor that lifts and tumbles the product to ensure exposure to the UV source (Figure 1.2). The unit can be used to treat fresh products in a wide range of processing applications such as fresh vegetables, fruits, meats, etc.; frozen products (vegetables, fruits, meats, seafood, bakery products, etc.); and cooked, refrigerated products (pasta, cheese, etc.). The C&S Equipment Co. designs solutions for these problems using the patented

FIGURE 1.2 UVC Tumbling Machine developed by C&S Equipment Company decontaminates food surfaces in a wide range of processing applications. (From http://www.cs-equipment.com.)

technology of Steril-Aire™ UV emitters. These emitters are sleeved in plastic to meet the food safety requirements of food processing facilities. The patented design allows emitters to work efficiently in the cold environment of refrigerated or chiller coils, where competitive units lose their effectiveness. Examples of UV units currently used in commercial processing facilities include: (a) UV tumbling drum in operation for chicken and beef fajita strips (cooked and individually quick frozen [IQF]), with a capacity 6000–7000 lb/h; (b) cooked and IQF hamburger patty treatment (hooded conveyor with turn over), with a capacity 3000 lb/h; and (c) a deli meat system (custom conveyor with UV-C hood) for formed deli ham logs, with a capacity of 10,000 lb/h.

1.3.1.2 Baguettes

UV treatment has also been applied to prolong shelf life of wrapped partially baked baguettes to minimize postbaking contamination (Doulia et al. 2000).

1.3.1.3 Shell Eggs

UV light has been documented to be effective in reducing various bacterial populations on eggshell surfaces, including total aerobic plate count (Chavez et al. 2002), *S. typhimurium* and *E. coli* (Coufal et al. 2003), and *Yersinia enterocolitica* (Favier et al. 2001). Kuo et al. (1997) reported UV inactivation of aerobic bacteria and molds in addition to *S. typhimurium*, and a 99% reduction of CFU (colony-forming units) of aerobic bacteria per egg was observed for all UV treatments (0, 15, and 30 min) at an intensity of 0.62 mJ/cm^2. Mold CFU per egg was either 0 or 1 for all treatments. Despite the urgent need to improve egg safety and the demonstrated UV-light inactivation efficiency, UV treatment of eggs has not yet been commercially implemented.

1.3.1.4 Whole and Fresh-Cut Fruits

UV treatment has a potential for commercial use as a surface treatment of fresh-cut fruits. The ability of UV light to sanitize and retard microbial growth on the surface of fresh cut fruits without causing undesirable quality changes has recently been recognized.

Irradiation with UV light may be a more effective germicidal treatment than either chlorine, hydrogen peroxide, or ozone. The effect of UV light was evaluated on the microbial population and quality of fresh-cut watermelon (Fonseca and Rushing 2006) and cantaloupe melon (Beaulieu 2007; Lamikanra et al. 2005) and for surface disinfection of apples, kiwifruit, lemons, nectarines, oranges, peaches, pears, raspberries, and grapes (Lagunas-Solar et al. 2006). The results reported by Fonseca and Rushing (2006) showed that exposing packaged watermelon cubes to UV light at 4.1 kJ×m^{-2} produced more than a 1-log reduction in microbial populations without affecting juice leakage, color, and overall visual quality. Lamikanra et al. (2005) compared the effect of processing cantaloupe melon under UV radiation on storage properties of the cut fruit with postcut UV-C fruit treatment. Results indicated that fresh-cut pieces from whole melon cut under UV light had lower populations of aerobic mesophilic and lactic acid bacteria relative to the control and postcut-treated

pieces. While postcut application of UV light improved shelf life, cutting fruit under UV radiation further improved product quality.

1.3.1.5 Broiler Breast Fillets

Lyon et al. (2007) reported that raw broiler breast fillets were subjected to germicidal ultraviolet (UV) light (dose of 1000 μW/cm^2 for 5 min at a wavelength of 254 nm) to evaluate its potential to reduce *Listeria monocytogenes* numbers on raw product before shipment to a poultry further-processing plant. Boneless, skinless breast fillets were inoculated with four different strains of *L. monocytogenes* 5 min before treatment. After the UV treatment, breast fillets were stored at 4°C for 24 h. An approximate 2-log reduction in viable *L. monocytogenes* was observed with all four strains on UV-treated breast fillets as compared with the nontreated breast fillets. The UV treatment caused only slight changes in meat color (lightness, redness, and yellowness) on the day of treatment or after 7 days of storage. This study suggested that UV treatment of raw breast fillets at a slaughter plant can significantly reduce *L. monocytogenes* without negatively affecting meat color. This process could be used to reduce the negative effect of raw poultry as a transmission vector of *L. monocytogenes* into a poultry further-processing plant.

1.3.1.6 Pulsed UV Light for Foods

A few studies recently reported an application of UV pulsed light for foods. A pulsed xenon UV-light treatment was applied to inactivate spores of *Aspergillus niger* in corn meal. However, low penetration power and excessive heat buildup inside the chamber were reported (Jun et al. 2003). Pulsed UV light was found to be effective for the inactivation of *Saccharomyces cerevisiae* (Takeshita et al. 2003). In addition, the pulsed UV light was used to control microbial levels on fresh processed lettuce. Allende and Artes (2003) reported that pulsed UV light was effective for reducing the levels of psychrotrophic and coliform bacteria as well as yeast without adversely affecting the sensory quality of the lettuce. Sharma and Demirci (2003) demonstrated that pulsed UV light holds promise for eliminating pathogens such as *Escherichia coli* O157:H7 from alfalfa seeds.

Fine and Gervais (2004) reported the efficiency of pulsed UV light on the destruction of dried microorganisms on fluidized glass beads and determined treatment parameters. The drying method used in the study allowed *S. cerevisiae* to remain viable on glass beads or dried powdered products. The dose of 58 J/cm^2 was required to decrease microbial population by 7 log using glass beads. However, it was found that, for black pepper and wheat flour, the thermal effect dominated the UV-light effect.

Inactivation of *E. coli* O157:H7 and *Listeria monocytogenes* inoculated on raw salmon fillets by pulsed UV-light treatment was investigated by Ozer and Demirci (2006). To enhance shelf life and enhance safety of seafood products, UV light was studied in terms of microbial inactivation efficiency. The outbreaks of fish and fish products are on the top of the list of foods associated with food-borne diseases. The sterilization system generated 5.6 J/cm^2 per pulse at the lamp surface and three pulses per second. To avoid overheating, the fillets were exposed to UV-light pulses

at the distance of 8 cm, and at least one $\log_{10}$ CFU reduction of *E. coli* and *L. monocytogenes* was achieved after a 1-min treatment.

1.3.2 UV Light for Liquid Foods and Beverages

UV light has considerable promise to reduce the levels of microbial contamination for a wide range of liquid foods and beverages. These liquids include juices, brines, liquid sugars, pharmaceuticals, process lubricants, and other semitransparent and opaque ingredients or foods. Due to the presence of color compounds, organic solutes, and suspended matter, liquid foods usually transmit relatively little UV light, and this low transmission lowers the performance efficiency of the UV pasteurization processes. In addition, the absorptivity and turbidity of clear fresh juices and juices with pulp vary considerably. Clear apple juice has a low absorptivity, with an absorption coefficient from 11 cm^{-1}, whereas orange juice can have absorption coefficients close to 100 cm^{-1} (Koutchma et al. 2004). Turbidity of juices is due to the presence of soluble and suspended solids and can be in a range from 1000 nephelometric turbidity units (NTU) for apple and other clear juices up to >4000 NTU for opaque varieties such as carrot, orange, and pineapple juices. The liquid foods, ingredients, juices, and beverages also have different °Brix (soluble solids content) and pH levels as well as varying viscosities (Figure 1.3) that significantly distinguish the approaches to treat them successfully using UV light. From a commercial perspective, an increase in viscosity significantly increases the power requirements to maintain the unique and desirable fluid flow characteristics of the individual reactor designs.

This means that the combination of physical properties, such as liquid density and viscosity, must be considered to meet the required pasteurization standard for a 5-$\log_{10}$ reduction in the number of the target pathogen of concern for fresh juices. Exposure of microorganisms to UV light or residence time in the UV reactor should be sufficient to achieve the required level of inactivation.

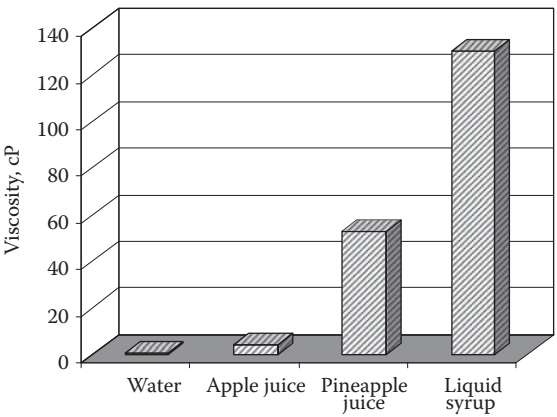

FIGURE 1.3 Comparison of viscosity of water, fresh juices, and liquid sugar syrups.

1.3.2.1 Fresh Apple Juice/Cider

FDA approval of UV light as an alternative treatment to thermal pasteurization of fresh juice products (U.S. FDA 2000a, 2000b) has led to a growing interest and research in UV technology. A number of UV-light static- and continuous-flow apparati were developed and validated for a variety of beverages ranging from exotic tropical juices to the more common apple cider and apple juice.

Apple cider poses a significant health risk if not pasteurized. Some research has examined the efficacy of UV light in the treatment of apple cider. Harrington and Hills (1968) studied the effect of UV irradiation on subsequent spoilage and flavor of fresh cider. The reduction in the total aerobic population was dependent on the clarity of juice and time of UV exposure. The reduction of any pathogenic population was not examined. Taste panel tests did not find a significant difference between UV-irradiated and control cider. The relationship between the degree of clarity of the juice and efficacy of microbial inactivation was not explored.

Extensive research of the application of UV light for fresh apple cider by Worobo (1999) yielded a design and production model of a thin-film CiderSure™ UV reactor. The flow rate in this reactor is controlled by a computer interface that reads the UV transmission using UV sensors. Worobo reported that apple cider of different varieties was used to test the ability of this unit to deliver a 5-log reduction of *E. coli* O157:H7. It was concluded that a greater than 5-log reduction was achieved after a single pass through the reactor. However, the absorptive properties of apple cider used for validation trials were not reported by this group.

Wright et al. (2000) examined the efficacy of UV light for reducing *E. coli* O157:H7 in apple cider. For their studies, a model CIDER-10uv (Ideal Horizons, Poultney, VT) was used to deliver dosages ranging from 9,402 to 61,005 $\mu W \times s/cm^2$ (9.4 to 61 J/m^2). This unit was stated to have 10 individual UV chambers connected in series through which the apple cider was pumped as a thin film. UV treatment significantly reduced the pathogen, with a mean reduction of 3.81 $\log_{10}$ CFU/mL. High background microflora in the cider adversely affected reduction of *E. coli* O157:H7. Absorbance, turbidity, pH, and other physical or chemical parameters of the juice were not examined.

A similar UV treatment system was used by Hanes et al. (2002) to determine the inactivation of *Cryptosporidium parvum* oocysts in fresh apple cider. For these studies, a CiderSure 3500A (FPE Inc., Rochester, NY) was used. The CiderSure system also treats a thin layer of liquid, similar to the CIDER-10uv; however, with the CiderSure unit, three individual treatment chambers are connected in tandem around eight concentrically located tubes. Juice was treated at 14.32 mJ/cm^2 for 1.2 to 1.9 s, resulting in dosages within the range tested by Harrington and Hills (1968). This level of treatment successfully reduced oocysts from 106/mL to below the lower limit of detection, which was 23 oocysts/mL.

A statistical evaluation of UV treatment efficacy in the treatment of apple cider can be found in Duffy et al. (2000). Here, calculated log reductions of CiderSure units shown to result in a 5-log reduction of a nonpathogenic *E. coli* were examined to determine the risk that failure to achieve a 5-log reduction would occur. Based on a statistical evaluation, the authors state that analysis of risk indicates a possible

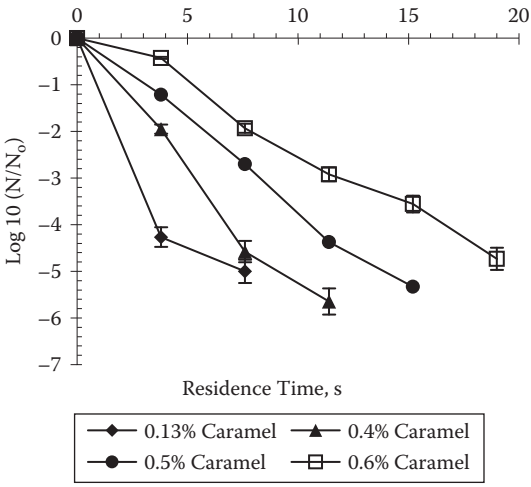

FIGURE 1.4 Inactivation curves of *E. coli* K12 in caramel buffer solutions. CiderSure UV reactor at 57 mL/s. (From Koutchma et al. 2004. With permission.)

failure rate of less than 0.2%. The evaluation is entirely statistical in nature and makes no effort to provide explanations for possible failure or for the variability in log reductions calculated for validated units.

Koutchma et al. (2002) examined individual physical and chemical factors in a model fluid that simulated pH, °Brix, and the range of absorbencies of apple juice and cider for their effects on the efficacy of UV light on the destruction of *E. coli* K12 bacteria using laminar- and turbulent-flow treatment systems. A thin-film flow-through laboratory UV unit (CiderSure Model 1500, FPE Inc., Macedon, NY) and a UV reactor (Aquionics, Hanovia Ltd., Slough, England) were used in the study.

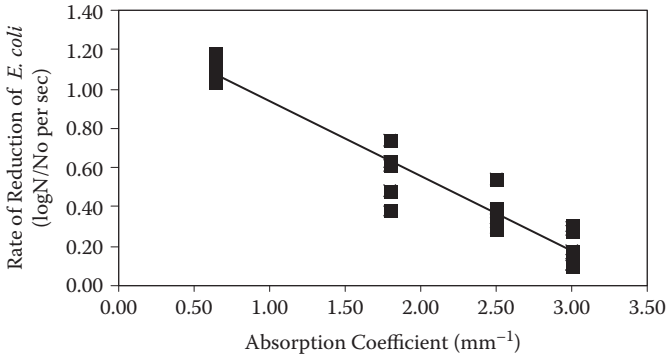

FIGURE 1.5 Inactivation of *E. coli* K12 exposed to UV light related to the absorption coefficients of a model system. (From Koutchma et al. 2004. With permission.)

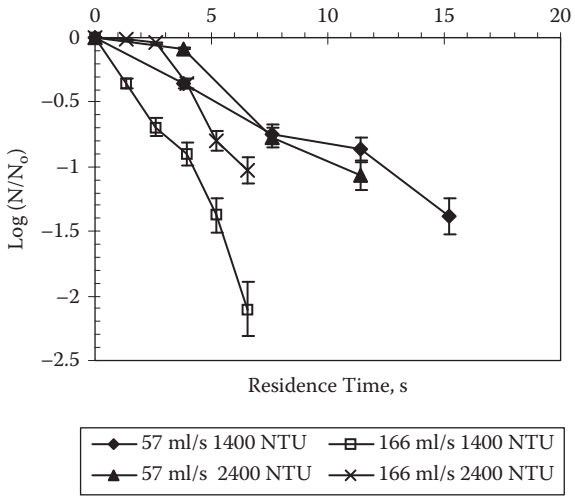

FIGURE 1.6 Effects of absorbance and turbidity on UV inactivation of *E. coli* K12 in caramel buffer solutions in the CiderSure 1500 UV reactor. (From Koutchma et al. 2004. With permission.)

Factors unique to juice, such as °Brix and pH, did not exhibit a large effect over the range tested when examined individually. The single factor found to consistently affect the efficacy of UV-light inactivation in juice was absorbance. The effect of absorbance of model solutions on the inactivation of *E. coli* K12 in a thin-film reactor is shown in Figures. 1.4 and 1.5.

To examine the effect of suspended particles on killing rate, the UV inactivation of *E. coli* K12 in commercial apple juices with turbidity values of 1400 and 2400 NTU was studied. The data shown in Figure 1.6 indicate faster killing of *E. coli* in the less turbid apple cider of 1400 NTU at the higher flow rate of 166 mL/s. No significant difference in inactivation was observed at the minimum flow rate of 57 mL/s. Higher flow rates resulted in increased mixing between the three tandem treatment chambers and thus a more complete irradiation of cider. Increasing the turbidity of apple cider to 2400 NTU negatively impacted the effectiveness of UV disinfection, resulting in a lower inactivation rate. The flow rates and mixing in the turbulent flow also affected microbial inactivation, with higher flow rates producing higher UV inactivation rates in the turbulent-flow reactor. Regression equations were developed to describe the relationship between the rate of reduction of *E. coli* K12 and the absorption coefficients in both a thin-film reactor and a turbulent-flow UV reactor.

Murakami et al. (2006) reported similar findings regarding the insignificant effects of pH and °Brix in apple juice on inactivation. A static irradiation vessel was used in this study to look at the inactivation kinetics of *E. coli* K12. The effect of suspended solids was also studied, and a two-component inactivation curve was used to describe their effects in the range of concentration up to 5.0 g/mL on inactivation kinetics.

Geveke (2005) processed apple cider with a single-lamp UV apparatus surrounded by a coil of UV-transparent Chemfluor tubing. *Escherichia coli* K12 and *L. innocua*

were used for inoculation of apple cider. The population of *E. coli* K12 was reduced by 3.4 ± 0.3 log after being exposed for 19 s to a 15-W low-pressure mercury (LPM) lamp. The population of *L. innocua* was more resistant to UV and was reduced by 2.5 ± 0.1 log after being exposed for 58 s. The energy for the process was calculated as the ratio of lamp power to the flow rate and was equal to 34 J/mL. The comparison of the average energy cost with heat treatments showed that energy consumption and cost for UV and heat treatments were approximately the same.

Forney et al. (2004) have developed a novel Taylor–Couette flow reactor to process commercial apple and grape juices inoculated with *E. coli*. The described design consists of an inner cylinder that rotates within a stationary larger cylinder. The flow characteristics of this reactor approached ideal plug flow, with a residence time that was uncoupled from the hydrodynamics or boundary-layer characteristics. At low rotation rates, a laminar flow was established within the annular fluid gap. A 3–5-log reduction of *E. coli* was reported to be achieved in the Taylor–Couette reactor. In addition, a dosage of roughly 9 mJ/cm^2 for a 4-log reduction in pathogen level was determined.

Guerrero-Beltran and Barbosa-Canovas (2005) studied inactivation of *Saccharomyces cerevisiae*, *E. coli*, and *L. innocua* by UV light in apple juice. Two annular single-lamp reactors from Atlantic UV Co. were connected in series using a LPM UV lamp of 25 W. The apple juice was recirculated in a system, and calculated Re numbers indicated that laminar flow was achieved during trials. Reductions of 1.34, 4.29, and 5.10 $\log_{10}$ after 30 min of UV treatment were reported for *S. cerevisiae*, *E. coli*, and *L. innocua*, respectively. An incident UV fluence of 450 kJ/m^2 was reported in this study.

1.3.2.2 Juices with Pulp

Guerrero-Beltran and Barbosa-Canovas (2006) processed mango nectar with UV light and examined inactivation of *S. cerevisiae* and polyphenoloxidase using the lab-scale UV reactors described above. The maximum 3-log reduction was achieved after treatment for 30 min. In addition, shelf-life extension up to 20 days for mango nectar was reported by these researchers.

According to Oteiza (2005), orange, apple, and multifruit juices were inoculated with *E. coli* K12 and treated in a static UV chamber using stirred and stagnant films and UV doses up to 6 J/cm^2. The absorptivity coefficients were determined in this study, and linear correlation was found with the *D*-values obtained. In addition, a linear relationship between *D*-values and absorbed energy was also found. The higher the absorbance of the medium, the greater were the values of *D* required to inactivate *E. coli* strains by UV light.

UV treatment of orange juice was also reported by Tran and Farid (2004). A vertical single-LPM UV lamp (6-W output power) thin-film reactor was designed and built for treatments. The thickness of the film was approximately 0.21–0.48 mm. The applied UV dose was in the range of 12–147.6 mJ/cm^2 in the conducted experiments, which resulted in a 3-$\log_{10}$ reduction of aerobic bacteria, yeasts, and molds.

Koutchma et al. (2007) validated the performance of a coiled UV module, Model 420 (Salcor Inc., Fallbrook, CA), with 24 lamps for pasteurizing fresh juices.

TABLE 1.3
Physicochemical Properties of Tropical Juices

Juice	Absorption Coefficient cm^{-1}/Std. Dev.		Turbidity NTU/Std. Dev.		pH	(°Brix)		Viscosity cP/Std. Dev.	
Apple	25.9	1.1	972	23	3.21	11.35	0.35	5.79	0.46
Carrot	52.9	0.9	3980	453	3.75	10.55	1.06	9.87	2.59
Guava nectar	45.8	12.6	>4500	>450	6.32	9.05	0.21	5.02	1.01
Orange	47.9	1.0	3759	21	3.30	7.37	0.29	51.77	17.81
Lilikoi	11.7	2.1	1392	503	3.01	11.40	0.28	5.55	0.46
Pineapple	73.1	1.95	4028	256	3.96	14.17	0.58	53.20	6.16
Watermelon	23.6	1.9	1502	200	5.19	8.10	0.57	6.72	3.22

Source: Koutchma et al. (2007).

The properties of seven varieties of tropical juice from Hawaii—apple, melon, lilikoi (yellow passion fruit), orange, carrot, guava, and pineapple—were measured and served as a basis for the models used in the study. All tested fruit juices highly absorbed UV light, with absorption coefficients ranging from 11 to 78 cm^{-1} for lilikoi and pineapple juice, respectively. Of the juices examined, pineapple juice appeared to be the "worst-case scenario" in terms of UV absorptivity and high viscosity. Table 1.3 summarizes critical properties of fresh fruit juices tested in this study.

A caramel model solution was developed to mimic juice absorption properties and then used for inoculation studies with *E. coli* K12 bacteria. The results of inactivation tests in model juice solutions after one, two, and three passes are given in Table 1.4. The 5-$\log_{10}$ reduction standard under turbulent flow, as required

TABLE 1.4
Inactivation of *E. coli* K12 in Model Juice Solutions

Juice	Absorption Coefficient (cm^{-1})	Caramel Juice Model (%)	Log Reduction		
			1 Pass	2 Passes	3 Passes
Lilikoi	12	0.2	6.3 ± 0.2	…	…
Apple	26	0.5	2.23 ± 0.016	3.60 ± 0.085	4.8 ± 0.18
Orange	48	1.0			
Carrot	53	1.1	0.35 ± 0.068	1.98 ± 0.17	3.1 ± 0.064
Guava	46	1.0			
Pineapple	73	2.0	0.48 ± 0.12	1.61 ± 0.12	2.87 ± 0.2

Source: Koutchma et al. (2007).

by the FDA, was achievable in juices that were characterized as having Newtonian liquid behavior with an absorption coefficient less than 15 cm^{-1} after one pass. Turbulent flow was not developed in the more-viscous orange and pineapple juices at the flow rates tested. A biodosimetry technique that utilizes *E. coli* as a tracer showed no distribution of UV dose in liquids with an absorption coefficient lower than 26 cm^{-1}.

The inactivation performance in relation to spoilage microflora of the Salcor coiled-tube UV reactor for treatment of tropical juices with pulp such as orange, pineapple, guava nectar, and carrot is shown in Figure 1.7(a, b). It can be seen that after two passes at flow rates of 4 gpm, no more than a 1-log reduction of aerobic plate count (APC) was achieved in orange, guava, and pineapple juices. However, the APC was reduced more than 3 log in carrot juice. Approximately 1.2–1.6-log reductions of yeasts and up to 1.6-log reduction of molds were achieved in treated juices.

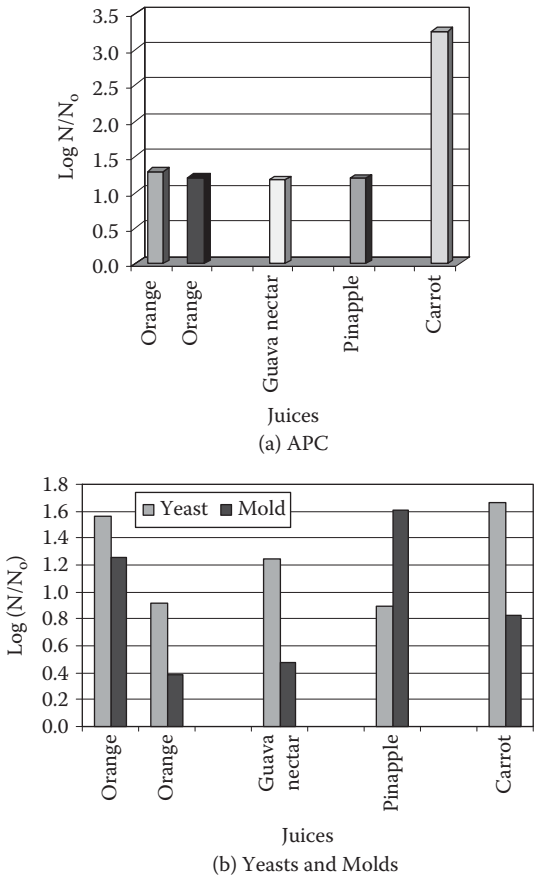

FIGURE 1.7 Inactivation performance of the "Salcor" UV reactor in tropical juices with pulp: (a) APC count, and (b) yeasts and molds count.

Keyser et al. (2008) reported that a novel system was used for the treatment of apple juice, guava and pineapple juice, mango nectar, strawberry nectar, and two different orange and tropical juices. Tests were performed using a pilot-scale UV system as well as the novel PureUV (Milnerton, South Africa) commercial-scale unit. According to the description, the reactor consisted of a stainless steel inlet and outlet chamber with a stainless steel corrugated spiral tube between the chambers. Inside the spiral tube is a UV lamp (100-W output, 30-W UV-C output) that is protected by a quartz sleeve. The liquid flows between the corrugated spiral tube and the quartz sleeve. The tangential inlet of the reactor creates a high-velocity turbulence in the inlet chamber that brings the liquid (product) into contact with the UV radiation. The liquid is pumped from the inlet chamber into the actual reactor, the gap between the quartz sleeve, and the corrugated spiral tubing at a minimum flow rate of 3800 L/h, with a Reynolds value (Re) in excess of 7500, which indicates turbulent flow.

Ultraviolet dosage levels of 0, 230, 459, 689, 918, 1148, 1377, 1607, and 2066 (J/L) were applied to the different juice products in the Keyser et al. (2008) study in order to reduce the microbial load to acceptable levels. In comparison to heat pasteurization, juices treated with UV light did not change taste and color profiles. UV-C radiation was successfully applied to reduce the microbial load in the different single-strength fruit juices and nectars. The commercial-scale unit presented 10 lamps in series, thereby delivering a UV-C dose of 230 J/L to the liquid being treated after one pass. The authors concluded that optimization was essential for each juice treated and recommended this novel UV technology as an alternative technology to pasteurization.

Table 1.5 summarizes the data of inactivation performance and technical characteristics of UV apparati used for treatments of various fresh juices that were reported in the studies cited above.

1.3.3 Liquid Sugars and Sweeteners

Liquid sugars are used extensively in the food and beverage industries. Sugar syrups (sucrose, fructose, honey) with high osmotic pressure can be subject to microbial growth, resulting in health problems and spoilage. In addition to the challenges of lower transmission of UV light, liquid sugars have high-viscosity characteristics. UV systems have been effectively designed and validated for manufacturing companies that produce soda, candy, honey, and a variety of other foods. In 1983, the Agricultural Experimental Station of Vermont published a report of UV-light treatment of maple syrup before storage (Morselli and Whalen 1984). It was found that UV light was effective in killing bacteria but was least effective on yeasts in sap. Hillegas and Demirci (2003) reported on the use of pulsed UV light to inactivate *Clostridium sporogenes* spores in clover honey. However, no detailed information regarding observed effects was given in the publication.

Lenntech Water Treatment and Air Purification Holding B.V. (The Netherlands) developed a special range of UV systems to disinfect sugar syrups. These systems were designed to treat sugar syrups with a viscosity up to 66°Brix. (Above 66°Brix, the osmotic pressure of the syrup prevents the growth of microorganisms.) The treatment with UV increases the shelf life and prevents problems with the odor and taste of the syrups. The capacity for a single unit to treat sugar syrup is up to 34 m^3/h.

TABLE 1.5
Inactivation Performance of UV Reactors Used to Process Fresh Juices

		Type of UV Reactor					
Juice	**Researcher**	**Flow Regime**	**Number/Type of UV Lamp [a]/Power**	**Gap Size (mm)**	**UV Dose (mJ/cm²)**	**Test Microorganism**	**Achieved Inactivation (log)**
Apple cider	Worobo (1999)	Laminar	8/LPML/39 W	0.8	n.d.	*E. coli* (ATCC 25922)	5–6
Apple cider	Wright et al. (2000)	Thin film	10/LPML/39 W	n.d.	9–61	*E. coli* O157:H7	3.8
Apple juice	Koutchma et al. (2004)	Laminar	8/LPML/39 W	0.8	14.5	*E. coli* K12	3–4
Apple cider		Turbulent	12/LPML/42 W	6–10	0.75	*E. coli* K12	less than 1
Apple juice	Guerrero-Beltran and Barbosa-Canovas (2005)	Laminar	2/LPML/25 W	n.d.	5135	*S. cerevisiae*	1.34
						L. innocua	4.29
						E. coli	5.10
Apple cider	Geveke (2005)	Coiled tube, 27–83 mL/min	1/LPML/15 W	ID 1.6	34 J/mL	*E.coli*	3.4
						L.innocua	2.5
Apple juice	Forney et al. (2004)	Taylor–Couette flow	4/MPML/0.684 W	5.5	21.7	*E.coli* 15597	3–5
Grape juice		Laminar		2		*E.coli* 15597	
Apple cider	Hanes et al. (2002)	Thin film	8/LPML/39 W	0.8	14.32	*C. parvum*	5
		Laminar				Oocyst	
Orange juice	Tran and Farid (2004)	Thin film	1/LPML/30 W	0.21	12.3-	APC, yeasts, molds	2
		Laminar Vertical		0.48	120		3
Mango nectar	Guerrero-Beltran and Barbosa-Canovas (2006)	Laminar	2/LPML/25 W	n.d.	5135	*S. cerevisiae*	2.71
						APC, yeasts, molds	2.94

(*Continued*)

TABLE 1.5 (CONTINUED)
Inactivation Performance of UV Reactors Used to Process Fresh Juices

		Type of UV Reactor					
Juice	**Researcher**	**Flow Regime**	**Number/Type of UV Lamp [a]/Power**	**Gap Size (mm)**	**UV Dose (mJ/cm²)**	**Test Microorganism**	**Achieved Inactivation (log)**
Models of tropical juices	Koutchma et al. (2004)	Turbulent Dean flow	24/LPML/65 W	ID 10–12	21.5	*E. coli*	Up to 6
Orange juice						APC, yeasts, molds	1.5
Guava							1.2
Carrot							3.2
Pinapple							1.0
Apple juice	Keyser et al. (2008)	Turbulent (Re> 7500)	1–10/LPML/100 W	n.d.	229.5 J/L	APC, yeasts, molds	3.5
							3.0
Guava-and-pineapple juice					1377 J/L	APC, yeasts, molds	3.31
							4.48
Mango nectar, strawberry nectar					2065 J/L	APC, yeasts, molds	1.32
Orange juices					167 J/L	APC, yeasts, molds	<1

Note: n.d. = no data available.

[a] LPML, low-pressure mercury lamp; MPML, medium-pressure mercury lamp.

1.3.4 Liquid Egg Products

Egg products are classified as refrigerated liquid, frozen, and dried products. Liquid egg products (LEP) are valuable due to their high protein content, low cost, and potential use as ingredients in a prepared meal in order to provide texture, flavor, structure, and moisture. In the production of ready-to-use and shelf-stable LEP, pasteurization is the fundamental process to eliminate pathogenic microorganisms, mainly *Escherichia coli* O157:H7 and *Salmonella enteritidis* from the product. The most common pasteurization method for liquid egg products is the thermal treatment, having the principle of inactivation of microorganisms by application of heat for certain periods of time. Minimum temperature and holding time requirements for the egg yolk are 60°C and 6.2 min.

Unluturk et al. (2008) explored the efficacy of UV radiation as a nonthermal pasteurization process for liquid egg products using a strain of *E. coli* (ATCC 8739) as the target microorganism. For this purpose, the effects of depth of liquid food medium, applied UV intensity (incident), and exposure time on the inactivation of *E. coli* (ATCC 8739) were explored in three liquid egg products, namely liquid egg yolk, liquid egg white, and liquid whole egg. UV irradiation of samples was conducted using a collimated beam apparatus as described by Bolton and Linden (2003). The apparatus consisted of a low-pressure mercury UV lamp with peak radiation at 254-nm wavelength. The UV radiation was collimated with a flat-black painted tube that was the same size as a petri dish. Samples were placed in 6-cm-diameter petri dishes directly below the collimated UV beam and stirred continuously during the irradiation with a vortex mixer. Absorption coefficients of liquid egg products were reported to be 104, 807, and 630 cm^{-1} for liquid egg white, whole egg, and egg yolk, respectively. Turbidity of the liquid egg product was in the range from 398 NTU for liquid egg white to 8400 NTU for liquid yolk and whole egg. The kinetic rate parameters (k) were reported based on the first-order reaction for the different fluid-medium depths and UV intensities. Maximum inactivation obtained was 0.675 log CFU/mL in liquid egg yolk and 0.316 log CFU/mL in liquid whole egg. On the other hand, a greater than 2-log reduction of *E. coli (*ATCC 8739) was achieved in liquid egg white.

It was concluded that UV light may not be the feasible inactivation process for liquid white egg and liquid egg yolk. Considering the lower treatment costs of UV systems compared with thermal pasteurization methods, it was suggested that UV-light treatment can be used as a pretreatment process or alternative method when combined either with mild heat treatment or nonthermal technologies to reduce the initial microbial load as well as the adverse effects of thermal pasteurization of liquid egg products. It may also be used in combination with other preventive methods, such as good manufacturing practices and sanitizing treatments of egg shells, as part of an approved hazard analysis and critical control point plan (U.S. FDA 2001).

Ngadi et al. (2003) reported effects of pH, depth of food medium, and UV-light dose on the inactivation of *E. coli* O157:H7 in UV-opaque products such as apple juice (pH 3.5) and egg white (pH 9.1). The applied UV dose ranged from 0 to

6.5 mW × min/cm^2, while the depths of the medium were 1, 3.5, 5, and 10 mm. The pH of the medium did not affect the inactivation of *E coli* O157:H7, since similar inactivation characteristics were obtained for both apple juice and liquid egg white. More than a 5-log reduction was obtained when the fluid depth and UV dose were 1 mm and 6.5 mW×min/cm^2, respectively. However, less than a 1-log reduction was obtained when the fluid depth was 10 mm. The visual appearance of the treated apple juice and egg white did not show any discoloration changes during 4 weeks of storage at ambient temperature (25°C).

1.3.5 Milk

In relation to UV treatment of milk, Matak et al. (2005) reported more than a 5-log$_{10}$ reduction in *Listeria monocytogenes* numbers in goat's milk by exposure to a cumulative UV dose of 15.8 ± 1.6 mJ/cm^2 with the use of a CiderSure 3500 UV apparatus (FPE Inc., Macedon, NY). Reinemann et al. (2006) reported that UV treatment of 15 kJ/L achieved a 3-log$_{10}$ reduction in total numbers of bacteria present in raw cow's milk, with coliforms showing the greatest reduction in numbers and spore formers showing only a modest reduction. The PureUV system (PureUV, South Africa) was used in this study.

UV-light inactivation of *Mycobacterium avium* subsp. *paratuberculosis* in Middlebrook 7H9 broth and whole and semi-skim milk was investigated by Altic et al. (2007) using a laboratory-scale UV unit that consisted of four UV lamps surrounding a UV-penetrable flow tube and incorporated static mixers within UV-penetrable pipes. UV treatment proved to be less effective in killing *M. avium* subsp. *paratuberculosis* suspended in milk (0.5- to 1.0-log$_{10}$ reduction per 1000 mJ/mL) than that suspended in Middlebrook 7H9 broth (2.5- to 3.3-log$_{10}$ reduction per 1000 mJ/mL).

Currently, different designs of continuous-flow UV reactors are being evaluated for use in juice pasteurization in order to overcome the interference of high UV absorptivity and turbidity associated with fresh juices/ciders. Two strategies are being employed (Koutchma et al. 2004). The first approach uses laminar flow in extremely thin-film UV units to decrease the path length of the UV light, thus avoiding the problems associated with the lack of penetration. The second approach increases the turbulence within a UV unit to bring all material into close proximity of the UV light during the treatment. The majority of the reactors tested were not specifically designed for juice treatments and therefore were not optimized with regard to geometrical configurations, flow regimes, and UV lamps.

Considering the differences in velocity profiles for laminar and turbulent regimes, a desirable design for UV units would be a pure plug flow such that every element of liquid resides in the unit for the same time period and, thus, all microorganisms would receive an equivalent UV dose if the UV irradiance were equal at all points. To achieve the latter, desirable additional mixing and a more uniform residence distribution was promoted in the coiled-tube (Koutchma et al. 2007) and Taylor–Couette flow reactors (Forney and Pierson, 2004). The correct choice and design of the UV unit, its flow characteristics, and UV source can reduce the interference of

high UV absorptivity and viscosity associated with fresh juices and will improve inactivation efficiency.

1.4 CURRENT STATUS OF U.S. AND INTERNATIONAL REGULATIONS

1.4.1 U.S. FDA: Continuous UV-Light Irradiation

The U.S. Food and Drug Administration (FDA) has approved UV light as an alternative treatment to thermal pasteurization of fresh juice products (U.S. FDA 2000b). In 2000, the FDA amended the food additive regulations to provide for the safe use of UV irradiation to reduce human pathogens and other microorganisms in juice products. This action was in response to a food additive petition filed by California Day-Fresh Foods, Inc. Under section 201(s) of the Federal Food, Drug, and Cosmetic Act (21 U.S.C. 321(s)), a source of radiation used to treat food is defined as a food additive. The additive is not, literally, added to food. Instead, a source of radiation is used to process or treat food such that, analogous to other food processes, its use can affect the characteristics of the food. In the subject petition, the intended technical effect is a change in the microbial load of the food, specifically, a reduction of human pathogens and other microorganisms in juice products.

FDA has evaluated the safety of the use of UV irradiation to reduce human pathogens and other microorganisms in juices. This safety assessment was based on the current understanding of the effects of UV irradiation on the major chemical components of food. Having evaluated the data in the petition and other relevant material in the agency's files, the agency concluded that any photochemical changes that may occur as a result of the UV irradiation are of no toxicological significance. FDA concluded that the proposed use is effective in reducing human pathogens in juices and that treated juices will be at least as safe as untreated juices currently on the market. However, the submitted microbiological data do not constitute the type of validation studies necessary to demonstrate the achievement of specific performance standards, e.g., 5-log reductions, for human-pathogen control programs. Therefore, users of this UV treatment who are subject to certain performance standards need to establish that this treatment meets their required level of human-pathogen reduction.

The petitioned UV radiation is produced by low-pressure mercury lamps, and the juice being treated passes through a transparent tube in which the juice is subjected to UV irradiation. Because most juices strongly absorb UV radiation, most of the UV radiation would be absorbed by the juice at the wall of the tube near the source of the UV irradiation. However, the amount of UV irradiation that would reach juice in the middle of the tube would be insufficient to reduce significantly human pathogens. Therefore, the petitioner proposed that the juices flow under turbulent conditions that produce eddies and swirls in the juice to ensure that as much juice as possible will reach the wall of the UV-transparent tube, where the juice would be exposed to UV irradiation. This would help to reduce human pathogens and other microorganisms throughout the juice. The conditions for turbulent flow are described mathematically by the unitless Reynolds number (Re). To ensure that sufficient turbulent flow

is achieved, the petitioner has requested that a limit of a Reynolds number of no less than 2200 be incorporated into the regulation. FDA concurs with this specification.

The amount of UV irradiation necessary for human-pathogen reduction will depend on various factors, such as the type of juice, the initial microbial load, and the design of the irradiation system (e.g., flow rate, number of lamps, and time exposed to irradiation). Therefore, FDA did not specify a minimum or maximum dose by regulation, but concludes that this should be achieved for individual usage situations in a manner consistent with good manufacturing practice. In addition, FDA expects that the maximum dose applied to the juice will be economically self-limiting due to the costs associated with UV irradiation. Additionally, the levels of UV irradiation applied to the juice will be limited by the possible alterations in organoleptic characteristics of the juice (i.e., changes in taste or color) after UV irradiation, changes that may result in decreased consumer acceptance.

1.4.2 Pulsed UV Light in the Production, Processing, and Handling of Food

Code 21CFR179.41, issued by the Food and Drug Administration (U.S. FDA 2005), Department of Health and Human Services, approves the use of pulsed UV light in the production, processing, and handling of food. As stated in the code, "Pulsed light may be safely used for the treatment of foods under the following conditions:

(a). The radiation sources consist of xenon flashlamps designed to emit broadband radiation consisting of wavelengths covering the range of 200–1000 nanometers (nm), and operated so that the pulse duration is no longer than 2 milliseconds (ms);
(b). The treatment is used for surface microorganism control;
(c). Foods treated with pulsed light shall receive the minimum treatment reasonably required to accomplish the intended technical effect; and
(d). The total cumulative treatment shall not exceed 12.0 joules/square centimeter (J/cm^2)."

1.4.3 Health Canada: Novel Food Information

The Department of Novel Foods, of Health Canada, has conducted a comprehensive assessment of UV-treated apple juice/cider according to its guidelines for the safety assessment of novel foods. These guidelines are based upon internationally accepted principles for establishing the safety of novel foods. The assessment conducted by Food Directorate evaluators determined (a) the effectiveness of the CiderSure 3500 UV-light unit in reducing the bacterial load of apple juice/cider, (b) how the composition and nutritional quality of UV-light-treated apple juice/cider compares with untreated and pasteurized apple juice/cider, and (c) the potential for toxicological or chemical concerns associated with the use of UV light on apple juice/cider (Health Canada 2004).

After reviewing the information presented in support of the CiderSure 3500, Health Canada concluded that there are no human food safety concerns associated

with the sale of unpasteurized and unfermented apple cider and juice that has been treated with the CiderSure 3500. The UV treatment can achieve a significant reduction in the microbial load of apple juice and cider products. However, it was noted that this reduction does not mean elimination of pathogenic organisms, especially in cases where the original microbial load of the juice product was extremely high. Therefore, manufacturers should continue to take steps to limit the risk of contamination in their production process. Health Canada has notified Moore Orchards that it has no objection to the sale of unpasteurized and unfermented apple juice and cider products that have been treated with the CiderSure 3500 UV-light unit. This opinion was solely with respect to the suitability of apple cider and juice treated using the CiderSure 3500 for sale as human food.

1.4.4 European Union Regulations

The European Union (EU) considers UV light as an irradiation. Regulations for the use of the irradiation process in the EU are not harmonized. The member states still discuss which foodstuffs should be allowed to be treated by ionizing radiation. Food irradiation may only be authorized if (a) there is a reasonable technological need, (b) it presents no health hazard and is carried out under the conditions proposed, (c) it is of benefit to the consumer, and (d) it is not used as a substitute for hygiene and health practice or for good manufacturing or agricultural practice.

1.4.5 Establishing the Equivalence of Alternative Methods of Pasteurization

The definition of "pasteurization" for foods was revised by the National Advisory Committee on Microbiological Criteria for Foods (NACMCF 2006). The NACMCF agreed on the following guidance for the pasteurization that now includes "any process, treatment, or combination thereof, which is applied to food to reduce the most microorganism(s) of public health significance to a level that is not likely to present a public health risk under normal conditions of distribution and storage." NACMCF recommended that regulatory agencies establish a Food Safety Objective (FSO) and a performance standard for food–pathogen combinations that can be used as the basis for judging equivalency when a proposed process is evaluated as an alternative to traditional pasteurization. The processes and technologies examined in the above-mentioned report that can satisfy the definition of pasteurization for certain foods also include UV radiation as an alternative to traditional thermal pasteurization.

The NACMCF recommended considering numerous factors when establishing the efficacy and equivalency of different pasteurization processes. This includes identification of the most resistant pathogens of concern in the food, the efficacy of the specific technology to reduce the pathogens of concern, the food matrix characteristics, and the intended use of food. In addition to the general considerations, the NACMCF identified research needs that are relevant to UV radiation of foods: identification of pathogens most resistant to UV in foods, optimization of critical process

parameters and development of protocols to monitor critical factors, identification of differences between pulsed and continuous UV treatments, and establishment of parameters such as suspended- and dissolved-solids concentration.

It was stated that all pasteurization processes need to be validated through the use of process authorities, challenge studies, and predictive modeling. All pasteurization processes must be verified to ensure that critical processing limits are achieved. As new technology is applied commercially, the research is needed to develop label statements about pasteurization that are understood by consumers.

REFERENCES

Allende, A., and F. Artes. 2003. Combined ultraviolet-C and modified atmosphere packaging treatments for reducing microbial growth of fresh processed lettuce. *Food Sci. Technol. (LWT)* 36: 779–786.

Altic, L., M. Rowe, and I. Grant. 2007. UV light inactivation of *Mycobacterium avium subsp. paratuberculosis* in milk. *Appl. Environ. Microbiol*. 73: 3728–3733.

Anonymous. 2000. Kinetics of microbial inactivation for alternative food processing technologies. Institute of Food Technologists. *J. Food Sci. Supplement* http//vm.cfsan.fda.gov/~comm/ift-pref.html.

Beaulieu, J. 2007. Effect of UV radiation on cut cantaloupe: Terpenoids and esters. *J. Food Sci*. 72 (4): 272–281.

Blatchley, E. R., and M. Peel. 2001. Disinfection by ultraviolet irradiation. In *Disinfection, Sterilization, and Preservation*, 823–851. New York: Lippincott Williams & Wilkins.

Bolton, J. R., and K. G. Linden. 2003. Standardization of methods for fluence UV dose determination in bench-scale UV experiments. *J. Environ. Eng*. 129: 209–215.

Chapman, S. 2003. New machines use tumbling process to decontaminate food. *Food Chem. News* 10: 20.

Chavez, C., K. Knape, C. Coufal, and J. Carey. 2002. Reduction of eggshell aerobic plate counts by ultraviolet irradiation. *Poultry Sci.* 81: 1132–1135.

Coufal, C. D., C. Chavez, K. D. Knape, and J. B. Carey. 2003. Evaluation of ultraviolet light sanitation of broiler hatching eggs. *Poultry Sci*. 82: 754–759.

Doulia, D., G. Katsinis, and B. Mougin. 2000. Prolongation of the microbial shelf life of wrapped part baked baguettes. *Int. J. Food Prop*. 3: 447–457.

Duffy, S., J. Churey, R. Worobo, and D. W. Schaffner. 2000. Analysis and modeling of the variability associated with UV inactivation of *Escherichia coli* in apple cider. *J. Food Prot*. 63: 1587–1590.

Favier, G., M. Escudero, and A. De Guzman. 2001. Effect of chlorine, sodium chloride, trisodium phosphate and ultraviolet radiation on the reduction of *Yersinia enterocolitica* and mesophilic aerobic bacteria from eggshell surface. *J. Food Prot.* 64: 1621–1623.

Fine, F., and P. Gervais. 2004. Efficiency of pulsed UV-light for microbial decontamination of food powders. *J. Food Prot*. 67: 787–792.

Fonseca, J., and J. Rushing. 2006. Effect of ultraviolet-C light on quality and microbial population of fresh cut watermelon. *Post Harvest Biol. Technol*. 40: 256–261.

Forney, L., and J. A. Pierson. 2004. Ultraviolet disinfection. *Resource* 11: 7.

Forney, L., J. A. Pierson, and Z. Ye. 2004. Juice irradiation with Taylor-Couette flow: UV inactivation of *Escherichia coli*. *J. Food Prot*. 67: 2410–2415.

FSIS. 2003. FSIS rule designed to reduce *Listeria monocytogenes* in ready to eat meat and poultry products. Food Safety and Inspection Service, USDA, Washington, DC. http://www.fsis.usda.gov/OA/background/lmfinal.htm.

Gardner, D., and G. Shama. 2000. Modeling UV induced inactivation of microorganisms on surfaces. *J. Food Prot.* 63: 63–70.

Geveke, D. 2005. UV inactivation of bacteria in apple cider. *J. Food Prot*. 68: 1739–1742.

Guerrero-Beltran, J. A., and G. V. Barbosa-Canovas. 2005. Reduction of *Saccharomyces cerevisiae, Escherichia coli* and *Listeria innocua* in apple juice by ultraviolet light. *J. Food Proc. Eng*. 28: 437–452.

Guerrero-Beltran, J. A., and G. V. Barbosa-Canovas. 2006. Inactivation of *Saccharomyces cerevisiae* and polyphenoloxidase in mango nectar treated with UV light. *J. Food Prot*. 69: 362–368.

Hanes, D. E., P. A. Orlandi, D. H. Burr, M. D. Miliotis, M. G. Robi, J. W. Bier, G. J. Jackson, M. J. Arrowood, J. J. Churey, and R. W. Worobo. 2002. Inactivation of *Cryptosporidium parvum* oocysts in fresh apple cider using ultraviolet irradiation. *Appl. Environ. Microbiol*. 68: 4168–4172.

Harm, W. 1980. *Biological effects of ultraviolet radiation*, Cambridge, UK: Cambridge University Press.

Harrington, W. O., and C. H. Hills. 1968. Reduction of the microbial population of apple cider by ultraviolet irradiation. *Food Technol*. 22 (11): 117–120.

Health Canada. 2004. Ultraviolet light treatment of apple juice/cider using the CiderSure 3500. Novel Food Information. http://www.hc-sc.gc.ca/fn-an/gmf-agm/appro/dec85_rev_nl3_e.html.

Hillegas, S. L. and Demirci, A. 2003. Inactivation of *Clostridium sprogenes* in clover honey pulsed UV-light treatment. CIGR-ejournal. 2003;5(5).

Jun, S., J. Iruddayaraj, A. Demirci, and D. Geiser. 2003. Pulsed UV-light treatment of corn meal for inactivation of *Aspergillus niger* spores. *Int. J. Food Sci. Technol*. 38: 883–888.

Keyser, M., I. Müller, F. P. Cilliers, W. Nel, and P. A. Gouws. 2008. UV radiation as a non-thermal treatment for the inactivation of microorganisms in fruit juice. *Innovative Food Sci. Emerging Technol*. 9 (3): 348–354.

Kim, T., J. Silva, and T. Chen. 2002. Effects of UV irradiation on selected pathogens in peptone water and on stainless steel and chicken meat. *J. Food Prot*. 65: 1142–1145.

Koutchma, T., R. Englert, and C. Adhikari. 2002. The effect of browning and suspended particles on the UV treatment of apple juice/cider. Paper presented at IFT Annual Meeting, Anaheim, CA, June 15–19, 2002. Technical programs abstracts, 228.

Koutchma, T., S. Keller, B. Parisi, and S. Chirtel. 2004. Ultraviolet disinfection of juice products in laminar and turbulent flow reactors. *Innovative Food Sci. Emerging Technol*. 5: 179–189.

Koutchma, T., B. Parisi, and E. Patazca. 2007. Validation of UV coiled tube reactor for fresh fruit juices. *J. Environ. Sci. Eng*. 6: 319–328.

Kuo, F., J. Carey, and S. Ricke. 1997. UV irradiation of shell eggs: Effect on populations of aerobes, molds and inoculated *Salmonella typhimurium*. *J. Food Prot*. 60: 639–643.

Lagunas-Solar, M., C. Pina, J. MacDonald, and L. Bolkan. 2006. Development of pulsed UV-light processes for surface fungal disinfection of fresh fruit. *J. Food Prot*. 69: 376–384.

Lamikanra, O., B. Garber, D. Kueneman, and D. Ukuku. 2005. Effect of processing under ultraviolet light on the shelf-life of fresh cut cantaloupe melon. *J. Food Sci*. 70: 534–539.

Lyon, S. A., D. L. Fletcher, and M. E. Berrang. 2007. Germicidal ultraviolet light to lower numbers of *Listeria monocytogenes* on broiler breast fillets. *Poultry Sci*. 86: 964–967.

Matak, K. E., J. J. Churey, R. W. Worobo, S. S. Sumner, E. Hovingh, C. R. Hackney, and M. D. Pierson. 2005. Efficacy of UV light for the reduction of *Listeria monocytogenes* in goat's milk. *J. Food Prot*. 68: 2212–2216.

Morselli, M., and M. Whalen. 1984. In-line ultraviolet treatment of sugar maple sap at different flow rates and on sap concentrated by reverse osmosis. Research report 37. Agricultural Experimental Station, University of Vermont, Burlington.

Murakami, E., L. Jackson, K. Madsen, and B. Schickedanz. 2006. Factors affecting the ultraviolet inactivation of *Escherichia coli* K12 in apple juice and a model system. *J. Food Proc. Eng*. 29: 53–71.

NACMCF (National Advisory Committee on Microbiological Criteria for Foods). 2005. Requisite scientific parameters for establishing the equivalence of alternative methods of pasteurization. *J. Food Prot*. 69 (5): 1190–1216.

Ngadi, M., J. Smith, and B. Cayouette. 2003. Kinetics of ultraviolet light inactivation of *Escherichia coli* O157:H7 in liquid foods. *J. Sci. Food Agric*. 83: 1551–1555.

Oteiza, J., Peltzer M., Gannuzzi L., and Zaritzky N. 2005.Antimicrobial efficacy of UV radiation on *Escherichia coli* O157:H7 in fruit juices of different absorptivities. *Journal Food Protection*, 68 (1): 49–58.

Ozer, N., and A. Demirci. 2006. Inactivation of *Escherichia coli* O157:H7 and *Listeria monocytogenes* inoculated on raw salmon fillets by pulsed UV-treatment. *Int. J. Food Sci. Technol*. 41: 354–360.

Reinemann, D. J., P. Gouws, T. Cilliers, K. Houck, and J. R. Bishop. 2006. New methods for UV treatment of milk for improved food safety and product quality. ASABE paper no. 066088. American Society of Agricultural and Biological Engineers (ASABE), St. Joseph, MI.

Sharma, R. R., and A. Demirci. 2003. Inactivation of *Escherichia coli* O157:H7 on inoculated alfalfa seeds with pulsed ultraviolet light and response surface modeling. *J. Food Sci*. 68: 1448–1453.

Sugarman, C. 2004. Pasteurization redefined by USDA committee. *Food Chem. News* 46 (3).

Takeshita, K., J. Shibato, and T. Sameshima. 2003. Damage of yeast cells induced by pulsed light irradiation. *Int. J. Food Microbiol*. 85: 151–158.

Tran, M. T., and M. Farid. 2004. Ultraviolet treatment of orange juice. *Innovative Food Sci. Emerging Technol*. 5: 495–502.

Unluturk, S., M. Atılgan, A. H. Baysal, and C. Tarı. 2008. Use of UV-C radiation as a non-thermal process for liquid egg products (LEP). *J. Food Eng*. 85: 561–568.

U.S. FDA. 2000a. Kinetics of microbial inactivation for alternative food processing technologies. Report prepared by Institute of Food Technologists for the U.S. Food and Drug Administration. Contract No. 223-98-2333. http://vm.cfsan.fda.gov/~comm/ift-pref.html.

U.S. FDA. 2000b. Irradiation in the production, processing and handling of food. *Code of Federal Regulations*. Title 21, part 179. *Federal Register*. 65: 71056–71058. U.S. Food and Drug Administration, Washington, DC.

U.S. FDA. 2001. Hazard analysis and critical control point (HACCP): Final rule. *Federal Register* 66 (13). U.S. Food and Drug Administration, Washington, DC.

U.S. FDA. 2005. *Code of Federal Regulations* 21CFR179.41. Title 21, Food and drugs. Part 179, Irradiation in the production, processing and handling of food. Subpart B, Radiation and radiation sources. Sec. 179.41, Pulsed light for the treatment of food. U.S. Food and Drug Administration, Washington, DC. http://edocket.access.gpo.gov/cfr_2005/aprqtr/21cfr179.41.htm.

Wallner-Pendleton, E. A., S. S. Sumner, G. Froning, and L. Stetson. 1994. The use of ultraviolet radiation to reduce salmonella and psychrotrophic bacterial contamination on poultry carcasses. *Poultry Sci*. 73: 1327–1333.

Wong, E., R. Linton, and D. Gerrard. 1998. Reduction of *Escherichia coli* and *Salmonella senftenberg* on pork skin and pork muscle using ultraviolet light. *Food Microbiol*. 15: 415–423.

Worobo, R. 1999. Efficacy of the CiderSure 3500 ultraviolet light unit in apple cider. Paper presented at U.S. FDA CFSAN Apple Cider Food Safety Control Workshop. http://www.cfsan.fda.gov/~comm/cidwworo.html.

Wright, J. R., S. S. Sumner, C. R. Hackney, M. D. Pierson, and B. W. Zoecklein. 2000. Efficacy of ultraviolet light for reducing *Escherichia coli* O157:H7 in unpasteurized apple cider. *J. Food Prot*. 63: 563–567.

2 Sources of UV Light

The general mechanism of UV-light generation was discussed in Chapter 1. In principle, the success of UV technology depends on the correct matching of the UV source parameters to the specific demands of the UV application. These determining parameters are principally the radiating properties of the UV source and their aging-related long-term effects. Low- and medium-pressure mercury lamps have been the traditional sources of radiation in most UV-based disinfection systems. The mercury-vapor UV-lamp sources have been successfully used in water treatment for nearly 50 years. They are both well understood and reliable sources for most disinfection treatments that benefit from their performance, low cost, and quality. For liquid foods and beverages, UV absorption can be relatively high; therefore, effective UV treatment requires development of alternative approaches to those normally employed for water. Concern over the impact of mercury release into the food plant environment has stimulated the development and validation of mercury-free lamps. The correct choice of UV source can enhance the efficiency of microbial inactivation by increasing UV penetration in the liquid as well as employing high UV intensity from pulsed sources.

In an effort to determine the best UV approach for food treatments, this chapter reviews the full range of commercially available UV sources, including low- and medium-pressure mercury lamps, mercury-free amalgam lamps, and excimer lamps. The advantages of pulsed UV-light sources that are currently under development are also discussed. It should be emphasized that, in a majority of cases, alternative UV sources have not been evaluated for food applications. More research in this important area can help ensure the effectiveness of UV light for microbial inactivation in foods, stimulate the growing interest in such nonthermal technologies, and assist in the successful commercialization of UV light for food-processing applications. The chapter concludes with a discussion of practical guidelines for the choice of UV-lamp technology.

2.1 INTRODUCTION

Three general types of UV lamps are typically used: low pressure (LP); low pressure, high output (LPHO); and medium pressure (MP). These terms are based on the vapor pressure of mercury when the lamps are operating. Vapor-discharge lamps consist of a UV-transmitting envelope made from a tube of vitreous silica glass sealed at both ends. An electrode is located at each end of the envelope connected to the outside through a seal. The envelope is filled with mercury and an inert gas. The lamp is typically powered using alternating current (AC). Stable operation also requires the presence of a ballast (Figure 2.1).

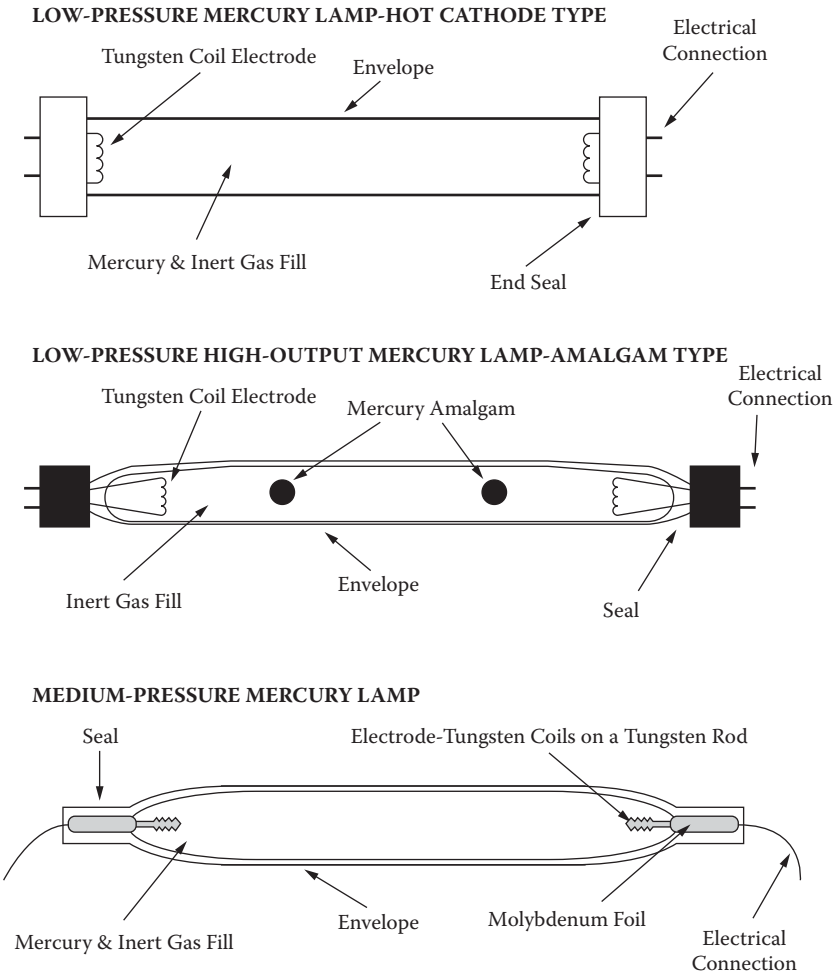

FIGURE 2.1 Schematics of LPM, LPHO, and MPM lamps.

Commercial UV reactors consist of an open- or closed-channel vessel that contains UV lamps separated from the treated liquid by a UV-transmitting sleeve. UV-intensity sensors, flow meters, and in some cases, UV transmittance monitors are used to monitor dose delivery by the reactor.

The reactor's control system allows the user to control and monitor its performance. The most important technical characteristics associated with UV lamps include operating temperature, electrical input (W/cm), germicidal UV output (W/cm), electrical-to-germicidal UV conversion efficiency (%), arc length, and rated lifetime (h). These characteristics will be used in this chapter to compare the operating performance of different types of lamps.

2.2 MERCURY-EMISSION LAMPS

In most cases, mercury-emission lamps contain a small amount of elemental mercury (Hg) and an inert gas (e.g., argon). The reasons for the prevalence of mercury are that it is the most volatile metal element for which activation in the gas phase can be obtained at temperatures compatible with the structures of the lamps. Moreover, it has an ionization energy low enough to enable the so-called avalanche effect, which is a chain reaction underlying the electrical discharge.

Argon is the filler gas that is most common, and has an ionization energy of 15.8 eV, whereas the lowest activated metastable state is at 11.6 eV. If collision takes place, the energy of this metastable state can be lost, but if there is collision with a mercury atom, ionization of mercury can take place, followed by the emission of light. Therefore, the primary role of the filling gases is not only to support the starting of the discharge, but also to promote the starting activation-ionization of the mercury. This process can be simplified by the subsequent equations (Masschelein 2002)

$$e + \mathrm{Ar} = \mathrm{Ar}^*(+e)$$

$$\mathrm{Ar}^*(+e) + \mathrm{Hg} = \mathrm{Hg}^+ + e + \mathrm{Ar}$$

Mercury lamps can operate at low and medium pressures.

Amalgam lamp technology has recently been developed and incorporated into disinfection applications. A subdivision of the low-pressure mercury lamps can be made into soft glass and fused quartz, while amalgam lamps can be made into fused-quartz lamps. Among the amalgam lamps, only low-pressure lamps exist. Figure 2.2

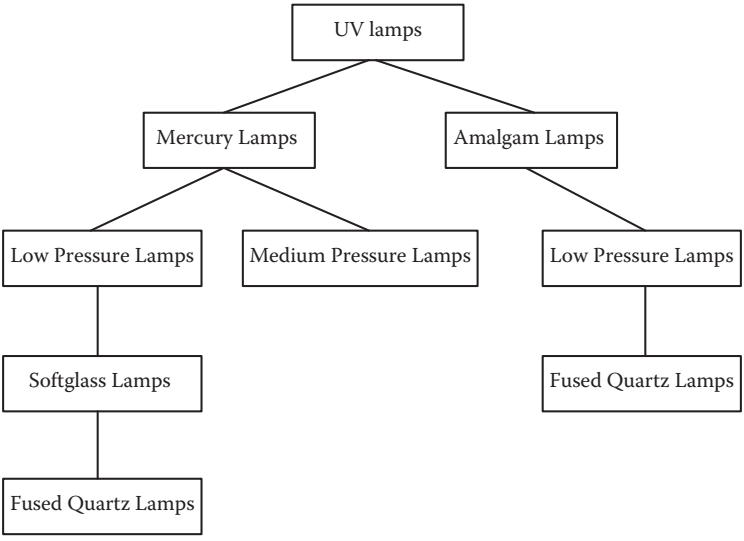

FIGURE 2.2 Overview of commercially available UV lamps.

presents an overview of the different UV-light sources currently available on the market.

2.2.1 Low-Pressure Mercury Lamp Technologies

Low-pressure mercury (LPM) lamps for the generation of UV light are operated at nominal total gas pressures in the range of 10^2 to 10^3 Pa or 90.01 to 0.001 mbar. The carrier gas is in excess in a proportion of 10 to 100. This corresponds to the vapor pressure of liquid mercury at an optimum temperature of 40°C at the lamp wall. The reaction by which a photon is emitted corresponds to

$$\text{Hg}^* \text{ (excited state)} \rightarrow \text{Hg (ground state)} + h\nu$$

or

$$\text{Hg}^* \text{ (excited state)} \rightarrow \text{Hg}^* \text{ (less excited state)} + h\nu$$

The emission of a photon by an atom in an excited electronic state is reversible; this means that, before escaping from the plasma contained in the lamp enclosure, the emitted photons can be reabsorbed by another mercury atom.

LPM lamps are usually cylindrical. They are currently available in lamp diameter ranges from 0.9 to 4 cm and lengths of 10 to 160 cm. According to Masschelein (2002), the electrical field along the length of a tubular discharge lamp is not uniform, and several zones can be distinguished, as shown in Figure 2.3. The Faraday dark zone, located at the cathode side of the lamp, is about 1 cm in length. The dark space remains constant, independent of the length of the lamp. Therefore, the useful emission length of a short lamp is proportionally shorter than for a long lamp. However, Masschelein does not talk about the reasons or possible solutions to avoid this disadvantage linked to UV lamps.

In practice, LPM lamps are powered by alternating current, with the cathode and anode sides constantly alternating, along with the Faraday dark space. The effect of voltage fluctuations in the power supply has a direct influence on the UV output yield of LPM lamps. The temperature outside the lamp is another factor that has a direct effect on the output yield. Temperature itself has a marginal effect; however, it directly influences the equilibrium vapor pressure of the mercury along the inner wall of the lamp. If it is too low, the emission yield drops due to partial condensation

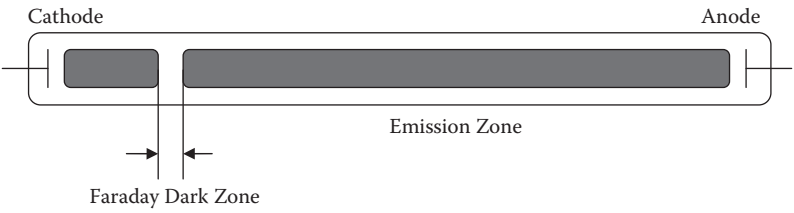

FIGURE 2.3 Different zones of a UV lamp.

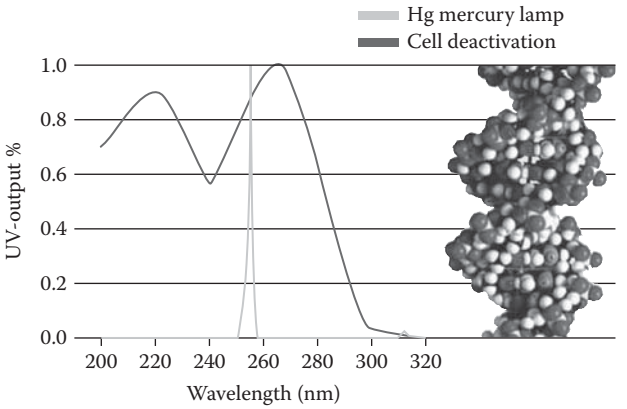

FIGURE 2.4 Cell deactivation, depending on the exposed wavelength of UV light and operated wavelength of mercury lamp. (Source: Heraeus Noblelight, http://www.heraeus-noblelight.com/fileadmin/user_upload/PDF/disinfection/Lampe_eng.pdf.)

of the Hg vapor as it is cooled. At high temperatures, the Hg pressure is increased, as long as there is an excess of liquid Hg. Therefore, the optimum pressure of mercury is about 1 Pa, and the optimum temperature is around 40°C. To minimize the cooling effect of liquids when treated, especially in the food industry, the lamp is mounted within a quartz tube, through which air is circulating freely.

The aging of LPM lamps also influences the emitted intensity. An initial drop in emission yield occurs during the first 100 to 200 h of operation. However, after this period of time, the emission is stable for months. Aging is caused by two factors: solarization of the lamp wall material and blackening due to deposits of sputtered oxides from the electrodes.

The typical LPM lamp emission spectrum is illustrated in Figure 2.4. The emission is concentrated at a limited number of well-defined lines, and the source is called *monochromatic*. The resonance lines at 253.7 and 185 nm are by far the most important. The 253.7-nm line represents around 85% of the total UV intensity emitted and is directly related to the germicidal effect. The wavelength of 253.7 nm is most efficient in terms of germicidal effect, since photons are most efficiently absorbed by the DNA of microorganisms at this specific wavelength. Light with a wavelength below 230 nm is most effective for the dissociation of chemical compounds. At wavelengths below 200 nm, such as 185 nm, ozone is produced from oxygen, and organic compounds can be oxidized. For the food industry, the production of ozone is not desired, not only because it has no germicidal effect on microorganisms, but because it can also cause side reactions with organic components in the food. Figure 2.4 shows the cell deactivation of *Escherichia coli* bacteria (according to DIN 5031-10) at different wavelengths in contrast to the effective wavelength of a low-pressure lamp.

If natural quartz is used as the glass, approximately 5% of the electrical input power is converted into 185-nm UV radiation. Synthetic quartz offers approximately 50% more transmission of UV light at a wavelength of 185 nm than natural quartz

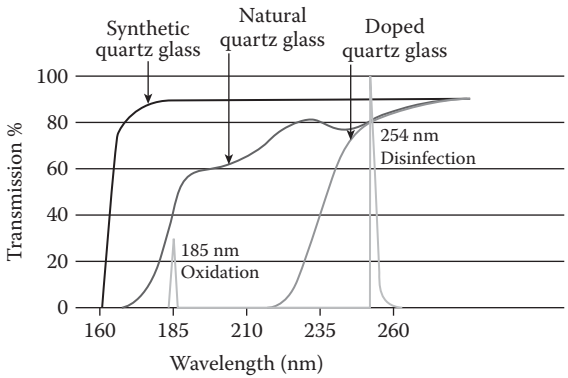

FIGURE 2.5 Comparison of different transmissions due to different glasses for UV lamps. (Source: Heraeus Noblelight, http://www.heraeus-noblelight.com/fileadmin/user_upload/PDF/disinfection/Lampe_eng.pdf.)

and, therefore, approximately 9% of the input power is converted into 185-nm UV radiation. If the 185-nm wavelength is unnecessary, for example if no oxidation is required, special lamps using doped quartz can be used to completely filter out this wavelength. The special combinations of natural quartz glass with doped quartz, called "combiquartz mercury low-pressure lamps," are available on the market. Their bodies are assembled from two different quartz glass materials that make it possible to emit radiation at wavelengths of 185 and 254 nm. To control the amount of ozone produced, the ratio of the two quartz materials can be adjusted. Figure 2.5 shows the transmission for different kinds of glasses used in LPM lamps.

The specific electrical loading in the glow zone, expressed in watts per centimeter, typically is between 0.4 and 0.6 W_e/cm. The linear total UV output of the discharge length for lamps appropriate for use in disinfection is in the range of 0.2 to 0.3 W_{UV}/cm. This means that the UV efficiency generally designed by total W_{UV} output vs. W_e input is between 0.25 and 0.45. The energy losses are mainly in the form of heat. For LPM lamps, the UV-C proportion of the UV-light wavelengths emitted are in the range of 80% to 90% of the total UV power emitted. Approximately 40% of the electrical power is converted into UVC radiation at 254 nm.

2.2.2 Medium-Pressure Mercury Lamps

Medium-pressure mercury (MPM) lamps are operated at a total gas pressure of approximately 10^4 to 10^6 Pa. Compared with the low-pressure mercury lamps, the coolest possible temperature of the medium-pressure lamp is about 400°C, which can go up to 600°C and even 800°C in a stable operation. Therefore, it is absolutely necessary to use an open (or even vented) quartz enclosure of the lamp to avoid direct contact of the surface of the lamp with the treated fluid. MPM lamps operate in the potential gradient range of 5–30 W/cm. The emission of medium-pressure mercury lamps is polychromatic. The spectrum covers wavelengths from about 250 nm up to almost 600 nm, which results from a series of emissions in the UV region and in the

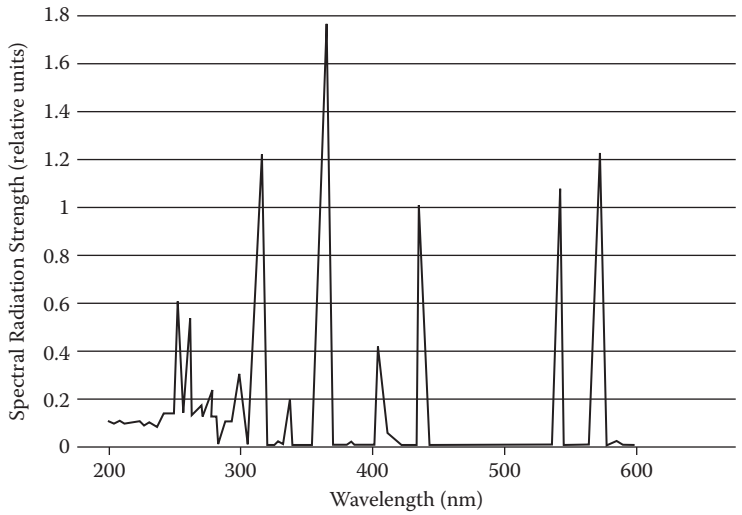

FIGURE 2.6 Typical emission spectrum of a MPM UV lamp. (Source: Heraeus Noblelight, http://www.heraeus-noblelight.com/fileadmin/user_upload/PDF/disinfection/Lampe_eng.pdf.)

visible range as well. Hence, such lamps are not considered to be useful for targeted germicidal treatment; however, their strong UV-radiation flux results in high penetration depth. Figure 2.6 shows the typical emission spectrum of a MPM UV lamp.

By varying the gas filling, doping, and the quartz material, the spectrum as well as the radiation flux of the UV lamps can be varied and matched to suit specific applications, especially for oxidation or photochemistry. Other than LPM lamps, MPM lamps are not affected by the temperature, as they already operate at high temperatures. The UV output is approximately directly proportional to the input voltage. At an input voltage of 160 V, the lamp reaches only about 30% of its maximum possible UV yield. At 250 V, close to 100% of the possible UV yield is reached (Masschelein 2002). If the goal is disinfection and not photochemical oxidation, and if the operated temperature is not a problem, the entire range under 220 nm can be cut off by the material of the lamp enclosure, as discussed previously.

Aging of the MPM lamp is a factor that affects the emission of the MPM lamp in a similar fashion as LPM lamps. After 4000 hours of operation, at least 80% of the emission of germicidal wavelengths is maintained. Aging affects not only the emission, but the emission spectrum is modified as well.

2.2.3 Low-Pressure Mercury Lamp for Producing Ozone

Ozone production by means of an LPM lamp discharge at 185 nm is a well-known technology, but according to a report by Voronov (2007), it is limited by economical and technical factors, most importantly the efficiency and lifetime of LPM lamps. A big advantage lies in the emission spectrum of the mercury discharge, since it emits with high efficiency at two resonance lines: the wavelengths of 254 and 185 nm.

The photons with a wavelength of 185 nm are responsible for ozone production, and the combination of both wavelengths is a very effective means for photochemical air treatment. The ratio of light at 185 nm to light at 254 nm varies from 12% to 34%, depending on the operating current, wall temperature, and inert gas. Heraeus Noblelight recently developed a new coating that increases efficiency and lifetime of the UV sources up to 10,000 h. It was reported that every VUV-watt at 185 nm can produce 0.54 g of ozone per hour. This means that a 200-W lamp will generate approximately 10 g of ozone per hour, with an ozone production efficiency of ≈50 g/kW×h.

The model for calculation of the ozone concentration generated by LPM lamps in air flow was suggested in Voronov's report based on the lamp power, lamp efficiency at 185 and 254 nm, distance from the wall, and velocity of air flow.

2.3 AMALGAM UV LAMPS

A concern over the impact of mercury release from lamps into the plant environment has encouraged research of mercury-free lamps. Instead of mercury, amalgam can be used in low-pressure amalgam (LPA) lamps, resulting in an extremely long life while ensuring high-power outlet. Up to 10 times the UV power density of an LPM lamp can be achieved, and they can be used at higher ambient temperatures of up to 90°C. The UV intensity of LPA lamps is insensitive to temperature fluctuations. The amalgam lamps do not show the transmission loss of quartz glass associated with LPM lamps, and they therefore produce a constant disinfection action over the total operating life of the lamp. Compared with LPM lamps with a UV-C output of approximately 40%, up to 90% of the UV-C output power is delivered with the use of amalgam lamps. Due to their high efficiency, long operating life, and low operating costs, amalgam lamps represent an alternative to MPM lamps and can be specifically used in the food industry, as very little heat is generated. Depending on the type of quartz used, ozone-free or ozone-generating lamps are available. Table 2.1 shows

TABLE 2.1
Differentiation of UV Lamps with Soft Glass and Fused Quartz

Characteristic	Soft Glass	Fused Quartz Mercury	Fused Quartz Amalgam
Available UV spectrum (nm)	254	185 and 254	185 and 254
Wall temperature (°C)	30–50	30–50	90–120
Electrical power (W)	5–80	5–80	40–500
Current (A)	0.2–0.5	0.3–0.5	1.2–5.0
Specific electric power (W/cm)	0.2–0.5	0.3–0.5	1.0–3.0
Specific UVC-flux (mW/cm)	<175	<200	<1000
UVC efficiency at 254 nm (%)	25–35	30–40	35
Influence of ambient temp.	High	High	Low

Source: Schalk 2005.

an operating differentiation of characteristics of soft glass (mercury), fused quartz (mercury), and fused quartz (amalgam).

2.3.1 UV-Lamp Breakage

There are health concerns regarding the potential of mercury exposure due to lamp sleeve breakage. As discussed earlier, all UV lamps contain some amount of mercury. Breakage is a concern due to potential for mercury release. LPM and MPM lamps generally contain elemental mercury, while LPHO lamps generally contain a mercury amalgam. The mercury contained within a UV lamp is isolated from exposure by a lamp envelope and surrounding lamp sleeve. For the mercury to be released, both the lamp and lamp sleeve must break. Breakage can occur when lamps are in operation as well as during maintenance. The mercury content in a single UV lamp used for water treatment typically ranges from 0.005 to 0.4 g (5–400 mg). LP lamps have less mercury (5–50 mg/lamp) compared with LPHO (26–150 mg/lamp) and MP lamps (200–400 mg/lamp). Depending on the state of mercury (gas, solid, or liquid), when a lamp breaks can be important in determining potential health risks. Mercury in the vapor phase may be released as very fine particles, which may readily dissolve in water, as opposed to solid or liquid mercury, which will tend to settle. There is very little information on determining the amount of mercury released relative to the amount of mercury in the lamp prior to breakage. Clarke (2006) indicated that the breakage of a UV lamp containing 150 mg mercury in a 50-L batch reactor resulted in a concentration of 2.5 μg/L of mercury in the reactor. However, it was not reported whether all 150 mg of mercury was recovered.

Little information exists regarding the fate of mercury released to the water or to a liquid food product as a result of UV-lamp breakage. The EPA established a maximum contaminant level (MCL) for mercury at 0.002 mg/L. The EPA has found mercury to potentially cause kidney damage from short-term exposures at levels above the 0.002 mg/L MCL (EPA 1995).

2.4 SPECIAL LAMP TECHNOLOGIES

Temperature sensitivity is another area in which special lamp technologies hold promise. The output and efficiency of a mercury lamp is dependent on the mercury vapor, which is a function of lamp temperature. Several alternative UV-source types, such as excimer lamps and pulsed-UV technologies, have been developed. These lamps show great promise for instant UV emission, are independent of temperature effects, and can be applied to foods. However, the efficacy and specific characteristics of these UV-light sources that are used today for water treatment have not been evaluated for food applications, and the results of only a few studies have been reported in the literature.

2.4.1 Excimer Lamps

Modern excimer lamps, or excilamps, are based on the formation of rare gas (Rg_2^*) or halogen excimers (X_2^*) or of rare gas–halide exciplexes (RgX^*) and the efficient

TABLE 2.2
Matrix of Excimers (X_2*, Rg_2*) and Exciplexes (RgX*) Obtained from Halogens and Rare Gases and Their Emission Maxima (nm)

			Rare Gas (Rg)				
			He	**Ne**	**Ar**	**Kr**	**Xe**
			74	84	**126**	**146**	**172**
Halogen (X_2)	F	157	…	108	193	248	354
	Cl	259	…	…	175	**222**	**308**
	Br	289	…	…	165	207	282
	I	342	…	…	…	190	253

Source: Oppenlander and Sosnin 2005.

Note: Commercially available excilamps are in boldface.

fluorescence of these molecules in different types of discharges. Excimer is an abbreviation of *excited dimer.* This is essentially a pair of atoms with one excited gas atom, which are normally not bonded in the ground state. (Xe + Xe* = Xe_2* [excimer]). Noble gases and noble gas/halogen mixtures can form excimers. The excimer state is very short lived. Upon decomposition of the excimers, a UV photon is emitted in a very tight, quasimonochromatic spectral range. Depending on the choice of gas, different narrow-band UV spectra can be produced, predominantly in a single spectral line. Today, there are several different excimer combinations that can produce UV radiation in the wavelength range between 120 and 380 nm (Table 2.2). The spectrum has no infrared component, and emitters provide the pure UV spectrum.

The gas discharge is created by a high-frequency electromagnetic field. Electrodes are therefore not needed in the gas discharge. These are so-called electrodeless lamps. High-power excimer emitters are operated with water cooling to prevent heating of the emitter. As such, the output of these lamps is "tunable" to the wavelength of interest.

Compared with conventional UV emitters, excimer emitters offer properties that improve and expand the use of UV radiation in industry. The monochromatic spectrum and the ability to select specific wavelengths allow photoprocesses to be carried out in a much more focused manner. In addition, there is no unwanted heating effect, as excimer UV emitters produce no infrared radiation in their spectrum. Excimers exhibit a very long lifetime (in the range of several thousand hours). Further, the use of dielectric barrier discharge or capacitive discharge gives a freedom with respect to the geometric design of excilamps, which allows for the first-time adjustment of the lamp's geometry to the optimum conditions of a desired process. The intrinsic efficiency of rare-gas excimer fluorescence emission was calculated to be in the range of 45% to 80%, but commercial XeCl*, KrCl*, XeBr*, and KrBr* lamps reach only radiant efficiencies of 5% to 18%.

There are no reports available, except for the study made by Warriner et al. (2002), of applications of excimer lamp technology for foods. UV excimer lamps can produce monochromatic output that can be tuned to the wavelength of interest

by the combination with gases. Excimer lamps also have an advantage of extremely low output and are able to operate at much lower surface temperatures. Thus they can provide an advantage by avoiding fouling behavior by liquid foods. Warriner et al. (2002) demonstrated that UV excimer light was effectively used for sterilization of packaging carton surfaces.

Recently, an excimer technology has been presented by Triton Thalassic Technologies (T^3I) (Ridgefield, CT). T^3I claimed that they had developed a new class of light sources that produce discretely tuned light, at significant powers. These sources allow for the controlled application of radiant energy (intensity, wavelength, power, and geometry) necessary to convert fundamental photochemical and photobiological processes into commercial tools.

T^3I's position is that the processing of delicate fluids and surfaces is best performed using monochromatic light delivered to the treatment volume (or surface) as uniformly as possible. Pulsed lasers are monochromatic but are not suited to treat large areas and produce damaging peak powers. Standard high-power lamps produce a range of wavelengths that both damage and heat the target. Further, flash lamps combine several undesirable characteristics (broadband and pulsed), while T^3I light sources operate in the optimal parameter space and are monochromatic and continuous.

T^3I has developed excimer lamps optimized for immersion that have been operated under field conditions at temperatures from 30°F to 170°F. This allows even high-power excimer lamps to operate at the same temperature as the fluid to be treated. T^3I's new class of dielectric-barrier-driven excimer sources are able to operate in high-mineral waters without fouling, since the lamp surface temperature is not significantly higher than the water. The systems emit light over a large active area and can be configured to operate at reduced temperatures. The near-monochromatic output of these sources can be tuned to produce high spectral irradiance (watts/nm) within peaks of the process action spectra to maximize the germicidal effectiveness (or other desired process) as a function of fluid quality, reactor design, and the required biological objective. The range of available geometries (including coaxial sources radiating either inwardly or outwardly, and planar sources emitting from one or both sides) and the capability to independently adjust irradiance and total power allow for more efficient reactor designs.

T^3I's current excimer sources produce 90% of their output within a 10-nm band that can be discretely adjusted across the VUV, UV-A, UV-B, and UV-C by changing the rare and/or halogen gases used. Efficiencies vary with gas mix and geometry from 10% to >30%, with demonstrated input powers from <1 W to >10 kW. One lamp, which has been manufactured for the last eight years, produces >1000 W of germicidal UV, with demonstrated lifetimes >10,000 hours. T^3I has a range of patents protecting this work that are granted, pending, and in process. Current activities using these sources include pathogen control in complex fluids, directed chemical synthesis, and rapid modification of surface characteristics.

Heraeus Noblelight (Germany) offers two excimer versions: high-power excimer systems with water cooling and BlueLight Compact excimer systems without cooling. Emitters for wavelengths 172, 222, 282, and 308 nm are offered as standard irradiation units, with illuminated lengths of 300 and 600 mm. High-power excimer units are available in the power range of 450 W to 3 kW.

2.4.2 Broadband Pulsed Lamps

In this technology, alternating current is stored in a capacitor and energy is discharged through a high-speed switch to form a pulse of intense emission of light within about 100 μs. The emission is similar in wavelength composition to solar light. The pulsed UV devices can deliver high-intensity UV that can penetrate opaque liquids better than mercury lamps and provide enhanced treatment rates. This technology is claimed to be promising but not yet thoroughly established in the field.

A few studies recently reported an application of pulsed UV light for foods. A pulsed xenon UV-light treatment was applied to inactivate spores of *Aspergillus niger* in corn meal. However, low penetration power and excessive heat buildup inside the chamber was reported (Jun et al. 2003). Pulsed UV light was found to be effective in the inactivation of *Saccharomyces cerevisiae* (Sharma and Demirci 2003). In addition, the pulsed UV light was used to control microbial levels on fresh processed lettuce. Allende and Artes (2003) reported that pulsed UV light was effective in reducing the levels of psychrotrophic and coliform bacteria as well as yeast without adversely affecting the sensory quality of lettuce. Sharma and Demirci (2003) demonstrated that pulsed UV light holds promise for eliminating pathogens such as *E. coli* O157:H7 from alfalfa seeds.

Flash lamps are pulsed lamps in which a pulse occurs in a rare gas between two electrodes enclosed inside an envelope. Flash lamps are commercially available, but have not been commercially successful for water treatment because of their relatively low efficiency and short lifetime. Initial research (Schaefer et al. 2007) shows, however, that flash lamps have much higher intensity than mercury lamps and enhance the inactivation rate of bacteria (no data are available for virus inactivation with flash lamps).

The Surface Discharge (SD) lamp developed by Phoenix Science & Technology Inc. (Chelmsford, MA) is a new pulsed lamp that overcomes the disadvantages of flash lamps. According to Schaefer et al. (2007), a high-power electrical pulse is discharged along the surface of a dielectric tube and generates a uniform plasma sheet along the substrate tube, producing an intense light pulse. The intensity and efficiency of the pulsed SD lamp is much greater than that of traditional mercury low- and medium-pressure lamps and commercially available pulsed flash lamps. The discharge is in a rare gas (xenon or krypton) that is nontoxic. The envelope serves only as a container for the rare gas and plays no role in the discharge (Figure 2.7). As a result, SD light pulses can have a much higher intensity than flash lamps (Figure 2.8). Also, tests show that the SD inactivates viruses with less than half the dose of MPM lamps and less than one-sixth the dose of LPM lamps. The SD lamp is currently under development by PS&T (with a grant from the National Science Foundation), with a product planned by 2009.

The sparker is another pulsed source, but it is different from lamps in that the pulsed discharge is in the liquid, which results in extremely high intensity. In addition, the sparker generates a strong pressure pulse that can lyse microorganisms. Thus, although the sparker's UV efficiency is less than the other sources, it is the only source with enhanced treatment rates from the pressure pulse. The limited research on water treatment with sparkers (Schaefer et al. 2007) showed large increases in disinfection rates. Sparkers are the newest water-treatment technology listed in

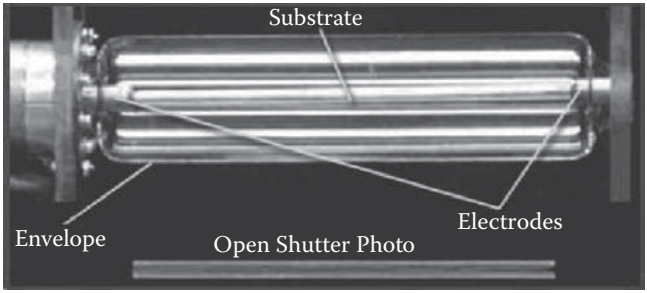

Pulsed electric discharge generates "light emitting" plasma along surface of a substrate

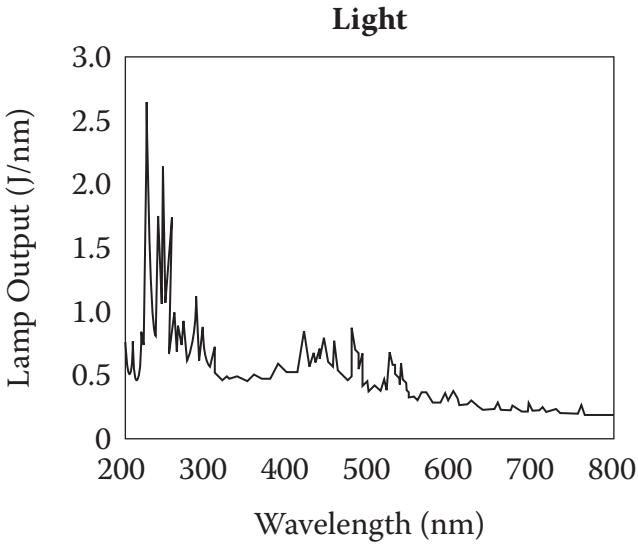

FIGURE 2.7 Surface-discharge lamps generate pulsed electric discharges along a dielectric between electrodes producing intense light pulses. (Source: Phoenix Science & Technology, http://www.phoenixsandt.com/sdl.htm.)

Table 2.3, but they have the potential for fast commercialization because of concurrent development for the U.S. Navy to protect its submarines and for sonar applications. Sparkers are also potentially low cost. In a sparker, a high-voltage, high-power electrical pulse discharges between electrodes in a liquid, as shown conceptually in Figure 2.9. The discharge creates a hot vapor channel between the electrodes that emits a bright flash of light, including significant output in the UV. The overpressure in the hot vapor channel produces a strong pressure wave. The high-pressure vaporized water cavity expands to a maximum diameter and then contracts and collapses, producing another light and pressure pulse (Figure 2.10). The vapor cavity continues to oscillate until its energy dissipates.

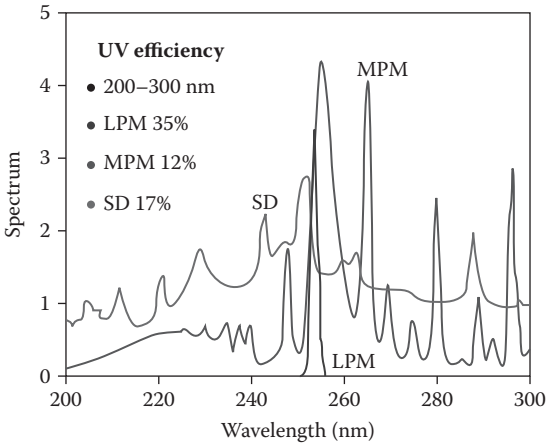

FIGURE 2.8 Spectrum and efficiency comparison of LPM and MPM lamps with SD lamp.

SD lamps and sparker sources are clamed to be effective mercury-free technologies for water treatment. SD lamps have higher UV efficiency than medium-pressure mercury lamps as well as increased treatment rates from the high-intensity pulsing and short-wavelength spectrum. Note that all the pulsed sources are instant-on and insensitive to the ambient temperature, in contrast to mercury lamps.

2.4.3 Microwave UV Lamps

A new UV-lamp technology that eliminates the need for electrodes is the microwave-powered electrodeless mercury UV lamp (Little 2007; Meier et al. 2007). Instead of

TABLE 2.3
Efficiency Comparison for Mercury Lamps, Flash Lamp, Surface Discharge, and Sparker

Lamp	UV Efficiency (%)	UV Intensity (W/cm^2)	Dose for Virus Inactivation (mJ/cm^2)	Pressure Pulse (psi)
LPM	38	0.01	150	None
MPM	12	12	48	None
Flash lamp	9	600	n.d.	None
Surface discharge [a]	17	30,000	22	None
Sparker [a]	7	100,000	n.d.	100

Source: Phoenix Science & Technology; http://www.phoenixsandt.com/sdl.htm

Note: n.d. = no data available.

[a] Patented by and being commercialized by Phoenix Science &Technology, Inc.

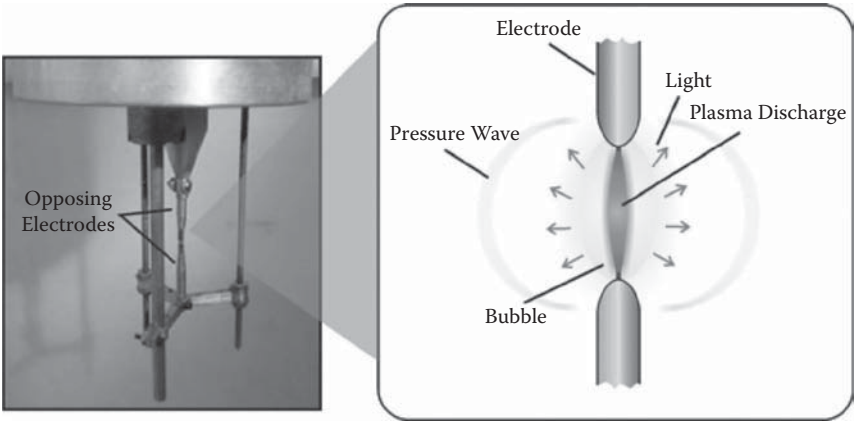

FIGURE 2.9 Conceptual design of the sparker. (Source: Phoenix Science & Technology, http://www.phoenixsandt.com/sparkers.htm.)

utilizing electrodes, microwave energy is generated by a magnetron and directed through a waveguide into the quartz lamp containing the gas filling. The directed microwave energy excites the argon atoms, which in turn excite the mercury atoms to produce radiation as they return from excited states to states of lower energy, as is the case with other mercury lamps. Electrodeless lamps operate at similar pressures and temperatures as a typical LPM lamp. There are two types of commercially available microwave-powered UV water-disinfection systems for drinking water and for small flows of wastewater that are using microwave lamps. The microwave UV-lamps assembly is shown in Figure 2.11.

The advantages of using microwave-powered lamps over conventional lamps with electrodes are as follows: They warm up quickly; the primary deterioration process associated with UV lamps is eliminated; and lamp life is approximately three times that of electroded lamps. Since there are no electrical connections in the water and there are no electrodes used, there is no electrical connection to fail, and the corrosion issue is also prevented. Moreover, lamps can be switched on and off whenever desired without deterioration. This technology has not been used in the food industry yet. However, the above advantages need to be taken into consideration by food-industry specialists.

2.4.4 UV-Light-Emitting Diodes

Recent advances have produced UV-light-emitting diodes (UV LEDs) in the range of 280–340 nm (Bettles et al. 2007). These UV LEDs are compact, rugged, and efficient, enabling new applications in existing markets as well as opening potentially new markets. A LED is a semiconductor device that emits lights when carriers of different polarities (electron and holes) combine, thereby generating a photon. The wavelength of the photon depends on the energy difference the carriers overcome in order to combine. The system for UV LED operating

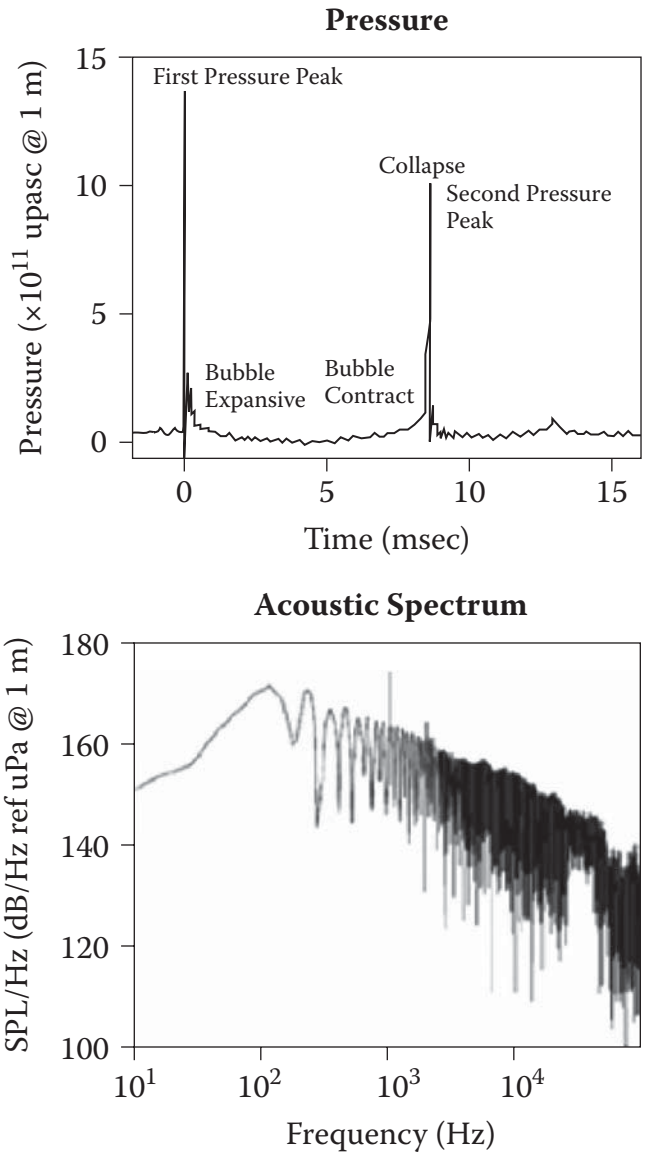

FIGURE 2.10 Sparkers generate pulsed electric discharges in water (or other liquid) between electrodes, producing pulsed sound (pressure) and light. (Source: Phoenix Science & Technology, http://www.phoenixsandt.com/sparkers.htm.)

between 210 and 365 nm is the one formed by aluminum nitride (AIN), gallium nitride (GaN), and intermediate alloys. Currently, UV LEDs are commercially available in research grade and in limited quantities, and their operational lifetime is on the order of 200 h.

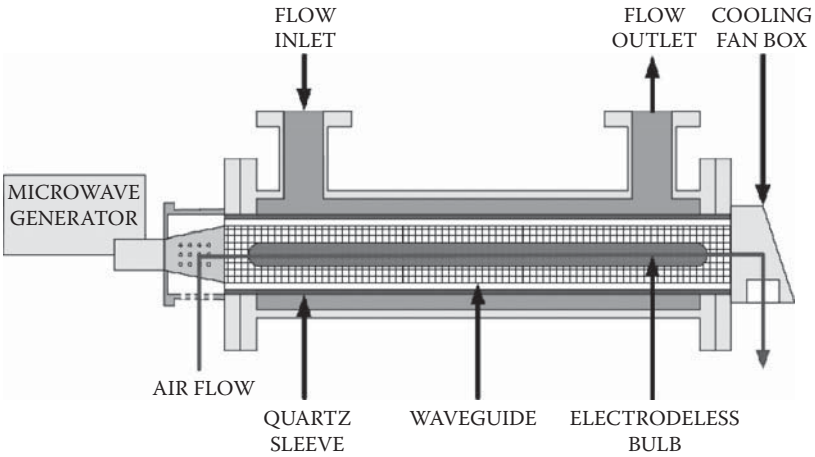

FIGURE 2.11 Cross section through the MicroDynamics™ microwave ultraviolet lamp. (Source: Severn Trent Services, http://www.severntrentservices.com/ultraviolet_disinfection/microdynamics_prod_350.aspx? PhotoID=1380.)

Compared with the visible-light LEDs, UV LEDS are in their initial stage of development because of the lack of an appropriate substrate. The application range is from analytical instrumentation to disinfection to homeland security. Among the newest security systems is a bioagent detection system. Rapid detection of an aerosol release in a critical building can enable timely implementation of protective measures to safeguard occupants and minimize the extent of contamination. It is very likely that, in the near future, many applications that today make use of mercury lamps will be carried out by UV LEDS. The other applications that have potential, such as portable purification systems, will also become a reality.

2.5 GUIDELINES FOR CHOICE OF LAMP TECHNOLOGY

Table 2.4 provides a summary of some of the basic characteristics of common UV sources that are in commercial use or under development. From this summary, it is evident that no single lamp technology represents the best source for all applications. However, situation-specific requirements may dictate a clear advantage for a given process technology.

Mercury-vapor lamps are highly developed and provide good efficiency, long life, and compact size for various applications. LPM lamps are easy to install and operate. They are readily available, with their emission spectrum well established and quantified, at comparatively low cost. MPM lamps have higher emission intensity in the UV-C range; however, the source is polychromatic. The lamp source operates at high temperatures and at higher electrical potential. The lamp materials and enclosures of MPM lamps also age faster than those of LPM lamps. Mercury lamps are the dominant sources for UV treatment. Special-technology lamps are promising due to instant start, robust packaging, and the elimination of mercury in the lamp.

TABLE 2.4
Summary of UV Sources and Their Basic Characteristics

UV Radiation Source	Electrical Efficiency (%)	UV Efficiency (%)	UV Intensity (W/cm^2)	Lamp Surface Temperature (°C)	Lifetime (months)	Output Spectrum
LPM	50	38	0.01	40	18–24	Monochromatic (253.7 nm)
MPM	15–30	12	600	400–1000	0.5	Polychromatic (200–300 nm)
Pulsed xenon	n.d.	n.d.	n.d.	n.d.	1	Polychromatic
Surface discharge [a]	15–20	17	30,000	n.d.	n.d.	Polychromatic
Excimer	10–35	10–40	n.d.	ambient	>6	Monochromatic tunable
Sparker [a]	n.d.	7	100,000	n.d.	n.d.	Polychromatic

Note: n.d. = no data available.

[a] Patented by and being commercialized by Phoenix Science &Technology, Inc.

Light sources such as pulsed lamps, excimer lamps, and UV-light-emitting diodes hold promise for future applications, but more research is needed to establish them for food applications.

REFERENCES

Allende, A., and F. Artes. 2003. Combined ultraviolet-C and modified atmosphere packaging treatments for reducing microbial growth of fresh processed lettuce. *Food Sci. Technol. (LWT)* 36: 779–786.

Bettles, T., S. Schujman, J. Smart, W. Liu, and L. Schowalter. 2007. UV-light emitting diodes: Their application and benefits. Paper presented at UV and Ozone World Congress, Los Angeles.

Clarke, S., and W. Bettin. 2006. Ultraviolet light disinfection in the use of individual water purification devices. Technical paper TIP #31-006-0206 15. Army Center for Health Promotion and Preventive Medicine. Aberdeen Proving Ground, MD.

EPA, Office of Water. 1995. National primary drinking water regulations contaminant fact sheets inorganic chemicals: Technical version. EPA 811-F-95-002-T. Washington, DC.

Jun, S., J. Iruddayyaaraj, A. Demirci, and D. Geiser. 2003. Pulsed UV-light treatment of corn meal for inactivation of *Aspergillus niger* spores. *Int. J. Food Sci. Technol.* 38: 883–888.

Little, R. 2007. An analysis of microwave generated UV devices, their track record and their potential. Paper presented at UV and Ozone World Congress, Los Angeles.

Masschelein, W. J. 2002. *Ultraviolet light in water and wastewater sanitation*. Ed. R. G. Rice. Boca Raton, FL: Lewis Publishers.

Meier, J., A. Slater, K. Bourgeous, and A. Salveson. 2007. Microwave UV: The future of UV disinfection. Paper presented at UV and Ozone World Congress, Los Angeles.

Oppenlander, T., and E. Sosnin. 2005. Mercury free vacuum-(VUV) and UV excilamps: Lamps of the future? *IUVA News* 7 (4): 16–20.

Schaefer, R., M. Grapperhaus, and K. Linden. 2007. Status report on the development and use of pulsed UV technologies for treating water. Paper presented at UV and Ozone World Congress, Los Angeles.

Schalk, S. 2005. Differentiation of soft glass (mercury) and two fused quartzes (mercury and amalgam). Paper presented at Third International Congress on Ultraviolet Technologies, Whistler, BC, Canada.

Sharma, R. R., and A. Demirci. 2003. Inactivation of *Escherichia coli* O157:H7 on inoculated alfalfa seeds with pulsed ultraviolet light and response surface modeling. *J. Food Sci*. 68: 1448–1453.

Takeshita K., Shibato, J., Sameshima, T. 2003. Damage of yeast cells induced by pulsed light irradiation. *Int. J. Food Microbiol.*, 85:151–158.

Voronov, A. 2007. New generation of low pressure mercury lamps for producing ozone. Paper presented at UV and Ozone World Congress, Los Angeles.

Warriner, K., J. Kolstad, J. Rumsby, and W. Waites. 2002. Carton sterilization by UV-C excimer laser light: Recovery of *Bacillus subtilis* spores on vegetable extracts and food simulation matrices. *J. Appl. Microbiol*. 92: 1051–1057.

3 Characterization of Foods in Relation to UV Treatment

The transmission of UV light through fresh juices and other liquid foods is small due to their high optical density. The presence of solids, organic solutes, and compounds leads to light scattering and absorbance, both of which strongly attenuate the effects of UV light. Moreover, suspended solids can also provide sites for the aggregation of bacteria to particle surfaces. As the UV absorbance of a liquid medium increases, the penetration and intensity of UV light delivered to the product in the UV reactor decreases, thereby reducing the antimicrobial effectiveness of the delivered UV dose.

The optical properties of liquid food products, along with the design of the UV reactor, are the major factors affecting UV inactivation of microbes in liquid foods with high absorptive properties. Physical and chemical properties that influence the effectiveness of UV treatment need to be properly assessed. This chapter discusses the characterization of UV-light absorbance in selected fresh juices that are currently processed by using UV light. The chapter also discusses the impact of UV absorbance and light scattering on the performance of UV reactors.

3.1 TERMS AND DEFINITIONS

The UV absorbance of a liquid food strongly influences the efficiency of the delivered UV dose. The Lambert–Beers law (equation 3.1) is the linear relationship between: absorbance (A); the concentration of an absorber of electromagnetic radiation (c); the extinction coefficient (ε), i.e., the molar absorptivity of the absorbing species (L/mol/cm), which is a measure of the amount of light absorbed per unit concentration absorbance or optical density; and the path length of light (d)

$$A = \varepsilon \times c \times d \tag{3.1}$$

If multiple species that absorb light at a given wavelength are present in a sample, the total absorbance at that wavelength is the sum due to all absorbers (equation 3.2)

$$A = (\varepsilon_1 \times c_1 \times d) + (\varepsilon_2 \times c_2 \times d) + \ldots \tag{3.2}$$

where the subscripts refer to the molar absorptivity and concentration of the different absorbing species that are present.

The liquid itself and the concentration of the suspended units can be transparent if $A << 1$, opaque if $A >> 2$, or semitransparent if $1 < A < 2$ for anything in between these extremes. In a majority of cases, liquid foods will absorb UV radiation. For

example, fresh juices can be considered as a case of semitransparent or opaque liquids if the juice contains suspended solids.

The *absorption coefficient* (α) base e (α_e) or base 10 (α_{10}) is also used in the calculations and is defined as the absorbance divided by the path length (m^{-1}) or (cm^{-1}) (equation 3.3).

$$\alpha_e = 2.303A_{254} \tag{3.3}$$

Experimental measurements are usually made in terms of *transmittance* of a substance (T), which is defined as the ratio of the transmitted to the incident light irradiance (equation 3.4).

$$T = I_1/I_0 \tag{3.4}$$

where I_1 is the irradiance of light after it passes through the sample and I_0 is the incident light irradiance. The relation between A and T is expressed by equation 3.5.

$$A = -\log(T) = -\log(I_1/I_0) \tag{3.5}$$

From the Beer–Lambert Law, the percent transmittance in a 10-mm path length (% T_{10}) is related to absorption coefficient α by equation (3.6).

$$\%T_{10} = 100 \times 10^{-\alpha_{10}d} \tag{3.6}$$

where $d = 1$ cm and α_{10} is in cm^{-1}.

The UV transmittance (UVT) is affected by absorption and scattering of light by the substance as well as the reflection at the interfaces. UVT directly affects dose delivery and, subsequently, inactivation capability. Decreased UVT decreases UV intensity delivered to the microbe. As turbidity increases, UVT decreases, UV absorbance increases, and UV intensity decreases.

Penetration depth (d) is the depth (cm) where the fluence rate drops by a specified percentage of its value at the quartz sleeve, for example, 95% or 99%.

It should be pointed out that UV absorbance and transmittance at 254 nm are important design parameters for UV reactors containing low-pressure mercury (LPM) or low-pressure, high-output mercury (LPHO) lamps. However, for broadband UV lamps, such as medium-pressure or pulsed UV mercury lamps, it is important to measure the full scan of absorbance or transmittance in the germicidal region from 200 to 300 nm. In addition, the molar absorption coefficient and its spectra should be collected for a variety of compounds.

3.2 ANALYTICAL MEASUREMENTS

The absorbance measurement techniques that were reported include direct spectrophotometric measurement of absorbance at 254 nm using cuvettes and an integrating sphere. Due to the low light transmittance of the samples, Koutchma et al. (2007, 2006, 2004) and Murakami et al. (2006) used matched demountable fused-quartz cuvettes with light path lengths of 0.1, 0.2, 0.5, and 1.0 mm. The absorption

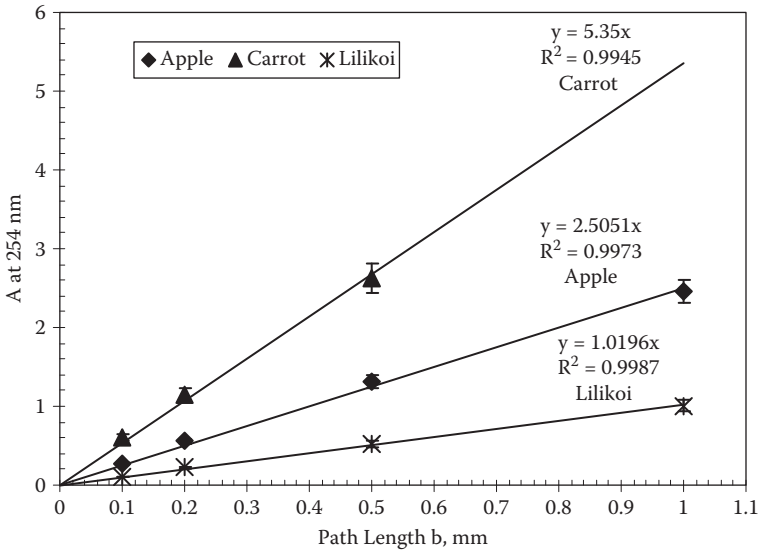

FIGURE 3.1 Measurement of absorption coefficient of fresh fruit juices. (From Koutchma et al. 2007. With permission.)

coefficient was determined as a slope of the linear plot of the absorbance versus light path length as shown in Figure 3.1 (Murakami et al. 2006).

$$A = a \times b \tag{3.7}$$

A similar approach was used by Forney et al. (2004). Oteiza et al. (2005) diluted fruit juices in sterile water first, and then the measurements were made using standard 1-cm light path cuvettes. The molar absorptivity coefficient was obtained as a regression curve slope by plotting absorbance versus sample concentration.

For the samples with suspended solids, the direct-measurement technique is controversial, since suspended particles can scatter light out of the detector, resulting in a high value of measured absorbance even though the light was not absorbed by the sample. The simplest and most popular approach, called *filtered transmittance*, is to filter the sample through a membrane filter and use the absorbance of the filtrate as the absorbance of the liquid medium. The latter approach provides a true measure of the liquid absorptivity but underestimates absorptivity of the bulk solution with particles. Standard spectrophotometric measurement of the UV transmittance of the unfiltered sample, called the *unfiltered transmittance*, provides an overestimate of the absorbance of the bulk liquid. The absorbance of the sample with suspended particles is also called the *apparent absorption*. To compensate for this error, Linden and Darby (1998) used integrating-sphere spectroscopy to measure the absorbance of water with particulates.

The use of the apparent absorption coefficient values may result in failure to accurately predict inactivation rates in solutions containing particles, which can be partially explained by light scattering, as reported by Koutchma et al. (2004).

Filtering the apple cider that was used in this study reduced the turbidity from 1420 to 2.5 NTU (nephelometric turbidity units) and the measured absorption coefficient from 21 to 7.0 cm^{-1}. When the absorption coefficient of the filtered cider (7.0 cm^{-1}) was used in calculations of the inactivation rates of tested bacteria (*Escherichia coli* K12) instead of the value of the unfiltered cider (21 cm^{-1}), it was reported that the predicted rate was not significantly different from the measured rate of bacterial destruction in the original apple cider.

3.3 ABSORPTIVE AND PHYSICOCHEMICAL PROPERTIES OF LIQUID FOODS

The effectiveness of UV treatments has to be optimized for applications in diverse types of liquid foods. In addition, a quantitative understanding of UV radiation dose is needed in relation to (a) the inactivation of pathogens in solutions with high absorptive properties and (b) the interference from particulates and dissolved materials. Product composition, solids content, color, and the overall chemistry of the food product have a major impact on both the absorption properties and the effectiveness of UV inactivation.

It is known that the absorption coefficient of pure distilled water is close to zero. Natural organic matter, iron, nitrate, and manganese absorb UV light and will increase the absorption coefficient of a water sample (AWWA 1999). Absorption coefficients in drinking water would be expected to be in the range of 0.01–0.2 cm^{-1}. According to EPA (1995), water with a Napierian absorption coefficient of 0.125 cm^{-1} would be considered of fair water quality. Bolton et al. (2001) studied solutions of various possible absorbers in drinking waters. Of the compounds studied, only ferric ion, ferrous ion, hydrogen peroxide, hypochlorite ion, permanganate ion, ozone, and sulfite ion absorbed significantly in the 200–300-nm region. A comparison of absorption coefficients of selected liquid foods, shown in Figure 3.2, indicates that the absorbance of apple juice/cider, orange juice, and liquid sugars is significantly higher than that for water.

3.3.1 Apple Cider

Fruit and vegetable products, including apple cider, have been identified as vehicles for infection caused by enterohemorrhagic *E. coli* (Centers for Disease Control and Prevention 1996; Harrington and Hills 1968). Apple cider was implicated in a disease outbreak caused by *E. coli* O157:H7 in the early 1980s in Canada (Steele et al. 1982), and the frequency of outbreaks has increased over the last decade. Fresh apple cider is defined as a fresh, unfermented, short-shelf-life juice extracted from apples that have not been clarified or heat treated. The presence of suspended solids distinguishes certain types of apple juice as cider. Soluble solids are responsible for flavor, aroma, and color of freshly pressed juice. Refrigeration and chemical preservatives are the main techniques used to prolong the shelf life of fresh apple cider. The UV irradiation process has shown its ability to inactivate pathogens in apple cider and other fresh fruit juices (Koutchma et al. 2004; Murakami et al. 2006; Oteiza et al. 2005).

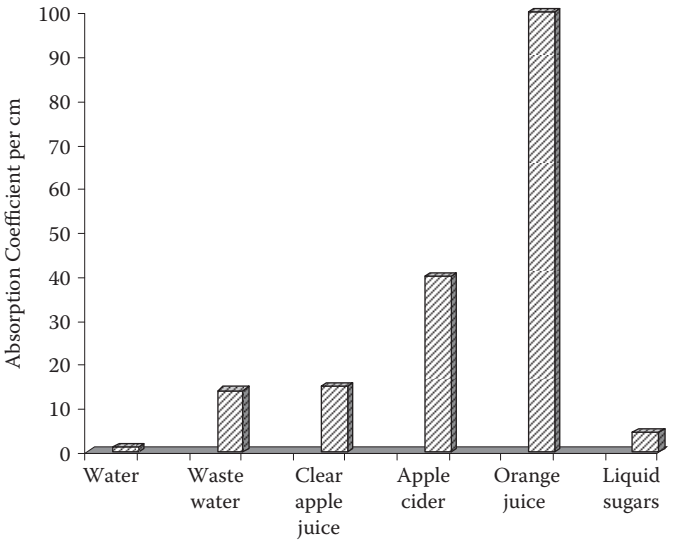

FIGURE 3.2 Comparison of absorption coefficients of water with fresh juices and liquid sugars.

It is apparent that transmission of UV light is poor through cider and apple juices due to the presence of organic compounds, vitamins, or suspended materials, and this results in ineffective UV-light pasteurization. The content of dissolved and suspended solids of apple cider and juice increases their absorption and scattering of UV light. Apple cider is made from different apple cultivars, so the physical and chemical properties of apple ciders are different. These properties are affected by season, variety, and storage conditions of apples, as reported by Basaran et al. (2004).

The color of apple cider is typical of freshly pressed apple juice. However, just after it is extracted from fruit and exposed to air, the cider becomes dark due to oxidative browning. Color development in apple cider due to browning can significantly change the absorbance of untreated samples. The increase in absorbance is up to 40% due to the browning that occurs in freshly pressed apple juice with time, as shown in Figure 3.3.

The absorbance and transmittance spectra of diluted commercial apple cider (dilution factor of 100) in a 1-cm quartz cuvette in a range from 1 to 1000 nm is shown in Figure 3.4. The absorption coefficient and transmittance of the tested apple cider at 254 nm corresponded to 19 cm^{-1} and 62%, respectively.

Apple cider and juice are also characterized by a wide pH range and a high sugar concentration, as characterized by °Brix. Table 3.1 provides examples of pH, °Brix, absorption coefficients, and turbidity for several types of commercially available apple juices and ciders. Turbidity—a measure of the quantity of particulates in a solution—is determined by shining an infrared beam of light through a 1-cm-thick sample and measuring light detected by sensors placed at 90° to the beam. Turbidity, commonly reported in NTU units, is not necessarily correlated with the absorption coefficient.

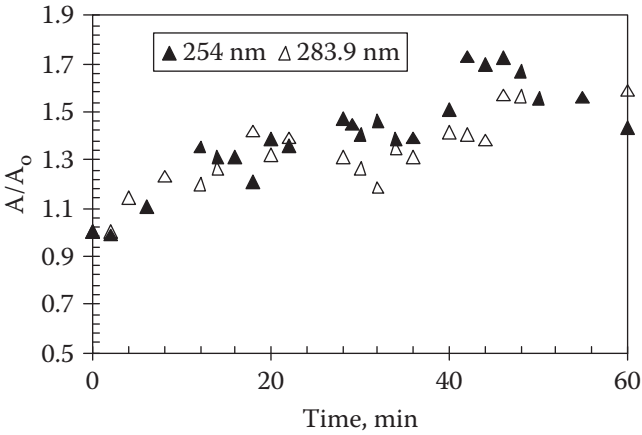

FIGURE 3.3 Increase of absorbance of fresh apple juice (Granny Smith green apples with peel) due to browning as measured at 254 and 283.9 nm.

As evident from Table 3.1, the UV absorptivity and turbidity of commercial brands of apple ciders vary considerably. Turbidity of apple ciders can range from 1000 to 2400 NTU, thus resulting in a range of absorption coefficients from 9.0 to 98 cm^{-1}. For clear, commercially prepared apple juice, the particles are so small (most or all being less than 0.1 mm in diameter) that they do not cause significant haze and turbidity in less than 2 NTU for well-prepared juices. Turbidity is often

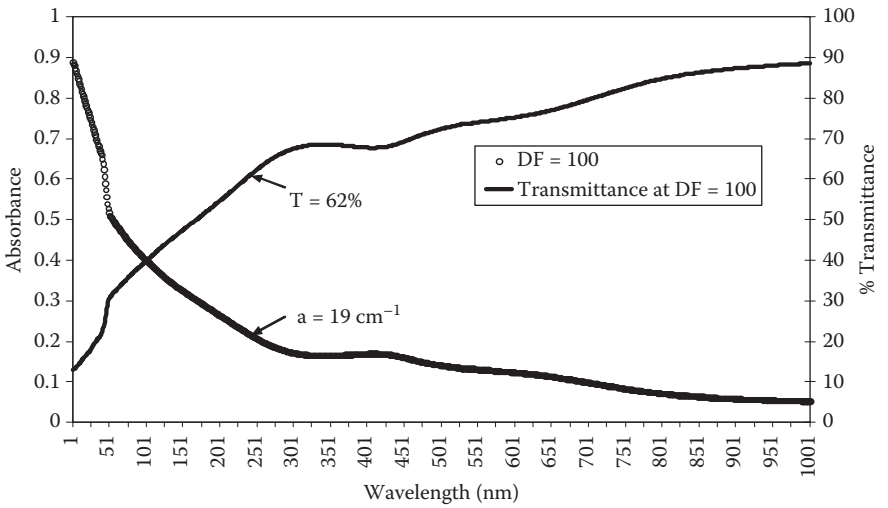

FIGURE 3.4 Absorbance and transmittance spectra of apple cider (100% apple cider, store brand). (From Unluturk et al. 2004. With permission.)

TABLE 3.1
The pH, °Brix, Absorption Coefficient, and Turbidity of Several Types of Apple Cider Commercial Products

Juice/Ciders	pH	°Brix	Absorption Coefficient, (cm^{-1}) α	Turbidity, (NTU)
Apple cider, "Yakima"	4.0	11	21	1420
Apple cider, fresh (Placerville, CA)	4.2–4.4	16.3	25.8	1024
Apple cider, "Zeiger's"	3.5	9.7	57	1400
Apple cider, "Tastee" (Newcomerstown, OH)	3.65	11.5	98	2400
Apple cider (Geneva, NY)	n.d.	n.d.	9.3	n.d.
Apple juice, light (without vitamin C added)	3.5	12	9	1.96
Apple juice (Gordon Food Service, Inc.)	3.5	13	19.8	0.8

Note: n.d. = no data available.

thought to be a limiting feature in UV disinfection. However, work has shown that particles, as long as they are not UV absorbers, do not significantly reduce the overall irradiance by either shading or scattering. The exception is the case when organisms are embedded within the particle. Particle suspensions, however, can increase the apparent absorption coefficient—as measured by a spectrophotometer—by scattering rather than absorbing light (Linden and Darby 1998).

The negative impact of suspended particles on both UV dose transmission and spectrophotometric absorbance is well documented for unfiltered water, as particles can absorb, scatter, and block UV light due to aggregation of bacteria to the particle surfaces (Christenen and Linden 2001). The effects of suspended particles on the absorbance characteristics of marginal effluents were studied and reported by Linden and Darby (1998). Very little research has been done to examine the effects of particles on UV processing of juices. The effects of high levels of suspended matter—a characteristic of fresh juices—on the UVT are not understood.

The range of particle size distributions in apple cider from a producer (Placerville, CA) was estimated by Unluturk et al. (2004). The particles showed a bimodal distribution (Figure 3.5). From 65% to 70% of the particles were distributed in a range from 1 to 26 μm with an average size of 7.6 μm. Particles ranging from 30 to 592 μm, with an average of 225 μm, contributed 30–35% of total volume. The smaller particle size class dominated with respect to total particle volume. Thus, the particles of apple cider were larger than the wavelength of UV light at 254 nm, possibly causing more light scattering in the forward direction because of enhanced backscattering.

The effect of the concentration of suspended particles on the absorption coefficient was studied and reported by Koutchma et al. (2004) using model solutions of caramel and dried apple particles. Dried particles were added to model solutions

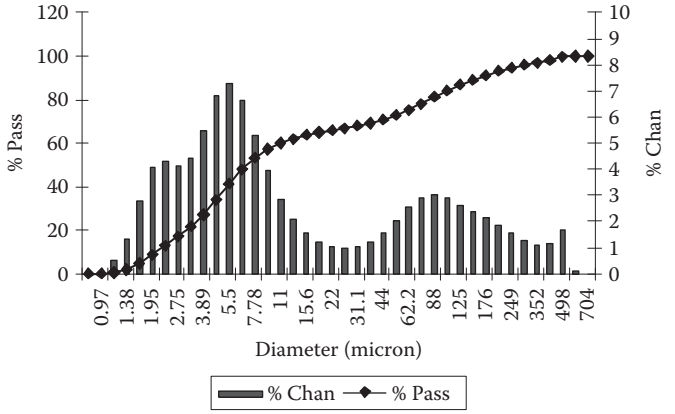

FIGURE 3.5 Particle size distribution of apple cider. (From Unluturk et al. 2001. With permission.)

with 0, 0.13%, and 0.40% of caramel, and absorption coefficients of the mixtures were determined. The absorption coefficients of model solutions were plotted versus content of suspended particles, as shown in Figure 3.6, demonstrating the apparent increase of absorption due to the light scattering by particles. The intercept of the linear plots represents the absorbance of the caramel solutions without suspended particles, and the slopes show the increase in absorption due to both the increase of particle concentration and the scattering effect. It was observed that the slopes of the linear plots were similar, indicating the scattering effect due to suspended solids.

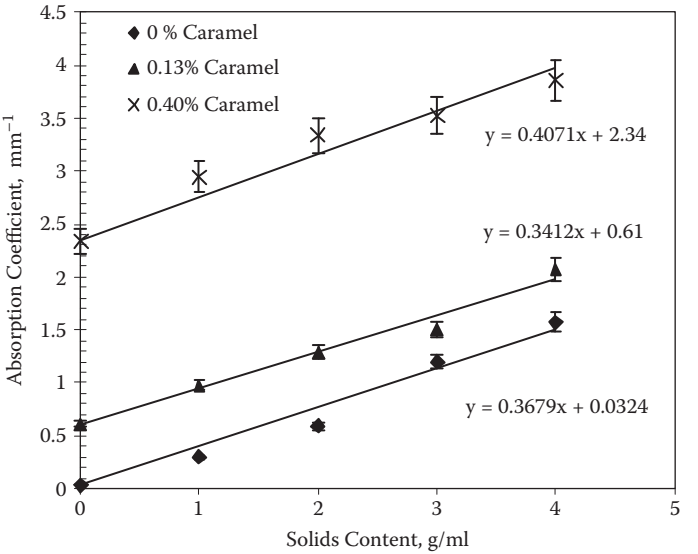

FIGURE 3.6 Effect of concentration of suspended solids on absorption coefficient of model caramel solutions. (From Koutchma et al. 2004. With permission.)

The absorbance by particles may be impacted by light-scattering properties, which will not be reflected in measurements made with a standard spectrophotometer. Since the average UV-light dose is generally calculated based on absorption coefficient measurements, the dose may be overestimated for fluids with a large particle concentration and a smaller soluble absorbance component.

3.3.2 Apple Juices

The essential properties of commercial brands of packaged apple juice (pasteurized, no preservatives) were characterized by Ye et al. (2007) in terms of their UV absorption effects. The pH, °Brix, vitamin C content, and color in terms of *L*-, *a*-, and *b*-values that were measured are summarized in Table 3.2. The selected four brands of juices were used for evaluation: Ocean Spray apple juice (OS), Sahara Burst (SB) apple juice, Gordon Food Service (GFS) apple juice, and Govinads apple juice from Hawaii. Sahara Burst and Gordon Food Service brands were enriched with vitamin C.

The small difference of pH and °Brix can be observed among brands of apple juice. However, the absorption coefficient of the tested juices varied in the range from 39.1 to 7.1 cm^{-1}. The correlation between absorption coefficients and vitamin C contents can be observed. In general, the larger values of vitamin C contents resulted in the larger absorption coefficients of juices. SB juice had the highest absorption coefficient of 39.1 cm^{-1}, and OS juice was the least absorptive (7.1 cm^{-1}) in terms of UV light. SB juice was enriched with vitamin C, whereas OS juice was not enriched with vitamin C and had the lowest magnitudes of *L* (lightness), *a* (yellowness), and *b* (greenness). For apple juices with higher values of absorption coefficients, the higher *L*-values were observed. Due to the correlation between vitamin C content and UV-light absorption,

TABLE 3.2
Physicochemical and Absorptive Properties of Commercial Brands of Apple Juices

Apple Juice	pH	°Brix	Absorption Coefficient, α (cm^{-1})	Vitamin C (mg/mL) Before UV Treatment	Color Space Values		
					L	*a*	*b*
Sahara Burst (SB)	3.49	11.9	39.1	0.30	5.74 ± 0.09	−0.667 ± 0.022	4.44 ± 0.25
Ocean Spray (OS)	3.44	11.65	7.1	0	4.03 ± 0.12	−0.35 ± 0.017	2.60 ± 0.04
Gordon Food Service (GFS)	3.51	11.75	37.1	0.45	4.67 ± 0.42	−0.39 ± 0.07	3.97 ± 0.12
Govindas (Hawaii)	3.21	11.35	25.9	n.d.	n.d.	n.d.	n.d.

Source: Ye et al. 2007.

Note: n.d. = no data available.

the understanding of UV-light effects on the destruction of vitamin C during treatment becomes critical in determining the optimal UV dose delivered.

Forney et al. (2004) used direct spectrophotometric measurements to report the values of absorption coefficients of 24.84 and 63.89 cm^{-1} for apple juice and grape juice, respectively.

3.3.3 Tropical Fruit and Vegetable Juices

Koutchma et al. (2007) reported optical and physicochemical properties of seven brands of tropical juices from Hawaii, and their results are summarized in Table 3.3. The variety of juices tested represented different °Brix and pH levels with varying viscosities. Lilikoi and apple juice represented less viscous, Newtonian fluids with low-pH products. Watermelon and guava juice had higher pH values in the similar range of viscosity typical for Newtonian liquids. The distinguishing characteristic of pineapple and orange juices was their low pH and viscosities, which were more than 10 times greater than apple and watermelon juices and were typical for non-Newtonian liquids.

Figure 3.7 demonstrates the comparison of absorption coefficients of tropical juices. UV absorption coefficients and turbidity of tropical juices varied considerably. Lilikoi juice had the lowest absorptivity, with an absorption coefficient of 11 cm^{-1}, followed by watermelon and apple juice. Orange and guava juices had somewhat similar absorption coefficients of 46 to 48 cm^{-1}, whereas carrot and pineapple juices were almost opaque juices containing particulate, pulpy materials. Turbidity of juices due to the presence of suspended solids was in a range from 1000 NTU for apple and lilikoi juices up to >4000 NTU. In this study, the absorption properties of the model caramel solution were adjusted to approximate those of tropical juices. For instance, absorbance of a 0.2% model caramel solution was comparable to the absorbance of a clarified lilikoi juice. Absorbance of a 0.5% model caramel solution matched to that of unfiltered apple juice. Model caramel solutions of between 1% to 1.1% were similar in absorbance to commercial orange, guava, and carrot juices, and a 2.0% model caramel solution was used to mimic the absorbance of pineapple juice.

TABLE 3.3
Physicochemical Properties of Tropical Juices

	Turbidity					Viscosity	
Juice	NTU	St. Dev.	pH	°Brix		cP	St. Dev.
Apple	972	23	3.21	11.35	0.35	5.79	0.46
Carrot	3980	453	3.75	10.55	1.06	9.87	2.59
Guava nectar	>4500	>450	6.32	9.05	0.21	5.02	1.01
Orange	3759	21	3.3	7.37	0.29	51.77	17.81
Lilikoi	1392	503	3.01	11.40	0.28	5.55	0.46
Pineapple	4028	256	3.96	14.17	0.58	53.20	6.16
Watermelon	1502	200	5.19	8.10	0.57	6.72	3.22

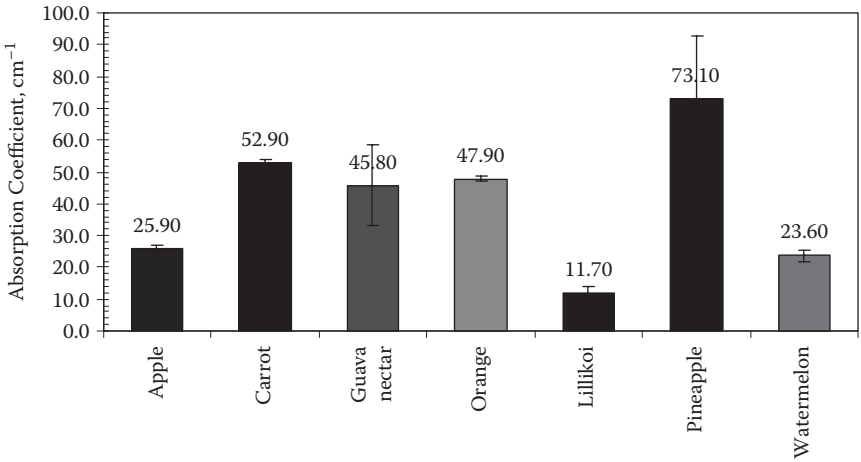

FIGURE 3.7 Comparison of absorption coefficients of tropical juices. (From Koutchma et al. 2007. With permission.)

Molar absorptivity of apple juice, orange juice, and multifruit juice was determined from the linear regression of absorbance at 254 nm versus concentration as reported by Oteiza (2005). The following absorptivities were reported: 0.0715, 0.3528, and 0.72330 L/mol/cm for apple, orange, and multifruit juice, respectively.

3.3.4 UV Absorption of Major Apple Cider Components

The major components of apple juice/cider are sugars, including fructose, sucrose, and glucose, followed by organic acids, mainly malic acid (Fan and Geveke 2007). Apple cider contains a very low amount of ascorbic acid. Fan and Geveke (2007) measured UV absorbance in the range of 190–360 nm for freshly made and commercial apple ciders and solutions of the three sugars, ascorbic acid, and malic acid using a Shimadzu UV-1601 spectrophotometer (Shimadzu Scientific Instruments, Columbia, MD). Apple ciders were filtered through a 0.45-μm Millipore (Billerica, MA) HV filter and then diluted 10 times. The sugar and malic acid solutions were undiluted, while ascorbic acid was diluted to 0.001% (10 ppm) before measurement.

The three sugars absorbed little UV in the range of 240–360 nm, although the fructose solution had higher UV absorbance at 260–280 nm than glucose and sucrose solutions. All three sugars had high absorbance around 200 nm (Figure 3.8a). Malic acid mainly absorbed UV at wavelengths less than 240 nm, while ascorbic acid had a strong absorbance between 220 and 300 nm, even at a very low concentration (0.001%) (Figure 3.8b). Apple ciders also had UV-C absorbance at wavelengths below 240 nm (Figure 3.8c). Overall, the commercial apple cider had higher UV-C absorbance than the freshly prepared cider. Soluble solids content, which measures mostly sugar content, was higher (11.9 vs. 11.1 g/mL) in the freshly prepared cider than the commercial cider. The higher sugar content presumably corresponds to higher concentration of fructose. The authors of this study concluded that apple cider with

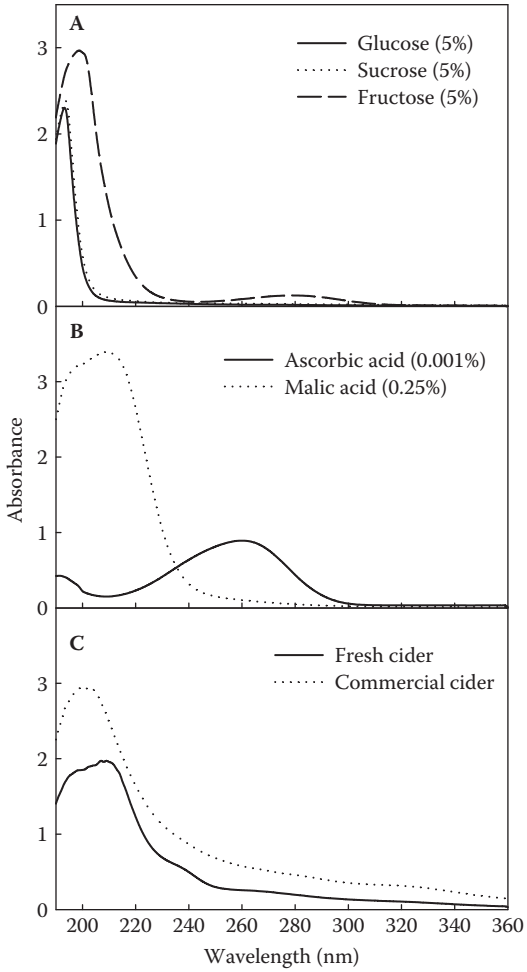

FIGURE 3.8 UV absorbance of (a) 5% glucose, sucrose, and fructose; (b) 0.001% ascorbic acid and 0.25% malic acid; and (c) diluted (10×) apple ciders. (From Fan and Geveke 2007. With permission.)

higher amounts of pigments (absorptivity) and suspended matter will reduce the penetration of UV-C. The apple cider prepared freshly in the lab had lower absorbance in the UV-C range than the commercial cider (Figure 3.8c), which may permit the penetration of UV-C treatment.

3.4 FOOD SOLIDS AND SURFACES

In the case of UV-light treatments of a surface, it is important to realize that UV light is strongly absorbed by most materials and cannot penetrate beyond the surface layers of solid objects. In such instances, for many types of foods, it is only

microorganisms that are present at the surface that can be inactivated. For some types of food this may well be sufficient; for example, muscle flesh from a healthy animal immediately after slaughter is, for all intents, sterile. Where contamination does occur, it will be as a result of contact with contaminated surfaces or fluids, and this will initially manifest itself at the surface.

According to Sharma (2007), the efficacy of UV surface treatment will be strongly influenced by surface topography. Crevices, and similar features, of dimensions comparable to the size of microorganisms (i.e., a few microns) may shield microorganisms from potentially lethal UV light and enable them to survive. This is why the UV treatment of fish fillets from a smooth-fleshed species was more effective than that of a rough-fleshed one. Another important factor determining survival is the intrinsic resistance of the microorganism to the effects of UV, a subject of discussion in Chapter 4.

Yet another protective strategy that has been adopted by some microorganisms is growth in the form of "biofilms." A biofilm may be thought of as a structured microbial community associated with solid surfaces. Attachment to surfaces occurs because certain members of the community are able to produce polysaccharides that serve as adhesives. Biofilms pose a very real threat in the food industry, and contact of foods with biofilms invariably results in contamination as cells are shed from the biofilm to the food.

The presence of Gram-negative enteric pathogens such as *E. coli* O157:H7 and *Salmonella enterica* on fresh produce presents a significant threat to public health and an economic challenge to the food industry. Enteric pathogens can originate from various sources such as soil, animal feces, irrigation water, and processing plants. Once the pathogen is attached in the field or during processing to the fresh cut surfaces, it can rapidly establish biofilms and is difficult to completely remove.

While there is no evidence that growth in the form of biofilms arose specifically as a protection against environmental UV light, organisms within biofilms are well protected from a variety of stresses, including UV. This is partly because the microorganisms within the biofilm are in a metabolic state that renders them less susceptible to environmental stresses, and partly because the polysaccharide matrix in which the cells are embedded offers a defense against both physical and chemical disinfectants. Many different approaches for neutralizing biofilms are being pursued, but the best current advice appears to be to effect physical removal and then to thoroughly disinfect the underlying surface using UV light. The efficiency of the current sanitation practices can be significantly improved by using innovative hybrid decontamination and cleaning technologies along with current advances in UV-lamp technologies.

3.5 CONCLUSIONS

Considerable information is available on critical process and product parameters in the UV treatment of water and wastewater. However, there is very limited data on the absorptive properties of liquid foods and fresh juices, which have a major effect on microbial inactivation under UV treatment and thus need to be properly assessed. It is highly desirable that sufficient UV absorbance data of liquid foods, beverages, and juices be collected, characterized, and reported. The absorbance measurement

techniques should account for the presence of the suspended particles and their effect on the estimation of the absorbed UV dose. In addition, the effect of some essential compounds such as vitamin C on the absorption effects of the sample needs to be taken into account during UV treatment. In determination of the UV absorbance design criteria, the full range of UV absorbance at the UV implementation point where the system will be installed should be determined. This enables selection of an appropriate UV absorbance range to ensure compliance at all times.

REFERENCES

AWWA. 1999. *Water quality & treatment: A handbook of community water supplies*. 5th ed. New York: McGraw-Hill.

Basaran, N., A. Quintero-Ramos, M. M. Moake, J. J. Churey, and R. W. Worobo. 2004. Influence of apple cultivars on inactivation of different strains of *Escherichia coli* O157:H7 in apple cider by UV irradiation. *Appl. Environ. Microbiol*. 70: 6061–6065.

Bolton, J., M. Stefan, R. Cushing, and R. Mackey. 2001. The importance of water absorbance/transmittance on the efficiency of ultraviolet disinfection reactors. Paper presented at First International Congress of UV Technologies, Washington, DC, June 14–16.

Centers for Disease Control and Prevention. 1996. Outbreak of *Escherichia coli* O157:H7 infections associated with drinking unpasteurized commercial apple juice: British Columbia, California, Colorado, and Washington. *Morb. Mortal. Wkly. Rep*. 45: 975.

Christenen, J., and K. Linden. 2001. Ultraviolet disinfection of unfiltered drinking water: Particle impacts. Paper presented at First International Congress on UV technologies, Washington, DC, June 14–16.

EPA, Office of Water. 1995. National primary drinking water regulations contaminant fact sheets: inorganic chemicals. Technical version. EPA 811-F-95-002-T. Washington, DC.

Fan, X., and D. Geveke. 2007. Furan formation in sugar solution and apple cider upon ultraviolet treatment. *J. Agric. Food Chem*. 55: 7816–7821.

Forney, L., J. A. Pierson, and Z. Ye. 2004. Juice irradiation with Taylor–Couette flow: UV inactivation of *Escherichia coli*. *J. Food Protection* 67: 2410–2415.

Harrington, W. O., and C. H. Hills. 1968. Reduction of the microbial population of apple cider by ultraviolet irradiation. *Food Technol*. 22: 117–120.

Koutchma, T., S. Keller, B. Parisi, and S. Chirtel. 2004. Ultraviolet disinfection of juice products in laminar and turbulent flow reactors. *Innovative Food Sci. Emerging Technol*. 5: 179–189.

Koutchma, T., B. Parisi, and E. Patazca. 2007. Validation of UV coiled tube reactor for fresh fruit juices. *J. Environ. Sci. Eng.* 6: 319–328.

Koutchma, T., B. Parisi, and S. Unluturk. 2006. Evaluation of UV dose in flow-through reactors for juices. *Chem. Eng. Commun.* 193: 1–14.

Linden, K., and L. Darby. 1998. Ultraviolet disinfection of marginal effluents: Determining UV absorbance and subsequent estimation of UV intensity. *Water Environ. Res*. 70: 214–223.

Murakami, E., L. Jackson, K. Madsen, and B. Schickedanz. 2006. Factors affecting the ultraviolet inactivation of *Escherichia coli* K12 in apple juice and a model system. *J. Food Process Eng.* 29: 53–71.

Oteiza, J., M. Peltzer, L. Gannuzzi, and N. Zaritzky. 2005. Antimicrobial efficacy of UV radiation on *Escherichia coli* O157:H7 in fruit juices of different absorptivities. *J. Food Protection* 68 (1): 49–58.

Sharma, G. 2007. UV disinfection in the food industry. *Controlled Environments Mag.* April 2007. http://www.cemag.us/articles.asp?pid=668.

Steele, B. T., N. Murphy, G. S. Arbus, and C. P. Rance. 1982. An outbreak of hemolytic uremic syndrome associated with the ingestion of fresh apple juice. *J. Pediatr.* 101: 963–965.

Unluturk, S., T. Koutchma, and H. Arastoopour. 2001. Modeling of dispersed particle-liquid (solid-liquid) phase flow and application to UV pasteurization of apple cider. In Proceedings of 7th Conference on Food Engineering (CoFE'01), AICHE Annual Meeting, Reno, NV. Book of abstracts, p. 75.

Unluturk, S., T. Koutchma, and H. Arastoopour. 2004. Modeling of UV dose distribution in a thin film UV reactor for processing of apple cider. *J. Food Eng.* 65 (1): 125–136.

Ye, Z., T. Koutchma, B. Parisi, J. Larkin, and L. J. Forney. 2007. Ultraviolet inactivation kinetics of *E. coli* and *Y. pseudotuberculosis* in annular reactors. *J. Food Sci.* 72: E271–E278.

4 Microbial Inactivation by UV Light

When discussing UV-light microbial inactivation capabilities, a distinction must be made between inactivating and killing microorganisms. For chemical disinfectants (e.g., chlorine, chlorine dioxide, iodine), inactivating and killing can be considered synonymous terms, since chemical disinfectants destroy and damage cellular structures, which interferes with metabolism, biosynthesis, and growth. In contrast, UV light does not destroy or damage cellular structures. Rather, UV light prevents microorganisms from reproducing. Microorganisms that cannot reproduce cannot infect and are thereby inactivated. The mechanism of microbial inactivation by UV light is discussed in this chapter.

The UV sensitivity of microorganisms of concern is a key factor affecting the efficacy of UV treatment of liquid foods. Knowledge of the UV decimal reduction dose is a requirement to design a preservation process. A clear understanding on how variations in product characteristics can affect UV inactivation must be established. In this way, appropriate operating parameters can be developed. Inactivation kinetics parameters and the impact of physical and chemical properties in foods on inactivation rates need to be properly measured and assessed. The objective of this chapter is to provide information regarding these important issues in UV treatment of liquid foods.

4.1 MECHANISMS OF MICROBIAL INACTIVATION BY UV LIGHT

UV light inactivates microorganisms by damaging their nucleic acid, thereby preventing microorganisms from replicating. The nucleic acid is either deoxyribonucleic acid (DNA) or ribonucleic acid (RNA). The nucleus of most cells is composed of double-stranded DNA. DNA contains the information necessary for the synthesis of ribosomal, transfer, and messenger RNA, which are responsible for synthesizing metabolic processes within the cell. The virus and bacteriophage genetic material is DNA or RNA, either single or double stranded.

DNA and RNA are long polymers comprising combinations of four nucleotides. In DNA, the nucleotides are the purines, adenine and guanine, and the pyrimidines, thymine and cytosine. In RNA, the nucleotides are the purines, adenine and guanine, and the pyrimidines, uracil and cytosine. The nucleic acid is double stranded, with nucleotides on one strand complementing those on the other strand. Adenine pairs with thymine in DNA and with uracil in RNA, while quinine pairs with cytosine. Hydrogen bonds form between each pair. Each nucleotide can be broken into two parts: a sugar phosphate and a nitrogenous base (Figure 4.1).

As shown in Figure 4.2, nucleic acid absorbs UV light from 200 to 310 nm. UV light kills microorganisms by disrupting their DNA or RNA structures by inducing

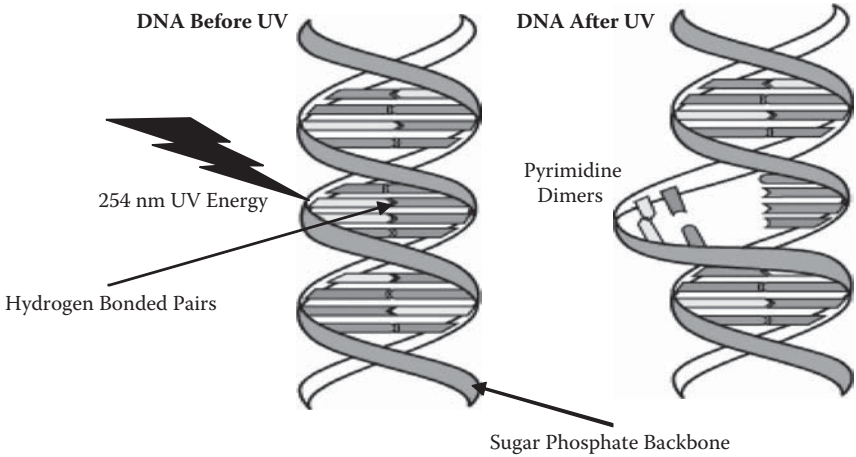

FIGURE 4.1 Structure of DNA before and after absorbing a photon of UV light. (Adapted from Wikimedia Commons. http://commons.wikimedia.org/wiki/Main_Page.)

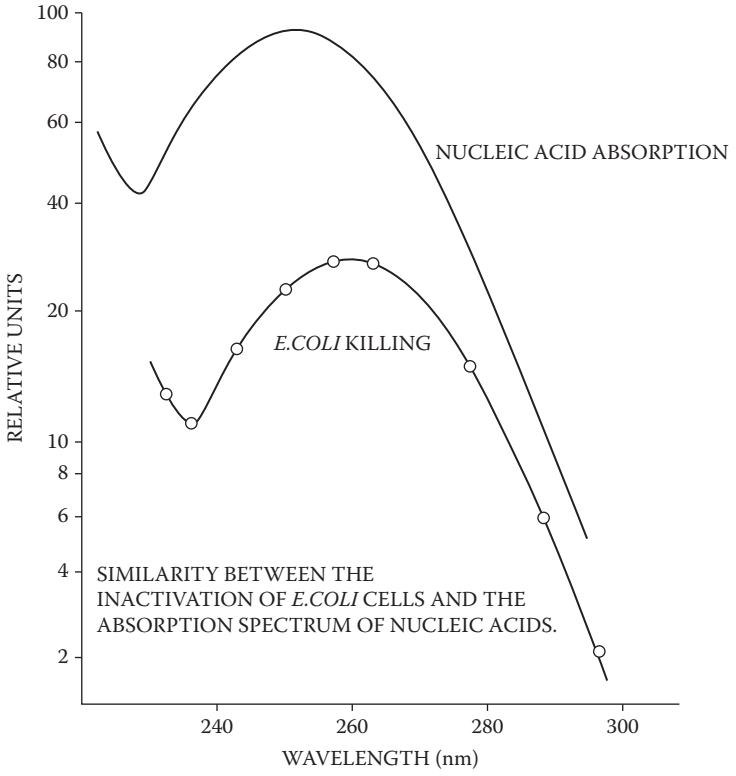

FIGURE 4.2 UV absorbance of nucleic acid.

six types of damage. The primary mechanism of inactivation by UV is the creation of pyrimidine dimers (Figure 4.1), which are bonds formed between adjacent pairs of thymine or cytosine pyrimidines on the same DNA or RNA strand. Dimers prevent microorganisms from replicating, thereby rendering them inactive and unable to cause infection. Figure 4.2 shows the similarity between the ability of UV light to destroy and the ability of this cell's nucleic acid to absorb UV light. The germicidal lamp emitting UV at 254 nm is operating very close to the optimized wavelength for maximum absorption by nucleic acids. However, damage to nucleic acid does not prevent the cell from undergoing metabolism and other cell functions. Enzyme mechanisms within the cell are capable of repairing some of the damage to the nucleic acid. It is possible for microorganisms to repair themselves to the extent where they will become infective again after exposure to UV light. Microorganisms have developed two mechanisms to repair damage caused by UV light. These mechanisms are termed light and dark repair. Repair to UV-light-induced DNA damage includes photoreactivation, excision or dark repair, recombinational repair, and inducible error-prone repair. The details of the repair mechanism have been reported by Jagger (1967), Shama (1992), and Harm (1980). As a result, the strategy in UV disinfection of water has been to provide a sufficiently high dosage to ensure that nucleic acid is damaged beyond repair.

Figure 4.3 illustrates the output spectra for low-pressure mercury (LPM) and medium-pressure mercury (MPM) UV lamps along with the microbial action spectra. A low-pressure UV lamp typically converts electrical input power into resonant radiation, mostly at 254 and 185 nm. The contribution of 185-nm UV to germicidal effect is negligible because the transmission in wastewater at this wavelength is very small, typically less than 0.2%. Consequently, the UV dose using a LPM UV lamp is a result of the near-monochromatic line at 254 nm. On the other hand, a MPM UV lamp

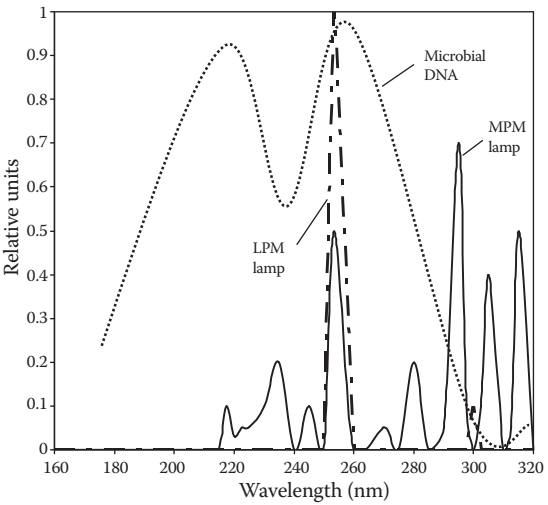

FIGURE 4.3 Output spectra of low-pressure and medium-pressure mercury lamps and microbial-action spectra. (From Kuo et al. 2003. With permission.)

typically generates a polychromatic spectral output over the entire UV range. The UV wavelength most effective at inactivating microorganisms occurs between 260 and 265 nm, and the biocidal effectiveness for microbial disinfection decreases from this peak as the wavelength either decreases or increases from this region. In other words, wavelengths other than 254 nm still possess disinfection power. Wright (2000) presented a method for calculating UV dose for MPM UV lamp systems. The method considered wavelength-dependent factors related to UV dose, including spectral output of the UV source, water absorbance, and germicidal response of the microbes. The development of a standard protocol needs to consider these wavelength-dependent factors.

4.2 UV SENSITIVITY OF PATHOGENIC AND SPOILAGE FOOD-BORNE MICROORGANISMS

4.2.1 Definition of UV Dose

In drinking-water applications, disinfection using UV light follows the familiar *CT* concept (disinfectant *concentration* × contact *time*). However, instead of using *CT* to describe UV disinfection, UV dose is used instead. UV dose is the product of UV fluence rate, *I*, and exposure time, *T*, i.e., *IT*, similar to the *CT* concept. UV dose is reported as mW×s/cm^2. However, UV dose is also commonly expressed as millijoules per square centimeter (mJ/cm^2), because 1 mW×s = 1 mJ.

4.2.2 Estimating UV Dose

Several complex models have been developed to estimate the UV fluence rate delivered to a microorganism. With the estimated UV fluence rate, the UV dose can be calculated based on various exposure times and compared with UV doses determined in the scientific literature. The simplest model used to estimate UV fluence rate is the radial model (equation 4.1). This model can be used to provide a rough evaluation of UV inactivation capability.

$$I(r) = (P_{\mathrm{L}} / 2\pi r) \times e^{-\alpha_e r} \tag{4.1}$$

where

$I(r)$ = UV fluence rate (mW/cm^2) at a distance r from the lamp
P_{L} = UV power emitted per unit arc length of the lamp (mW/cm)
r = radial distance from the lamp (cm)
α_e = base e absorption coefficient (cm^{-1}), $\alpha_e = 2.303 \times A_{254}$

UV doses required for reducing populations of microbial groups by a single order of magnitude, a quantity referred to as the "D_{10} dose," is often used to characterize the UV sensitivity of microorganisms. Survival curves (UV dose response) are constructed to demonstrate the susceptibility of a specific organism to different doses of UV light.

Microorganisms differ in their sensitivity to UV light. This variation may be due to cell-wall structure, thickness, and composition; to the presence of UV-absorbing proteins; or to differences in the structure of the nucleic acids themselves. Three pathogen groups are of primary concern in water treatment: bacteria, viruses, and protozoa.

A summary of reported data on the UV dose response of various organisms that are pathogens, indicators, or organisms encountered in the application, testing of performance, and validation of UV disinfection technologies was published by Cairns (2006). These tables reflect the current state of knowledge, but they also include the variations in techniques and biological response that currently exist in the absence of standardized protocols. In most cases, the data were generated from low-pressure monochromatic mercury arc lamp (LPML) sources for which the lamp fluence rate (intensity) can be measured empirically and multiplied by exposure time to obtain a UV dose. None of the data incorporated any impact of photorepair processes. Only the response to the inactivating UV dose was documented. Another review that can be recommended to the reader is the report by Hijnen et al. (2006). The review summarized published data for viruses, bacteria, and protozoa. However, it should be emphasized that both reports reviewed the literature for UV disinfection of water.

4.3 UV SENSITIVITY OF WATERBORNE PATHOGENS

UV disinfection technology is of growing interest in the water-treatment industry, since it was demonstrated that UV radiation is very effective against (oo)cysts of *Cryptosporidium* and *Giardia*, two pathogenic microorganisms of major importance for the safety of drinking water. Generally, in water-disinfection practice, UV light is most effective at inactivating *Cryptosporidium* and *Giardia*, followed by bacteria. UV light is least effective against spores and viruses

Cryptosporidium and *Giardia* > Bacteria > Spores > Viruses

Table 4.1 provides a summary of numerous UV disinfection studies and shows the ranges of average D_{10} doses of various microbes. The range for bacteria excludes *Deinococcus radiodurans*, which are the most UV-resistant bacteria isolated to date. The D_{10} dose of *Deinococcus* ranged from 19.7 up to 145 mJ/cm^2. Fortunately, this bacterium is something of an oddity and is highly unlikely to be found in normal food-processing operations (Shama 2007). The doses for 1-log inactivation of yeast, fungi, and algae are given for inactivation in air.

TABLE 4.1
D_{10} UV Inactivation Doses (mJ/cm^2) Measured at 253.7 nm for Various Microbial Groups

Microbial Group	D_{10} UV Dose (mJ/cm^2)
Enteral bacteria	2–8
Cocci and micrococci	1.5–20
Spore formers	4–30
Enteric viruses	5–30
Yeast	2.3–8
Fungi	30–300
Protozoa	60–120
Algae	300–600

Adenovirus is recognized as the most UV-resistant waterborne pathogen of concern to public-health microbiologists (Linden et al. 2007). As reported by Cairns (2006), the value of D_{10}-dose for adenoviruses type 40 and 41 varies in the range of 40–55 mJ/cm^2. According to recently published EPA regulations (U.S. EPA 2003), the inactivation of adenoviruses to a level of 4 log requires a UV fluence of 186 mJ/cm^2 based on an 80% credible interval. Typical doses used for drinking-water disinfection would not be effective for treatment of adenoviruses. The EPA-regulated UV fluence for inactivation of all viruses is now based on the conservative case of adenoviruses. As mentioned above, all peer-reviewed studies were performed using LPML-generated UV. Linden et al. (2007) reported inactivation data using polychromatic UV sources and indicated the significant enhancement of inactivation. When a full-spectrum medium-pressure mercury lamp (MPML) was used, 4-log inactivation of adenovirus type 40 was achieved at a UV fluence less than 60 mJ/cm^2. Surface-discharge pulsed UV sources required a fluence of less than 40 mJ/cm^2.

MS-2 is an F-specific single-stranded RNA virus about 20 nm in diameter that is often used as a viral surrogate. The reported D_{10} values of MS-2 viruses differ significantly, from 4 mJ/cm^2 for MS-2 DSM 5694 host *Escherichia coli* NCIB 9481 up to 20 mJ/cm^2 for MS-2 host *E. coli* ATCC 15997 and *E. coli* ATCC 15597 (Weidenmann et al. 1993; Sommer et al. 1999).

The UV sensitivity of bacteria is positively correlated to the thymine content of its DNA. Spore-forming and gram-positive bacteria are more resistant to UV light than gram-negative bacteria. With microbes larger than 1 micron, absorption of UV light by cytoplasm affects UV sensitivity. The UV sensitivity is also strongly related to the ability of the microbe to repair UV damage. *Bacillus subtilis* spores are also commonly used as a bioassay organism in water treatment because of their resistance to inactivation, requiring about 36 mJ/cm^2 for a 1-log reduction (Chang et al. 1985). Sommer et al. (1999, 2000) showed that UV inactivation of eight strains of *E. coli* differed considerably, with a 6-log reduction of the most sensitive strain being achieved with a fluence of 1.2 mJ/cm^2 and the most resistant strain requiring 12.5 mJ/cm^2.

Bacteria and (oo)cysts of *Cryptosporidium* and *Giardia* are more susceptible, with a fluence requirement of < 20 mJ/cm^2 to achieve 3-log reduction. When evaluating UV disinfection capability, assays that measure *Giardia* cyst and *Cryptosporidium* oocyst infectivity, not viability, must be used. Excystation assays measuring viability are not accurate indicators of UV disinfection capability.

The protozoan *Acanthamoeba* is also highly UV resistant (Hijnen et al. 2006). Fungi and molds can also be very UV resistant, depending on the species. Blue-green algae are very resistant to UV light because they have evolved very effective repair mechanisms. A maximum dose of UV light is needed to ensure coverage for this wide variation of UV sensitivities.

4.4 UV SENSITIVITY OF FOOD-BORNE PATHOGENS

Food-borne diseases may be caused by a wide variety of pathogenic microorganisms. According to the U.S. FDA (2000), in the United States food-borne diseases caused by microorganisms can be attributed primarily to pathogenic

bacteria, enteric viruses, and protozoa. The following bacteria are known to be responsible for causing food-borne disease: *Aeromonas hydrophila*, *Bacillus cereus*, *Campylobacter jejuni*, *Clostridium botulinum*, *Clostridium perfringens*, *pathogenic Escherichia coli*, *Listeria monocytogenes*, *Salmonella*, *Shigella*, *Staphylococcus aureus*, pathogenic *Vibrio* spp., and *Yersinia enterocolitica*. The viruses of concern in foods are hepatitis A, Norwalk, Norwalk-like, and rotavirus (CDC 2000; Mead et al. 1999). *Cryptosporidium parvum*, *Cyclospora cayetanensis*, *Giardia lamblia*, and *Toxoplasma gondii* are all parasites of concern, in part because they produce resistant cysts. *Escherichia coli* O157:H7 is a non-spore-forming bacterium that has been implicated in numerous food-borne illness outbreaks of contaminated, raw apple cider. *Cryptosporidium parvum* is a protozoan parasite that has the capability of forming oocysts and has also been implicated as the causative agent in a food-borne illness outbreak of apple cider in New York State (USFDA 2000). In general, the microorganism of public health significance for a specific process depends on its resistance, the process, the initial numbers present, and its ability to grow in the food.

Hanes et al. (2002) demonstrated the effectiveness of UV light for inactivating *Cryptosporidium parvum* in apple cider. A 3.8-log reduction could be achieved for *E. coli* O157:H7 in apple cider, with turbidity of the cider impacting the effectiveness of the treatment (Koutchma et al. 2004). A 5-log reduction was achieved in cider containing low initial levels of yeast and mold with high UV doses and low flow rates. However, Duffy et al. (2000) and Quintero-Ramos et al. (2004) have demonstrated at least a 5-log reduction of an *E. coli* surrogate for O157:H7 in multiple trials using the CiderSure™ UV pasteurizer. Data on UV effectiveness against *L. monocytogenes* are not available, and data on *Salmonella* are limited.

The degree of inactivation of microbes by UV radiation is directly related to the UV dose applied to the food product. Key factors identified in the efficacy of the UV treatment include UV reactor design and the fluid dynamics parameters and absorptive properties. In general, absorptivity and suspended particles, even those found in wastewater, do not approach levels encountered in juices. In addition, water is unlikely to present in a wide a pH range or contain the high sugar concentrations of juice products.

4.5 UV INACTIVATION KINETICS AND COMPETITIVE EFFECTS IN FOODS: ABSORBANCE, PH, SOLIDS, AND OTHER COMPONENTS

The process and product parameters that influence the rate of microbial destruction in liquid foods during UV-light processing need to be characterized. Food products have a wide range of chemical and physical properties. Consequently, product characteristics like pH, dissolved solids, suspended solids, and absorbance vary from one lot to another. A clear understanding must be established on how variations in product characteristics can affect UV inactivation parameters. In this way, appropriate operating parameters can be developed.

4.5.1 pH and Dissolved Solids

Little data are available on factors that are critical for inactivation efficacy in juices. Koutchma et al. (2004) reported the effects of pH and dissolved solids (°Brix) on UV-inactivation of *E. coli* K12 in a laminar-flow, thin-film UV reactor manufactured by CiderSure. The tests were conducted in model apple juice/cider that was made of malate buffer and 0.13% caramel solution at the extreme ranges of pH (3–5) and °Brix (10–20) that were found for apple juice/cider. Absorbance of a 0.13% solution of caramel was comparable to the absorbance of a clarified (filtered) apple cider. Absorbance of a 0.6% caramel solution or a 0.13% caramel solution with added particles matched that of unfiltered apple cider. Caramel solutions of between 0.4% to 0.5% were similar in absorbance to commercial clear apple juice. It was found that, individually, pH and °Brix had no significant effect on the rate of *E. coli* destruction under the conditions tested. At the pH levels 3 and 5 at °Brix 10, the inactivation rates were not significantly different (t-test, $\alpha = 0.03$). At the °Brix levels of 10 and 20, results showed that the inactivation rates were also not significantly different from each other at both low- and high-absorbance solutions (t-test, $\alpha = 0.05$, two-tail). The effect of °Brix was expanded to °Brix levels of 15 and 25, and these levels also had an insignificant ($p = .05$) effect on inactivation rates. A small but statistically significant effect was noted when both pH and °Brix were changed, and a combined effect was observed. The similar findings of independence of UV dose response of the pH were reported for water by Hijner et al. (1987).

Bazaran et al. (2004) examined the effect of different apple cultivars upon the UV inactivation of *Escherichia coli* O157:H7 strains within unfiltered apple cider. Among the apple cultivars, an average log reduction range of 5.78 (Red Delicious) to 6.74 (Empire) was observed, with two statistically significant log reduction groups represented. Within the paired cultivar-strain analysis, five of eight ciders showed statistically significant differences in at least two of the *E. coli* strains used. Comparison of log reductions among the *E. coli* strains to the cider parameters of °Brix, pH, and malic acid content failed to show any statistically significant relationship.

4.5.2 Absorbance

It was reported by Koutchma et al. (2004) and Murakami et al. (2006) that the inactivation rate of *E. coli* K12 was affected by the absorbance of the model solution (Table 4.2). The inactivation rates of the solutions with $\alpha = 6$ and 21 cm^{-1} were 0.71- and 0.16-log reduction per mJ/cm^2, respectively. In comparison, the inactivation rate of a commercial clear apple juice with similar physical and chemical properties was 0.23-log reduction per mJ/cm^2. Inactivation plots demonstrating the effects of absorbance are shown in Figure 4.3b. They show that in order to achieve a 3-log reduction, it would take an exposure time of about 11.5 s in the buffer solution with $\alpha = 6$ cm^{-1} and about 36 s in the buffer with $\alpha = 20$ cm^{-1}. These results are consistent with the Beer–Lambert–Bouger's law, which states that light intensity decreases with increasing absorbance. Downey et al. (1998) reported that the inactivation rates of pathogen in irrigation water increased with decreasing absorbance. Similar findings on the effect of absorbance were reported by Oteiza et al. (2005). A linear relationship was

TABLE 4.2
Effects of Dissolved Solids, pH, and Absorption Coefficient (α) on the UV Inactivation Rates of *E. coli* K12 in Malate Buffer (turbidity = 0.5 NTU)

Caramel (%)	Dissolved Solids (°Brix)	pH	Absorption Coefficient, α (cm^{-1})	Inactivation Rate (log reduction per mJ/cm^2)
0.13	10	3	6.0	0.71
		5	6.2	0.60
	20	3	6.5	0.49
		5	6.3	0.50
0.4	10	3	17.8	0.13
		5	20.4	0.14
	20	3	21.5	0.16
		5	22.2	0.12

Source: Murakami et al. (2006).

found between the D-values obtained for the *E. coli* strains and absorptivity coefficients of the fresh fruit juices tested.

The effect of absorption coefficient on survival of *E. coli* K12 was studied for clear malate buffer and 0.13%–0.6% caramel solutions at pH 3.75 in a turbulent-flow UV reactor (Koutchma et al. 2004). The inactivation of bacteria followed first-order kinetics. Those results were similar to those observed in the CiderSure UV reactor, where survival increased with absorption coefficient. Greater than a 5-log reduction was achieved after one pass for clear malate buffer. Almost seven passes were needed to obtain a 5-log reduction of bacteria in apple juice with an absorption coefficient of 9 cm^{-1}. Inactivation rate decreased as absorbance of the model system increased and was close to zero when the absorption coefficient of the model solution was higher than 15 cm^{-1}. *Escherichia coli* K12 inactivation in apple cider ($\alpha = 57$ cm^{-1}, 1383 nephelometric turbidity units [NTU]) confirmed this observation when only a 1-log reduction was obtained after six passes through the reactor at a flow rate of 75 L/min.

4.5.3 Suspended Solids

The amount of particles or suspended solids (SS) in water is a major concern in UV-treated wastewater. Loge et al. (1996) reported that SS are the major cause of tailing, a phenomenon where microorganisms continue to survive despite continued exposure to high amounts of UV-light energy. Particles have high light absorbance and are impenetrable to light unless they have a high porosity (Abughararah 1994). However, porosity can provide effective shields for microorganisms, allowing them to survive during UV processing. Murakami et al. (2006) reported the effect of suspended solids using model apple cider. Apple solids obtained by centrifuging commercial apple cider were added to the buffer solution to simulate cider or juice with

TABLE 4.3
Effects of Suspended Solids on the UV Inactivation Rates of *E. coli* K12 in a Malate Buffer (caramel 0.13%, pH 5, 10°Brix, 0.2-mm cuvette)

Suspended Solids (g/mL)	Turbidity (NTU)	Absorption Coefficient, α (cm^{-1})	Inactivation Rate (log reduction per mJ/cm^2)
0	0.5	6.0	0.71[b]
2.5	256	10.3[a]	0.38[b]
5.0	858	22.0[a]	0.25[c]; 0.06[c]

Source: Murakami et al. (2006).

[a] Apparent values.

[b] Average of three replicates.

[c] Calculated from a two-component plot, as shown in Fig. 4.4.

high SS. Initial test levels were pH = 3 and 5, °Brix = 10 and 20, caramel = 0.13% and 0.40%, and SS = 0.0, 2.5, and 5.0 g/mL.

The inactivation rates of *E. coli* K12 in malate buffer solutions containing 0, 2.5, and 5 g/mL of suspended solids (SS) are given in Table 4.3. Inactivation plots in malate buffer at SS = 0 and 2.5 g/mL of solids were linear, however, indicating the decrease in inactivation rate due to the particles. In the solution with SS = 5 g/mL, the inactivation plot was interpreted as having two linear components, indicating that the bacteria were not equally exposed to UV light (Figure 4.4). To achieve a 4-log reduction, a solution with SS 5.0 g/mL and an apparent absorption coefficient $\alpha = 22\ cm^{-1}$ would require UV energy of about 16 mJ/cm^2. With shielding, the required dose is 32 mJ/cm^2 for a 140% increase (data were not reported).

Koutchma et al. (2004) examined the effect of suspended particles on UV inactivation of *E. coli* K12 in commercial apple juices with different turbidity values of 1400 and 2400 NTU. A laminar thin-film continuous UV reactor (CiderSure 1500)

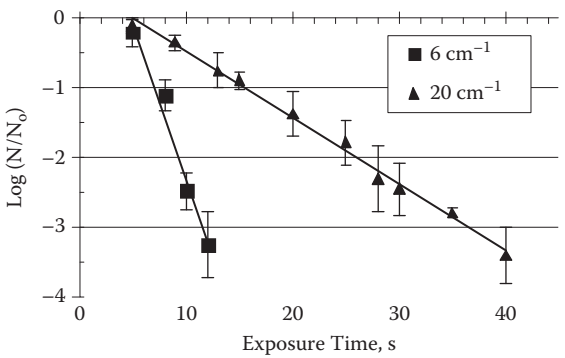

FIGURE 4.4 Effects of absorbance on inactivation curves of *E. coli* K12 in malate buffer with pH = 5 and BRIX = 20. (From Murakami et al. 2006).

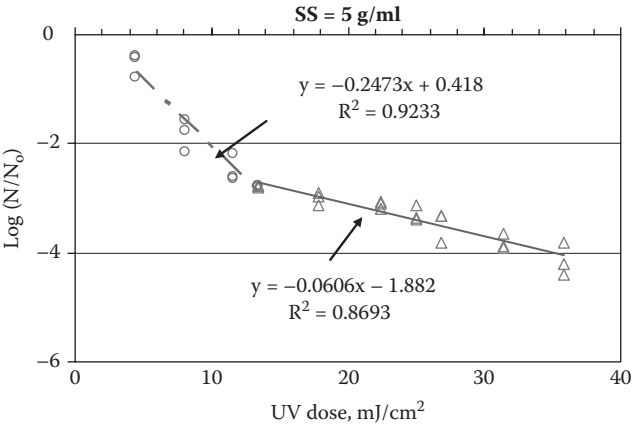

FIGURE 4.5 Two-component inactivation curve of *E. coli* K12 in malate buffer with 5 g/mL of suspended solids from composite data of three replicates. (From Murakami et al. 2006. With permission.)

was used in the experiments. The data shown in Figure 4.5 indicated faster inactivation of *E. coli* in less turbid apple cider of 1400 NTU at a higher flow rate of 166 mL/s. No significant difference in inactivation was observed at minimum flow rates of 57 mL/s. Higher flow rates resulted in increased mixing between the three tandem treatment chambers in the CiderSure reactor and more sufficient irradiation of cider. Increasing the turbidity of apple cider to 2400 NTU negatively impacted the effectiveness of UV inactivation, resulting in a lower inactivation rate.

Filtered apple particles were added to the model solution to determine their effect on rates of inactivation by UV irradiation. In addition, the rate of microbial inactivation in the model solution with and without suspended solids was compared to actual apple juice and cider (Table 4.4). Predicted values for both model fluids and cider or juices were calculated based on measured absorption coefficient and compared with measured values at three different flow settings. One of these settings was an "auto" setting that adjusts flow rate based on sensor readings (UV-light transmittance) at two points within the flow path. Flow rate is adjusted using an algorithm based on the transmittance of the UV light through the treated fluid. The rate of microbial destruction in apple juice and cider was measured using the "auto" setting and compared with rates obtained at the constant-speed settings. The rate of destruction on the "auto" setting was comparable with that obtained at constant flow rates (Table 4.4).

While the addition of particles had a dramatic effect on the measured absorption coefficient, it did not bring about the predicted change in inactivation rates. Increasing the concentration of the caramel to 0.5% resulted in an increase in absorption coefficient similar to that obtained through the addition of SS. The inactivation rate in this clear 0.5% caramel solution was significantly lower than the inactivation rate of the 0.13% solution containing suspended solids (SS) despite the similar absorption coefficient values. Unlike the 0.13% caramel solution containing SS, the inactivation rate measured in the 0.5% caramel solution closely matched its predicted value (Figure 4.6).

TABLE 4.4
Effect of Suspended Solids on the Rate of Destruction of *E. coli* K12 by UV Light

Model or Juice	Turbidity (NTU)	Absorption Coefficient, α (cm^{-1})	Predicted Inactivation[a]	Actual Inactivation, mean (SE) @ 56.8 mL/s	Actual Inactivation, mean (SE) @ 165.7 mL/s	Actual Inactivation, mean (SE) Auto Mode
0.13% caramel with solids	1400	26	0.32	1.01[b] (0.05)	1.21[b] (0.12)	n.d.
0.13% caramel	0.6	6.4	1.07	1.11 (0.04)	1.13 (n.d.)	n.d.
0.5% caramel	0.6	25	0.36	0.32 (0.02)	0.47 (0.08)	n.d.
Apple cider	1420	21	0.52	1.19[b] (0.10)	1.64[b] (0.06)	1.33[b]
Apple juice (clear)	0.8	19.8	0.56	0.20[b] (0.02)	0.18[b] (0.08)	0.14[b]

Note: Rate of destruction = [−log (N/N_0)]/s, with initial level of inoculation at log 6 CFU/mL; n.d. = no data available.

[a] Based on absorbance model regression line.
[b] Indicates mean falls outside of absorbance-based regression two-sided 95% prediction limits.

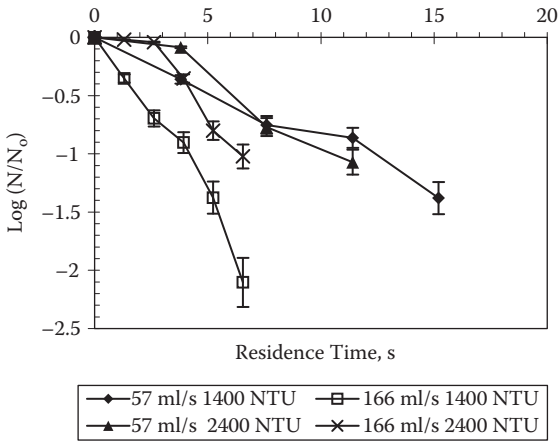

FIGURE 4.6 Effect of turbidity on UV inactivation of *E. coli* K12 in apple cider in a CiderSure 1500 UV reactor.

The failure of the absorption coefficient values to accurately predict kill rates in solutions containing particles may be partially explained by light scattering (Linden and Darby 1998). Suspended particles can scatter light away from the detector, resulting in an artificially high value of measured absorbance or apparent absorbance.

4.5.4 Temperature

Temperature affects the configuration of nucleic acid and the activity of repair enzymes. Severin at al. (1983) found the dose required for a given log reduction of *E. coli*, *Candida parapsilosis*, and f2 phage increased slightly as temperature decreased. While the rate of repair is temperature dependent, UV dose is typically reported after repair processes have saturated. Accordingly, UV dose response is considered independent of temperature. The UV-light transmittance through the liquid and reflectance at the air–liquid surface are temperature dependent because the physical properties of the liquid change with changing temperatures. The water sample temperature of a pilot operation can be quite different from that in the laboratory. To have a more meaningful comparison, the effects of temperature should be taken into consideration.

4.5.5 Wavelength

Microbial UV dose response varies with the wavelength of UV light. The action spectrum of a microbe is a plot of its UV sensitivity as a function of the wavelength. The dependence of the first-order inactivation constant k on wavelength is similar to the dependence of the UV absorption of nucleic acid. The inactivation constant peaks at or near 260 nm, has a minimum near 230 to 240 nm, and drops to zero near 300 to 320 nm. The inactivation constant increases below 230 nm; however, the strong absorption of UV light by water at these wavelengths limits germicidal action.

4.6 METHODS TO MEASURE, QUANTIFY, AND MATHEMATICALLY MODEL UV INACTIVATION

Conventional UV inactivation kinetics is obtained by irradiating suspensions of cells in either water or buffer. The UV dose response of microbes is determined by measuring the concentration of microbes capable of replication after exposure to a measured UV dose.

4.6.1 Collimated-Beam Tests

Several approaches may be used to measure microbial dose response (Sommer et al. 1995; Ye et al. 2007). The bench-scale collimated beam (CB) device (Qualls et al. 1983; Kuo et al. 2003) has evolved as a standard method. Laboratory dose-response data from collimated-beam tests are commonly used as a basis for determining the necessary delivered UV dose for full-scale UV systems.

A typical configuration of the CB apparatus is described by Kuo and illustrated in Figure 4.7. It is constructed by housing two low-pressure, low-intensity UV lamps in a

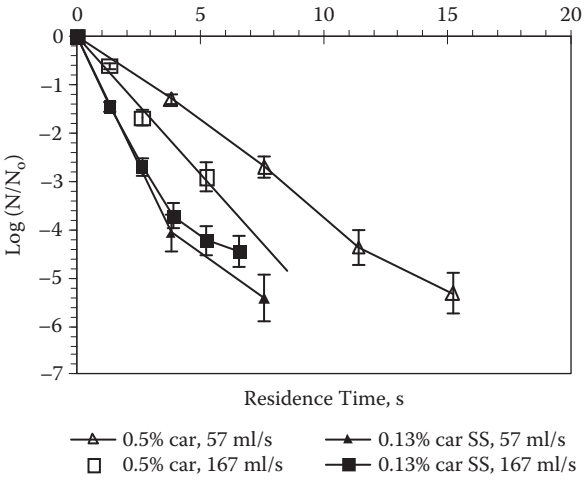

FIGURE 4.7 Comparison of the effects of absorbance and turbidity on UV inactivation of *E. coli* K12 in caramel buffer solutions in a CiderSure 1500 UV reactor. (From Koutchma et al. 2004. With permission.)

horizontal copper pipe ≈50.8 mm in diameter. A tee extends downward from the horizontal pipe to achieve collimation of the UV light, where the collimating tube length-to-diameter ratio is approximately 15. The intensity of UV light is measured at the point of application using a radiometer. Ten millimeters of water sample is placed into a sterilized petri dish of 50-mm ID containing a stir or spin bar. The end of the collimating tube is covered with an opaque sheet of cardboard, and the petri dish is positioned approximately 10 mm from the end of the collimating tube. Mixing is initiated, the cardboard is removed, and the irradiation timer is started simultaneously. After the specified amount of irradiation time, the cardboard is inserted between the collimating tube and the petri dish. An automatic shutter mechanism can alternatively be used instead of the opaque sheet of cardboard.

The UV light can be either 254-nm light from an LPML, bandpass-filtered from an MPML, or monochromatic light from a UV excimer lamp. During UV exposure, the sample is often stirred using an insulated magnetic stirrer plate with a small spin-bar to ensure thorough mixing of the liquid. For a completely mixed liquid sample of a depth d, each liquid sample parcel would receive an average UV intensity that can be determined using equation (4.2).

$$\text{UV Dose} = I_{\text{avg}} t = \frac{I_0 t(1-R)(1-e^{-\alpha_e d})}{\alpha_e d} \tag{4.2}$$

where

I_{avg} = average intensity within suspension (mW/cm^2)
t = exposure time (s)
I_0 = intensity measured at the suspension surface (mW/cm^2)

R = reflection of light at the suspension surface
α_e = Napierian absorption coefficient of the suspension (cm^{-1})
d = suspension depth (cm)

The assays that are used to measure the microbial response to UV light measure the concentration of microbes capable of replicating. They include

- Colony-forming assays to measure the concentration of bacteria within a sample from the UV survivors
- Plaque-forming assays to measure virus within a sample from the UV survivors
- MPN (most probable number) method (among other methods) to determine metabolic response of populations grown from the UV survivors
- Infectivity assays to measure the ability of microbes within a sample from the UV survivors to infect a host

Bench-scale CB tests are typically conducted in a controlled environment. They are much less expensive and time consuming, and can be used to supplement pilot-plant tests. However, even using microbial species and water of similar characteristics, the reported dose-response relationships varied considerably among researchers. One possible cause of the discrepancies is that protocols for collimated-beam tests have not been standardized. Numerous factors may affect the test results to some extent. Potential factors include apparatus setup, column dimensions, UV lamp type and output, intensity measurement, shutter type and operation, petri dish specifications, sample volume and depth of the liquid, mixing condition, laboratory settings, and water temperature as well as the types of microbial organisms/strains, age, and assay methods to quantify the inactivation. The methodology used to calculate the UV dose for collimated beam tests is also a critical factor. To ensure reproducibility or to have a meaningful comparison of results from different collimated-beam tests, a standardized protocol for collimated-beam testing and its dose calculation is necessary. Kuo et al. (2003) started developing a standardized collimated-beam testing protocol for water that would be acceptable by researchers, industries, and regulatory agencies.

4.6.2 Measurement of UV Inactivation Kinetics in Annular Reactors

The CB test procedure is not appropriate for high-absorptive food products such as fresh juices due to a nonuniform fluence in the sample. In addition, the collimated beam is not perfectly parallel. Ye et al. (2007) proposed a novel method to overcome the disadvantages of the traditional CB approach for liquid foods to measure UV inactivation using a single-lamp annular UV reactor.

The schematic diagram of the UV treatment system used in the experiments is shown in Figure 4.8. The thin-film annular reactor used in the study was an UltraDynamics model TF-1535 (Severn Trent Services Inc., Colmar, PA). The system included a UV lamp, protective quartz sleeve, and a remote power supply with a built-in lamp-failure indicator. The single low-pressure mercury UV lamp was

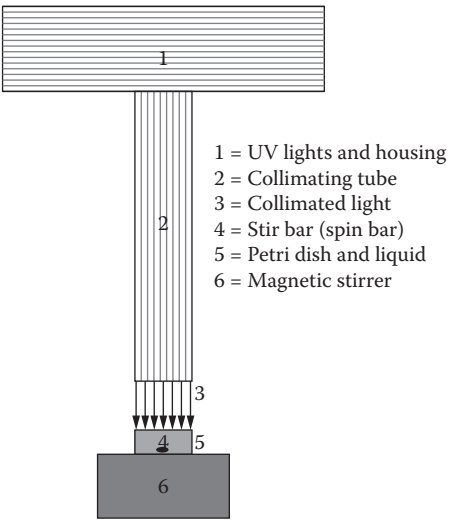

FIGURE 4.8 Typical collimated-beam apparatus.

positioned in a 316 stainless steel reactor chamber. The whole system consisted of three chambers with lengths of 20, 40, and 87.5 cm. All three single-bulb UV reactors were used separately. Each reactor was mounted in the vertical position with the fluid flowing from the bottom to the top in order to fill the annular gap fully and avoid bubbles. Samples for microbial analysis were taken after steady state for both UV lamps and flowing conditions was reached. The flow rate of the pump was varied from 3 to 36 mL/s and was controlled by a shielded flow meter. The range of axial Reynolds number was from 67 to 800 and indicated that the flow pattern in the reactor was within the laminar flow regime.

The test model caramel solutions at concentrations of 0.04%, 0.05%, 0.1%, and 0.2% were inoculated with bacteria, and control samples were taken to measure absorbance and initial microbial concentration. The flow rate was preset, and the solution was pumped into the UV reactors through the inlet. Then the irradiated samples were taken at the outlet after a volume of six times the volumetric average had passed because, according to numerical simulation, 99.51% of fluid held by the UV reactors has exited the system at this time. These two steps were repeated for each flow rate. The flow rates chosen were 3, 6, 12.5, and 36 mL/s. The objective of the study was to characterize resistance of *Yersinia* species to UV treatment using a single-lamp annular UV reactor. *Yersinia pseudotuberculosis* was chosen as a surrogate of *Y. pestis*. *Escherichia coli* K12 (ATCC 25253) was chosen as a reference microorganism to test UV inactivation rate.

The theoretical background of the novel method to measure UV inactivation kinetics was based on the following considerations. The flow of the liquid in the radiation section can be approximated as annular Poiseuille flow. According to the

Navier–Stokes equations of laminar flow for Newtonian fluids, the velocity profile can be computed based on equation (4.3).

$$u(r)=C_1\left[1-\frac{r^2}{R_2^2}+\frac{1-\kappa^2}{\ln(1/\kappa)}\ln\left(\frac{r}{R_2}\right)\right]U_{\text{avg}} \tag{4.3}$$

The steady-state radiative transfer equation (RTE) in a homogeneous medium may be written as equation (4.4)

$$\frac{dI(s,\Omega)}{ds}=-\alpha I(s,\Omega) \tag{4.4}$$

If UV fluence rate varies only in the radial direction,

$$\frac{d(Ir)}{dr}=-\alpha Ir \tag{4.5}$$

For the boundary condition at $I = I_0$ at $r = R_1$, the fluence rate in an annular gap can be approximated by equation (4.6)

$$I(r)=I_0\frac{R_1}{r}\exp[-\alpha(r-R_1)] \tag{4.6}$$

Even when the model caramel solution with the lowest absorption coefficient (2.4 cm^{-1}) was used, the fluence rate on the opposite wall of the incident radiation source was about 4.1% of the incident fluence rate. The maximum fluence rate of radiation that was reflected was only about 0.8% of the incident fluence rate and, therefore, reflected UV was neglected.

Because stream lines of the annular Poiseuille flow are parallel, and axial dispersion and diffusion between neighboring layers are negligible, UV fluence *It* (the product of fluence rate *I* and exposure time *t*) can be described by equation (4.7)

$$It(r)=I(r)L/u(r) \tag{4.7}$$

If UV inactivation kinetics is known as a function of fluence *It*,

$$\frac{N}{N_0}=f(It) \tag{4.8}$$

the average concentration of viable organisms at the outlet of the reactor, N_{avg}, can be obtained by integrating equation (4.9),

$$\frac{N_{\text{avg}}}{N_0}=\frac{\int_0^{2\pi}\int_0^{R_2} f[It(r)]u(r)rdrd\theta}{\int_0^{2\pi}\int_0^{R_2} u(r)rdrd\theta} \tag{4.9}$$

The number of survivors N_{avg} was measured experimentally. The parameters in the inactivation kinetics model were obtained by mathematical methods such as the least-squares method. Compared with the traditional collimated-beam approach, neither the collimated-beam apparatus nor uniform fluence was required in the novel method.

4.6.3 Modeling of UV Inactivation Kinetics

4.6.3.1 First-Order Inactivation Model

Various modeling approaches have been proposed to describe and predict UV inactivation kinetics (Collins and Selleck 1972; Severin et al. 1983; Kowalski 2001). Among them, the first-order inactivation model is the simplest. It assumes that the inactivation rate changes with respect to pathogen concentration, N, and fluence rate, I, such that

$$\frac{dN}{dt} = -k_1 IN \tag{4.10}$$

where k_1 is the first-order inactivation constant in units of cm^2/mJ. The first-order inactivation reaction was also defined as a pseudo-first-order model or a mixed second-order model (Severin et al. 1983; Chiu et al. 1999). If k_1 and I are constant, by integration,

$$\frac{N}{N_0} = \exp(-k_1 It) \tag{4.11}$$

The first-order model was able to reasonably predict microbial inactivation when the fluence was within certain limits. However, the predicted data did not agree well with experiments at low UV fluence levels (Severin et al. 1984). Sigmoidally shaped inactivation curves were often observed and reported (Harris et al. 1987). At first, the value of the first-order inactivation constant is low at relatively low UV fluence. This phenomenon is also referred to as a shouldered survival curve (Harm 1980). The first-order inactivation constant increased with fluence and remained constant within a certain fluence range. Finally, when the fluence was larger than a certain value, the first-order inactivation constant decreased with the increase of UV fluence. This is referred to as a tailing phenomenon.

A lag in microbial inactivation at low levels of UV fluence (the shouldered survival curve) can be observed because microorganisms exposed to a sublethal UV fluence may repair injuries and continue multiplying. The sublethal UV fluence has a slight adverse effect with the analytical procedure to quantify microbial viability. Also, the tailing phenomenon (the decline in the slope of the fluence-log reduction curve) at high UV fluence may be observed. The tailing phenomenon may be attributable to the result of heterogeneity among a population of microorganisms. Some organisms may be relatively less resistant to UV radiation, while other organisms in the same population may be more resistant. Another reason for the tailing effect is the presence of particles such as pulp in fresh juices. Particles may serve as a hiding space for a viable organism or an opaque surface to shade microorganisms from UV radiation.

Because the tailing phenomenon is mostly observed when the log reductions are larger than 5, it is not very important in commercial applications of UV disinfection. Other models, for example, the multitarget (Severin et al. 1983; Kowalski 2001), series-event (Severin et al. 1983), and Collins–Selleck models (Collins and Selleck

1972), were developed to account for deviations from the first-order model at low UV fluence.

4.6.3.2 Series-Event Inactivation Model

As stated before, a lag in microbial inactivation at low UV fluence can be observed for various kinds of microorganisms. The series-event inactivation model was proposed by Severin et al. (1983) to account for the lag at low fluence. It assumes that inactivation of microorganism elements takes place in a stepwise fashion,

$$M_0 \xrightarrow{k_{SE}I} M_1 \xrightarrow{k_{SE}I} \ldots M_i \xrightarrow{k_{SE}I} \ldots M_{n-1} \xrightarrow{k_{SE}I} M_n \xrightarrow{k_{SE}I} \ldots. \quad (4.12)$$

The inactivation rate at each step is of the first order with respect to the fluence rate I,

$$\frac{dN_i}{dt} = k_{SE} I (N_{i-1} - N_i) \quad (4.13)$$

where subscript i is the event level and k_{SE} is the inactivation constant in the series-event inactivation model. The value of k_{SE} is assumed to be the same for different event levels. When n elements (a threshold) of microorganisms have been inactivated, the microorganisms will become nonviable. If k_{SE} and I are constant, the concentration of surviving microorganisms N is determined by equation (4.14)

$$\frac{N}{N_0} = \exp(-k_{SE} It) \sum_{i=0}^{n-1} \frac{(k_{SE} It)^i}{i!} \quad (4.14)$$

where n is a threshold. It is obvious that if $n = 1$, the above equation will be reduced to the first-order model.

The physical meaning behind equation (4.12) is that more than one hit is required for UV inactivation of an individual microorganism. At the beginning of the UV inactivation process (low fluence), the probability of an individual microorganism to obtain n hits (where $n > 1$) is rather low. As the UV inactivation continues, more surviving microorganisms have accumulated $n - 1$ hits and require only one additional hit to be inactivated completely (Harm 1980), so that the inactivation curve becomes steeper with increasing fluence. Larger threshold values of n represent microorganisms that are more resistant at low UV fluence. Figure 4.9 illustrates this trend. The inactivation constants in Figure 4.9 were obtained by fitting the same experimental data of *E. coli* K12 (ATCC 25253) with different thresholds. At low fluence, the first-order model cannot account for the shouldered survival curve and overestimates log reductions. At high fluence, the series-event model predicts higher log reductions than the first-order model. Moreover, the difference of the microbial log reductions between the first-order model and the series-event model increases with an increase in fluence and the threshold. The series-event and the first-order models, however, predict similar log reductions with intermediate fluence values, which are about 14–20 mJ/cm^2.

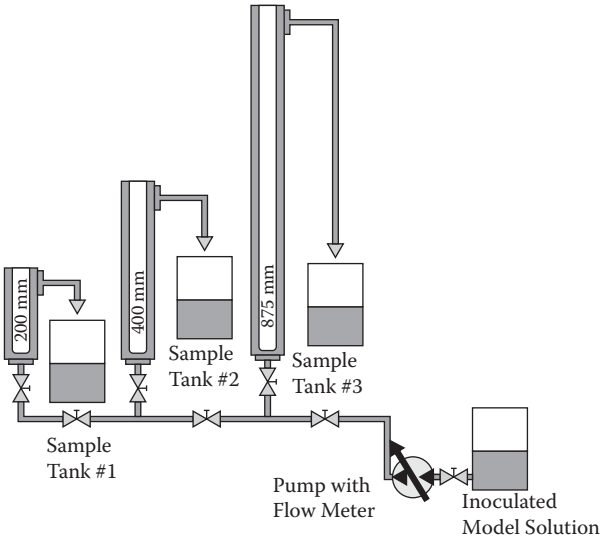

FIGURE 4.9 Schematic diagram of UV-treatment system. (From Ye et al 2007. With permission.)

The shouldered survival curve can be observed in UV inactivation of many types of microorganisms. The first-order model ($n = 1$) was valid only for some viruses whose sensitive material is single-stranded DNA or single-stranded RNA (Harm 1980). For example, it was reported that $n = 1$ for f2 bacterial virus (Severin et al. 1984).

Both the first-order inactivation model and series-event inactivation model (Severin et al. 1983) were used in numerical simulations.

4.6.4 UV Inactivation Kinetics of *E. coli*

4.6.4.1 First-Order Inactivation Model

Figure 4.10 is the comparison of *E. coli* $\log_{10}$ reductions between experiments and fitted data with the first-order inactivation model. The experiments were conducted in different reactors (and, correspondingly, different incident fluence rates) in model solution with different absorption coefficients. After 38 experimental points of *E. coli* K12 inactivation were fitted by the first-order inactivation model, the values of the first-order inactivation constant of *E. coli* K12 $k_1 = 0.325$ cm^2/mJ, with the coefficient of determination $R^2 = 0.907$ and the standard deviation of $\log_{10}$ reductions $\sigma_y = 0.354$, were obtained. The maximum absolute $\log_{10}$ reduction error was 0.929 when the $\log_{10}$ reduction is 5.3. The maximum relative error of $\log_{10}$ reduction was 277% when $\log_{10}$ reduction is 0.17. Because of the shouldered survival curve of *E. coli*, the first-order model overestimates inactivation at low log reduction and underestimates inactivation at high log reduction.

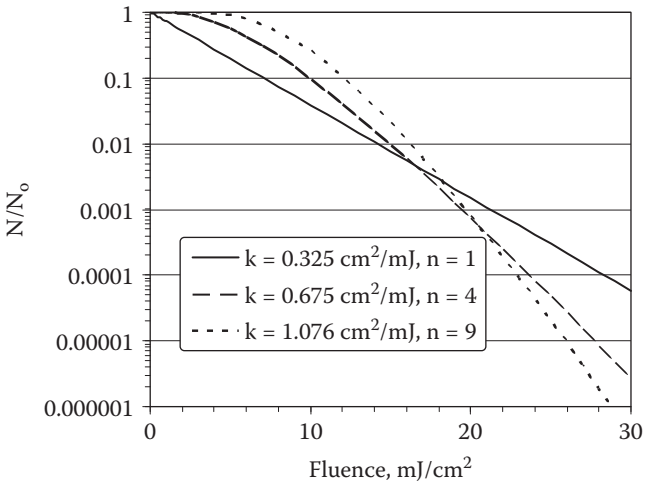

FIGURE 4.10 UV inactivation curves with different thresholds.

The fluence required for 90% inactivation of *E. coli* with the first-order inactivation model is reported in some references (Table 4.5). No names of strains were revealed, and water or wastewater was used in most references. Because of different strains and culturing conditions, it was common that the first-order inactivation constants measured by different authors were not the same. It was reported by Koutchma et al. (2004) that *E. coli* K12 (ATCC 25253) had a lower inactivation rate than *E. coli* O157:H7 (DHS1) and *E. coli* O157:H7 (H3482). The measured value, $k_1 = 0.325$ cm^2/mJ, is similar to the latest value (k_1 = 0.371–0.658 cm^2/mJ), and it is within a reasonable range.

TABLE 4.5
Reported Ultraviolet Decimal Reduction Fluence and Inactivation Constant of *E. coli*

Medium	Fluence Required for 90% Inactivation (mJ/cm^2)	First-Order Inactivation Constant (cm^2/mJ)	Reference
Waste water	2.57	0.893	Severin et al. (1984)
Potable water	2.99	0.77	Wolfe (1990)
Drinking water	3.2	0.72	Cairns (1991)
Drinking water	1.33	1.73	Wilson et al. (1992)
Water	3.5–6.2	0.371–0.658	Taghipour (2004)

Source: Ye et al. (2007).

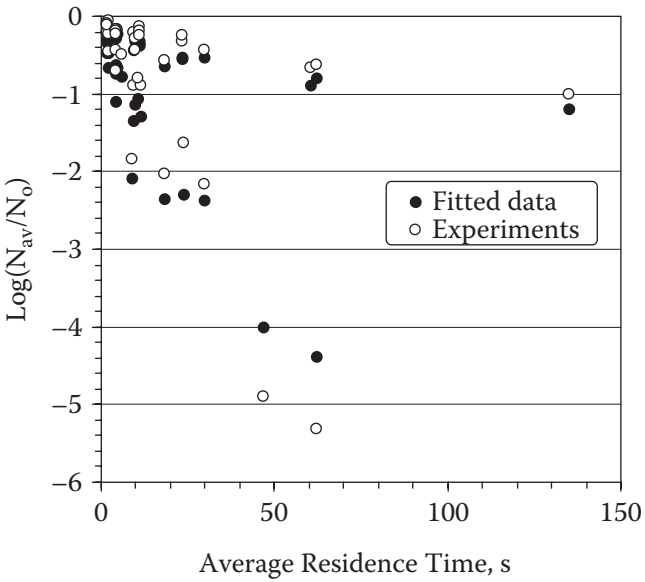

FIGURE 4.11 Comparison of *E. coli* K12 $\log_{10}$ reductions between experiments and fitted data with the first-order inactivation model. (From Ye et al. 2007. With permission.)

4.6.4.2 Series-Event Inactivation Model

As stated before, the first-order model overestimates inactivation at low log reduction and underestimates inactivation at high log reduction. If 38 experimental points of *E. coli* K12 inactivation were fitted by the series-event inactivation model, the values of inactivation constant $k_{SE} = 0.67474$ cm²/mJ and threshold $n = 4$, with $R^2 = 0.987$ and $\sigma_y = 0.133$, were obtained. Figure 4.11 is the comparison of *E. coli* K12 $\log_{10}$ reductions between experiments and fitted data with the series-event inactivation model. The maximum absolute error of $\log_{10}$ reduction is 0.434 when the $\log_{10}$ reduction is 2.1. The maximum relative error of $\log_{10}$ reduction is 72.5% when the $\log_{10}$ reduction is 0.1745.

It was found that compared with the first-order inactivation model, the series-event inactivation model was better suited to fit the experimental data of *E. coli* K12. The R^2 increased from 0.907 to 0.987, and the σ_y decreased from 0.354 to 0.133. Both the maximum absolute error and maximum relative error are decreased. The reason was that the fluence distribution was so broad that it included both low and high fluence, especially when absorption coefficients of the model solutions are high. Therefore, deviation from the first-order model had to be accounted for.

4.6.5 UV Inactivation Kinetics of *Y. pseudotuberculosis*

4.6.5.1 First-Order Inactivation Model

Next, the inactivation tests for *Y. pseudotuberculosis* were conducted in model caramel solutions. After 19 experimental points of *Y. pseudotuberculosis* inactivation

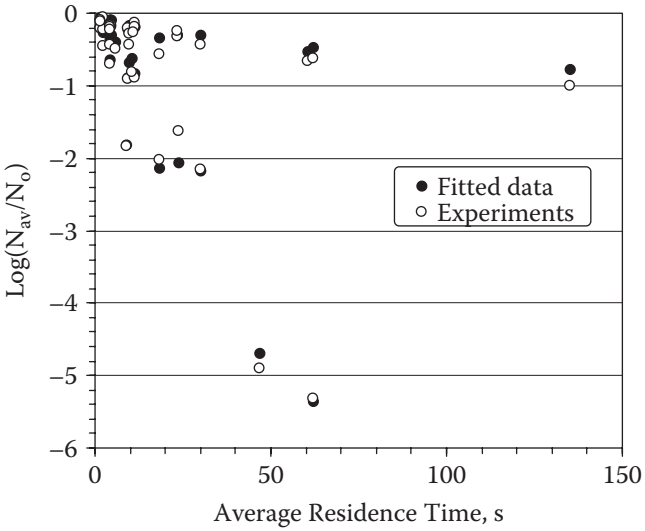

FIGURE 4.12 Comparison of *E. coli* K12 $\log_{10}$ reductions between experiments and fitted data with the series-event inactivation model. (From Ye et al. 2007. With permission.)

were fitted by the first-order inactivation model, the values of the inactivation constant $k_1 = 0.557$ cm^2/mJ, with $R^2 = 0.916$ and $\sigma_y = 0.402$, were obtained. Figure 4.12 is the comparison of *Y. pseudotuberculosis* $\log_{10}$ reductions between experiments and fitted data with the first-order inactivation model. The maximum absolute error of $\log_{10}$ reduction is 1.19 when the $\log_{10}$ reduction was 4.9. The maximum relative error of $\log_{10}$ reduction is 124% when the $\log_{10}$ reduction was 0.41. When these results are compared with the inactivation rate of *E. coli* K12, it is apparent that *Y. pseudotuberculosis* was less resistant to UV light.

No UV inactivation data of *Y. pseudotuberculosis* have been reported in any references. The fluence required for 90% inactivation of *Yersinia enterocolitica*, one of three main *Yersinia* species, with the first-order inactivation model is reported in Table 4.6. It shows that the first-order inactivation constant of *Y. pseudotuberculosis* was of the same order as that of *Y. enterocolitica*.

4.6.5.2 Series-Event Inactivation Model

Figure 4.13 is the comparison of *Y. pseudotuberculosis* $\log_{10}$ reductions between experiments and fitted data with the series-event inactivation model. After 19 experimental points of *Y. pseudotuberculosis* inactivation were fitted by the series-event inactivation model, the values of the inactivation constant $k_{SE} = 0.984$ cm^2/mJ and threshold $n = 3$, with $R^2 = 0.972$ and $\sigma_y = 0.212$, were obtained. The maximum absolute error of $\log_{10}$ reduction is 0.6 when the $\log_{10}$ reduction is 2.5. The maximum relative error of $\log_{10}$ reduction is 34.1% when the $\log_{10}$ reduction is 0.24.

TABLE 4.6
Reported UV Decimal Reduction Fluence and Inactivation Constant of *Y. enterocolitica*

Medium	Fluence Required for 90% Inactivation (mJ/cm²)	First-Order Inactivation Constant (cm²/mJ)	Reference
Drinking water	1.07	2.15	Wilson et al. (1992)
n.d.	0.921	2.5	Hoyer (1998)
Eggshell surface	7647–3342	n.d.	Favier et al. (2001)

Source: Ye et al. (2007).
Note: n.d. = no data available.

As for *E. coli*, the series-event inactivation model was better suited to fit experimental data of *Y. pseudotuberculosis* than the first-order inactivation model. The R^2 increased from 0.916 to 0.927, and the σ_y decreased from 0.402 to 0.212. Both the maximum absolute error and maximum relative error decreased.

4.6.6 UV Inactivation of *Bacillus subtilis* Spores in the Annular UV Reactor

The set of experiments was conducted on UV inactivation of spores using a bench-scale single-lamp UV-disinfection system (120 V, 60 Hz) from Sunlight System/

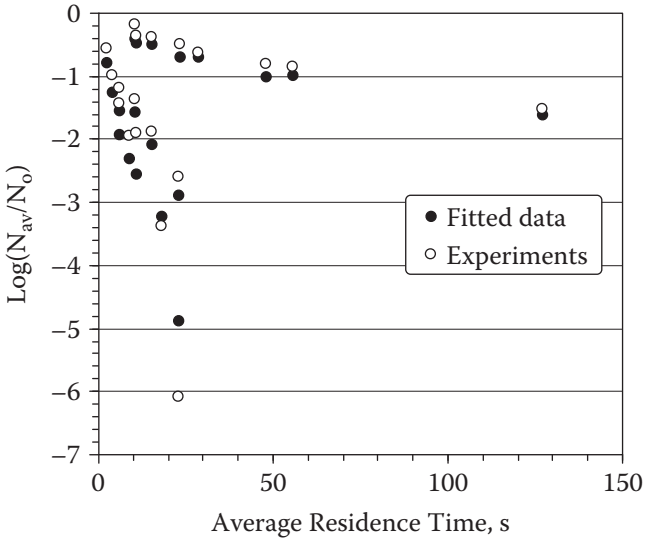

FIGURE 4.13 Comparison of *Y. pseudotuberculosis* $\log_{10}$ reductions between experiments and fitted data with the first-order inactivation model. (From Ye et al 2007. With permission.)

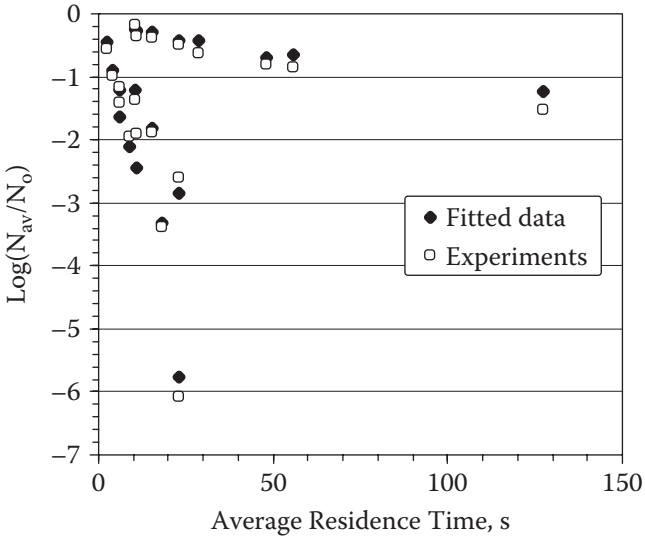

FIGURE 4.14 Comparison of *Y. pseudotuberculosis* $\log_{10}$ reductions between experiments and fitted data with the series-event inactivation model. (From Ye et al 2007. With permission.)

Siemens (Allendale, NJ). The UV setup shown in Figure 4.14 can be assembled with a low-pressure mercury arc lamp, with nominal output power of either 320 or 450 W, mounted within a quartz sleeve running centrally through the chamber and allowing the liquid to pass the sleeve on all sides. Experiments were run with both types of the lamp. The unit had a single chamber covered by a stainless steel cylinder. The viscous liquid food model with absorption coefficient of 0.42 cm^{-1} was pumped through a 1.005-cm annular gap between the inner surface of the chamber and the outer surface of the quartz sleeve, which allowed exposure of a thin film of liquid to UV light. Tests were conducted to determine the level of inactivation of *Bacillus subtilis* ATCC 6633 spores after one pass of the liquid model through the annular reactor. Flow rates varied in the range from 151.2 to 308.7 mL/s to construct a dose-response curve. The inactivation constant of *Bacillus subtilis* was determined by fitting experimental data using first-order and series-event reaction models (Figure 4.15).

The results of computation of inactivation rate constants are summarized in Table 4.7. When eight and nine experimental points of *B. subtilis* inactivation data were fitted by the series-event inactivation model with threshold $n = 4$, the obtained values of the inactivation constant $k_{SE} = 0.094$ and 0.096 cm^2/mJ, with $R^2 = 0.97$ and 0.92; correspondingly, values resulted in the decimal reduction dose of *B. subtilis* spores in the range of 23.86–24.47 mJ/cm^2. The UV dose for a 1-log reduction of *B. subtilis* ATCC 6633 reported by Chang et al. (1985) was 36 mJ/cm^2. Sommer et al. (1989, 1998) reported the dose of 20–22 mJ/cm^2 for a 1-log reduction of this strain. CB procedure was used in both studies. The measured D_{10} dose using an annular UV reactor in a food model system was comparable with earlier reported data.

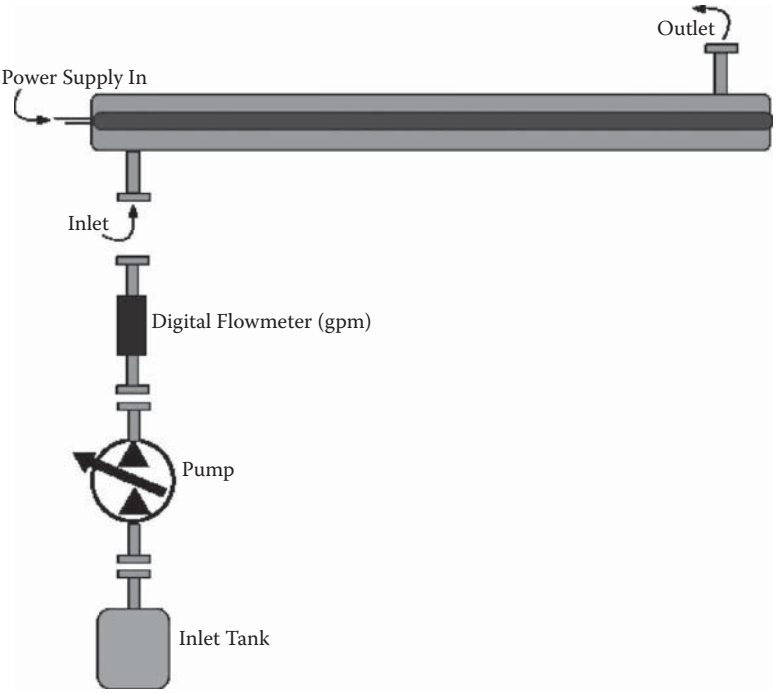

FIGURE 4.15 Bench scale of the annular single-lamp UV reactor experimental setup.

4.7 EFFICACY OF LOW-PRESSURE, HIGH-INTENSITY LAMP FOR INACTIVATION OF FOOD PATHOGEN

Gorlitt (2007) studied the effects of the output power of the low-pressure, high-intensity amalgam lamps (LPAL). Here, the absorbance of model solutions on inactivation of *E. coli* K12 using a bench-scale single-tube annular UV reactor was studied, as described above. The reactor could be assembled with two lamps with nominal output power of either 320 or 450 W. According to the manufacturer (American Ultraviolet Co, Lebanon, MI), 90% of UV output was within the range 233.7–273.7 nm. The lamp warranty is 9000 hours. The lamp arc length is 149 cm, with an OD of 19 mm. The lamp's sleeve is clear fused-quartz circular tubing rated for transmission of 94%.

TABLE 4.7
Inactivation Parameters of *Bacillus subtilis* Spores

Event Level, n	Inactivation Rate, k (cm²/mJ)	Global Min. SSD	R^2	D_{10} (mJ/cm²)
1	0.0204	75.30	–1.21	112.72
4 (9 points)	0.096	1.93	0.92	23.86
4 (8 points)	0.094	0.66	0.97	24.47

After the UV lamps were turned on for 10 min, an IL 1700 Research Radiometer equipped with an SUD240 detector (International Light, Inc., Newburyport, MA) was used to measure the incident irradiation fluence rate. The fluence rate was measured along the entire length of the quartz sleeve and averaged. The obtained value of the average irradiation fluence rate on the surface of the quartz sleeves was 49.7 and 60.4 mW/cm^2 for the 320- and 450-W LPALs, respectively. The measured values were used in the calculations of UV fluence.

A water-caramel-syrup solution with absorption coefficients varied in the range from 1.58 to 4.42 cm^{-1} was used to mimic the absorbance of typical fresh juices. The model solutions were inoculated with *E. coli* K12 and treated by UV light at the flow rates of 15, 38, and 49 mL/s, respectively. The calculated Reynolds numbers were between 104 and 341, indicating the laminar flow regime in the reactor.

The measured inactivation of *E. coli* was compared with the results calculated using the first-order model and the series-event model. Using equations (4.3–4.7), the velocity, residence time, UV fluence rate, and UV fluence distribution along the reactor radius were computed for each flow rate, absorption coefficient, and lamp intensity, and graphical representations are shown in Figure 4.16.

The UV fluence rate attenuation increased with the increase of absorption coefficient from 1.54 to 4.4 cm^{-1}. The nonuniform UV fluence distribution was observed in the annulus of the reactor and was approximately 10 J/cm^2 at the quartz sleeve surface, falling to 0.5 J/cm^2 in the center of the annulus in the model solution with the highest absorption coefficient of 4.45 cm^{-1}.

Figure 4.17 shows the effect of the increase of the absorption coefficient for the model solution on inactivation of K12 when the 320-W output power LPAL was

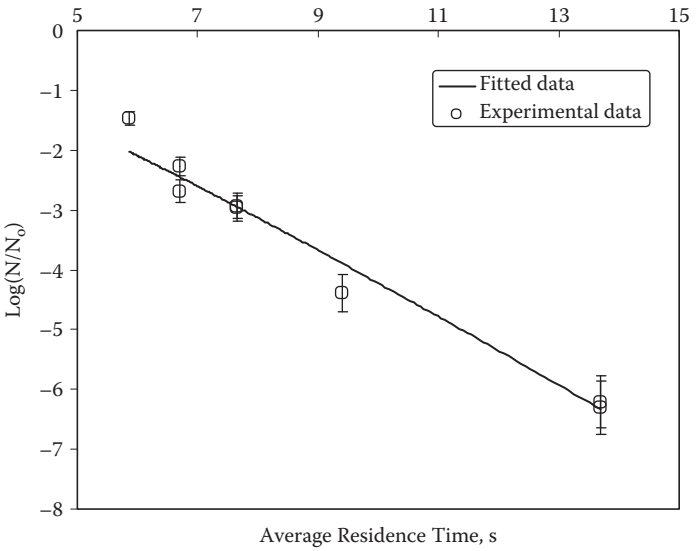

FIGURE 4.16 Inactivation curve of *B. subtilis* spores in the annular UV reactor.

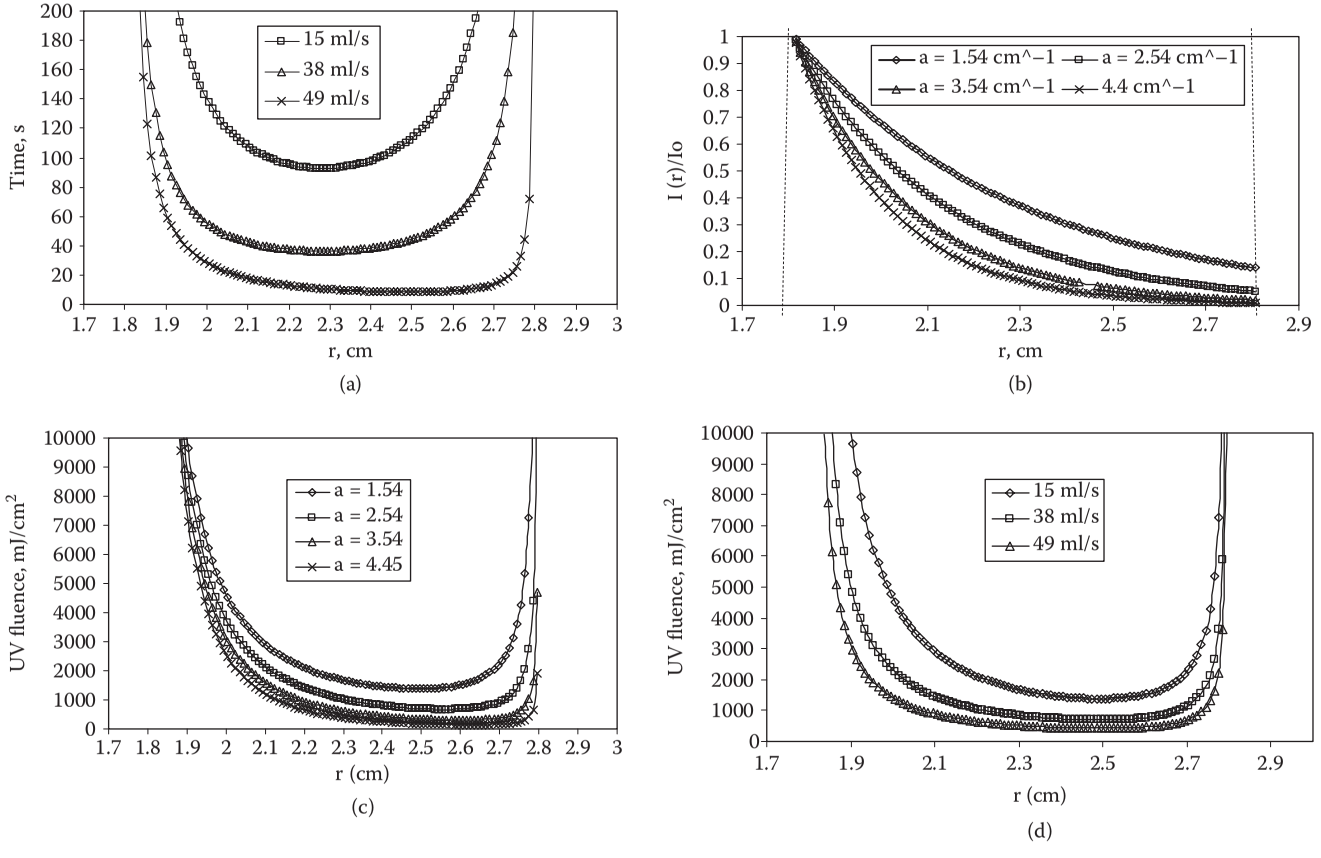

FIGURE 4.17 Distribution of (a) residence time, (b) UV fluence rate, and (c, d) UV fluence in the UV reactor annulus in model caramel solution at $I_0 = 50$ mW/cm^2.

TABLE 4.8
Comparison of Microbial Log Reduction (averaged) for the 320- and 450-W LPAL at 254 nm

Absorption Coefficient @ 254 nm, α (cm^{-1})	Microbial Log Reduction (320 W)	Microbial Log Reduction (450 W)	Δ Microbial Log Reduction
1.58 ± 0.043	4.33 ± 0.45	4.46 ± 0.33	0.13
2.56 ± 0.02	3.49 ± 0.04	3.51 ± 0.25	0.02
3.20 ± 0.014	1.72 ± 0.2	2.28 ± 0.24	0.56
3.52 ± 0.02	1.16 ± 0.25	2.06 ± 0.3	0.9
3.98 ± 0.02	1.35 ± 0.24	1.41 ± 0.13	0.06
4.42 ± 0.01	1.06 ± 0.3	1.17 ± 0.25	0.11

installed in the UV reactor. The higher the absorption coefficient of the solution, the lower is the microbial log reduction of *E. coli*. With an absorption coefficient of 1.55 cm^{-1}, a microbial log reduction of 4.7 was achieved, whereas the increase of the absorption coefficient to 4.4 cm^{-1} reduced the microbial log reduction to 1.0. When the 450-W LPAL was installed, a similar microbial inactivation efficiency was found. At the absorption coefficient of the model solution of $\alpha = 1.54$ cm^{-1}, a 4.7-log reduction was measured compared with a 1.2-log reduction at $\alpha = 4.45$ cm^{-1}. The comparison of inactivation parameters at tested absorption coefficients is summarized in Table 4.8. The experiment at each absorption coefficient was run in triplicate.

The difference in microbial inactivation between 320- and 450-W LPALs did not achieve more than 0.56 log for all tested model solutions. The largest difference in inactivation of *E. coli* K12, equal to 0.9 log, was found in the model solution with an absorption coefficient of 3.52 cm^{-1}. A one-way ANOVA statistical analysis confirmed that there was no significant difference ($\alpha = 0.05$) in inactivation performance between lamps in the range of absorbencies tested except for $\alpha = 3.524$ cm^{-1}. In addition, the first-order model and the series-event model were evaluated for prediction of inactivation of *E. coli* K12 in the UV reactor. The inactivation rate constant $k = 0.325$ cm^2/mJ reported by Ye et al. (2007) was used in calculations. After comparison of predicted data with experimental results, it was evident that both the models underestimated microbial inactivation. However, the first-order model was found to be more accurate for the prediction of LPAL at 320-W output power in the range of absorption coefficients of 2.6–3.5 cm^{-1}.

Figure 4.18 shows the performance of the first-order inactivation model in predicting log reduction of *E. coli* K12 when a 320-W UV source was used. Based on the comparison of predicted performance, both the first-order and series-event models can be used to calculate microbial inactivation for a range of absorbencies of model solutions tested. However, the models have to be validated to predict inactivation in food matrices, taking into account the physical and chemical properties of real foods.

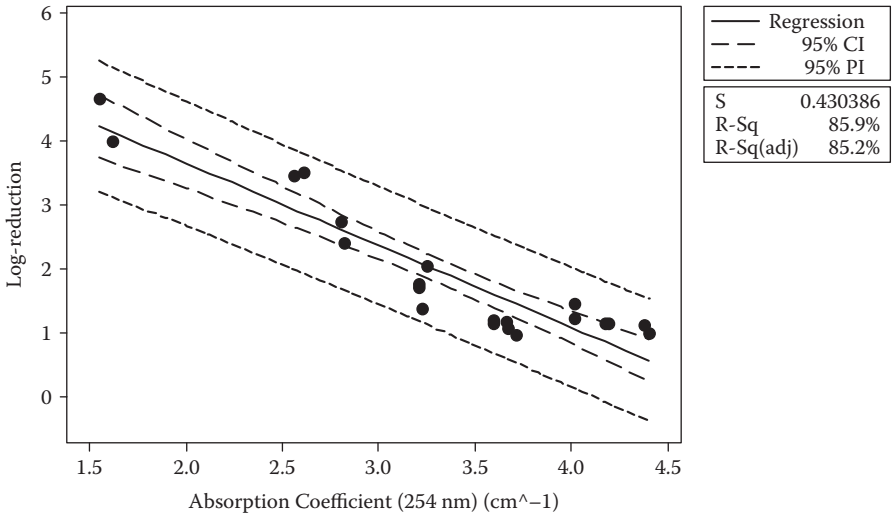

FIGURE 4.18 Effect of absorption coefficient of the model solution upon inactivation of *E. coli* K12 achieved in the single-lamp UV reactor with the 320-W LPAL.

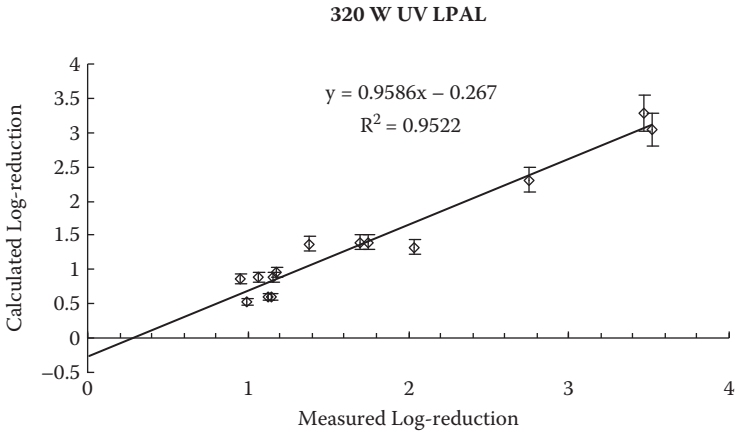

FIGURE 4.19 Comparison of experimental and calculated reduction of *E. coli* using first-order reaction model.

4.8 CONCLUSIONS

Although there have been numerous studies published on inactivation of microorganisms by UV light, the most-resistant microorganisms of public-health significance have not yet been fully determined. Bacterial spores and viruses appear to be the most resistant forms; however, they may not be of concern when water, fruit

juices, or other beverages are the products undergoing treatment. UV treatment does not demonstrate linear inactivation kinetics. Initial treatment damages or injures cells, as demonstrated by a shoulder in the inactivation curve. Rapid inactivation is often followed by a tailing of survival. Some of the tailing effect can be explained by shielding effects of the microbes in the food matrix. Within a given food product, several factors can influence the delivery of the UV dose. The presence of particles could provide a means of shielding microorganisms from the UV irradiation. The single factor found to consistently affect the efficacy of UV-light inactivation in a liquid system was absorbance. Changes and variations in UV absorbance of food products should be considered. However, a simple absorbance reading may prove inadequate to predict the microbial destruction within most juice systems.

A novel method to measure inactivation kinetics using annular reactors was proposed for use in measuring inactivation rate constants in liquid foods. The novel method can overcome the disadvantages of the traditional collimated-beam approach for high-absorptive liquids.

Moreover, since many UV devices in industry are continuous-flow annular reactors, the parameters of inactivation kinetics obtained from the novel method may be more reliable and accurate. Both first-order and series-event inactivation models can be used to predict microbial inactivation in high-absorptive fluids. However, these models should be combined with knowledge of other factors, such as the physical and chemical properties of the real liquid foods and beverages.

REFERENCES

Abughararah, Z. 1994. Effect of temperature on the kinetics of wastewater disinfection using ultraviolet radiation. *J. Environ. Sci. Health A* 29: 585–603.

Cairns, B. 2006. UV dose required to achieve incremental log inactivation of bacteria, protozoa and viruses. *IUVA News* 8 (1): 38–45.

CDC. 2000. Surveillance for foodborne disease outbreaks: United States, 1993–1997. *Morbidity and Mortality Weekly Reports*. 49: 1–51.

Chang, J. C. H., S. F. Ossoff, D. C. Lobe, M. H. Dorfman, C. M. Dumais, R. G. Qualls, and J. D. Johnson. 1985. UV inactivation of pathogenic and indicator microorganisms. *Appl. Environ. Microbiol*. 49 (1): 361–1365.

Chiu, K., D. A. Lyn, P. Savoye, and E. R. Blatchley. 1999. Effect of UV system modification on disinfection performance. *J. Environ. Eng.* 125: 7–16.

Collins, H. F., and R. E. Selleck. 1972. Process kinetics of wastewater chlorination. SERL Report. University of California, Berkeley, 72–75.

Downey, D., D. K. Giles, and D. Delwiche. 1998. Development and validation: Biologic efficacy of UV reactors against water. *Trans. ASAE* 41: 849–867.

Duffy, S., J. Hurey, R. W. Worobo, and D. W. Schaffner. 2000. Analysis and modeling of the variability associated with UV inactivation of *Escherichia coli* in apple cider. *J. Food Prot*. 63: 1587–1590.

Favier, G., M. Escudero, and A. DeGuzman. 2001. Effect of chlorine, sodium chloride, trisodium phosphate and ultraviolet radiation on the reduction of *Yersinia enterocolitica* and mesophilic aerobic bacteria from eggshell surface. *J. Food Prot*. 64: 1621–1623.

Gorlitt, M. 2007. Experimental and theoretical evaluation of performance of the single-tube annular UV reactor for high absorptive liquid models. Master of Science in food process engineering, Illinois Institute of Technology, Chicago.

Hanes, D. E., P. A. Orlandi, D. H. Burr, M. D. Miliotis, M. G. Robi, J. W. Bier, G. J. Jackson, M. J. Arrowood, J. J. Churey, and R. W. Worobo. 2002. Inactivation of *Cryptosporidium parvum* oocysts in fresh apple cider using ultraviolet irradiation. *Appl. Environ. Microbiol*. 68: 4168–4172.

Harm, W. 1980. *Biological effects of ultraviolet radiation*. Cambridge, U.K.: Cambridge University Press.

Harris, G. D., V. D. Adams, D. L. Sorensen, and M. S. Curtis. 1987. Ultraviolet inactivation of selected bacteria and viruses with photoreactivation of the bacteria. *Water Res.* 21: 687–692.

Hijnen, W. A. M., E. F. Beerendonk, and G. J. Medema. 2006. Inactivation credit of UV radiation for viruses, bacteria and protozoan (oo)cysts in water: A review. *Water Res*. 40: 3–22.

Jagger, J. 1967. *Introduction to research in UV photobiology*. Englewood Cliffs, N.J.: Prentice Hall.

Koutchma, T., S. Keller, B. Parisi, and S. Chirtel. 2004. Ultraviolet disinfection of juice products in laminar and turbulent flow reactors. *Innovative Food Sci. Emerging Technol.* 5: 179–189.

Kowalski, W. J. 2001. Design and optimization of UVGI air disinfection system. PhD thesis, Pennsylvania State University.

Kuo, J., C. Chen, and M. Nellor. 2003. Standardized collimated beam testing protocol for water wastewater ultraviolet disinfection. *J. Environ. Eng*. 129: 773–779.

Linden, K., and L. Darby. 1998. Ultraviolet disinfection of marginal effluents: Determining UV absorbance and subsequent estimation of UV intensity. *Water Environ. Res.* 70: 214–223.

Linden, K., J. Thurston, R. Schaefer, and J. Malley. 2007. Enhanced UV inactivation of adenovirus under polychromatic UV lamps. *Appl. Environ. Microbiol*. 73: 7571–7574.

Loge, F., R. Emerick, M. Heath, J. Jacangelo, G. Tchobanoglous, and J. Darby. 1996. Ultraviolet disinfection of secondary wastewater effluents: Prediction of performance and design. *Water Environ. Res*. 68: 900–916.

Mead, P. S., L. Slutsker, V. Dietz, L. F. McCaig, J. S. Breese, C. Shapiro, P. M. Griffin, and R. V. Tauxe. 1999. Food-related illness and death in the United States. *Emerging Infectious Diseases* 5: 607–625.

Murakami, E., L. Jackson, K. Madsen, and B. Schickedanz. 2006. Factors affecting the ultraviolet inactivation of *Escherichia coli* K12 in apple juice and a model system. *J. Food Process Eng*. 29: 53–71.

Oteiza, J., M. Peltzer, L. Gannuzzi, and N. Zaritzky. 2005. Antimicrobial efficacy of UV radiation on *Escherichia coli* O157:H7 in fruit juices of different absorptivities. *J. Food Prot*. 68: 49–58.

Qualls, R. G., M. P. Flynn, and J. D. Johnson. 1983. The role of suspended particles in ultraviolet disinfection. *J. WPCF* 55: 1280–1285.

Quintero-Ramos, A., J. J. Churey, P. Hartman, J. Barnard, and R. W. Worobo. 2004. Modeling of *Escherichia coli* inactivation by UV irradiation at different pH values in apple cider. *J. Food Prot*. 67: 1153–1156.

Severin, B. F., M. T. Suidan, and R. S. Engelbrecht. 1983. Kinetic modeling of UV disinfection of water. *Water Res.* 17: 1669–1678.

Severin, B. F., M. T. Suidan, B. E. Rittmann, and R. S. Engelbrecht. 1984. Inactivation kinetics in a flow-through UV reactor. *J. WPCF* 56: 164–169.

Shama, G. 1992. Ultraviolet irradiation apparatus for disinfecting liquids of high ultraviolet absorptivities. *Lett. Appl. Microbiol*. 15: 69–72.

Shama, G. 2007. UV disinfection in the food industry. *Controlled Environments* 10 (4): 10–15. http://www.cemag.us/articles.asp?pid=668.

Sommer, R., A. Cabaj, T. Sandu, and M. Lhotsky. 1999. Measurement of UV radiation using suspensions of microorganisms. *J. Photochem. Photobiol*. 53 (1–3): 1–5.

Sommer, R., A. Cabaj, D. Schoenen, J. Gebel, A. Kolch, A. Havelaar, and F. Schets. 1995. Comparison of three laboratory devices for UV-inactivation of microorganisms. *Water Sci. Technol*. 31 (5–6): 147–156.

Sommer, R., M. Lhotsky, T. Haider, and A. Cabaj. 2000. UV inactivation, liquid-holding recovery, and photoreactivation of *Escherichia coli* O157 and other pathogenic *Escherichia coli* strains in water. *J. Food Prot*. 63: 1015–1020.

Sommer, R., G. Weber, A. Cabaj, J. Wekerle, G. Keck, and G. Schauberger. 1989. UV inactivation of microorganisms in water. *Zentralbl. Hyg*. 189: 214–224.

Taghipour, F. 2004. Ultraviolet and ionizing radiation for microorganism inactivation. *Water Res.* 38: 3940–3948.

U.S. FDA. 2000. Kinetics of microbial inactivation for alternative food processing technologies. Institute of Food Technologists. *J. Food Sci. Suppl*. http://vm.cfsan.fda.gov/~comm/ift-pref.html.

Wiedenmann, A., B. Fischer, U. Straub, C.-H. Wang, B. Flehmig, and D. Schoenen. 1993. Disinfection of hepatitis A virus and MS-2 coliphage in water by ultraviolet irradiation: Comparison of UV-susceptibility. *Wat. Sci. Tech*. 27: 335–338.

Wilson, B. R., P. F. Roessler, E. VanDellen, M. Abbaszadegan, and C. P. Gerbal. 1992. Coliphage MS2 as a UV water disinfection efficacy test surrogate for bacterial and viral pathogens. Paper presented at 1992 Water Quality Technology Conference. Toronto, May 1992.

Wolfe, R. L. 1990. Ultraviolet disinfection of potable water. *Environ. Sci. Technol*. 24: 768–773.

Wright, H. B. 2000. Comparison and validation of UV dose calculations for low- and medium-pressure mercury arc lamps. *Water Environ. Res*. 72: 439.

Ye, Z., T. Koutchma, B. Parisi, J. Larkin, and L. Forney. 2007. Ultraviolet inactivation kinetics of *E. coli* and *Y. pseudotuberculosis* in annular reactors. *J. Food Sci.* 72 (5): E271–E278.

5 UV Processing Effects on Quality of Foods

The UV light in food processing is typically used to prolong the shelf life of food products or to reduce health hazards associated with certain products due to the presence of pathogenic microorganisms. The treatments may be applied for different purposes, as was discussed in the previous chapters. These may include prolongation of the shelf life and prevention of food-borne diseases in fresh juices, drinks, and other beverages; in fresh produce, meat, poultry, and seafood; and in retardation of ripening and aging of fruit and vegetables. This chapter presents background information on the photodegradation in foods during UV-light processing. It starts with a brief overview of the kinds of photochemical processes involved in the photodegradation of organic molecules. Recent papers are reviewed to illustrate the effect of UV light on different groups of foods from the point of view of quality and nutritional aspects. This review includes information on the susceptibility of certain vitamins to degradation by UV light that may occur during treatments of fresh juices and milk. Information is provided on the possible formation and degradation of chemical compounds that may present a health threat occurring from the UV treatment of foods.

5.1 BASIC CONSIDERATIONS

The effects of UV light on food quality are measured in two major ways. The first way involves an evaluation of the organoleptic qualities of the food or sensory evaluation involving taste, smell, appearance, and texture by trained food-tasting panels. The second one involves physical and chemical measurements, including spectrophotometric measurement of color, pH, chemical analysis of vitamin content, etc. Foods vary enormously in their sensitivity to light. Heiss and Radtke (1968) categorized a number of foods into four groups on the basis of their ability to maintain their organoleptic qualities under continuous exposure to 500 lux of daylight fluorescent light. The most sensitive group includes sour cream, whipped cream, dried vegetable soups, butter, margarine, milk, and mayonnaise. The foods in this group developed off-flavors after a few hours of exposure. Sugar, cookies, cheese, chocolate, fat bacon, raw sausage, green peas, and salted peanuts deteriorated in 24–70 h. Rice, potato chips, and soft caramels showed changes in 4 to 7 days. The least-sensitive group—egg noodles, almonds, and yellow peas—required exposures ranging from 10 to more than 30 days. A number of variables are involved in addition to the inherent light sensitivity of the food. This includes the light intensity in the spectral band effective on a given food, the optical properties of packaging, the level of light exposure, the oxygen concentration in the food, and temperature.

5.2 CHEMISTRY OF THE PHOTODEGRADATION OF ORGANIC COMPOUNDS

Photochemical reactions can be initiated in two ways. The first category of reactions, termed *direct*, is based on the central principal of photochemistry: absorption of a photon of light by a molecule can produce a chemical reaction and change. The extent of chemical reaction depends upon the quantum yield and fluence of incident photons. A quantum yield is a ratio of absorbed photons that cause a chemical change to the total absorbed photons. UV light at 253.7 nm has a radiant energy of 112.8 kcal/Einstein (one Einstein represents one mole of photons). It is theoretically possible for 253.7-nm light to affect the O-H, C-C, C-H, C-N, H-N, and S-S bonds if it is absorbed.

In the other category, termed *photosensitized*, the action of one component in the system causes some other component to undergo reaction because of light. The kinds of processes that occur in direct photochemical reactions depend on the wavelength (photon energy) of the light and the structure of the absorbing molecule. After absorbing a photon, a molecule is raised to an electronically excited level and undergoes a photochemical process that can include dissociation into radicals, decomposition into molecular products, isomerization, dimerization, and ionization. Typically, the reactive intermediates, such as radicals and ions, react further in the thermal process to give the final products.

The most common type of photosensitizing reaction is photooxidation. Typically, photosensitizers are excited from the ground state to a short-lived singlet excited state that undergoes conversion to a long-lived triplet state that mediates the process. The triplet sensitizer can react further by two major pathways: by hydrogen- or electron-transfer processes (free radical) or by energy-transfer reactions. Hydrogen peroxide or superoxide anion, as produced in type-one reactions, also reacts with many kinds of molecules.

Nucleic acids are the strongest 253.7-nm light absorbers. Only the purine and pyrimidine bases on the nucleic acid strands absorb, and the polymeric backbone does not absorb. At 253.7 nm, only compounds containing conjugated bonds, such as aromatic-ring and double-ring molecules, plus compounds containing disulfide bonds are effective absorbers. Approximately 10% of the proteins contain aromatic amino acids and amino acids with disulfide bonds, and UV-light absorption is confined to only that percentage. It is usually stated that the following nutrients are "light sensitive": vitamin A, carotenes, cyanobalamin (vitamin B_{12}), vitamin D, folic acid, vitamin K, riboflavin (vitamin B_2) tocopherols (vitamin E), tryptophan, and unsaturated fatty acid residues in oils, solid fats, and phospholipids (Spikes 1981). It has been reported in the literature that vitamin D is photochemically altered by UV light. The superoxide radical reacts with vitamin K. Light at 350 to 750 nm had no significant effect on ascorbic acid in pure solution. However, at 254 nm, ascorbic acid is a strong absorber of UV light. It must be emphasized that the nutrients identified above differ greatly in their basic photosensitivity and in the wavelength of the light involved. Some are quite stable in the absence of photosensitizers. In addition to nutrients, certain food pigments are also light sensitive. Photodegradation of organic compounds that are usually important in foods were studied in simple

model solutions under laboratory conditions. Thus, the conclusions and results of these findings may not always reflect the reactions that might occur in the much more complex mixtures represented by foods.

In general, only unsaturated organic molecules absorb at wavelengths greater than 220 nm. The longer the conjugated chain in the molecule, the longer is the wavelength of maximum absorption. Aromatic heterocyclic molecules, such as the nucleic acid bases and the aromatic amino acids (phenylalanine, tryptophan, and tyrosine), absorb strongly at 254 nm. In some cases, the absorption spectrum extends well above 300 nm.

Carbohydrates are not especially sensitive to light; they do not absorb appreciably and thus are not directly sensitive. In the presence of certain type-one photosensitizers, hexiols (e.g., sorbitol) are photooxidized to the corresponding hexoses and hexonic acids. Singlet oxygen and hydroxyl radicals can produce some sensitized photoreactions, which can result in the photochemical depolymerization of polysaccharides in foods, producing softening in fruits and vegetables.

Spikes (1981) reported that UV light accelerates oxidative changes in fats and oils. Three of the amino acids (histidine, phenylalanine, and tryptophan) that are considered as essential for human health are degraded by UV light. Moreover, UV light causes the degradation of proteins in complex reactions that lead to changes in solubility, sensitivity to heat, mechanical properties, and digestion by proteases. It is also possible that the photodegradation of proteins might alter their physical properties sufficiently to result in detectable organoleptic changes and off-flavors, for example in milk.

Foods have characteristic colors, depending on the presence of natural pigments and artificial colorants. Many of these food colorants can be altered upon exposure to light, leading to changes in the colors of foods. Examples of such changes are presented in the following sections, which discuss UV processing of various groups of foods. Some pigments in real foods synthesize the photooxidative degradation of many kinds of nutrients in foods. In contrast, some food compounds protect other components against these changes. For example, tocopherols can act as protective agents against photodegradative processes (Spikes 1981).

5.3 SHELF LIFE AND QUALITY CHANGES IN FRESH JUICES

Fresh juices are popular beverages in the world market. They are perceived as wholesome, nutritious, all-day beverages. For items such as juices or juice beverages, minimal processing techniques are expected to be used to retain fresh physical, chemical, and nutritional characteristics with extended refrigerated shelf life. The overall quality parameters that are typically controlled include soluble solids content (°Brix), pH, acid content, turbidity, and color. There are only a few recently published studies that have examined the effects of UV light on flavor, color, and nutrient content of fresh juices, including apple juice/cider, orange juice, and mango nectar.

Tandon et al. (2003) conducted a comparison study of the effect of hot-fill pasteurization at 63°C and UV irradiation at 14 mJ/cm^2 on the quality and shelf life of apple cider. UV irradiation of cider was carried out using a CiderSure model 3500 UV unit (FPE Inc., Rochester, NY). The processed cider was stored at 7°C for up

to 14 weeks in the first study and 4 weeks in the second. The authors did not find significant differences among the fresh processed ciders with regard to taste and preference. The sensory tests confirmed the results obtained from the analytical and microbiological evaluation: Similar quality was observed at the beginning of the storage study, but quality significantly declined after that due to fermentation of the UV-treated samples. The scores for preferences and the average ranking showed no statistical differences between UV and thermal pasteurization at week 0. However, the UV samples did not maintain this quality after 1 week of storage. The authors concluded that an extended shelf life of more than 12 weeks without the use of chemical preservatives can be achieved if the apple cider is produced from healthy apples under sanitary conditions followed by hot fill. The effects of UV-light processing and hot-fill treatment on nutrient contents, e.g., for some essential vitamins, were not reported in this study.

Tran and Farid (2004) reported the results of UV treatment of reconstituted orange juice. In addition to the decimal-reduction dose for the standard aerobic plate count, effects on shelf life, pH, color, vitamin C, and degradation of pectin methylesterase (PME) enzyme were studied. The shelf life of fresh-squeezed orange juice was extended to 5 days as a result of limited exposure of UV light of 73.8 mJ/cm^2. The color and pH of the orange juice were not significantly impacted. The measured degradation of vitamin C was 17% under UV exposure of 100 mJ/cm^2, which was similar to that found in thermal treatment. No degradation of PME (5%), which is a major cause of cloud loss of juices, was reported, whereas the activity of this enzyme was significantly decreased (70%) by mild heat treatment at 70°C for 2 s.

Guerrero-Beltrán and Barbosa-Cánovas (2006) studied the inactivation of *Saccharomyces cerevisiae* and polyphenoloxidase activity (PPO) in mango nectar (pH of 3.8, 13.0°Brix) treated with UV light. A single low-pressure mercury UV lamp (LPML, 25 W at 254 nm) continuous system was used in the study over a range of flow rates from 0.073 to 0.45 L/min. Decimal-reduction values for PPO activity in UV-light-processed mango were reported between 299,100 and 235,000 mJ/cm^2 for the range of flow rates studied. The remaining PPO activity after 30-min treatment at a flow rate of 0.45 L/min was approximately 19%. UV-treated mango nectar maintained yellow and orange-yellow colors for 26 days of storage. PPO activity remained constant after 30 days of storage.

Noci et al. (2008) investigated the influence of UV irradiation, pulsed electric fields (PEF), and heat treatment at 72°C and 94°C on microbial inactivation, selected quality attributes (color, pH, °Brix, nonenzymatic browning index [NEBI]), antioxidant capacity, and enzymatic activity of polyphenol oxidase (PPO) and peroxidase (POD) of fresh apple juice. Exposure of the juice to UV was performed under batch conditions. Freshly squeezed apple juice (800 mL) was distributed as a thin layer in sterile Pyrex oven dishes (25-cm diam.) and then exposed to a 30-W UV-light source. The greatest decrease ($p < .05$) in total phenolic compounds compared with fresh juice was caused by both heat treatments, and such decrease was greater ($p < .05$) than that observed in juices processed by PEF alone or in combination with UV. Compared with the fresh juice, the level of total phenolic compounds was significantly decreased ($p < .05$) in apple juice treated by UV, although the magnitude of this decrease was less than that observed in juices processed by heat. The relative

antioxidant capacity was not affected by either UV, PEF, UV + PEF, or PEF + UV, as no difference was observed compared with fresh juice. However, it was reported that processing the juice by heat at 94°C had a significant effect ($p < .05$) in reducing the relative antioxidant capacity compared with fresh juice, and the observed value was significantly lower ($p < .05$) than those in juices processed by PEF, UV + PEF, or PEF + UV. The relative activity of PPO and POD observed after applying heat at 72°C was higher than in samples processed by PEF, UV + PEF, or PEF + UV. Relative to fresh juice, PPO and POD were unaffected by UV, but they were significantly decreased ($p < .05$) by PEF. The color analysis revealed significant differences only between fresh juice and heat-processed juices. It was concluded that the quality attributes measured in juice processed by PEF or by the combined approach with UV were similar to those observed in juice treated by the milder heat process (72°C) and consistently superior when compared with the severe heat treatment (94°C), with the exception of enzyme inactivation. These results indicated the potential for the use of these technologies for processing freshly squeezed apple juice.

5.4 EFFECTS OF UV LIGHT ON DEGRADATION OF ESSENTIAL VITAMINS

Vitamins, even though they may be present in small amounts in fresh juices, are of concern because some vitamins, as was discussed earlier, are considered light sensitive. Water-soluble, light-sensitive vitamins include C (ascorbic acid), B_{12} (cobalamin), B_6 (pyridoxine), B_2 (riboflavin), and folic acid. Fat-soluble, light-sensitive vitamins include A, K, E (alpha-tocopherol), and carotene. Most studies were conducted on the effects of light on vitamins in the wavelength range of 290 to 700 nm, which includes both UV and visible light. They have involved exposure to fluorescent lamps, but there are little data available at 254 nm.

Ye et al. (2007) measured the physicochemical properties of three commercial brands of apple juices, including soluble solids content, pH, color (*L*, *a*, and *b* values), and vitamin C content before (see Table 3.2) and after UV treatment. Three brands of packaged apple juice (pasteurized, no preservatives) were purchased locally and stored at 4°C for the trial. Sahara Burst and Gordon Food Service brands were enriched with vitamin C. The UV-treatment system used in the experiments was described by Ye (2007). The whole system consisted of four chambers with lengths of 87.5, 87.5, 40, and 20 cm with a single LPML bulb at output power of 25 W and 254 nm. The *L*-values of juices were correlated directly with measured values of absorption coefficients; the higher the *L*-value, the higher was the observed absorption coefficient of apple juice. Approximately 50% degradation of vitamin C was observed after one complete pass through the system at the slowest flow rate.

Because vitamin C is characterized by high UV absorbance within the germicidal wavelength range (peak at approximately 260 nm) but does not absorb light significantly above 300 nm, the contents of vitamin C also affected the absorption coefficient. The relationship between vitamin C concentration in model solution and absorbance at 254 nm is shown in Figure 5.1.

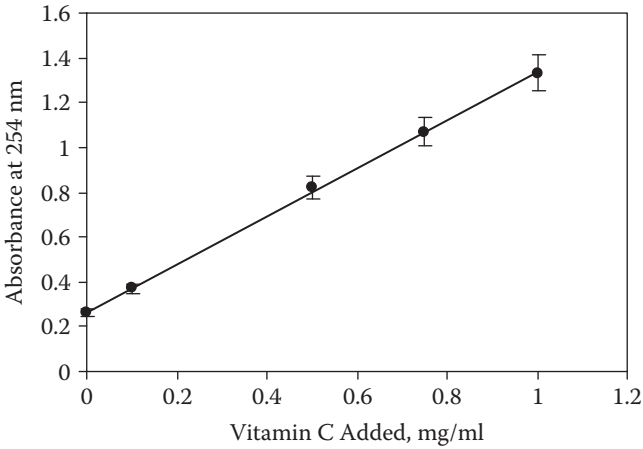

FIGURE 5.1 Relationship between vitamin C content in model buffer solution and absorbance at 254 nm.

The degradation of vitamin C during exposure to UV light may alter the absorption properties of treated juice. The effect of vitamin C degradation on the value of the absorption coefficient in apple juice enriched with this vitamin was measured. After three passes through the UV reactor at a flow rate of 4 mL/s, the absorption coefficient of apple juice was reduced to approximately 20% of its initial value, as demonstrated in Figure 5.2. By this means, it was concluded that juices enriched with vitamin C require significantly higher doses of UV irradiation for pasteurization purposes.

The degradation kinetics of vitamin C in clear apple juice enriched with ascorbic acid at concentrations levels from 34.1 mg/100 mL up to 66 mg/100 mL is shown in

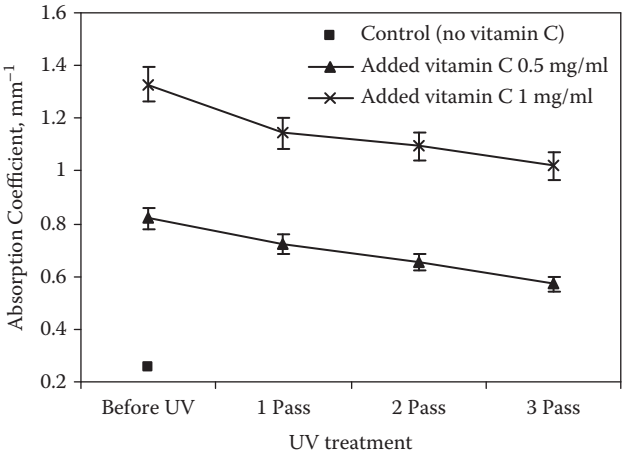

FIGURE 5.2 Effect of degradation of vitamin C on absorption coefficient of apple juice.

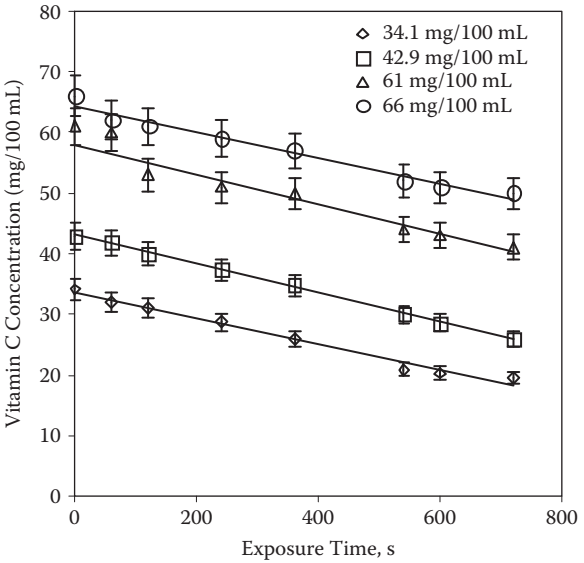

FIGURE 5.3 Degradation of vitamin C in clear apple juice after exposure to UV light at fluence rate of 1.0 mW/s.

Figure 5.3. The degradation curves were obtained by exposing 5 mL of apple juice in a petri dish with stirring bar to a stationary UV source at 254 nm (LPML) when the fluence rate at the surface of the juice was 1.0 mW/s. The degradation of vitamin C in apple juice followed zero-order reaction kinetics with the constant rate $k = -0.025$ s^{-1}, which was independent of initial concentration C in equation (5.1),

$$C = C_0 - (k \times t) \tag{5.1}$$

where t is exposure time.

Figure 5.4 presents a comparison of vitamin C degradation and inactivation of *Escherichia coli* K12, a surrogate bacteria of *E. coli* O157:H7, in commercial apple juice (Motts) exposed to UV irradiation at the fluence rate of 1.0 mW/s. It can be seen that *E. coli* bacteria were more sensitive to UV-light exposure, with a degradation rate almost 2.5 times higher compared with samples containing vitamin C.

When degradation of vitamin C in apple juice was measured after processing using a commercial multiple-lamp UV unit (CiderSure 1500), it was found that after three consecutive passes through the system at the slowest flow rate of 57 mL/s, approximately 50% to 60% of the initial concentration of vitamin C (25 mg/100 g) remained.

Figure 5.5 shows a comparison of degradation of vitamin C in clarified apple juice (absorption coefficient $\alpha = 15$ cm^{-1}) and orange juice ($\alpha = 54$ cm^{-1}). After exposing both juices to the identical levels of UV fluence of 1.0 mW·s in a petri dish, it was found that the degradation rate was 8 times faster in clarified apple juice due to greater levels of available absorbed energy.

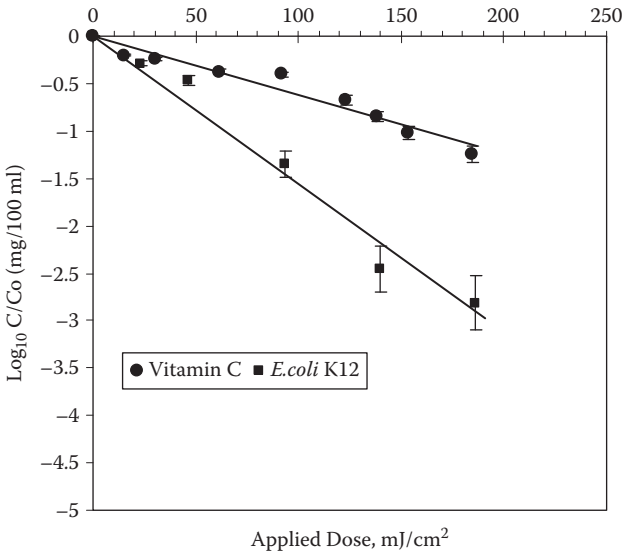

FIGURE 5.4 Degradation kinetics of vitamin C and *E. coli* K12 in apple juice exposed to UV irradiation. (From Adhikari and Koutchma, 2002.)

Vitamin A is another vitamin of great importance along with vitamin C in fresh juices because they both contribute more than 2% nutritional value to the recommended daily allowance (RDA). Figure 5.6 shows the sensitivity of vitamin A in malate buffer to UV light. After solution of vitamin A was exposed to UV light at the dose level of 200 mJ/cm^2, approximately 50% of vitamin A initial concentration remained.

The degradation of the essential vitamins in orange juice and carrot juice was reported (California Day-Fresh Foods Inc. 1999) after treatment in the commercial

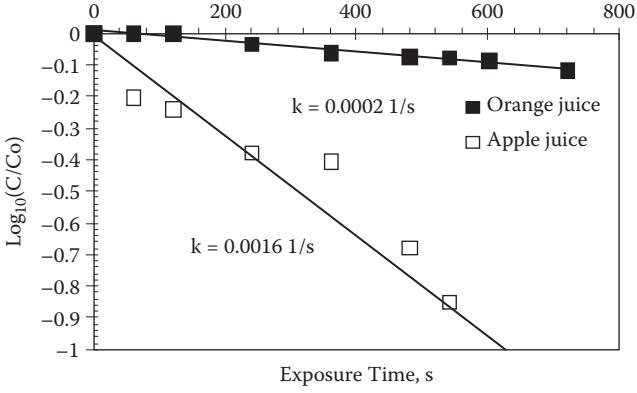

FIGURE 5.5 Effect of UV light on vitamin C degradation in apple and orange juice. (From Adhikari and Koutchma, 2002.)

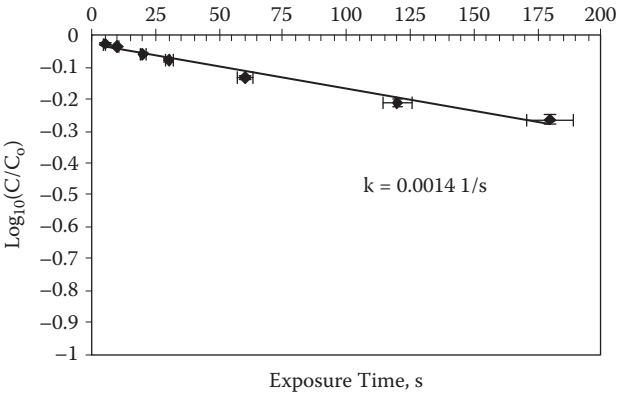

FIGURE 5.6 Effect of UV irradiation on vitamin A degradation in malate buffer at pH 3.5. (From Adhikari and Koutchma, 2002.)

Salcor UV module (Salcor Co.) at a flow rate of 7.5 gpm after seven passes through a system when total accumulative UV dose was 298.9 mJ/cm^2.

Orange juice is an essential source of vitamin C and A. One 8-fl. oz. serving of orange juice contributes approximately 210% of RDA vitamin C and 10% RDA vitamin A to the diet. Table 5.1 is a summary of the UV treatment impact on the contents of eight essential vitamins listed (California Day-Fresh Foods Inc. 1999). The highest degradation of riboflavin and beta-carotene (≈50%) may be observed. However, in terms of vitamins C, B_6, and A, only 16.6% to 11% of those vitamins were destroyed after exposure to UV light.

One 8-fl. oz. serving of carrot juice contributes approximately 8% of RDA vitamin C and 690% of RDA vitamin A to the diet. From the results in Table 5.2, it can be concluded that all treated samples did not show significant differences, as might be expected.

TABLE 5.1
Summary of Essential Vitamin Contents in Orange Juice before and after UV Treatment in the Salcor UV Module

Orange Juice	Vitamin C (mg/ 100 g)	Vitamin B_6 (mg/ 100 g)	Folic Acid (mg/ 100 g)	Thiamine B_1 (mg/ 100 g)	Riboflavin (mg/ 100 g)	Vitamin E (IU/ 100 g)	Vitamin A (IU/ 100 g)	Beta-Carotene (IU/ 100 g)
Treated	28.2	0.031	4	0.03	0.01	0.16	49	19
Untreated	33.8	0.037	4	0.05	0.02	0.16	55	37
Remaining, %	83.4	83.8	100	60	50	100	89.1	51.4

Source: California Day-Fresh Foods Inc. (1999).

TABLE 5.2
Summary of Essential Vitamins Contents in Carrot Juice before and after UV Treatment in the Salcor UV Module

Carrot Juice	Vitamin C (mg/100 g)	Retinol (IU/100 g)	Vitamin A (IU/100 g)	Beta-Carotene (IU/100 g)
Treated	<2.0	<5.0	8870	8870
Untreated	<2.0	<5.0	8700	8700
Remaining, %	100	100	100	100

In addition to vitamins C and A, carrot juice is a source of beta-carotene. The sensitivity of vitamin C and beta-carotene in carrot juice to UV light is compared in Figure 5.7. Beta-carotene demonstrated much higher stability in carrot juice than vitamin C under identical exposure to UV light at the fluence rate level of 4.0 mW/s at the surface of a petri dish.

In summary, the degradation of vitamin C in apple juice after exposure to a UV dose of 600 mJ/cm^2 ranged from 30% to 40% when present at initial concentrations of 66 to 32 mg/100 g. Exposure of orange and carrot juices to a similar UV dosage resulted in 18% and 25% degradation of vitamin C. Koutchma and Shmalts (2002) reported that microwave heating of apple juice to a temperature of 83°C for 50 s (total absorbed energy of 1450 J/s) destroyed 20% of the vitamin C. Gamma-irradiation of orange juice to the dose of 20 kGy resulted in 89% degradation of vitamin C, with strong oxidative off-flavors.

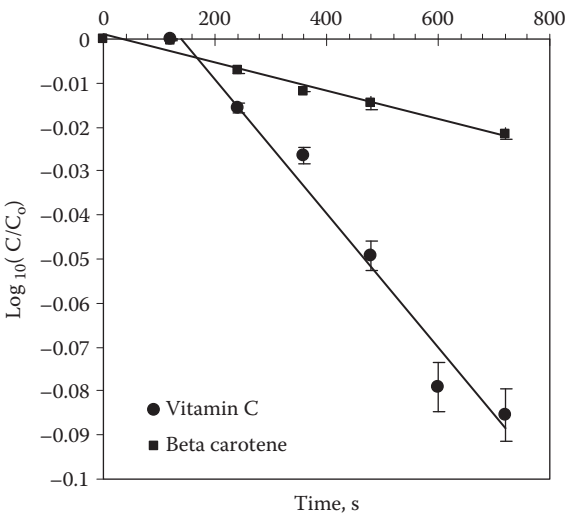

FIGURE 5.7 Degradation of beta-carotene and vitamin C in carrot juice. (From Adhikari and Koutchma, 2002.)

5.5 EFFECT OF UV PROCESSING ON MILK QUALITY

It is well known that milk and milk products are highly light-sensitive products. Loss of quality is most rapid for milk in clear glass containers and polycarbonate containers. The use of standard and opaque cardboard containers gives absolutely complete protection against light. The off-flavor that develops in milk includes components derived from several sources, and this characteristic flavor is termed as "burnt," "burnt protein," and "cabbage" (Spikes 1981). Another type of photochemical off-flavor in whole milk is "oxidized" flavor that results from oxidation of unsaturated fatty acid residues in milk lipids and phospholipids. It is a well-known technology that uses short-wavelength UV light to produce vitamin D. However, this wavelength range also produces off-flavors and destroys certain nutrients. The doses of UV light that are typically used in the preparation of vitamin D milk do not reduce the concentration of carotene, vitamin A, thiamine, or riboflavin.

Sensory and chemical consequences of treating goat milk using a UV fluid processor were assessed by Matak et al. (2007). Milk was exposed to UV light for a cumulative exposure time of 18 s and targeted UV dose of 15.8 ± 1.6 mJ/cm^2. A triangle test revealed differences between the odor of raw milk and UV irradiated milk. Oxidation and hydrolytic rancidity were measured by thiobarbituric acid-reactive substances and acid degree values (ADV). As UV dose increased, there was an increase in thiobarbituric acid-reactive substance values and ADV of the milk samples. A separate set of samples was processed using the fluid processor but with no UV exposure to see if lipase activity and agitation from pumping contributed to the differences in odor. The ADV increased at the same rate as the samples exposed to UV; however, sensory studies indicated that the increase of free fatty acids was not enough to cause detectable differences in the odor of milk. Solid-phase microextraction and gas chromatography were utilized for the analysis of volatile compounds as a result of UV exposure. There was an increase in the concentration of pentanal, hexanal, and heptanal (relative to raw goat milk) after as little as 1.3-mJ/cm^2 UV dose. The researchers concluded that UV irradiation at the wavelength of 254 nm produced changes in the sensory and chemical properties of fluid goat milk.

5.6 SHELF LIFE AND QUALITY CHANGES IN FRESH PRODUCE

According to the International Fresh-Cut Produce Association, fresh produce is one of the fastest growing food categories in the U.S. supermarkets. In the fresh produce industry, as in many other food applications, the product is exposed to UV radiation right before and after packaging when the product has been fresh-cut processed. UV light may induce hypersensitive defense responses in plant tissues. The effect of UV light on product degradation during processing and storage—including such properties as overall visual quality, enzyme activity, and texture properties—is an essential aspect of process feasibility.

5.6.1 Lettuce

Allende et al. (2006) exposed fresh processed "red oak leaf" lettuce (*Lactuca sativa*) to three doses of UV-C at 254-nm radiation at doses levels of 2.36, 4.74, and 14.22 kJ/m^2.

The UV-C radiation effects on microbial growth, chemical composition, and sensory quality were evaluated. All three doses reduced growth of microorganisms tested in this study (total aerobic bacteria, Enterobacteriaceae, lactic acid bacteria, and yeasts) when compared with the control. UV-C treatments used in this experiment had little or no effects on sugar or organic acid content of the lettuce. The highest dose induced tissue softening and increased browning after 7 days of storage at 5°C. The 4.74-kJ/m^2 treatment and lower doses reduced the microbial growth without damaging the product tissue. It was concluded that UV-C radiation at proper doses could reduce microbial loads without adversely affecting quality of "red oak leaf" lettuce.

In another study, Allende et al. (2003) reported the results of the application of UV light to reduce microbial growth and maintain quality of fresh processed lettuce. Red-pigmented "Lollo Rosso" lettuce, freshly processed following standard industrial methods, was exposed to UV-C radiation from germicidal lamps before modified-atmosphere packaging. Depending on distance and exposure time (1, 5, and 10 min), three intensities—0.81, 4.06, and 8.14 kJ/m^2—were applied. Throughout shelf life, changes in gas composition within bags were monitored, and the effects of UV-C radiation on microbial growth and on quality attributes of the product were determined. A panel test of 12 people evaluated the sensory quality. Results showed that microbial growth was inhibited by UV-C radiation at least until day 6 of storage, with the exception of lactic acid bacteria. When UV-C-treated product was compared with the control, lower microbial counts for total psychrotrophic microorganisms, coliforms, and yeast were found. However, only the highest UV-C intensity was efficient in reducing mold growth. Higher CO_2 and lower O_2 concentrations were generated within bags containing "Lollo Rosso" lettuce treated with higher UV-C radiation, which means that treatment increased the respiration rate of lettuce pieces. Between 0.81- and 4.06-kJ/m^2 treatments and the control, only slight differences in overall appearance were found. However, when the highest UV-C treatment at the level of 8.14 kJ/m^2 was applied, the lettuce tissue became brighter, probably due to the segregation of wax by the lettuce tissue as a protection against the UV-C stress.

5.6.2 Fresh-Cut Fruits

Lamikanra et al. (2005) studied the effect of processing cantaloupe melon under UV-C radiation on the storage properties of the cut fruit at 10°C and compared these results with post-cut UV-C fruit treatment and an untreated control. Cutting fruit under UV-C light induced a hypersensitive defense response that resulted in increased accumulation of ascorbate peroxidase relative to the other two treatments. Fruit processed under UV-C had the lowest esterase activity throughout the storage period. It was found that lipase activity was higher in post-cut-treated fruit than fruit processed under UV-C light and the control fruit. Lipase activity decreased rapidly in fruit processed under UV-C and was undetectable after 7 days of storage. Human sensory aroma evaluation indicated reduced rancidity, and instrumental texture measurements suggested improved firmness retention in fruit cut under UV-C. The treatment also reduced respiration during cut-fruit storage. Results of this study indicated

that while post-cut application of UV improved shelf life of cut cantaloupe melon, cutting under UV-C radiation further improves product quality.

Fonseca and Rushing (2006) reported the influence of UV-C light (140–1370 mJ/cm^2 at 254 nm) on the quality of fresh-cut watermelon. The UV treatment was compared with results obtained for the common sanitizing solutions used for fresh produce. Dipping cubes in chlorine (40 μL/L) and ozone (0.4 μL/L) was not effective in reducing microbial populations, and quality was lower in cubes receiving these aqueous treatments compared with UV-irradiated cubes or the control sample. In commercial trials, exposing packaged watermelon cubes to UV-C at 410 mJ/cm^2 produced more than a 1-log reduction in microbial populations by the end of the product's shelf life without affecting juice leakage, color, and overall visual quality. Higher UV doses (1370 mJ/cm^2) did not show any difference in microbial populations and resulted in quality deterioration. Spray applications of hydrogen peroxide (2%) and chlorine (40 μL/L) without subsequent removal of excess water failed to further decrease microbial load of cubes exposed to UV-C light at 410 mJ/cm^2. It was concluded that when properly utilized, UV-C light is the only method tested in this study that could be potentially used for sanitizing fresh-cut watermelon.

A recent study (Beaulieu 2007) demonstrated that UV radiation enhanced terpenoids and decreased esters in thin-sliced cantaloupe. UV-enhanced terpenoid production appeared to be both cultivar- and maturity-dependent. Concomitant decreases in the ester content of UV-treated samples occurred using a 15-W UV lamp. Ester losses occurred in thinly sliced laminar tissue receiving 60-min UV exposure. The finding supported the observation that UV was not responsible for chemical transformations to ester bonds or for esterase and lipase decrease in stored cantaloupe; no lipid oxidation volatiles were observed in thin-sliced control tissue. Information gathered indicated that improper cutting, handling, sanitation treatment, and storage can radically alter the desirable volatile aroma profile in cut cantaloupe, and potentially leads to decreased consumer acceptance.

5.6.3 Whole Fruits and Vegetables

Traditionally, UV-light applications for treatment of whole fruits and vegetables were focused on the disinfection role, with the objective of extending the duration of storage. This type of treatment requires that every surface of the object be exposed to UV light for a time sufficient for any microorganisms present to accumulate a lethal dose. This also means that the topography of the surface determines the efficacy of treatment and presents its limitation due to shielding effects. An example of such a process involves the use of UV irradiation at 254 nm on sweet potatoes in an effort to decrease the percentage of rot during storage (Stevens et al. 1990). The UV light was found to be effective in the control of *Fusarium* rot but did not impact nutrients except for starch. However, a new way of exploiting UV light is beginning to emerge that has particular relevance to plant foods such as fruits and vegetables.

Shama (2007) reported about a new role of UV that consists in extending the shelf life of plant foods by UV-induced effects. In this relatively new role, exposure to UV triggers a series of biochemical events within the plant tissue, and a number of quite distinct responses have been identified. Some responses involve the synthesis

of enzymes that have activity against molds, while others result in the generation of a host of so-called phytoalexins, which are inhibitory to microorganisms. These effects are produced by the use of very low UV doses, and the time scale for the induction of such events is measured over hours or even days; the term *hormesis* has been applied to this type of treatment. According to Shama, "hormesis involves the use of small doses of potentially harmful agents directed against a living organism or living tissue in order to elicit a beneficial or protective response."

Hormetic UV treatment is distinguished from conventional UV treatment. In conventional treatment the UV is directed at microorganisms present on the surfaces of an object, whereas in hormetic UV treatment the object itself is the target of the incident UV. The objective of the treatment is to elicit an antimicrobial response in the fruit and vegetable tissue. Both types of UV treatment employ the same wavelengths, but for hormetic treatments only low UV doses are required. These doses, recently reviewed for fruit by Shama and Alderson (2005), vary according to the type of fruit, with the doses ranging from 10 to 900 mJ/cm^2. The literature contains numerous reports of hormetic UV treatments resulting in protective effects against microorganisms throughout the entire tissue rather than at its surface only. For example, Stevens et al. (1999) showed that sweet potatoes inoculated with spores of *Fusarium solani* as deep as 12 mm below the surface could successfully be protected from infection following hormetic UV treatment. The literature on UV hormesis in fresh produce reveals two distinct effects. The first is protection against attack by phytopathogens (mainly fungi), and the second is delaying the onset of ripening. Both effects are obviously desirable and would contribute to reducing losses.

The greatest attention has focused on citrus fruit, where enhancement of resistance to phytopathogens such as *Penicillium digitatum* has been attributed to accumulation of the phytoalexin scoparone. For example, Ben-Yehoshua et al. (1992) reported that UV illumination of lemon fruit reduced its susceptibility to *P. digitatum*. Expression of this effect was directly related to the level of scoparone in illuminated fruit. In carrots, UV treatment has been shown to result in accumulation of the phytoalexin 6-methoxymellein (Mercier et al. 2000).

Maneerat et al. (2003) investigated the effect of UV-A light at 315 and 400 nm at 0.02, 0.5, and 2 mW/cm^2 during storage on tomato fruit injury at 25°C. The fruit temperature did not change, no physiological disorders were found, and the SOD activity did not differ from that for control fruits. It was concluded that UV-A light might not induce reactive oxygen species in UV-A-irradiated fruit. Some of the compounds induced by UV are known to have beneficial health effects, the most well studied of these being resveratrol synthesis in grapes. Nigro et al. (1998) treated grapes with low doses of UV and attributed increased resistance in the treated grapes to resveratrol. Resveratrol has been claimed to have cardioprotective, anti-inflammatory, and antitumorogenic properties, and perhaps most intriguingly, that it extends the life span of lower organisms.

Three types of fluorescent lamps with peak emissions at 254, 310, and 352 nm were compared to increase the flavonoids content of harvested strawberries and onions (Higashio et al. 2005). The flavonoids play physiological functions in the human diet. The irradiation of shaded sides of strawberries followed by storage in the dark induced the synthesis of anthocyanins in strawberries and quercetin in onions.

Color differences between the sunlit and shaded sides of strawberry fruit disappeared, and the content of quercetin in onion doubled, especially at peak emission of 352 nm and 184 μW/cm^2. The results of the study suggested that UV radiation after harvest has a potential to improve the quality of these fruits and onions.

5.6.4 Meats, Poultry, Fish

The potential of UV light to reduce bacterial contamination on meats and poultry and its impact on quality attributes has not been well studied or extensively reported. Studies have shown that UV exposure does not have a deleterious effect on the color of meat, nor does it cause oxidative rancidity.

The UV-treated poultry carcasses were evaluated for color changes and rancidity along with evaluation of the effect of UV light on *Salmonella* (Wallner-Pendleton et al. 1994). This study suggested that UV radiation can reduce *Salmonella* without negatively affecting color or increasing rancidity of the meat.

Raw broiler breast fillets were subjected to germicidal UV light (dose of 1000 μW/cm^2 for 5 min at a wavelength of 254 nm) to evaluate its potential to reduce *Listeria monocytogenes* numbers on raw product before shipment to a poultry further-processing plant. Boneless, skinless breast fillets were inoculated with four different strains of *L. monocytogenes* 5 min before treatment. After the UV treatment, breast fillets were stored at 4°C for 24 h. Enumeration of remaining *L. monocytogenes* was performed using the spread-plate method on modified Oxford agar. An approximate 2-log reduction in viable *L. monocytogenes* was observed with all four strains on UV-treated breast fillets as compared with the nontreated breast fillets. The UV treatment caused only slight changes in meat color (lightness, redness, and yellowness) on the day of treatment or after 7 days of storage. This study suggests that UV treatment of raw breast fillets at a slaughter plant can significantly reduce *L. monocytogenes* without negatively affecting meat color. This process could be used to reduce the negative effect of raw poultry as a transmission vector of *L. monocytogenes* into a poultry further-processing plant (Lyon et al. 2007). However, when pulsed UV-light was used to inactivate *Escherichia coli* and *L. monocytogenes* on raw salmon fillets, visual color and quality changes occurred due to temperature increase on the surface of fish samples (Ozer and Demirci 2006).

5.7 DEGRADATION AND FORMATION OF CHEMICAL COMPOUNDS IN FOODS

5.7.1 Furan in Apple Cider

The presence of furan in processed foods is a concern because furan is listed as "reasonably anticipated to be human carcinogen" in the Department of Health and Human Services Report on Carcinogens (1) and is considered "possibly carcinogenic to humans" by the International Agency for Research on Cancer (1995). In a recent survey, the U.S. FDA found that furan is present in many thermally processed foods purchased from supermarkets, with furan levels of ≈100 ppb in some of the foods (Food and Drug Administration 2004). Apple juice as a baby food contained furan

levels ranging from 2.5 to 8.4 ppb (Food and Drug Administration 2004). Furan is formed from carbohydrates, ascorbic acid, fatty acids, and a mixture of the three upon heating (Locas and Yaylayan 2004; Fan 2005).

Fan and Geveke (2007) investigated whether UV-C induced furan in apple cider and its components, and they determined furan levels in apple cider exposed to UV-C at doses that would inactivate *E. coli* by 5 log. The UV-C intensity reached at the surface of tested solutions was approximately 9.5–10 mW/cm^2. The results showed that more furan was formed at higher doses (>3.5 J/cm^2) in the freshly prepared cider than in the commercial one. In the commercial fresh apple cider, UV-C induced little furan at doses less than 3.5 J/cm^2. Afterward, furan formation increased to approximately 14 ppb with UV-C dose at 8.8 J/cm^2. Similarly, in freshly prepared apple cider, no furan was formed at the UV-C dose of 1.8 J/cm^2. However, furan formation increased linearly at a rate of 11 ppb per J/cm^2 UV-C in the dose range of 3.5–8.8 J/cm^2, reaching about 60 ppb at 8.8 J/cm^2.

When fresh apple ciders were UV treated to achieve the 5-log reduction of *E. coli*, as required by the U.S. FDA, less than 1 ppb furan was found. It was concluded that a significant amount of furan could be accumulated if apple cider was overtreated. Overall, these results suggested that little furan is induced in apple cider if UV-C processing is used for the purpose of apple cider pasteurization.

To determine the source(s) of furan formation, the effect of UV treatment on furan formation was tested in major components of apple cider such as sugars (fructose, sucrose, and glucose) and organic acids (mainly malic acid). It was reported that UV-C treatment of fructose solution produced a high amount of furan (Figure 5.8), and slightly higher furan was produced from fructose solution prepared in 0.25% malic acid than that in water. Fructose in 0.25% malic acid had a lower pH than fructose solution in water, indicating that pH may have an effect on furan formation. Very low amounts of furan were produced from glucose or sucrose solutions prepared in either water or malic acid. Exposure of malic acid to UV-C did not

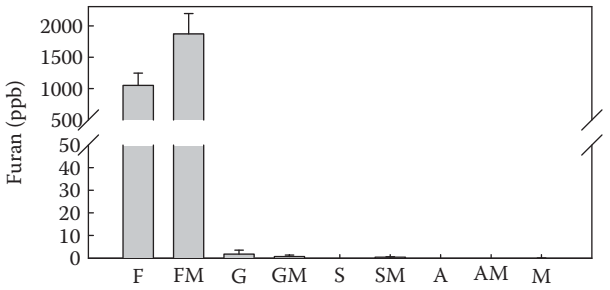

FIGURE 5.8 Formation of furan from sugars and ascorbic acid in aqueous and malic acid solutions. Vertical bars represent standard deviations. Solutions of 5% fructose (F), 5% fructose in 0.25% malic acid (FM), 5% glucose (G), 5% glucose in 0.25% malic acid (GM), 5% sucrose (S), 5% sucrose in 0.25% malic acid (SM), 5% ascorbic acid (A), 5% ascorbic acid in 0.25% malic acid (AM), and 0.25% malic acid (M) were exposed to ≈9 J/cm^2 UV-C at ambient temperature (≈23°C). (From Fan and Geveke 2007. With permission.)

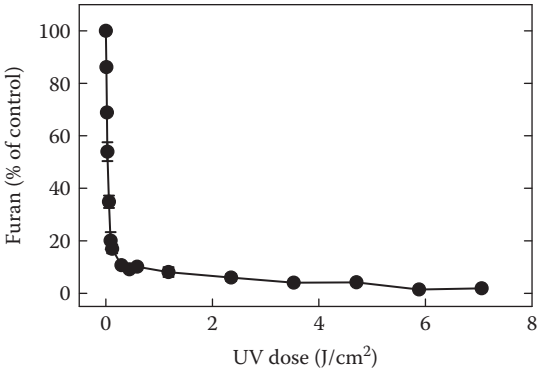

FIGURE 5.9 Reduction of d_4-furan in 5% fructose solution as a function of UV-C doses. Vertical bars represent standard deviations (n = 4). (From Fan and Geveke 2007. With permission.)

induce furan formation, and virtually no furan was formed from UV-C treatment of ascorbic acid.

The degradation of d_4-furan by UV-C in different solutions and apple cider was also analyzed in the study by Fan and Geveke (2007). There was little degradation of d_4-furan at a dose of ≈0.9 J/cm^2 when d_4-furan in water, glucose, sucrose, ascorbic acid, or apple cider was UV treated, but in fructose solutions, nearly all of d_4-furan (88%) was destroyed. In a dose-response study, it was demonstrated that most d_4-furan was degraded even at the low dose (<0.1 J/cm^2) (Figure 5.9). It is possible that the degradation products of fructose may react with furan. Identification of the specific mechanism requires further study.

5.7.2 Dioxins in Fish Meal

Dioxins are ubiquitous polychlorinated organic pollutants mainly introduced in the environment through industrial activity, pesticide production, and waste management. Dioxins generally include two classes of compounds: polychlorinated dibenzo-*p*-dioxins (PCDDs) and polychlorinated dibenzofurans (PCDFs). Only 7 congeners for dioxins and 10 for furans are considered toxic. Dioxins accumulate in the fat of foodstuffs, and the food chain represents more than 90% of the human exposure to dioxins. Due to their adverse health effects and their persistence in the environment, the presence of dioxins in the food chain and in animal feed have received increasing public attention. It is believed that the most important mechanism for dioxin degradation in the environment is by the UV component of sunlight. Studies have reported photolytic decomposition of dioxins in water (Friesen et al. 1990), in organic solutions (Colombini et al. 1996), in gases (Jones et al. 1993), and also in soils (Miller et al. 1989).

Baron et al. (2005) reported that UV-B light can be used to selectively remove dioxin from fish meal. Fish-meal samples were placed under UV-A and UV-B light for 2, 5, and 10 days. Obviously, a much shorter exposure time would be needed in

industrial environments. Analysis of amino acids content, lipid oxidation marker, ethoxyquin content, dioxin, and polychlorinated biphenyl (PCB) profiling was carried out in this study. Exposure of fish meal for 5 days to UV-B light resulted in the degradation of approximately 70% of the dioxin content, while UV-A had little effect, only resulting in the degradation of 10% of the dioxin content. UV-B did not affect the protein and amino acid content of fish meal; however, it did trigger lipid oxidation. Addition of ethoxyquin prevented oxidation but simultaneously slowed dioxin breakdown. Increasing UV-B intensity at the surface from 300 to 4800 μW/cm^2 resulted in more efficient dioxin degradation. Therefore, a higher intensity lamp would shorten the exposure time. However, oxidation of unsaturated fatty acids was found to be the main drawback. The degradation of furans (PCDFs) was also investigated, and results presented showed that PCDFs were also degraded by UV light to the same extent as PCDDs. The possible mechanism of dioxin decontamination remained unsolved in the report due to the complex matrix. It was found that more than one pathway effectively contributed to the degradation of dioxins.

5.7.3 Photolysis of Nitrates

The concern that surrounds the use of UV light for water treatment is whether nitrite (NO_2^-) formed from nitrate (NO_3^-) photolysis will pose a health threat. Research has shown that, with regard to NO_2^- formation during UV disinfection, there is little concern when LPML is used. NO_2^- formation is negligible at UV dose levels relevant to UV disinfection up to 250 mJ/cm^2. However, the potential of NO_2^- formation during disinfection with a polychromatic medium-pressure mercury UV lamp (MPML) source is greater, since it is known that quantum yield for NO_2^- formation is higher at shorter wavelengths.

The research of Sharpless and Linden (2001) addressed the effects of pH, wavelength, natural organic matter (NOM), and dissolved inorganic carbon on NO_2^- formation during UV disinfection with polychromatic MPML. Quantum yields measured at 228 nm were approximately two times higher than at 254 nm under all conditions studied. In the absence of NOM, NO_2^- quantum yields decreased with time. At 15 ppm dissolved organic carbon as NOM, the quantum yield increased with time. Dissolved inorganic carbon significantly decreased NO_2^- formation at pH 8 but not at pH 6. The results of this study indicated important and previously unrecognized roles of NOM and CO_2 in nitrate photolysis. When photolysis was carried out using the full-spectrum MPML UV lamp and germicidally relevant UV dose, NO_2^- concentrations remained well below the U.S. maximum contaminant level of 1 ppm N, even with nitrate initially present at 10 ppm N.

5.8 CONCLUSIONS

Ultraviolet (UV) light processing can be a viable nonthermal alternative for eliminating or reducing the levels of undesirable microorganisms in foods and beverages. However, UV light can adversely affect food by generating free radicals in products by a wide variety of organic photochemical reactions. Possible undesirable effects

include damage to vitamins and proteins, degradation of antioxidants, oxidation of lipids, changes in texture and color, and formation of off-flavors and aromas.

Exposure to UV can result in flavor changes to citrus products. Tests of light-sensitive vitamins in apple, carrot, and orange juices have shown that beta-carotene, vitamin C, and vitamin A are degraded by UV treatment. Loss of nutrients and development of off-flavors during UV processing of juices needs further investigation, and attempts should be made to minimize the damaging effects of UV light on different groups of food products. In addition, knowledge of the kinetics of vitamin degradation from UV irradiation will enable optimization of microbial inactivation while minimizing vitamin losses.

Photochemical decomposition of UV absorbers—vitamin A, riboflavin, ascorbic acid, and some pigments in milk—was also reported. Antioxidants such as vitamin A and beta-carotene were destroyed only in the presence of visible light. Ascorbic acid photooxidation was initiated from the superoxide anion produced in milk in the presence of riboflavin.

It is well documented that exposure to UV light has a significant effect on food compositions that are high in unsaturated fats and lipids, which are oxidized due to the generation of free radicals, resulting in the development of rancidity, off-flavors, and degradation of antioxidants. A better understanding of the effects of UV processing on lipid oxidation and antioxidant degradation will result in increased use of this technology.

The concept of employing low doses of UV to elicit hormetic responses in fresh produce has been firmly established by a host of laboratory studies. However, further research is needed before this treatment method can be applied commercially.

The effects of UV light on the potential formation of chemical compounds in foods that may present a health threat should be evaluated to determine whether there are any toxicological or chemical safety concerns associated with products that have undergone UV treatment. Closer examination of the potential of UV light to destroy undesirable compounds or pollutants deserves more attention.

REFERENCES

Adhikari, C., and T. Koutchma. 2002. Effects of UV radiation on lipids, antioxidants, and vitamins in foods. Abstract of presentation at the AOCS Annual Meeting. 93rd AOCS Annual Meeting, Montreal.

Allende, A., J. McEvoy, Y. Luo, F. Artes, and C.-Y. Wang. 2006. Effectiveness of two-sided UV-C treatments in inhibiting natural microflora and extending the shelf-life of minimally processed "red oak leaf" lettuce. *Food Microbiol.* 2: 241–249.

Allende, A., E. Padilla, and F. Artés. 2003. Changes in microbial and sensory quality of fresh processed UV-C treated "Lollo Rosso" lettuce. *Acta Horticulturae* 628 (2): 753–760.

Baron, C., T. Borresen, and C. Jacobsen. 2005. UV treatment of fishmeal: A method to remove dioxins. *J. Agric. Food Chem.* 53: 7091–7097.

Beaulieu, J. 2007. Effect of UV radiation on cut cantaloupe: Terpenoids and esters. *J. Food Sci.* 72 (4): S272–S280.

Ben-Yehoshua, S., V. Rodov, J. Kim, and S. Carmeli. 1992. Preformed and induced antifungal materials of citrus fruit in relation to the enhancement of decay resistance by heat and ultraviolet treatment. *J. Agric. Food Chem.* 40: 1217–1221.

California Day-Fresh Foods Inc. 1999. A food additive petition for the use of ultraviolet light in the reduction of microorganisms on juice products. Submitted to FDA regarding CFR 21 179. Glendore, CA: California Day-Fresh Foods Inc., pp. 1–117.

Colombini, M. P., F. Di Francesco, and R. Fuoco. 1996. Photodegradation of polychlorinated dibenzo-*p*-dioxins in liquid samples by near UV light radiation. *Microchem. J.* 54: 331–337.

Fan, X. 2005. Formation of furan from carbohydrates and ascorbic acid following exposure to ionizing radiation and thermal processing. *J. Agric. Food Chem.* 53: 7826–7831.

Fan, X., and D. Geveke. 2007. Furan formation in sugar solution and apple cider upon ultraviolet treatment. *J. Agric. Food Chem.* 55 (19): 7816–7821.

Fonseca, J., and J. Rushing. 2006. Effect of UV-C light on quality and microbial population of fresh-cut watermelon. *Postharvest Biol. Technol.* 40 (3): 256–261.

Food and Drug Administration. 2004. Exploratory data on furan in food: Individual food products. U.S. Food and Drug Administration, Center for Food Safety and Applied Nutrition. http://vm.cfsan.fda.gov/~dms/furandat.html.

Friesen, K., M. Foga, and M. Loewen. 1990. Evidence of sensitized photolysis of polychlorinated dibenzo-*p*-dioxins in natural waters under sunlight conditions. *Environ. Sci. Technol.* 1739–1744.

Guerrero-Beltrán, J. A., and G. V. Barbosa-Cánovas. 2006. Inactivation of *Saccharomyces cerevisiae* and polyphenoloxidase in mango nectar treated with UV light. *J. Food Protection* 69 (2): 362–368.

Heiss, R., and R. Radtke. 1968. Uber den einfluss von licht, sauerstoff und temperatur auf die haltbarkeit verpackter lebensmittel. *Verpak. Rundsch.* 19 (3): 17–24.

Higashio, H., H. Hirokane, F. Sato, S. Tokuda, and A. Uragami. 2005. Effect of UV irradiation after harvest on the content of the flavonoids in vegetables. Proc. 5th Int. Postharvest Symposium. *Acta Horticulturae* 682 (2): 1007–1012.

International Agency for Research on Cancer. 1995. IARC monographs on the evaluation of carcinogenic risks to humans: Dry cleaning, some chlorinated solvents and other industrial chemicals. Lyon, France: IARC, vol. 63, pp. 393–407.

Jones, P. H., J. de Gerlache, E. Marti, G. Misher, M. Scherrrer, W. Bontinck, and H. J. Niessen. 1993. The global exposure of man to dioxins: A perspective on industrial waste incineration. *Chemosphere* 26: 1491–1497.

Koutchma, T., and M. Shmalts. 2002. Degradation of vitamin C after alternative treatments of juices. Paper presented at IFT conference, New Orleans, 2002.

Lamikanra, O., B. Garber, D. Kueneman, and D. Ukuku. 2005. Effect of processing under ultraviolet light on the shelf-life of fresh cut cantaloupe melon. *J. Food Sci.* 70: 534–539.

Locas, C. P., and V. A. Yaylayan. 2004. Origin and mechanistic pathways of formation of the parent furan-a food toxicant. *J. Agric. Food Chem.* 52: 6830–6836.

Lyon, S. A., D. L. Fletcher, and M. E. Berrang. 2007. Germicidal ultraviolet light to lower numbers of *Listeria monocytogenes* on broiler breast fillets. *Poultry Sci.* 86 (5): 964–967.

Maneerat, C., Y. Hayata, N. Muto, and M. Kuroyanagi. 2003. Investigation of UV-A light irradiation on tomato fruit injury during storage. *J. Food Protection* 66 (11): 2168–2170.

Matak, K. E., S. S. Sumner, S. E. Duncan, E. Hovingh, R. W. Worobo, C. R. Hackney, and M. D. Pierson. 2007. Effects of ultraviolet irradiation on chemical and sensory properties of goat milk. *J. Dairy Sci.* 90: 3178–3186.

Mercier, J., D. Roussel, M. T. Charles, and J. Arul. 2000. Systemic and local responses associated with UV- and pathogen-induced resistance to *Botrytis cinerea* in stored carrot. *Phytopathology* 90: 981–986.

Miller, G. C., V. R. Hebert, M. J. Miille, R. Mitzel, and R. Zepp. 1989. Photolysis of octachlorodibenzo-*p*-dioxin on soils: Production of 2,3,7,8-TCD. *Chemosphere* 18: 1256–1274.

Nigro, F., A. Ippolito, and G. Lima. 1998. Use of UV-C to reduce storage rot of table grape. *Postharvest Biol. Technol.* 13: 171–181.

Noci, F., J. Riener, M. Walkling-Ribeiro, D. A. Cronin, D. J. Morgan, and J. G. Lyng. 2008. Ultraviolet irradiation and pulsed electric fields (PEF) in a hurdle strategy for the preservation of fresh apple juice. *J. Food Eng.* 85: 141–146.

Ozer, N., and A. Demirci. 2006. Inactivation of *Escherichia coli* O157:H7 and *Listeria monocytogenes* inoculated on raw salmon fillets by pulsed UV treatment. *Int. J. Food Sci. Technol.* 41: 354–360.

Shama, G. 2007. A new role for UV? Extensions to the shelf life of plant foods by UV-induced effects. Paper presented at 2007 IOA-IUVA Joint World Congress. Los Angeles, August 27–29, 2007.

Shama, G., and P. Alderson. 2005. UV hormesis in fruits: A concept ripe for commercialisation. *Trends Food Sci. Technol.* 16: 128–136.

Sharpless, C., and K. Linden. 2001. UV photolysis of nitrate: Effects of natural organic matter and dissolved inorganic carbon and implications for UV water disinfection. *Environ. Sci. Technol.* 35 (14): 2949–2955.

Spikes, J. 1981. *Photodegradation of foods and beverages*. In Vol. 6 of *Photochemical and photobiological reviews*, ed. K. C. Smith, 39–81. New York: Plenum Press.

Stevens, C., V. A. Khan, J. Y. Lu, C. L. Wilson, E. Chalutz, S. Droby, M. K. Kabwe, Z. Haung, O. Adeyeye, L. P. Pusey, and A. Y. A. Tang. 1999. Induced resistance of sweet potato to *Fusarium* root rot by UV-C hormesis. *Crop Prot.* 18: 463–470.

Stevens, C., V. Khan, A. Tang, and J. Lu. 1990. The effect of ultraviolet radiation on mold rots and nutrients of stored sweet potatoes. *J. Food Protection* 53 (3): 223–226.

Tandon, K., R. Worobo, J. Churley, and O. Padilla-Zakour. 2003. Storage quality of pasteurized and UV-treated apple cider. *J. Food Processing Preservation* 27: 21–35.

Tran, M. T., and M. Farid. 2004. Ultraviolet treatment of orange juice. *Innovative Food Sci. Emerging Technol.* 5 (4): 495–502.

Wallner-Pendleton, E. A., S. S. Sumner, G. Froning, and L. Stetson. 1994. The use of ultraviolet radiation to reduce *Salmonella* and psychrotrophic bacterial contamination on poultry carcasses. *Poultry Sci.* 73: 1327–1333.

Ye, Z. 2007. UV disinfection between concentric cylinders. PhD thesis, Georgia Institute of Technology, Atlanta.

Ye, Z., T. Koutchma, B. Parisi, J. Larkin, and L. J. Forney. 2007. Ultraviolet inactivation kinetics of *E. coli* and *Y. pseudotuberculosis* in annular reactors. *J. Food Sci.* 72: E271–E278.

6 Transport Phenomena in UV Processing

6.1 UV IRRADIANCE IN LIQUID FOODS

The process of inactivating microbes by UV radiation involves two steps that occur in series with some overlap. In the first step, microbes must diffuse toward the radiation surface. When the microbes reach a distance λ from the radiation surface, photons are absorbed by the microbes that become inactivated. The distance λ represents the radiation penetration depth, where the photon flux is 10% of the initial flux I_0 at the radiation surface. The penetration depth λ within a fluid of absorbance A is defined by

$$\frac{I(\lambda)}{I_0} = 10^{-\lambda A} \tag{6.1}$$

where $\lambda A = 1$ and the penetration depth is thus defined by $\lambda = 1/A$.

Of the two steps representing diffusion followed by inactivation, the diffusion step is much slower and is called the rate-limiting step in the microbe inactivation process (Forney et al. 2008). One must therefore focus on the diffusion process to predict microbe inactivation rates in a UV reactor. Here, the nature of the diffusion process will depend on flow conditions that can be either laminar, turbulent, or dominated by secondary flow such as Taylor or Dean vortices, as discussed in Chapter 8. In all cases, however, the microbes must diffuse across a laminar sublayer of thickness δ next to the radiation surface, where $\delta > \lambda$ for most liquid foods.

Determination of the momentum boundary thickness δ begins with the definition of the dimensionless mass-transfer coefficient k_c, where

$$k_c \propto \frac{Đ}{\delta_c} \tag{6.2}$$

and Đ is the microbe diffusivity, and δ_c is the microbe concentration boundary layer thickness. Here, the ratio of the concentration and the momentum boundary layers are given by

$$\frac{\delta}{\delta_c} = \mathrm{Sc}^{1/3} \tag{6.3}$$

where Sc is the Schmidt number. It is now possible to define the dimensionless mass-transfer coefficient in terms of the Sherwood number Sh, where

$$\mathrm{Sh} \propto \frac{k_c d}{Đ} \tag{6.4}$$

and d is the channel width.

Substituting equations (6.2) and (6.3) into equation (6.4), one obtains

$$\mathrm{Sh} \propto \left(\frac{d}{\delta}\right) \mathrm{Sc}^{1/3} \tag{6.5}$$

It is now possible to determine the normalized momentum boundary layer thickness δ/d for a variety of geometries. Here, we consider either turbulent or Taylor–Couette flow between concentric cylinders of diameters $R_1 < R_2$ for $d = R_2 - R_1 << R_1$.

Simple forms of the Sherwood number Sh for axial flow between concentric cylinders (Incropera and DeWitt 1996; Baier et al. 1999) are

$$\text{laminar: } \mathrm{Sh} = 4.86, \text{ where } \mathrm{Re_h} < 4 \times 10^3 \tag{6.6}$$

$$\text{turbulent: } \mathrm{Sh} = 0.023\mathrm{Re_h}^{4/5}\mathrm{Sc}^{1/3}, \text{ where } \mathrm{Re_h} > 4 \times 10^3 \tag{6.7}$$

$$\text{Taylor–Couette: } \mathrm{Sh} = 1.0\mathrm{Ta}^{1/2}\mathrm{Sc}^{1/3}, \text{ where } 10^2 < \mathrm{Ta} < 5 \times 10^2 \tag{6.8}$$

Here, $\mathrm{Re_h}$ is the channel Reynolds number based on the hydraulic diameter $D_h = 2d$ or

$$\mathrm{Re_h} = \frac{\mathrm{v}D_h}{\nu} \tag{6.9}$$

Values of the normalized momentum boundary layer thickness δ/d can now be determined from equation (6.5), where the Sherwood number is defined by equations (6.6), (6.7), and (6.8), where

$$\mathrm{Sh} = \frac{2d}{\delta_c} = \frac{2d}{\delta}\mathrm{Sc}^{1/3} \tag{6.10}$$

and the ratio becomes

$$\frac{\delta}{d} = \frac{2\mathrm{Sc}^{1/3}}{\mathrm{Sh}} \tag{6.11}$$

where $2d = D_h$ is the hydraulic channel diameter. Estimates of the Schmidt number are defined by

$$\mathrm{Sc} = \frac{\nu}{Đ} \tag{6.12}$$

where, for *E. coli* in water, the microbe diffusivity is (Fenchel 2001)

$$Đ \approx 2 \times 10^{-9}\ \mathrm{m^2/s} \tag{6.13}$$

and the kinematic viscosity of water is $\nu = 1 \times 10^{-6}$ m^2/s. These parameters provide values of the Schmidt number Sc ≈ 500 for bacteria in water.

Correlation and prediction of UV inactivation for flow between concentric cylinders is now possible from the expression (Ye 2007; Ye et al. 2008)

$$\ln\left(\frac{N}{N_0}\right) = \frac{-ckI_0\tau R_c}{\alpha d\delta} \tag{6.14}$$

where $R_c = 2R_2/(R_1 + R_2)$ for radiation introduced through the outer transparent cylinder. Here, $k = k_1$ is the inactivation rate constant for the microbe, τ is the average fluid residence time, $\alpha = 2.3$ A where A is the fluid absorbence, and N is the number of active microbes per unit volume of fluid.

6.2 GENERAL HYDRAULIC CONDITION

The power requirements for steady flow of liquid foods through a UV reactor are developed below. Here, one considers an incompressible fluid with both a constant Newtonian viscosity μ and kinematic viscosity $\nu = \mu/\rho$. Under these conditions, the fluid pump must supply power equal to the friction losses in both the reactor and the total pipe system at the reactor inlet and outlet. The mechanical energy equation for this case becomes (Welty et al. 2001)

$$\sum F_i = -W_s \tag{6.15}$$

where F_i is the frictional loss within various elements of the flow system, and W_s is the shaft work supplied by the pump.

Consider the steady flow through a concentric cylinder reactor of radius $R_2 > R_1$ and length L. The friction loss in units of J/kg is

$$F_1 = 4f_f\left(\frac{L}{D_h}\right)\left(\frac{v^2}{2}\right) \tag{6.16}$$

where $D_h = 2d$ is the hydraulic diameter, $d = R_2 - R_1$ is the gap width, and v is the average axial fluid velocity. An explicit expression for the Fanning friction factor f_f is given by Haaland (1983) in the form

$$\frac{1}{\sqrt{f_f}} = -3.6\log_{10}\left[\frac{6.9}{Re_h} + \left(\frac{\varepsilon}{3.7D_h}\right)^{\frac{10}{9}}\right] \tag{6.17}$$

for $4 \times 10^4 < Re_h < 10^8$, and $\varepsilon/D_h < 0.05$.

The remaining friction losses in the pipe system due to valves, elbows, and tubing are of the form (Welty et al. 2001)

$$\sum F_i = \sum K_i\left(v_i^2\right)/2 \tag{6.18}$$

for $i > 1$, where K_i are the loss factors for the pipe elements and v_i is the average velocity in the pipe leading to each fitting.

Substitution of the frictional losses F_i into equation (6.15) provides the required pump shaft work W_s delivered by a pump with a pump efficiency η. One computes the required pump or output power W_p from the expression

$$\eta W_p = -W_s \tag{6.19}$$

where the pump efficiency $\eta < 1$ is provided by the pump manufacturer.

6.2.1 Hydraulic Diameter

If the cross section of a conduit or channel is noncircular, then an equivalent hydraulic diameter must be used to compute the Reynolds number, friction loss, and friction factor from equations (6.9), (6.16), and (6.12). The hydraulic diameter is defined as the ratio of the cross-sectional area of the channel to the wetted perimeter.

One example of a noncircular channel often encountered in practice is flow between two concentric cylinders of diameters $D_0 > D_i$. The hydraulic diameter for this geometry is calculated by multiplying 4 times the ratio of the cross-sectional area to the wetted perimeter, or

$$D_h = 4\left[\frac{\text{cross sectional area}}{\text{wetted perimeter}}\right] \tag{6.20}$$

Thus, since the

$$\text{cross sectional area} = \pi/4(D_0^2 - D_i^2) \tag{6.21}$$

and the

$$\text{wetted perimeter} = \pi(D_0 + D_i) \tag{6.22}$$

the hydraulic diameter D_h becomes

$$D_h = (D_0 - D_i) = 2d \tag{6.23}$$

where d is the gap width. The hydraulic diameter defined by equation (6.23) is used in Chapter 8 for laminar, turbulent, and Taylor–Couette flow between concentric cylinders.

Another common example is the flow field between cylindrical lamps suspended within a larger cylindrical or rectangular channel. For lamps parallel to the channel axis, the flow area is

$$\text{flow area} = A_c - nA_L \tag{6.24}$$

where A_c and A_L are the cross-sectional area of the empty channel and lamp, respectively, and n is the number of lamps. The wetted perimeter is the sum of the channel and lamp perimeters, or

$$\text{wetted perimeter} = P_c + nP_L \tag{6.25}$$

Thus, the hydraulic diameter D_h is

$$D_h = 4\left[\frac{A_c - nA_L}{P_c + nP_L}\right] \tag{6.26}$$

6.2.2 Channel Entrance Length

When a liquid enters a channel, the flow characteristics are different from those downstream, where the flow is considered fully developed. Computation of microbe inactivation in UV reactors normally assumes that the flow is fully developed. The only exception is the numerical computations for both the flow field and microbe inactivation rates.

Specifically, at the entrance to a channel, the fluid may have a uniform velocity profile, depending on the geometry of the inlet tubing. The maximum entry length L_e would correspond to a uniform velocity profile and is a function of the hydraulic Reynolds number Re_h. The entrance length may be calculated for laminar flow, where $Re_h < 4000$, in the form (Singh and Heldman 2001)

$$\frac{L_e}{D_h} = 0.06 Re_h \tag{6.27}$$

and for turbulent flow, where $Re_h > 4000$, in the form

$$\frac{L_e}{D_h} = 4.4(Re_h)^{1/6} \tag{6.28}$$

Substitution of Re_h for values in the range $100 < Re_h < 1000$ for laminar flow, the maximum normalized entry length is calculated to be in the range of $6 < L_e/D_h < 60$. In contrast, substitution of Re_h for values in the range $4000 < Re_h < 20{,}000$ for turbulent flow, the maximum normalized entry length is calculated to be in the range of $17 < L_e/D_h < 23$.

Two UV reactor geometries that are discussed in Chapter 8 involve flow that contains secondary vortices. These geometries include either (a) flow between concentric cylinders when one or both cylinders are rotating about their axis or (b) flow within a tube wound in a helix geometry, called Dean flow. Numerical computations of both secondary flows indicate that fully developed secondary flow exists in less than five normalized hydraulic diameters, or $L_e/D_h < 5$ (Ye 2007).

The remaining effect of the entrance length to a channel is an increase in the friction factor/unit length of channel above that computed for the fully developed region of flow. The latter leads to an increase in the friction loss compared with a similar length in the fully developed region of flow. As an approximation, the friction factor f_f for the entry length can be taken as two to three times the value of the friction factor in fully developed flow (Geankoplis 1978). In this case, the friction loss F_e given by equation (6.16) for the entry length can be estimated by substituting $L = L_e$ and $3f_f$ for the friction factor f_f.

REFERENCES

Baier, G., T. M. Grateful, M. D. Graham, and E. N. Lightfoot. 1999. Prediction of mass transfer in spatially periodic systems. *Chem. Eng. Sci.* 54: 343–355.

Fenchel, T. 2001. Eppur si muove: Many water column bacteria are motile. *Aquatic Microbial Ecology* 24: 197–201.

Forney, L.J., Z. Ye and T. Koutchma. 2008. UV disinfection of *E. coli* between concentric cylinders: effects of the boundary layer and a wavy wall. *Ozone: Science and Engineering* (in press).

Geankoplis, C. J. 1978. *Transport processes and unit operations*. 3rd ed. Boston: Allyn and Bacon.

Haaland, S. E. 1983. Simple and explicit formulas for the friction factor in turbulent pipe flow. *Trans. ASME (JFE)* 105: 89–90.

Incropera, F. P., and D. P. Dewitt. 1996. *Introduction to heat transfer*. 3rd ed. New York: John Wiley & Sons.

Singh, R. P., and D. R. Heldman. 2001. *Introduction to food engineering*. 3rd ed. New York: Academic Press.

Welty, J. R., C. E. Wicks, R. E. Wilson, and G. L. Rorrer. 2001. *Fundamentals of momentum, heat and mass transfer*. 4th ed. New York: John Wiley & Sons.

Ye, Z. 2007. UV disinfection between concentric cylinders. PhD thesis, School of Chemical & Biomolecular Engineering, Georgia Institute of Technology, Atlanta.

Ye, Z., L. J. Forney, T. Koutchma, A. Giorges, and J. A. Pierson. 2008. Optimum UV disinfection between concentric cylinders. *Ind. Eng. Chem. Res.* 47: 3444–3452.

7 UV Process Calculations for Food Applications

Preservation is a process by which chemical agents or physical treatments prevent biologic deterioration of a substance. Microbial growth in foods is one of the leading causes of food spoilage, with the subsequent development of undesirable sensory characteristics. The pathogenicity of certain microorganisms is a major safety concern in the processing of foods. A wide range of physical treatments and chemical agents are employed to preserve foods with a high level of quality and safety. Based on the mode of action, major food preservation techniques can be categorized as: (a) inhibiting chemical deterioration and microbial growth, (b) directly inactivating bacteria, yeasts, molds, or enzymes, and (c) avoiding recontamination before and after processing. Methods of slowing down (inhibiting) microbial growth include refrigeration and freezing, reduction of water activity, acidification, adding preservatives, and adding or removing gases (oxygen or carbon dioxide). Direct inactivation can be performed during blanching, cooking, frying, pasteurization, and sterilization. Packaging, hygienic processing, and storage are the common approaches to avoid recontamination.

Of the many techniques used to preserve foods, only pasteurization and sterilization rely on killing the most resistant pathogens of public health concern. As defined by the U.S. Food and Drug Administration (2000), sterilization is a process to remove or destroy all viable forms of microbial life, including bacterial spores. Pasteurization was defined as a process of mild heat treatment to significantly reduce or kill the number of pathogenic and spoilage microorganisms. In September 2004, the USDA National Advisory Committee on Microbiological Criteria for Foods (NACMCF) redefined the term pasteurization. This was done in response to the fact that new physical methods of treatment are emerging as a result of the current consumer demands for foods that are more fresh, natural or minimally processed, and additive free. The use of thermal treatment leads to overcooking, an undesirable cooked flavor, and nutritional deterioration. To satisfy these demands, some changes in traditionally used preservation techniques must be made. However, the definition of a traditional pasteurization process relied only on thermal treatment, since this was the most widely used process in the category. The new definition of "pasteurization" includes "any process, treatment, or combination thereof, that is applied to food to reduce the most microorganism(s) of public health significance to a level that is not likely to present a public health risk under normal conditions of distribution and storage" (Food Chemical News 2004). UV radiation was one of the emerging techniques examined in the NACMCF report as an alternative to thermal pasteurization.

The knowledge of the physical nature of the process as well as the microbial resistance is essential for establishing a preservation process. The efficiency of the process is dependent on a number of parameters that are unique to each technology. To confirm the validity of the process, the effect of critical process and product

parameters on the inactivation capacity of that particular treatment must be demonstrated and will be briefly described in this chapter. The objective of this chapter is to review requirements for establishment of the preservation process specification. The requirements must be based on current practices and methods to measure the delivery of the scheduled UV process.

7.1 ESTABLISHMENT OF SPECIFICATIONS FOR PRESERVATION

For design of a "preservation specification" of a thermal pasteurization or sterilization process, processing time F_p (min) is traditionally defined by the initial load of resistant organisms (N_0), the end point of the process (N_F), the logarithmic resistance of target bacteria under defined conditions or D_T-value, and the specific log reduction of the process (SLR) (equation 7.1)

$$F_p = D_T \times (\log N_0 - \log N_F) = D_T \times \mathrm{SLR} \tag{7.1}$$

Traditionally, three approaches are used to define the treatment level, or sterility assurance level (Heldman 2003). The first approach comprises processes with a specific target end point, or probability of finding a nonsterile unit (PNSU). Within the PNSU concept, the final surviving level of microbial hazard defines product safety. The second approach comprises processes designed to consistently deliver a specific log reduction SLR (5*D*, 12*D*) of the microbial load. The resulting process is represented by equation (7.2), where SLR is the number of log reductions

$$F_P = \mathrm{SLR} \times D_T \tag{7.2}$$

The process target of making the food product "free from" microorganisms of concern is the third process design approach used for sterilization.

A similar concept can be applied for specifying a preservation process using any other physical or chemical lethal treatment or combination of treatments. Adoption and use of this convention will provide standardized calculations of microorganisms' resistance and facilitate comparability between processes. However, in order to design a process using treatments other than heat, the resistance of the most-resistant microorganism to the specific lethal agent must be determined from laboratory studies. The pathogen with the greatest resistance to one treatment, e.g., heat, usually will not be the most resistant to another type of treatment, e.g., irradiation.

In order to evaluate the degree of safety of any pasteurization process, the following procedure is usually employed: The initial number of "target" microorganisms and their resistance to the pasteurizing process (UV light) is determined, and then the final number of indicators surviving the process is calculated. Current knowledge of microbial UV resistance and "normal" levels of contamination will define the margins of a process. In any pasteurization process validation study, the target or pertinent pathogen of concern must be identified first. Records of normal microbial counts in industrial food products are known for their irregular, fluctuating character. The fluctuation pattern is determined primarily by variations in the initial load and numerous random factors, which tend to promote or inhibit the microbial growth. Since our understanding of the complex and dynamic microbial ecosystems

in food-production environments is still relatively superficial, food-preservation and safety-assurance systems must remain crude at best and be guided by a few general principles that apply to both spoilage and pathogenic species.

1. Expect fluctuations, and possibly increases, in the resistance of microbial contaminants to destructive or inhibitory agents.
2. Expect process failure if contamination levels are uncontrolled.
3. Anticipate the eventual emergence (recognition) of new food-borne pathogens.

Although generally artificial with respect to the "normal" levels seen on fruit or in juice-processing operations, the use of a convenient contamination level of $>10^6$/mL (or per gram) can be applied under appropriate treatment conditions to give a measurable level of survivors, which facilitate comparisons of the effects of different process variables.

The minimum infectious dose is an expression of the lowest number of organisms required to initiate an infection in any individual under given circumstances. The infectious dose for *Escherichia coli* O157:H7 is not yet known. However, based on the relatively high attack rates during outbreaks, it appears that the number of bacteria required to cause illness is very low. *Listeria monocytogenes* is present in a large number of foods but normally in very low numbers, i.e., less than one colony-forming unit (CFU) per gram of food.

Traditional kinetic parameters of microbial destruction such as reaction rate constant (k) and decimal reduction times (D) are used in thermal-process calculations. The determination of D-values is based on the assumption that microbial destruction follows an exponential decay or first-order kinetic mode (equation 7.3). For many foods, a first-order model adequately describes the destruction of bacteria under the action of various physical agents. When inactivation follows a first-order model, the thermal resistance of microorganisms is described by means of the D-values and can be calculated using the following equation (7.3)

$$D_T = 2.303/k \tag{7.3}$$

7.2 DELIVERY OF THE SCHEDULED PROCESS

Determination of the physical nature of the treatment is essential for the validation of process capacity to deliver the specified inactivation. The characteristic of the physical agent's action or exposure should uniquely determine the response of the microorganism and define the yield of the biological effect or kill of the treatment being used. The exposure is analogous to the "exposed dose," which is the amount of energy supplied to the object or energy "incident upon" an object and does not imply that the energy is "absorbed" by the object. In general, the exposed dose (ED) of any lethal physical or chemical agent could be expressed as a product of the agent's intensity and exposure time. The intensity of the lethal agent (temperature, concentration, light intensity) can be constant or varied in time (increasing, decreasing) or fluctuating (pulses). In some instances, the intensity of physical or chemical treatment varies with time, such as nonisothermal heating, intensity of UV light, or concentration of chemical agent.

In order to estimate the dose of the agent of varied intensity, the equivalent or effective time at a reference temperature, intensity, or concentration can be calculated. This approach has been traditionally used in the thermal process calculations.

The lethal action of irradiation or "exposure to irradiation" is defined in terms of *dose* or *absorbed doses,* both of which are used interchangeably. Absorbed dose is the energy absorbed per unit weight of product and is measured in gray (Gy). One kilogray (kGy) is equivalent to 1 kilojoule (kJ) of absorbed energy per kilogram (kg). In addition, it was found that 1 kGy could raise product temperature by approximately 0.24°C if all energy is converted to joule heating. A few thousand gray is a typical dose for processing food.

In photobiology, UV dose is defined in terms of *incident energy* and *absorbed energy*. Fluence (UV dose) is the total amount of radiant energy from all directions incident on an infinitesimally small sphere of cross-sectional area *dA*. The UV dose divided by *dA* is stated in units of J/m^2 or mJ/cm^2. The volume-averaged absorbed UV dose is UV energy absorbed by the medium as defined by Beer's law. Effective or delivered germicidal UV dose is a radiant energy delivered to the molecule or microorganism. Microbial inactivation depends primarily on the effective dose.

7.2.1 Reactor Performance

Important aspects of UV system performance include dose delivery and dose delivery monitoring. Both are affected by the design of the reactor and the liquid foods being treated. Figure 7.1 is a representation of how the elements of a unit operation such as UV-light processing manifest themselves in the microbial reduction kinetics that is measured and/or modeled for the targeted performance objective. The main elements include the transport phenomenon relevant in treating the liquid, the physical or chemical characteristics, and the resistance of the microorganisms to UV treatment. However, the achievement of the performance objective may result in the destruction of nutritional components and the formation of undesired compounds.

The delivery of UV dose within a reactor at full-scale is one of the challenges to ensure a 5-log reduction in numbers of the most resistant pathogen in fresh juices. For the UV pasteurization process, this indicates that a detailed knowledge of microbial UV inactivation and a complete representation of radiation irradiance and velocity fields are required in the development of the UV process.

Commercial UV reactors are flow-through systems, which have a distribution of exposure time (RTD) and light irradiance distribution (LID) due to attenuation following the Beer–Lambert law. Consequently, there is a variation in UV dose (product of LID and RTD) that any given microorganism is exposed to, and this can alter the performance of the reactor. The dose received by any individual microorganism may be calculated as the integral of the irradiance history throughout its residence time within the irradiated zone (equation 7.4)

$$\text{Dose}_i = \int_0^{\tau_i} I(t)dt \tag{7.4}$$

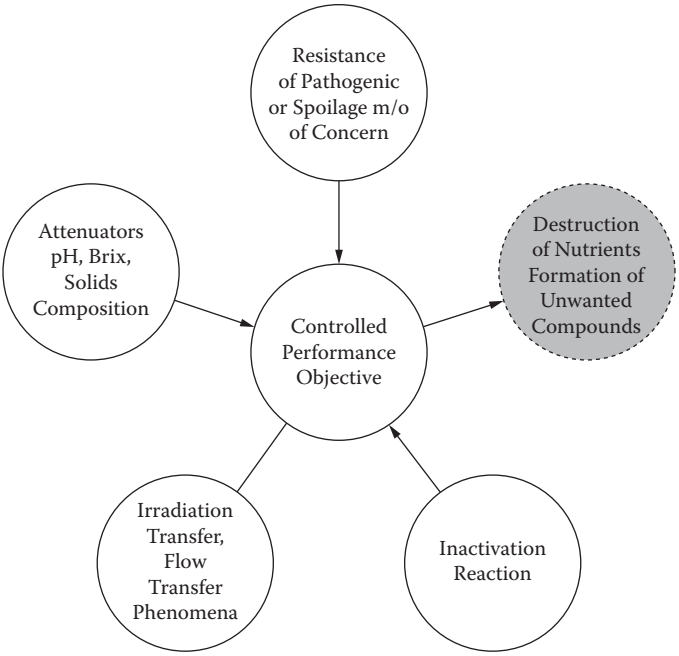

FIGURE 7.1 Critical elements affecting performance of UV reactors for processing liquid foods.

where Dose_i is the radiation dose received by the ith particle (mJ/cm^2), $I(t)$ is the time-dependent radiation irradiance (mW/cm^2), and τ_i is the period of exposure for the ith particle.

Therefore, estimation of the UV dose received by an individual microorganism requires knowledge of its trajectory through the irradiated zone. Understanding of UV transmission in the carrier fluid with high absorptive properties in relation to inactivation of pathogens is needed in order to establish inactivation efficiency.

The magnitude of the level of irradiance $I(r)$ from the lamp surface depends on transmission (or absorbance) of UV light through the liquid. The Beer–Lambert law (equation 7.5) serves as the main mathematical basis for computation of the UV fluence rate distribution in a medium,

$$I_r = I_0 \frac{r_0}{r} \exp[-a_\lambda (r - r_0)] \tag{7.5}$$

where I_r is the UV fluence rate at a distance r from the center (W/cm^2), I_0 is the UV fluence rate at the surface of the UV source (W/cm^2), r is the radial distance between the center of the source to the point at which irradiance is measured, r_0 is a radius of the UV lamp (cm), and α_λ is the absorption coefficient of the medium (cm^{-1}). Typical curves of UV fluence rate attenuation are shown in Figure 7.2 for malate buffer, clear apple juice, and apple cider (Koutchma and Parisi 2004). The higher the UV absorptivity of

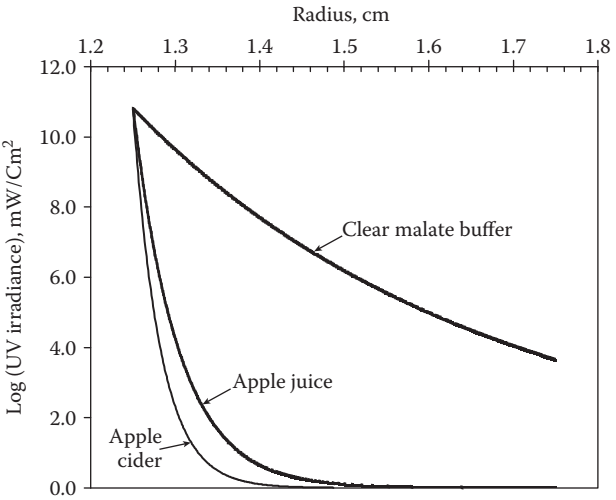

FIGURE 7.2 UV fluence rate distribution in malate buffer and apple juice/cider within an annular UV reactor of radius 1.75 cm. (From Koutchma and Parisi 2004. With permission.)

the medium to be disinfected, the higher is the inhomogeneity of the fluence rate field or the gradient of intensity between the lamp surface and the reactor wall.

As can be seen, UV fluence rate in juice/cider was strongly related to the distance outward from the lamp as opposed to high-transmission liquids, where the intensity of light striking the microorganisms is independent of its position from the lamp. This signifies that accumulated or absorbed UV dose in a juice volume will be primarily dependent on the radial position of the liquid and the time during which the liquid element resides at this position in the reactor. The flow pattern inside the UV reactor strongly influences the summed dose, since the position and the residence time of the microorganisms in certain regions of the irradiation field can vary significantly. Another reason for establishing flow characteristics is to obtain an indication of the mixing behavior of the fluid and how it can affect inactivation. Flow simulations using a computational fluid dynamics (CFD) program (Unluturk et al. 2004) showed that there was a variation in the dose received by the particles due to the broad range of the particle residence time distribution and the variation of fluence rate within the system.

The dispersed-phase model (DPM) was used to calculate particle residence time and locations in the CiderSure 1500 UV reactor. Figure 7.3 shows that some particles had a shorter duration time than the others, and some particles were exposed to lower UV intensity in the system. In addition, the simulation showed that some particles had the same residence time in the reactor, but received a different UV dose. For example, the particles that move close to the lamp side in the annular gap were exposed to a higher UV dose.

Stimulus-response techniques can be used for the experimental determination of RTD in UV reactors. Residence time is determined by pulse injections of sodium

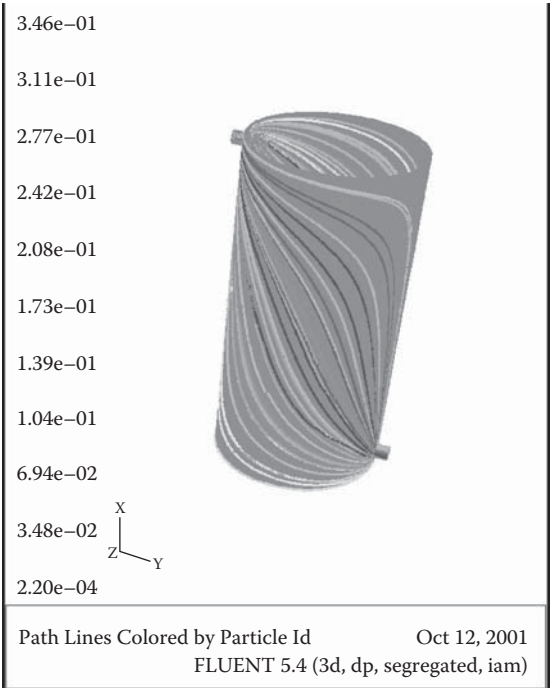

FIGURE 7.3 Particle tracks in the CiderSure 1500 UV reactor. (From Unluturk et al. 2004. With permission.)

chloride into the carrier fluid flow under steady-state flow conditions at the entrance of the reactor and then measuring the change in the salt concentration with time at the output of the UV reactor. The distribution of salt concentration $c(t)$ reflects the RTD in the UV reactor. The following information was obtained from experimental analysis of the $c(t)$ curve:

$E(t)$ is the age distribution function which represents a normalized curve for the fraction of fluid leaving the system at each time. $E(t)$ is constructed from the $c(t)$ curve or RTD function using a summation technique (equation 7.6)

$$E(t) = \frac{c(t)}{\int_0^t c(t)dt} \tag{7.6}$$

The mean residence time of the flow is calculated from the function $E(t)$ and time t using the summation technique (equation 7.7)

$$\bar{t} = \int_0^t tE(t)dt \tag{7.7}$$

The examples of $c(t)$ and $E(t)$ functions in a model solution at two flow rates for a vertical flow configuration of a single-lamp annular UV reactor are shown

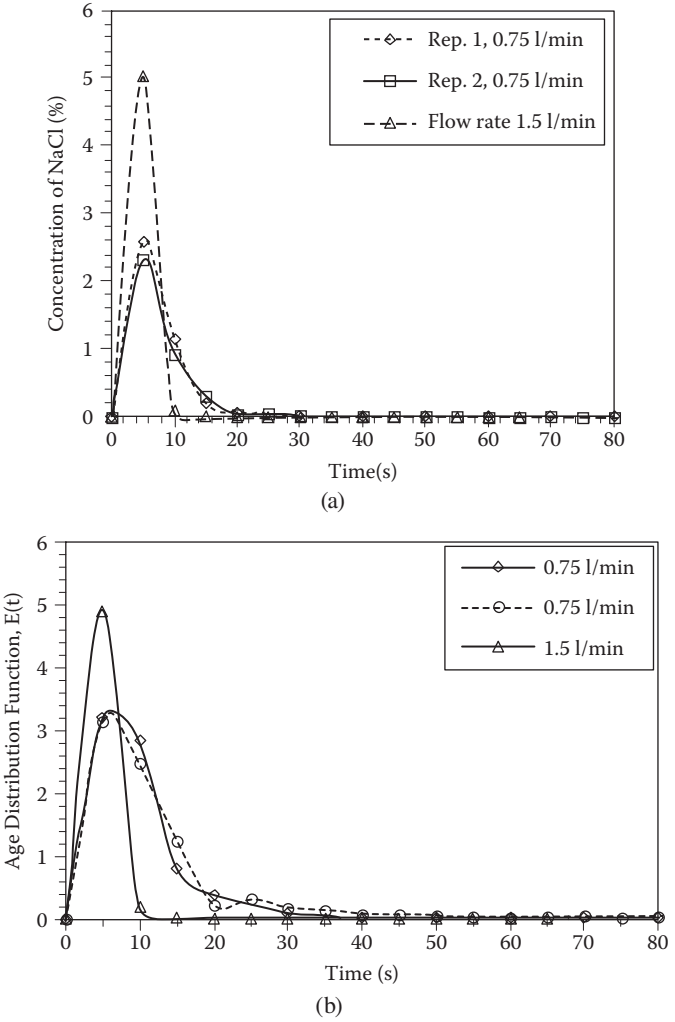

FIGURE 7.4 Exit concentration of sodium chloride in model solution—$c(t)$ function and $E(t)$ function—after pumping through the vertical annular UV reactor.

in Figure 7.4. The theoretical residence time ($t = V/Q$) can be calculated from the fill volume of the reactor V and volumetric flow rate Q. The ratio of $\bar{t}/t$ indicates whether full use is made of the reactor volume. If the ratio is less than 1, it indicates that the effective volume is much less than the actual volume of the reactor (Downey et al. 1998). In practice, microorganisms leaving a UV reactor experience different doses. Some microorganisms traveled close to the lamp and experienced a high dose while others that traveled close to the walls or between lamps experienced a lower dose. Some microorganisms short-circuit through the reactor quickly while others are trapped in eddy zones and dead spaces.

7.3 MEASUREMENT OF UV-DOSE DELIVERY

7.3.1 Biodosimetry

Biodosimetry or bioassay is a practical method commonly used for measuring the UV dose delivery by a UV reactor. Biodosimetry is a biological approach, since inoculated liquid product is passed through the reactor. Inactivation of microorganisms is determined by comparing the concentration of viable microorganisms in the samples taken from the reactor's influent (N_0) and effluent (N_F). The relationship between UV dose and specific log survival of the target bacteria is first developed using a collimated beam (CB) low-pressure mercury lamp (LPML) in a static UV system. *Escherichia coli* K12 can be used as a target bacterium for biodosimetry in juice products, since it is a surrogate of *E. coli* O157:H7. UV irradiance on the surface of the fluid can be determined using a calibrated radiometer that can also be used for UV dose calculations. When the count of surviving target bacteria in a UV reactor is determined, the delivered germicidal dose can be back-calculated knowing the decimal reduction (D_{10} dose) that is obtained from the dose-response curve constructed using a CB system. This measured dose value is termed the reduction equivalent dose (RED). The measured RED has a value lying between the minimum and average dose in the dose distribution. The drawbacks of this method are that the results are presented as the most probable results associated with the confidence interval of the microorganisms' enumeration (Linden and Darby 1997). Higher dose-response observations can be obtained for the collimated beam apparatus compared with the flow-through reactor. A correct dose measurement would result from biodosimetry only in the case that all microorganisms receive the same dose (ideal reactor). If a dose distribution occurs among the microorganisms, biodosimetry gives the volume average decimal reduction dose, which is lower than the arithmetic mean of the dose distribution.

7.3.1.1 Modified Biodosimetry Method

While there is currently no practical method available for measuring the UV dose distribution, a modified bioassay method employing the injection of target bacteria as a tracer reported by Koutchma et al. (2004, 2007) can be used to provide information on the distribution of the dose delivered in the UV reactor. To conduct a bioassay of UV dose distribution in the annular UV reactor, target bacteria can be used in a manner analogous to that for a salt tracer injection study. As an example, the pulse injection of *E. coli* bacteria as a tracer in model caramel solutions was employed, and the concentration of bacteria was measured at the outlet. The bacterial suspensions were injected into the flow stream at the entrance of the tube after steady-state conditions were achieved. The outflow fractions were collected as a function of time after injection. The injection was performed twice with the UV lamps on and repeated with the UV lamps off. The distribution of unirradiated bacteria reflected the RTD within the UV reactor. The distribution of surviving UV-irradiated bacteria reflected the combined effects that flow distribution (RTD) and light irradiance distribution (LID) can have on UV radiance exposure of bacteria. The level of inactivation of *E. coli* K12 in each volume fraction was obtained by subtracting the $\log_{10}$ of bacterial concentrations in the corresponding UV-unirradiated and UV-irradiated model solutions at a given time after injection.

The plots of concentration of viable bacteria versus time on semi-log scale after injection in 0.5% ($\alpha = 25.8$ cm^{-1}) and 1.0% ($\alpha = 51.5$ cm^{-1}) model caramel solutions at a flow rate of 5 gpm in a coiled UV reactor (Salcor Inc., Fallbrook, CA) with UV lamps "off" and "on" are shown in Figure 7.5. No survivors were detected at the outlet in model caramel solutions of 0.2% and 0.35%. The curve of distribution of the concentration of UV-unirradiated bacteria reflects the residence time distribution

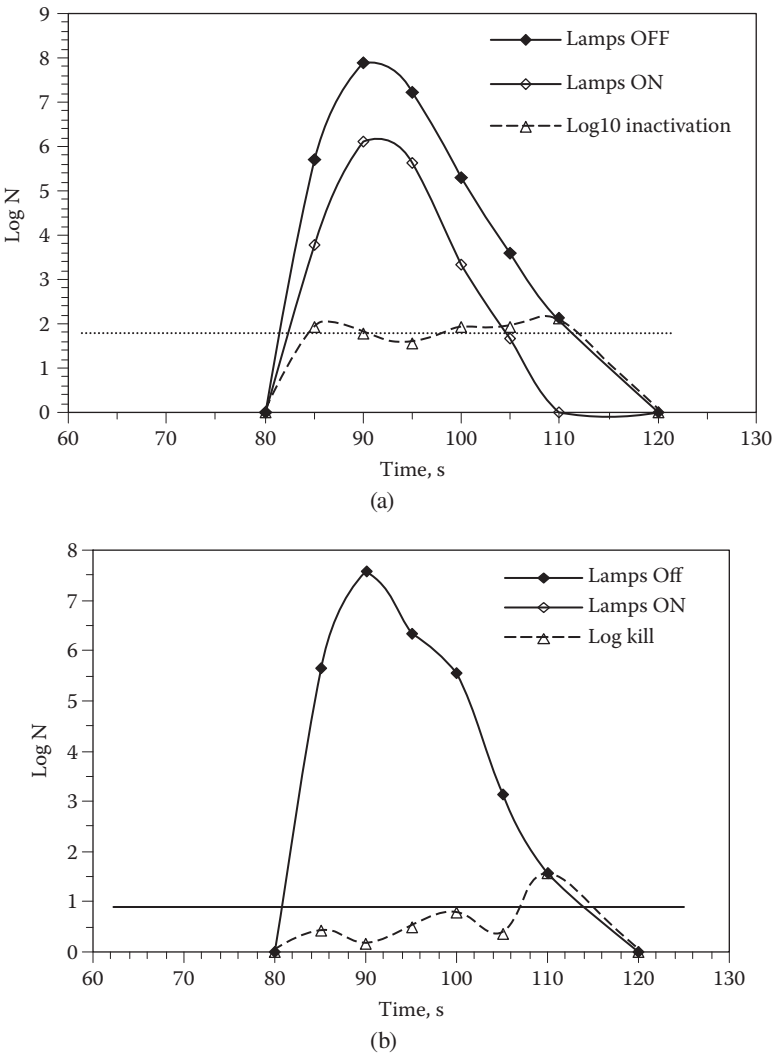

FIGURE 7.5 Bioassay of UV dose distribution in the coiled UV reactor at the flow rate of 5 gpm. Concentration of *E. coli* K12 as a function of residence time when irradiated and not irradiated by UV light. (a) 0.5% caramel model solution ($\alpha = 25.8$ cm^{-1}); (b) 1% caramel model solution ($\alpha = 51.5$ cm^{-1}).

(RTD) within the UV reactor. The curve of distribution of surviving UV-irradiated bacteria reflects the combined effects of the flow distribution (RTD) and UV-light irradiance distribution (LID) on the distribution of doses that any injected microorganism received within the UV reactor.

It can be seen (Figure 7.5a) that the distribution of the inactivated *E. coli* K12 in 0.5% model caramel solution was close to uniform, with an average of 1.86-$\log_{10}$ reduction and with maximum and minimum values of 2.1- and 1.6-$\log_{10}$, respectively. However, in 1.0% model caramel solutions, the microbial inactivation was broadly distributed from 1.6-$\log_{10}$ to 0.2-$\log_{10}$ reduction in the sample volumes, with an average inactivation of 0.47 $\log_{10}$. This reflected the higher gradient of UV-light irradiance between lamp surface and the wall region that depends on absorption of UV light through the liquid. The use of this approach can help in the interpretation of biodosimetry results of actual reactor performance and to improve the efficiency of the process.

7.3.2 Chemical Actinometry

Chemical actinometry is a photochemical method for measuring the number of photons in a light beam integrally or per unit time. A chemical sensitive to UV light at the wavelength of interest is exposed, and the resulting photochemical changes are measured. With chemical actinometry, photochemical conversion is directly related to the number of photons absorbed. In principle, some of the requirements for an effective chemical actinometer are constant quantum yield (i.e., number of molecules of product formed per photon absorbed) over a wide range of wavelengths, high sensitivity to UV light, and compatibility with the sample matrix. Some of the most widely used chemical actinometers used to measure dose during UV processing of water are potassium ferrioxalate ($K_3Fe(C_2O_4)_3$) and potassium iodide (KI). Although these standard actinometers have been used to measure UV dose in dilute aqueous solutions, no work has been published on the use of these actinometers in high acid solutions having large amounts of soluble solids, insoluble solids, and UV-absorbing compounds such as juices. In general, absorptivity and suspended particles, even those found in wastewater, do not approach absorbance levels encountered in juices.

Apple juice and cider can have different physical and chemical properties, depending on the variety of apple, time of harvest, type and length of storage, and method(s) of processing. Because UV dosage is the most critical parameter and it relates directly to the performance of a UV reactor, it would be useful to identify a chemical actinometer that could be effectively used for periodic verification of dose during UV processing of apple juices of different physical and chemical properties. The specific objectives of this study were to (a) evaluate the standard actinometers such as ferrioxalate and potassium iodide as well as 4,4′,4″-tris-di-B-hydroxyethyla minotriphenylacetonitrile (HHEVC; Far West Technology, Inc., Goleta, CA), a light-sensitive dye, for measuring dose during UV processing of apple juice of different physical and chemical properties; (b) measure the quantum yield of HHEVC dye using a static UV system; (c) calibrate HHEVC actinometer against a standard biodosimeter *E. coli* K12; (d) identify chemical and physical properties of apple juice that affect UV dose; and (e) evaluate UV dose in a continuous-flow UV reactor

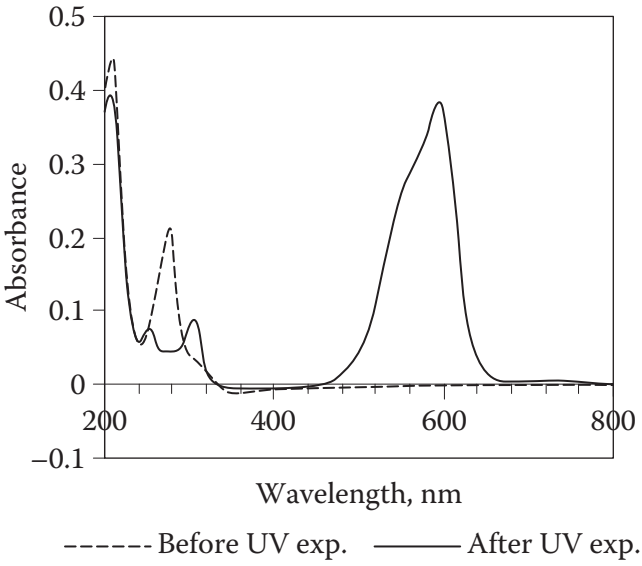

FIGURE 7.6 UV-Vis spectrum of HHEVC dye before and after UV exposure at 254 nm. (From Adhikari et al. 2005. With permission.)

(Adhikari et al. 2005). Static UV processing studies were conducted using demountable quartz cuvettes (NSG Precision Cells, Inc., Farmingdale, NY) with an opening at the side (10 × 40 mm) and path lengths of 0.1, 0.2, 0.5, and 1.0 mm.

The absorbance spectrum of the HHEVC shows the peak of absorbance of the dye at 254 nm, as illustrated in Figure 7.6, indicating that it has potential for measuring the UV dose. The photochemical reaction of the dye with electron-beam or UV-light photon results in the cleavage of CN- group from the rest of the molecule, causing a change in color from white to purple.

The dose-response curves in Figure 7.7 show that HHEVC dye was the most sensitive actinometer in the UV dose ranges studied (1–10 mJ/cm^2) compared with other standard chemical actinometers (potassium ferrioxalate and potassium iodide). It was found that potassium ferrioxalate and KI could not be used as actinometers in apple juice due to the chemical properties of the juice.

Estimation of the quantum yield of HHEVC dye provided an accurate calculation of UV dose. UV dose is defined as the delivered photons from a UV source that reacts with the actinometer, resulting in a chemical change at a particular wavelength. Thus, delivered UV dose (Einstein/cm^2 or mJ/cm^2) is the ratio of the number of moles of actinometer reacted per cm^2 in relation to the quantum yield of the actinometer. The quantum yield of HHEVC dye at 254 nm was calculated based on equation (7.8) (Lu 1981)

$$Q = \frac{-dc/dt}{I_0/b(1-10^{-kbc})} \tag{7.8}$$

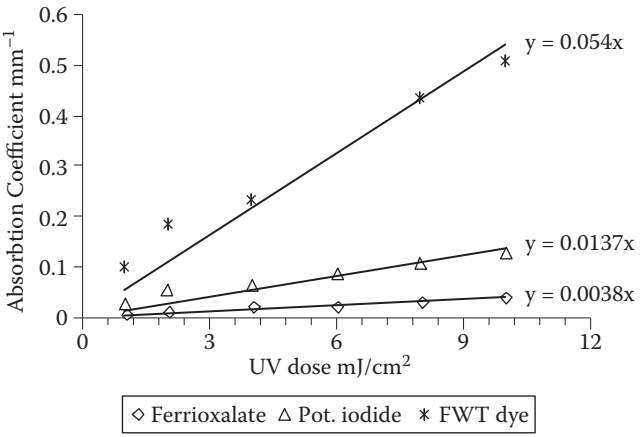

FIGURE 7.7 Comparison of UV dose-response curves of ferrioxalate, potassium iodide, and HHEVC dye in water at $I_0 = 1.02$ mW/cm^2. (From Adhikari et al. 2005. With permission.)

where

Q is the quantum yield of the HHEVC dye (mol/Einstein)
$-dc/dt$ is the change in concentration of the HHEVC dye with time (mol/L×s)
I_0 is the incident UV intensity (mW/cm^2)
b is the path length (cm)
k is the molar absorption coefficient of the dye at 254 nm (L/mol/cm)
c is the initial concentration of the dye (mol/L)

An incident intensity of 1.02 mW/cm^2 was used in all experiments. Samples were exposed to the UV light for different times to vary the applied dose. Table 7.1 shows the results of the calculations (equation 7.8) of the quantum yields of the HHEVC dye in various juice simulants and commercial apple juice. The quantum yields of HHEVC dye in all tested solutions ranged from 0.228 to 0.298 mol/Einstein and were not significantly different. These results were consistent with the fact that the quantum yield of an actinometer at a specific wavelength is a constant and it is not affected by the properties of the medium (Jagger 1967).

7.3.2.1 Effect of Chemical and Physical Properties of Apple Products on UV Dose

Chemical components of juice that can affect UV absorbance include proline, total acid, sorbitol, sucrose, fructose, and glucose as well as the elements cadmium, calcium, iron, lead, phosphorus, potassium, sodium, and zinc. Hence, it was important to study some of the key chemical variable product parameters that could have an influence on the UV dose, so the factors chosen for this study included absorbance, °Brix, suspended particles, and pH.

TABLE 7.1
Quantum Yield of HHEVC Dye at 254 nm in Model Juice Solutions and in Apple Juice

Solution [a]	Absorption Coefficient, (cm^{-1})	Quantum Yield of HHEVC Dye, (mol/Einstein) [b]
MB, pH3, °Brix 10	0	0.228 + 0.013
MB, pH3, 0.13 g/100 g, °Brix 10	6.4	0.252 + 0.015
MB, pH5, 0.13 g/100 g, °Brix 10	6.4	0.298 + 0.034
Clear apple juice, pH 3.5, °Brix 16	18.0	0.228 + 0.030

Source: Adhikari et al. (2005).

[a] MB = malate buffer.

[b] Significantly different at $p < .05$ confidence level.

7.3.2.1.1 Absorbance

It is generally known that the efficiency of UV disinfection reactors decreases as the absorbance of the liquid increases or as the percent of transmittance of UV through the fluid decreases. However, little was known about the quantitative impact of this parameter on UV dose delivery in liquids with high absorptive properties, such as juice products. The effect of absorbance on UV degradation of the dye was studied for pH-3.0 malate buffer containing 0.13 g/100 g or 0.6 g/100 g caramel and in clear apple juice with an absorption coefficient of 18 cm^{-1}. Increasing concentration of the caramel resulted in a decrease of UV dose in the malate buffer, as shown in Figure 7.8. Due to the high absorption coefficient (29 cm^{-1}) for a caramel concentration of 0.6 g/100 g in malate buffer, the penetration of UV radiation was attenuated, resulting in significant lowering of delivered dose compared with a 0.13-g/100 g caramel concentration (absorption coefficient 6 cm^{-1}) ($p < .05$). The dose range

TABLE 7.2
UV Dose in the CiderSure 1500 Reactor to Achieve 5-log Reduction of *E. coli* K12 at Flow Rate of 3.41 L/min

Product	Absorption Coefficient (cm^{-1})	Log Reduction per Single Pass	UV Dose, (mJ/cm^2 Actinometry)	UV Dose for 5-log Reduction, (mJ/cm^2)
Caramel solution (0.13 g/100 g)	6.4	4.26	2.75	3.22
Apple juice	18	0.74	2.52	17.03
Apple cider	30	0.36	0.28	3.89

Source: Adhikari et al. (2005).

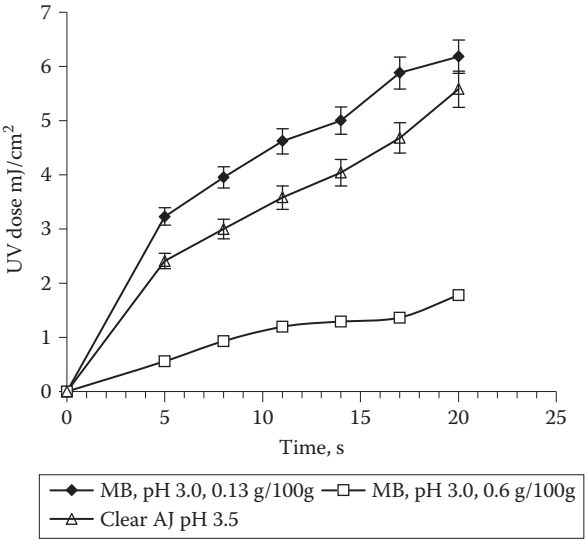

FIGURE 7.8 Effect of absorbance of model buffer caramel solution and apple juice (AJ) on UV dose in a static system. (From Adhikari et al. 2005. With permission.)

calculated for the model juice in an exposure interval of 20 s was up to 1 mJ/cm^2 at an absorption coefficient of 29 cm^{-1} and increased to 7 mJ/cm^2 at an absorption coefficient of 6 cm^{-1}. Thus, the absorption coefficient of the solution is a factor that influences the delivered dose in UV-treated apple juice: the lower the absorption coefficient, the higher is the rate of photochemical reaction. Downey et al. (1998) reported an increased inactivation rate of pathogens in irrigation water with decreasing absorbance. However, it can be concluded that HHEVC dye is suitable to be used in a matrix with an absorption coefficient less than 30 cm^{-1}.

7.3.2.1.2 pH and °Brix

HHEVC dye was found to be chemically stable in malate buffer in the pH range of 3.0 to 5.0 for a 0.13-g/100 g caramel concentration. However, at pH > 5.0, the solubility of the HHEVC dye is reduced with time, resulting in precipitation of the dye, which makes the solution appear cloudy (results not shown). It was found that soluble solid levels ranging from 10 to 20°Brix did not significantly affect the delivered UV dose in 0.13-g/100 g caramel model buffer solutions. Hence it is recommended that the HHEVC dye can be used to measure UV dose in acidic solutions (i.e., pH < 5) rather than alkaline or less acidic solutions.

7.3.2.1.3 Suspended Solids

Suspended apple solids (SS) (1–4 g/100 mL) were added to a malate buffer (pH 3.0; 0.13 or 0.4 g/100 g caramel) to simulate apple cider with turbidities of 100–1200 NTU (nephelometric turbidity units). Figure 7.9 illustrates the effect of the concentration of SS in caramel solutions on UV dose delivering in malate buffer. The obtained

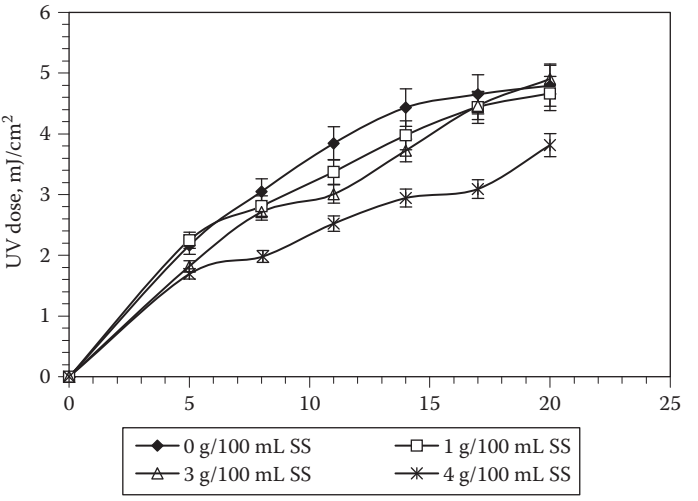

(a) 0.13 g/100 g Caramel with SS

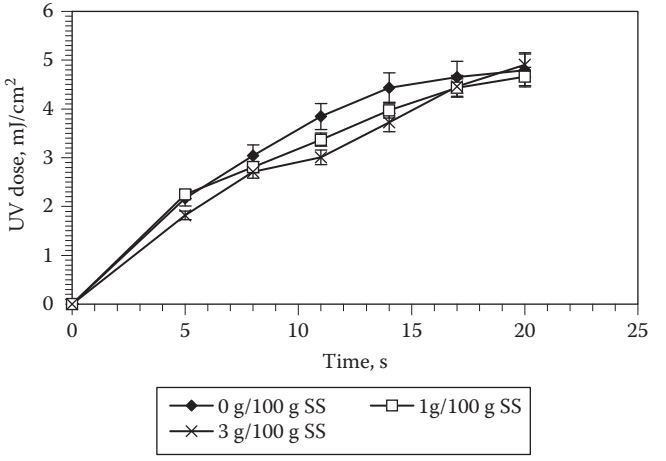

(b) 0.4 g/100 g Caramel with SS

FIGURE 7.9 Effect of suspended solids (SS) (turbidity) on UV dose delivery in a malate buffer containing 0.13 or 0.4 g/100 g caramel at pH 3.0. (From Adhikari et al. 2005. With permission.)

results indicated that, at a caramel concentration of 0.13 g/100 g, the dose response decreased with increased concentration of SS. It was found that solutions of 0–3 g SS/100 mL had a UV dose of approximately 4.7 mJ/cm², whereas in the solution containing 4 g SS/100 mL, only 3.8 mJ/cm² or 81% of the UV dose was delivered (Figure 7.9a). This observation can be explained by increased scattering of light as SS levels increased. Scattering reduces the fraction of UV light available for reacting with the HHEVC dye due to the increased path of scattered light traveling through a liquid medium. When the effects of SS in caramel malate solutions at concentrations

of 0.13 g/100 g and 0.4 g/100 g were compared, it was observed that in solutions with higher absorbance (0.4 g/100 g), the scattering effect of SS on dose delivery was less pronounced (Figure 7.9b). Given that the turbidities of juice can range from 1000 to 2400 NTU, the effects of SS on delivered dose in juice are more pronounced than in wastewater and can have a negative impact on the effectiveness of UV light for microbial destruction.

7.3.2.2 Calibration of HHEVC against a Standard Biodosimeter

In order to correlate the quantum yield of the dye with the inactivation levels of a biodosimeter, a suspension of the bacteria (concentration up to 10^6 CFU/mL) and HHEVC dye were prepared in 0.13-g/100 g caramel model solution and exposed to UV light under identical conditions. A linear relationship ($R^2 = 0.98$) between the number of log reductions and absorbance of the dye solution after exposure to UV light was observed within the dose range up to 10 mJ/cm^2, as illustrated in Figure 7.10. Knowing the absorbance reading and quantum yield of the HHEVC dye after UV treatment, a calibration curve can be used to estimate the UV dose required to achieve a 5-log inactivation of *E. coli* K12 in the flow-through reactor.

HHEVC dye was used to estimate the UV dose delivered during continuous UV processing in the CiderSure 1500 reactor. The UV dose was estimated in 0.13-g/100 g caramel buffer solutions, apple juice, and apple cider at three flow rates, as shown in Figure 7.11. As expected, the low flow rates (higher residence time) resulted in the highest UV doses delivered in the reactor. The actinometry data obtained from the CiderSure 1500 reactor matched the trend observed in static UV studies. As in static studies, as the absorbance of the model solution increased with 0.13-g/100 g to 0.6-g/100 g concentration of caramel at pH 3, the delivered UV dose in a continuous

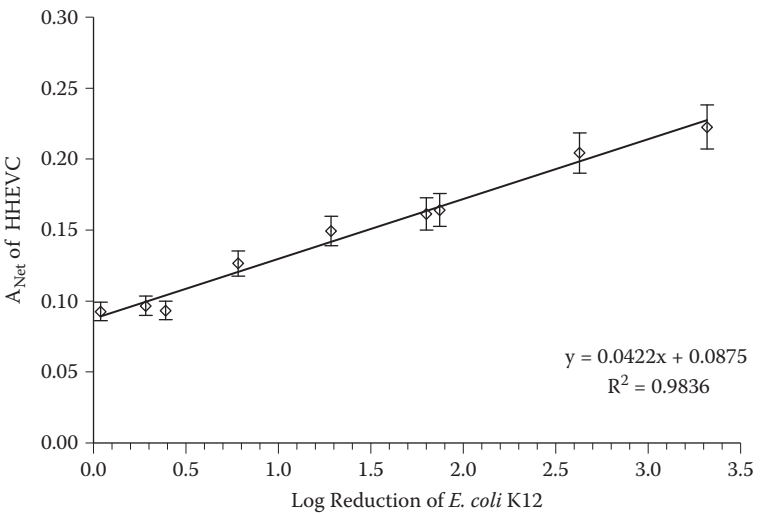

FIGURE 7.10 Correlation curve of log reduction of *E. coli* K12 vs. absorbance of HHEVC in 0.13-g/100 g caramel buffer exposed to UV light. (From Adhikari et al. 2005. With permission.)

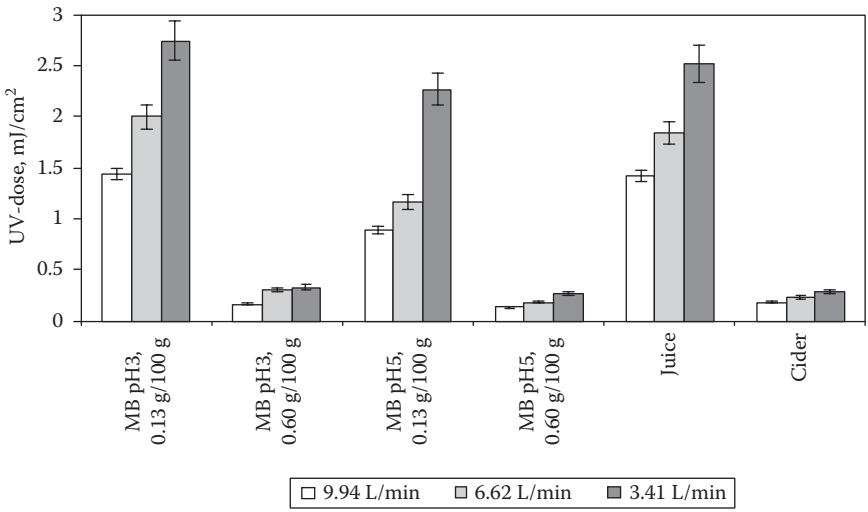

FIGURE 7.11 UV dose in caramel solutions, apple juice, and apple cider treated in a continuous flow CiderSure 1500 UV reactor. (From Adhikari et al. 2005. With permission.)

UV reactor decreased. In the case of a 0.13-g/100 g caramel in malate buffer (pH 3), the dose varied from 1.4 to 2.75 mJ/cm^2, while the dose was reduced to 0.14–0.88 mJ/cm^2 in a 0.6-g/100 g caramel in malate buffer (pH 3) in all flow rates studied. Similarly, the UV dose range in pH 5 malate buffer (for the malate buffer) containing 0.13-g/100 g caramel was from 0.9 to 2.28 mJ/cm^2. The UV dose decreased to 0.20–0.41 mJ/cm^2 in the buffer containing 0.6% caramel (pH 5). In contrast to the static UV studies, continuous UV treatment of pH-5 buffer showed a significant reduction of delivered dose, perhaps due to a loss in dye stability with time in solutions of low acidity. The delivered dose range in clear apple juice was from 1.28 to 2.52 mJ/cm^2. This dose delivered to clear apple juice was comparable with that of the malate buffer with 0.13-g/100 g caramel coloring added. The UV dose delivered in commercial apple cider (absorption coefficient of 30 cm^{-1}, pH 3.7, 1360 NTU) varied between 0.18 and 0.28 mJ/cm^2 due to the effects of suspended solids. Suspended solids that absorb and scatter the UV photons resulted in a lower rate of photochemical reaction of the HHEVC dye and reduced the UV dose delivered to the molecule.

Chemical actinometry was used to estimate the delivered UV dose in the CiderSure 1500 thin-film reactor that would achieve a 5-log reduction of *E. coli* K12 bacteria in apple juice and cider (Table 7.2). The log reduction of *E. coli* K12 in 0.13-g/100 g caramel, apple juice, and cider was measured after one pass through the reactor at a flow rate of 3.41 L/min. As expected, lower inactivation was observed in apple cider, the solution with the highest absorption coefficient. Nevertheless, the data indicate a similar range of delivered UV dose in 0.13-g/100 g caramel and apple cider. The observed phenomenon correlates well with data presented earlier by Koutchma et al. (2004). It was found that the relative transmittance readings of apple cider were similar to that of model 0.13-g/100 g caramel buffer with suspended solids. Surprisingly,

the transmittance of clear apple juice was lower than that of apple cider containing suspended solids. From the results presented, it can be concluded that transmittance of UV light through the annular gap in the CiderSure 1500 reactor is proportional to UV dose absorbed by the solution. Juice properties affect the efficacy of the UV-light absorption and destruction of microorganisms.

7.3.3 Mathematical Modeling

Mathematical modeling is an essential tool in the design of a UV process for liquid foods and beverages. Modeling can be used for a number of purposes. First, mathematical modeling can be used to predict the efficiency of microbial inactivation in a UV reactor for a specific application based on inactivation kinetics and transport phenomena, as shown schematically in Figure 7.1. Secondly, mathematical modeling of UV fluence in the reactor can assist in understanding the fluence distribution and identify the location of the least-treated liquid or dead spot in the reactor. The critical process and product parameters affecting UV fluence distribution in the reactor are shown schematically in Figure 7.12. Because commercial UV reactors are of a flow-through type, they are expected to have a distribution of exposure time or residence time distribution (RTD) and fluence rate distribution (FRD) resulting from UV-light attenuation in a medium with high absorptive properties. It can be seen that the emitting characteristics of the UV-light source and absorptive properties of the treated medium, the RTD in the annulus, and the annulus size and geometry will determine the UV fluence distribution in the reactor.

Computing the UV fluence is another way to evaluate the performance of UV processing reactors, since software is capable of modeling UV fluence and predicting particle and fluid velocities, particle mixing, and the residence time distribution. A further application of the mathematical modeling of UV processing is to calculate the optimal dimensions and geometry of the UV reactor for maximum inactivation performance, taking into account the specific physical properties of food and the requirements of the process. Mathematical modeling was used to estimate the UV

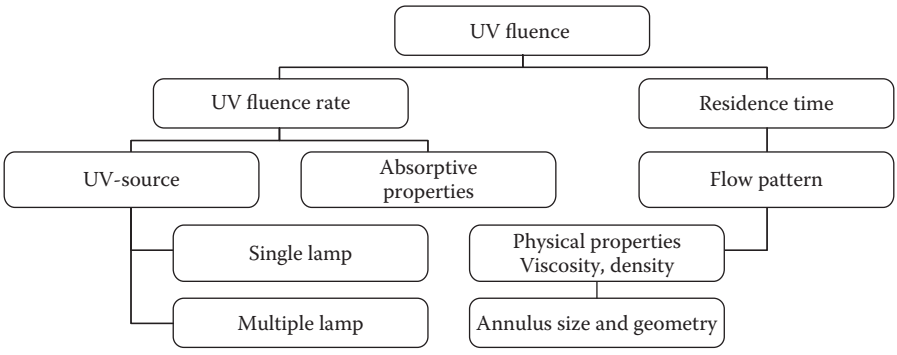

FIGURE 7.12 Critical process and product parameters affecting UV fluence distribution in the reactor.

fluence rate and UV fluence in apple juice and apple cider in multiple-lamp reactors such as the thin-film CiderSure (eight lamps) and the turbulent flow Aquionics reactor (Koutchma et al. 2006).

The CiderSure UV reactor incorporates three individual chambers connected in tandem with outside tubing. Eight low-pressure mercury arc lamps are mounted within the quartz inside cylinder running centrally through all three chambers. The manufacturer declared that each lamp emits UV radiation at a minimum fluence of 60 mJ/cm^2. A stainless steel outside cylinder covers all three chambers and lamps. Apple juice is pumped through a 0.08-cm annular gap between the inner surface of each chamber and the outer surface of the quartz sleeve. The CiderSure Model 1500 allows three flow-rate settings to regulate the UV fluence.

In the Aquionics UV reactor, the treatment was achieved by passing apple juice or apple cider through a stainless steel chamber containing 12 UV-emitting low-pressure mercury arc tubes. Each single arc tube is mounted in a quartz sleeve and fitted within the chamber, allowing the liquid to pass the sleeve on all sides (Koutchma et al. 2006). A sealed UV monitor, fitted to the chamber, measures the intensity of UV light being emitted from the arc tube. A temperature sensor is fitted on top of the chamber. The flow rate of 75 L/min was used in the experiments.

7.3.3.1 Flow Dynamics

Flow dynamics was first evaluated for water and apple cider at the entrance section of the UV reactors. The average velocity U_{av} was calculated as ($U_{av} = Q/A_{inlet}$), where Q is a volumetric flow rate and A is the inlet cross-sectional area. Reynolds numbers (Re) were calculated next as ($\mathrm{Re} = U_{av}\, d_{inlet}\, \rho/\mu$) based on the measured flow rate in each reactor, where d is characteristic dimension, ρ is density of fluid, and μ is dynamic viscosity. The magnitude of the Reynolds number (<2000) indicated that, at the selected flow rate of 56.8 mL/s, the hydraulic regime was laminar in the CiderSure UV reactor. However, in the Aquionics UV reactor at flow rates of 75 L/min, the flow dynamics can be characterized as a fully developed turbulent flow with Re > 10,000.

7.3.3.2 UV Fluence Rate Distribution

A finite-line source model (MPSS) was employed to simulate fluence rate and fluence distribution in the laminar-flow CiderSure UV reactor (Unluturk et al. 2004). Equation (7.9) was used to estimate the total UV-light energy received at any point of the receptor site at the reactor I_λ

$$I_\lambda(r,z) = \sum_{i=1}^{n} \frac{\frac{\Phi}{m}}{4\pi {l_i}^2} \exp[-(a_q t_q + a(r - r_q))] \frac{l_i}{r} \tag{7.9}$$

where Φ is power of the UV lamp (W); l is the distance (cm) from a point source to a receptor site; m is the number of point sources; r is radial distance from the UV lamp axis to the receptor site (cm); r_q is the outside radius of the UV lamp (cm); a is the absorption coefficient of the medium (cm^{-1}); a_q is the absorption coefficient of the quartz tube (cm^{-1}); and t_q is the thickness of the quartz tube (cm). The necessary

inputs used for calculation were as follows. The lamps are 39-W, 6-in. (15.24 cm) length, low-pressure mercury arc with a 2.5-cm diameter quartz sleeve that emits primarily at 253.7 nm. The manufacturer stated that each lamp emits UV radiation at a minimum fluence of 60 mJ/cm^2. The cider was pumped as a thin film at the rate of 56.8 mL/s. The number of computational fluid cells, used to create a computational domain for the given fluid flow system, was 443,514.

The detailed analysis of the modeling approach and the results obtained in this reactor were reported by Unluturk et al. (2004). These modeling results of UV fluence rate in apple cider with an absorption coefficient of 30 cm^{-1} were used in the current study to calculate UV fluence in the CiderSure reactor. Examples of radial UV fluence rate profiles at the selected vertical distances $z = 0$, 1, and 39.1 cm were calculated based on the MPSS model (equation 7.9) that is shown in Figure 7.2. The computation results showed a variation of UV fluence rate across the annular gap from 90 mW/cm^2 near the UV source down to 1.81 mW/cm^2 near the wall. The resulting average fluence rate was 19.7 mW/cm^2 in apple cider with an absorption coefficient of 30 cm^{-1}. Based on an average theoretical residence time in this reactor (3.82 s at a flow rate of 56.7 mL/s), an average value of UV fluence of 75.25 mJ/cm^2 was obtained in the CiderSure UV reactor.

UV Calc 2, a software program for multiple-lamp ultraviolet reactors (courtesy of Bolton Photoscience Inc., Edmonton, AB, Canada), was used to compute three-dimensional fluence rate (irradiance) distribution, average fluence rate, and hence the fluence in the turbulent-flow Aquionics UV reactor. The program is based on the Multiple Point Source Summation Method with full reflection and refraction accommodation at the air/quartz/water interface (Bolton 2000).

In order to calculate UV irradiance in multiple-lamp reactors using UV Calc, the reactor was divided into four quadrants with the center as the origin. Since the quadrants were not symmetrical, the UV fluence rate was computed for each quadrant and the results were averaged. First, the rate was computed only in the central plane through the lamp centers giving the "uncorrected" average fluence rate. The product of the "correction factor" and the "uncorrected" average fluence rate resulted in the "corrected" average fluence rate. The use of the correction factor is based on the fact that, at a fixed distance r from the center of one lamp, the ratio of the average fluence rate from $x = 0$ to the bottom (or top) of the reactor to that at $x = r$ (r is the "longitudinal" coordinate parallel to the lamp axis) is virtually independent of r. This ratio is called the longitudinal "correction factor." The input required was as follows: absorption coefficient of apple cider of 5.7 mm^{-1} or transmittance $T = 0.0001\%$, lamp power of 42 W, efficiency of 35%, lamp length of 94 cm, lamp sleeve radius of 1.4 cm, and maximum cylinder radius of 9.1 cm.

The calculation of UV fluence rate was made for each of 12 lamps in the quadrants. UV fluence rates "uncorrected" and "corrected" were calculated for the four quadrants and then the results averaged for all four quadrants (Table 7.3). The variation of the average fluence rate in the quadrants was explained by the nonsymmetrical positions of the lamps in each quadrant. The product of the "corrected" fluence rate and the hydraulic residence time resulted in the average UV fluence or dose. It can be seen that the UV fluence in apple cider varied from 17.8 to 29.99 mJ/cm^2 in each of the four quadrants of the reactor. The UV fluence rate gradient was observed along

TABLE 7.3
Fluence Rate in Quadrants of the Aquionics UV Reactor

	Average Fluence Rate (mW/cm^2 Uncorrected)	Average Fluence Rate (mW/cm^2 Corrected)	Average Fluence (mJ/cm^2)
1 Quadrant	1.91	1.79	26.71
2 Quadrant	1.27	1.19	17.84
3 Quadrant	2.14	2.01	29.99
4 Quadrant	2.14	2.01	29.99

the lamp length ranging from 2 to 15 mW/cm^2. Consequently, the UV fluence in apple cider (fluence rate times residence time) varied from 17.8 to 29.99 mJ/cm^2 in each of the four quarters of the reactor. Observed destruction of *E. coli* K12 was about 0.2-log reduction per pass through the reactor at the flow rate of 75 L/min, with a mean residence time of 15 s. Thus, the estimated value of absorbed UV dose required for 90% reduction of *E. coli* bacteria in apple cider ranged from 90 to 150 mJ/cm^2.

7.4 CONCLUSIONS

UV treatment has received the least attention when compared with other nonthermal processing procedures. There is sufficient evidence in the literature on the success of this method for reducing most types of microorganisms. Recent developments in UV lamp technology are encouraging; however, more work is needed in the design of UV reactors capable of providing sufficient UV doses to all parts of the treated liquid.

Dose distribution among bacteria passing through UV reactors must be taken into detailed consideration in UV treatment of juices, since commercial UV reactors are flow-through systems. Such systems have a distribution of exposure time due to the flow distribution and light irradiance distribution because of UV-light attenuation in media with high absorptive properties such as fresh juices. Consequently, the variation in UV doses for any given microorganism during the disinfection process must be understood, since the dose distribution will alter the disinfection performance of the reactor.

Biodosimetry and actinometry are reliable means of determining dose delivery in solutions with suspended solids such as fresh juices. The bioassay method employing the injection of bacteria as a tracer can also be used to provide separate information of the UV fluence distribution in juices when the lamps are "on" and mean residence time and RTD when the lamps are "off." The use of this approach can help in the interpretation of biodosimetry results for the actual performance of the reactor and to improve the efficiency of the process. Hydraulic characteristics of UV reactors can also be determined through the tracer experiments.

However, within a juice system, several factors can influence the delivery of the effective dose. In the actinometry tests using HHEVC dye, it was found that the

significant factors that consistently affected the efficacy of UV-light inactivation in a liquid system such as juice were the absorbance of the liquid medium and suspended solids.

Average UV dose based on direct absorbance measurements may be overestimated for fluids with a high particle concentration and smaller soluble absorbance component. Because the relationship between absorption coefficient and delivered dose does not necessarily apply in systems that demonstrate scattering effects due to suspended solids, it is also necessary to compare biological dose response curves to actinometry data. The obtained values of delivered UV dose can be used for periodically verifying the status of the UV lamps in the reactor.

More work needs to be done to (a) develop a chemical actinometer for validation and verification of UV dose delivery in juices and (b) address the effect of UV treatments on the loss of sensory characteristics and nutritional parameters due to the phenomenon of photodegradation.

REFERENCES

Adhikari, C., T. Koutchma, and T. Beecham-Bowden. 2005. Evaluation of HHEVC (4,4′,4″-tris-di-B-hydroxyethyl aminotriphenylacetonitrile) dye as a chemical actinometer in model buffers for UV treatment of apple juice and cider. *Food Sci. Technol. (LWT)* 38: 717–725.

Bolton, J. R. 2000. Calculation of ultraviolet fluence rate distributions in an annular reactor: Significance of refraction and reflection. *Water Res.* 34: 3315–3324.

Downey, D., D. Giles, and M. Delwiche. 1998. Finite element analysis of particle and liquid flow through an ultraviolet reactor. *Comput. Electron. Agric.* 21: 81–105.

Heldman, D. R., and R. L. Newsome. 2003. Kinetic models for microbial survival during processing. *Food Technology-Chicago*, 57 (8): 40–46.

Jagger, J. 1967. *Introduction to research in ultra-violet photobiology*. Englewood Cliffs, NJ: Prentice Hall.

Koutchma, T., S. Keller, S. Chirtel, and B. Parisi. 2004. Ultraviolet disinfection of juice products in laminar and turbulent flow reactors. *Innovative Food Sci. Emerging Technol.* 5: 179–189.

Koutchma, T., and B. Parisi. 2004. Biodosimetry of *E. coli* UV inactivation in model juices with regard to dose and RTD distribution in annular UV reactor. *J. Food Sci.* 69: 14–22.

Koutchma, T., B. Parisi, and E. Patazca. 2007. Validation of UV coiled tube reactor for fresh fruit juices. *J. Environ. Sci. Eng.* 6: 319–328.

Koutchma, T., B. Parisi, and S. Unluturk. 2006. Evaluation of UV dose in flow-through reactors for juices. *Chem. Eng. Commun.* 193: 1–14.

Linden, K. G., and J. L. Darby. 1997. Estimating effective germicidal dose from medium pressure UV lamps using mathematical, bioassay, and chemical actinometry approaches. *ASCE J. Environ. Eng.* 123: 1142.

Lu, Y. C. 1981. The determination of the quantum yield of benzoquinone by a modified method of actinometry. Ph.D. Thesis, University of Cincinnati.

Sugarman, C. 2004. Pasteurization redefined by USDA committee. *Food Chem. News* 46 (3).

Unluturk, S., T. Koutchma, and H. Arastoopour. 2004. Modeling of UV dose distribution in a thin film UV reactor for processing of apple cider. *J. Food Processing* 65: 125–136.

U.S. Food and Drug Administration. 2000. Irradiation in the production, processing and handling of food. *FR* 65 (230): 71056–71057.

8 Reactor Designs for the UV Treatment of Liquid Foods

An ideal UV reactor would provide a uniform dosage of photons to the fluid. A second objective would be to provide a uniform dosage on a continuous basis to large volumes of fluid. These objectives are particularly difficult when the absorbance of the fluid is large and the penetration depth of the UV radiation is small. For example, the absorption coefficients of juices typically vary from $A = 10$ to 40 cm^{-1}, providing a small radiation penetration depth of 1 mm down to roughly 0.25 mm.

These objectives are possible in concept with an ideal plug-flow reactor (PFR). Useful geometries to approach these characteristics are continuous flow between concentric cylinders and flow through a channel or tube. Such geometries can provide a large surface-to-volume ratio for the application of radiation. However, reactors will subject the fluid to a nonuniform fluid velocity distribution near solid walls. A second problem is the exponential reduction in the radiation flux with distance from the reactor walls, as described previously. These problems can broaden the fluence and radiation distributions to microbes within the device and reduce the reactor effectiveness.

Data for the UV disinfection of juices in laminar Poiseuille and turbulent flow are presented in the literature (Wright et al. 2000; Hanes et al. 2002; Koutchma and Parisi 2004; Unluturk et al. 2004; Koutchma et al. 2007; Ye 2007; Ye et al. 2007). Furthermore, Forney et al. (2003, 2004) investigated the possibility of applying laminar Taylor–Couette flow to the UV disinfection of juices. To complement the latter study, possible design improvements are also suggested that explore the effects of a wavy wall geometry for the inner cylinder (Forney et al. 2008). Useful comparisons of microbe inactivation levels are made in the present discussion between all of the above geometries.

In the present discussion, inactivation data are considered for the three types of flow between concentric cylinders: laminar, turbulent, and Taylor–Couette flow. Moreover, inactivation data are presented for the two commercial designs of (a) turbulent channel flow (Aquionics, Hanovia Ltd., Slough, England) and (b) Dean flow in a helical tube (Salcor Inc., Fallbrook, CA). Comparisons are made for the predicted fluence distribution between the various flow patterns. The relative boundary-layer thickness for each flow pattern is also compared and discussed. Finally, useful correlation procedures are suggested for plotting the inactivation data for all devices on a single graph.

8.1 LAMINAR FLOW IN CONCENTRIC CYLINDERS

8.1.1 Thin-Film Annular Reactors

The UV-treatment system used in laminar Poiseuille flow, as shown in Figure 8.1, consisted of thin-film annular reactors from UltraDynamics model TF-1535 (Severn Trent Services Inc., Colmar, PA). The whole system consisted of four chambers with various UV effective irradiation lamp lengths of 11.2, 29.2, and 77.9 cm. The fluence rates on the quartz surface were 15.4, 16, and 12 mW/cm^2, respectively. Each thin-film annular reactor included a UV lamp, protective quartz sleeve, and a remote power supply for (120 Vac) (220 Vac) 50/60 operation with a built-in lamp failure indicator. The single low-pressure, germicidal UV lamp was positioned in a 316L stainless steel reactor vessel. The quartz sleeve inner diameter is 2.45 cm and the stainless steel outer diameter is 3.48 cm. Correspondingly, the gap formed by the two cylinders is 0.515 cm wide. All four reactors were used separately for laminar Poiseuille flow.

8.1.2 UV Fluence Distribution

The UV fluence profile across the gap for the UltraDynamics model TF-1535 reactor is investigated. The inner radius of the quartz sleeve is $R_1 = 1.225$ cm and the outer diameter of the stainless steel tube is $R_2 = 1.74$ cm. The single low-pressure, germicidal UV lamp is 77.9 cm long. The UV fluence profile across the fluid gap with d at

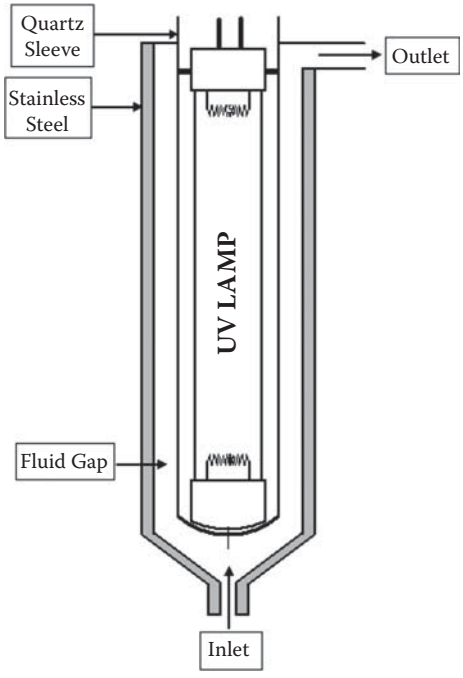

FIGURE 8.1 Schematic of thin-film reactor. (From Ye 2007. With permission.)

the reactor outlet is calculated from the product of the radiation intensity $I(r)$ within the fluid and the fluid residence time $t(r)$ along the laminar fluid streamlines. Here, the radiation intensity $I(r)$ in units of mJ/cm^2 is

$$I(r) = I_0 \frac{R_1}{r} \exp(-\alpha(r - R_1)) \tag{8.1}$$

where I_0 is the radiation flux at the inner wall, $r = R_1$, and the fluid absorbance $\alpha = 2.3A$. The fluid residence time is $t(r) = L/u(r)$ in units of s, where $u(r)$ is defined by

$$u(r) = C_1 \left[1 - \frac{r^2}{R_2{}^2} - \frac{1 - \left(\frac{R_1}{R_2}\right)^2}{\ln\left(\frac{R_1}{R_2}\right)} \ln\left(\frac{r}{R_2}\right) \right] \tag{8.2}$$

and

$$C_1 = \frac{2v}{\left[1 + \left(\frac{R_1}{R_2}\right)^2 + \frac{1 - \left(\frac{R_1}{R_2}\right)^2}{\ln\left(\frac{R_1}{R_2}\right)} \right]} \tag{8.3}$$

where v in equation (8.3) represents the average fluid velocity within the gap.

Figure 8.2 depicts the UV fluence profile when the flow rate equals 12 mL/s and the absorption coefficients range from $A = 0$ to 12 cm^{-1}. In Figure 8.2, the hydraulic

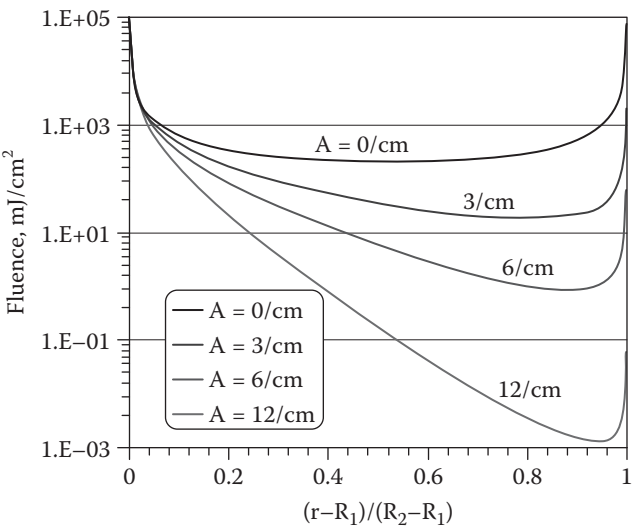

FIGURE 8.2 UV fluence profile in laminar flow with different absorption coefficients and $Q = 12$ mL/s. Vertical order in caption is identical to line position on graph. (From Ye 2007. With permission.)

Reynolds number is $Re_h = 285$, where $Re_h = D_h v/\upsilon = 2(R_2 - R_1)v/\upsilon = 2dv/\upsilon$. Here, $D_h = 2d$ is the hydraulic diameter, v is the average fluid velocity, and υ is the kinematic viscosity. Figure 8.2 shows that the UV fluence varies from roughly 10^{-3} mJ/cm^2 to 10^5 mJ/cm^2. Because UV is irradiated from the inner cylinder, the combination of high fluence rate and long residence time leads to a high fluence near the inner cylinder. With increasing distance from the inner cylinder, the combination of decreasing fluence rate and residence time results in a decrease in fluence. After $(r - R_1)/(R_2 - R_1) > 0.5$, the residence time begins to lengthen. However, if the absorption coefficients of juices are high, e.g., $A = 12$ cm^{-1} in Figure 8.2, the decreasing fluence rate is more important than longer residence times. As expected, the lowest fluence is not the position with the shortest residence time—$(r - R_1)/(R_2 - R_1) \approx 0.5$ or the farthest position from the radiation source ($r = R_2$)—but, rather, near the outer cylinder.

The UV fluence profile can be processed further to generate the UV fluence distribution. The definition of the fluence distribution function is similar to that of the age distribution function (Froment and Bischoff 1990). Because the UV fluence distribution is so broad for photochemical reactors, the fluence distribution function has to be defined as the fraction of fluid leaving the reactor that has fluence of (log *It*) to [log *It* + *d*(log *It*)] instead of (*It*) to [*It* + *d*(*It*)]. Thus, one defines

$$E(\log It)d(\log It) = \text{Fraction of fluid with fluence of } [\log It, \log It + d(\log It)] \tag{8.4}$$

The fluence distribution can be used to compare the effects of different flow patterns within a plug-flow reactor. The fluence distribution is computed numerically by following a large number of microbes through the reactor while summing the number of photons incident on each microbe. In the present study, a large number of microbes N_T distributed evenly across the reactor inlet were numerically tracked through each of the reactors. The results are presented in Figure 8.3, where the fluence distribution function $E(\log It)$ is defined by the expression (Forney et al. 2004)

$$E(\log It) = \frac{1}{N_T}\frac{dN}{d(\log It)} \tag{8.5}$$

In Figure 8.3, the area under the curve for each reactor design represents all microbes tracked for each design, or $\int E(\log It)d(\log It) = 1$. In simple terms, reactor designs with the highest peaks in the distribution function are superior. In such designs, all microbes are subject to a nearly uniform number of photons, and the required incident radiation flux for inactivation is reduced.

In equation (8.5), it is often practical to use the dimensionless fluence of $It/I_{av}\tau$, where the average fluence I_{av} of an ideal plug-flow reactor (PFR) assumes a uniform velocity v such that

$$I_{av} = \frac{2\pi \int_{R_1}^{R_2} I_0 \frac{R_1}{r} \exp[-\alpha(r - R_1)] r dr}{2\pi \int_{R_1}^{R_2} r dr} = \frac{I_0 R_1 \{1 - \exp[-\alpha(R_2 - R_1)]\}}{0.5\alpha(R_2^2 - R_1^2)} \tag{8.6}$$

and $\tau = L/v$ is the fluid residence time, where L is the reactor length.

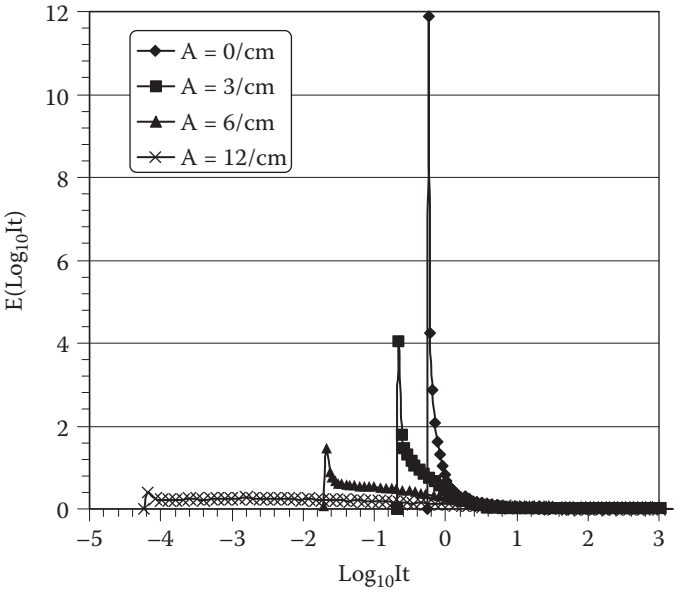

FIGURE 8.3 UV fluence distribution in laminar flow with different absorption coefficients and $Q = 12$ mL/s. (From Ye 2007. With permission.)

When the absorption coefficient is fixed, the fluence proportionally increases with the average residence time (the reciprocal of the flow rate). When the flow rate is fixed, large absorption coefficients result in broad fluence distributions, as shown in Figure 8.3. The dimensionless UV fluence distribution can easily demonstrate the deviation of real reactors from ideal plug-flow reactors. For example, when juices do not absorb UV radiation ($A = 0$ cm^{-1} in Figure 8.3), the performance of laminar reactors approaches that of ideal plug-flow reactors. With the increase in absorption coefficients, however, the performance of laminar reactors deviates from that of ideal plug-flow reactors. Moreover, decreasing the flow rate increases the inactivation levels in laminar UV reactors. The increased inactivation levels resulting from the decreased flow rates in laminar UV reactors, however, are at the cost of the reactor's decreased processing capability. The disadvantage of the broad fluence distributions for laminar reactors is alleviated only by decreasing the gap width or changing the flow pattern, such as applying turbulent or Taylor–Couette flow.

8.1.3 UV Inactivation Kinetics

The first order inactivation model is the simplest used to describe UV inactivation kinetics, since the model depends on a single rate constant, k_1. The model assumes that the inactivation rate changes with respect to pathogen concentration and fluence rate such that

$$\frac{dN}{dt} = -k_1 IN \tag{8.7}$$

where k_1 is a first-order inactivation constant, with units of cm^2/mJ. If k_1 and I are constant, by integration,

$$\frac{N}{N_0} = \exp(-k_1 It) \tag{8.8}$$

Because a lag in microbial inactivation at low fluence (the shouldered survival curve) is often observed, the first-order model overestimates inactivation at low log reductions.

The series-event inactivation model (Severin et al. 1983) was proposed to account for the lag at low fluence by introducing a second constant n, called the *threshold level*. It assumes that the inactivation of microorganism elements takes place in a stepwise fashion and that the rate at each step is first order with respect to fluence rate I,

$$\frac{dN_i}{dt} = k_{SE} I(N_{i-1} - N_i) \tag{8.9}$$

where k_{SE} is the inactivation constant in the series-event inactivation model, and subscript i is the event level. Here, k_{SE} is assumed to be the same for different event levels. When n elements of the microorganisms (a threshold) have been inactivated, the microorganisms will become nonviable. If k_{SE} and I are constant, the concentration of surviving microorganisms N is determined by

$$\frac{N}{N_0} = \exp(-k_{SE} It) \sum_{i=0}^{n-1} \frac{(k_{SE} It)^i}{i!} \tag{8.10}$$

where n is the threshold. One can show that if $n = 1$, equation (8.10) reduces to the first-order model.

8.1.4 UV Disinfection of *E. coli*

Figure 8.4 is the comparison of *E. coli* reductions between experiments and theoretical predictions for an $L = 29.2$-cm reactor. The theoretical predictions for the average residence time $\tau = L/v$ and total microbe reduction were made by the procedure described in Section 8.1.2. The total number of viable microbes at the reactor outlet is determined by summing the viable microbes on each streamline at the reactor outlet. The first-order model with $k_1 = 0.325$ cm^2/mJ and series-event model with $k_{SE} = 0.675$ cm^2/mJ and $n = 4$ are used for theoretical predictions. As expected, the log reductions do not have a linear relationship with average residence times because of the nonuniform fluence distribution and fluid boundary-layer effects.

According to Figure 8.4, it can be seen that the first-order model overestimates inactivation in regions with low fluence compared with experimental data and underestimates inactivation in regions with high fluence. These errors are reduced somewhat with the series-event model. Moreover, in Figure 8.4, the log reductions with

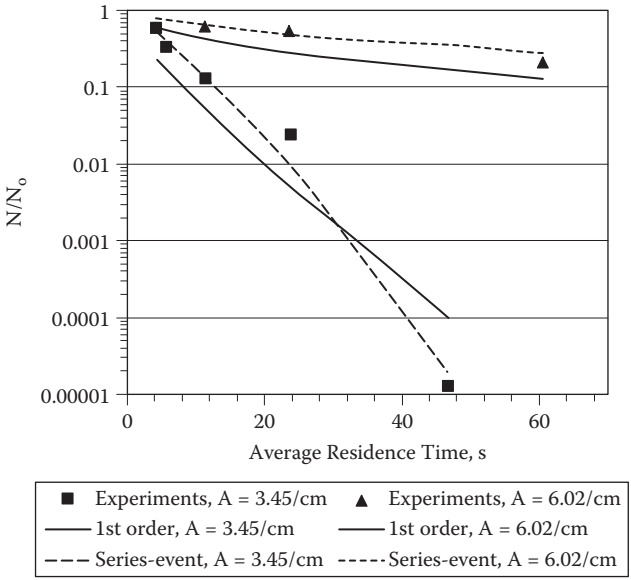

FIGURE 8.4 Comparison of *E. coli* log reductions between experiments and theoretical prediction for $L = 29.2$-cm reactor. (From Ye 2007. With permission.)

$A \approx 6$ cm^{-1} are much less than half the log reductions with $A \approx 3$ cm^{-1} when the absorption coefficients are increased by a factor of two (from 3 to 6 cm^{-1}). This is because fluence rates decrease exponentially with the path length from the radiation source, and small increases in the absorption coefficient result in a large increase in under-irradiated volumes.

8.1.5 Optimum Gap Width

Absorption coefficients A of juices vary widely, depending on brand and processing conditions. The normal range is $10 < A < 40$ cm^{-1}, with values as high as 60 cm^{-1}. Large absorption coefficients mean that thin-film annular UV reactors have to be used to inactivate juices. In designing thin-film annular UV reactors, one of the most important parameters is the gap width d. Because the velocity distribution across a narrow gap is not broad (the maximum velocity is about 1.5 times the average velocity), the distribution of residence time does not significantly affect the overall disinfection efficiency.

If the processing capability or flow rate Q of the UV reactor is kept constant, the gap width has opposing effects on the overall disinfection efficiency. When the gap width is increased, the longer average residence time may improve the overall disinfection efficiency (i.e., decrease N/N_0). On the other hand, a wide gap results in a broader fluence distribution because fluence rate decreases exponentially with the path length from the radiation source. Thus with large gap widths, the overall disinfection efficiency may become worse (i.e., increase N/N_0) because of larger

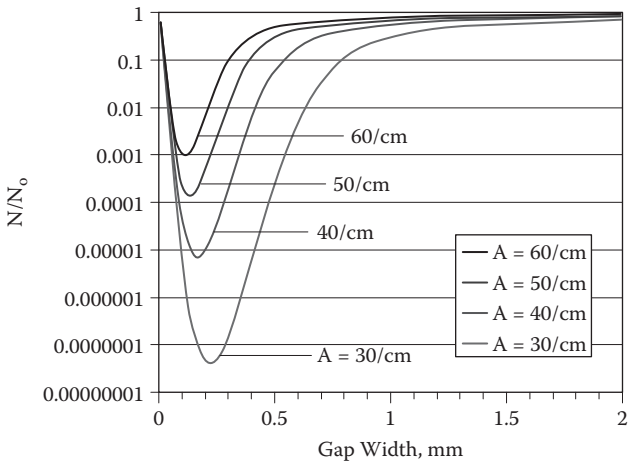

FIGURE 8.5 Log reductions when $Q = 1.25$ mL/s. Vertical order in caption is identical to line position on graph. (From Ye 2007. With permission.)

under-irradiated volumes. The final results, therefore, are determined by which of the two factors is dominating. As a result, for each absorption coefficient there is an optimum gap width.

Figure 8.5 shows how log reductions change with gap width d when the radius of the inner cylinder is constant at 1.225 cm and radiation comes from the inner cylinder with a fluence rate of $I_0 = 12$ mW/cm^2 and a UV effective lamp length $L = 77.9$ cm. It is useful to define the radiation penetration depth λ as the radiation path length at which the fluence rate is 10% of the incident radiation fluence rate I_0. The penetration depth is therefore the reciprocal of the absorption coefficient (base 10), or $\lambda = 1/A$. Therefore, one concludes from Figure 8.5 that an optimum gap width exists for each absorption coefficient A ($= 1/\lambda$).

Replotting the data from Figure 8.5, it is found that the optimum λ/d is constant for all fluids and independent of the fluid flow rates Q. As shown in Figure 8.6, the optimum $\lambda/d = 1.5$ (minimum N/N_0) for laminar thin-film reactors. Also shown in Figure 8.6, inactivation levels decrease (larger N/N_0) when $\lambda/d < 1.5$ because of the reduction in the exposed fraction of microbes with wider gap widths. In contrast, when $\lambda/d > 1.5$, the inactivation levels decrease because of smaller residence times.

8.1.6 Correlation of UV Disinfection in Laminar Reactors

The UV disinfection levels in laminar reactors with concentric cylinders can be obtained theoretically by integrating the following expressions

$$\frac{N}{N_0} = \frac{2\pi \int_{R_1}^{R_2} [I(r)t(r)]u(r)rdr}{2\pi \int_{R_1}^{R_2} u(r)rdr} \tag{8.11}$$

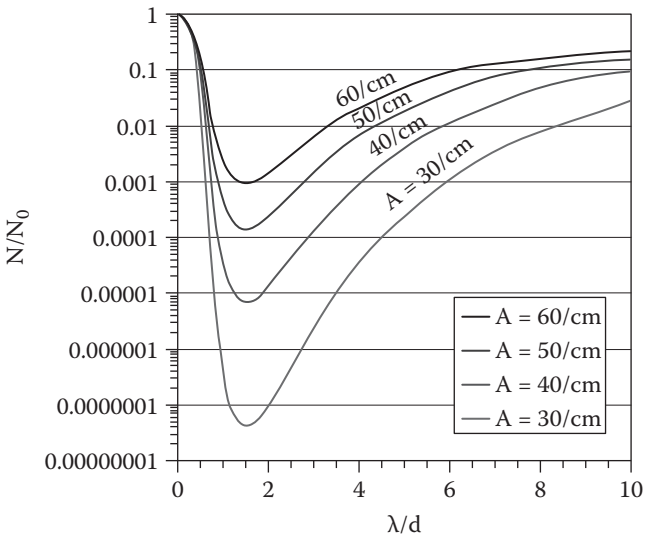

FIGURE 8.6 Log reduction with λ/d when $Q = 1.25$ mL/s. Vertical order in caption is identical to line position on graph. (From Ye 2007. With permission.)

However, it is desirable to find a simple correlation for log reductions with other parameters such as absorption coefficients and fluid residence times, etc. If the velocity profile is approximated by an average velocity v such that the fluid residence time $\tau = L/\text{v}$ and first-order inactivation kinetics is used, then equation (8.11) becomes

$$\frac{N}{N_0} = \frac{2}{(R_2^2 - R_1^2)} \int_{R_1}^{R_2} \exp\left(-kI_0\tau \frac{R_1}{r} \exp[-\alpha(r - R_1)]\right) r dr \tag{8.12}$$

According to the mean value theorem, there is at least one radius R_m such that $(R_1 \le R_m \le R_2)$ for the integration of equation (8.12) such that

$$\frac{N}{N_0} = \frac{2}{R_2^2 - R_1^2} \exp\left(-\frac{kI_0\tau R_1}{R_m} \exp[-\alpha(R_m - R_1)]\right) R_m (R_2 - R_1) \tag{8.13}$$

Assuming a dimensionless group $m = \frac{R_m - R_1}{R_2 - R_1} = \frac{R_m - R_1}{d}$, one can show that $m = 0.92$ and is approximately a constant for thin-film reactor geometries. Taking the natural logarithm of both sides of equation (8.13), substituting for m and neglecting the term $\ln[2R_m/(R_2 - R_1)]$, one obtains

$$\ln\left(\frac{N}{N_0}\right) = -\frac{kI_0\tau}{1 + m(R_2/R_1 - 1)} \exp(-\alpha d m) \tag{8.14}$$

where the term $[1 + m(R_2/R_1 - 1)] \approx 1$ for thin-film geometries.

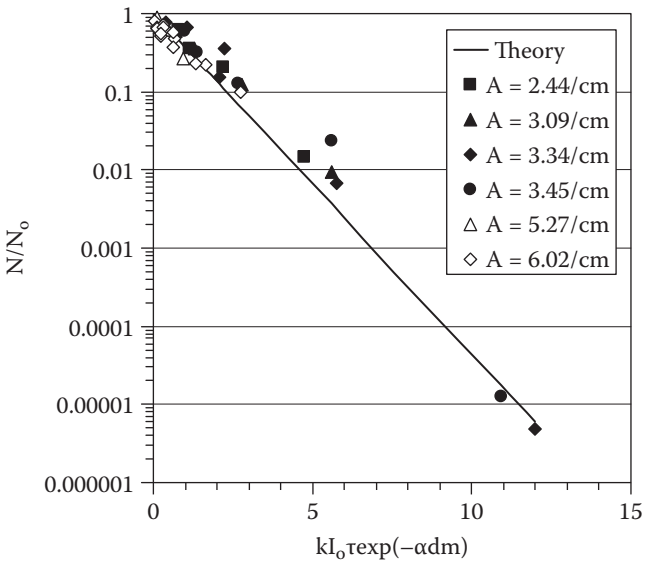

FIGURE 8.7 Correlation of UV disinfection in laminar reactors. (From Ye 2007. With permission.)

Figure 8.7 is the correlation obtained according to equation (8.14) and shows that log reductions are proportional to 1/exp(αdm). Figure 8.7 indicates that log reductions decrease rapidly with the increase in absorption coefficients, especially when the gap is wide. It is apparent that increasing the fluence rate of the UV lamp and decreasing the flow rate will increase the fluence proportionally. However, these effects cannot overcome the disadvantage of a broad fluence distribution when the absorption coefficient of the fluid is high and the radiation penetration depth is small.

With regard to laminar flow in concentric cylinders, it is demonstrated that there is an optimum gap width for each absorption coefficient. The optimum λ/d for laminar UV reactors is about 1.5. Because the normal absorption coefficients of juices are 10–40 cm^{-1}, the optimum gap width is in the range of 0.17–0.67 mm. Therefore, the gap width of laminar UV reactors used for juice disinfection should not be more than 1 mm. Existing commercial devices such as the CiderSure UV reactor (Koutchma et al. 2004) attempt to overcome the absence of radial mixing of the fluid in laminar devices by pumping the fluid through several stages.

8.2 TURBULENT FLOW IN CONCENTRIC CYLINDERS

8.2.1 Thin-Film Annular Reactor

The turbulent UV treatment system consists of the same concentric cylinder reactors used for the laminar-flow studies. A schematic of the flow in an annular reactor

is shown in Figure 8.8. However, for the case of turbulent flow, the reactors are connected in series to increase the short residence time because of high flow rates. For the experiments described, four reactors connected in series were used with sampling ports between each reactor. The four-reactor system consists of one short (effective irradiation length of 11.2 cm), one medium (29.2 cm), and two long (2 × 77.9 cm) connected in series. The fluid hydraulic Reynolds number $Re_h = 2500$ for a flow rate of 120 mL/s for juices within the inlet tube connecting the pump and the first reactor used in this study. Thus, $Re_h > 2100$ (Bird et al. 2002), and the flow is turbulent within the inlet to the annular reactors at flow rates of 120–240 mL/s for the juices used in this section.

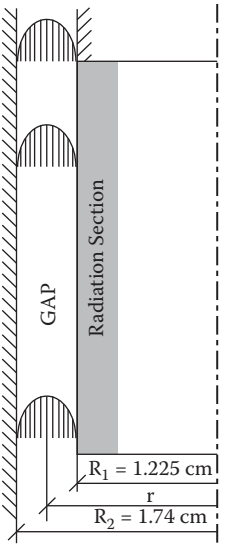

FIGURE 8.8 Schematic of laminar and turbulent flow in the annular reactor. (From Ye 2007. With permission.)

8.2.2 UV Fluence Distribution

Figure 8.9 is the fluence distribution for turbulent flow when $\lambda/d = 0.25$ and the absorption coefficient equals $A = 10\ cm^{-1}$ for a gap width $d = 4$ mm. The fluence distribution is defined as shown in equations (8.4) and (8.5). Here, the horizontal axis has dimensionless units of $It/I_{av}\tau$, where I_{av} is defined by equation (8.6) and $\tau = L/v$ is the total fluid residence time, where L is the total effective irradiated length for the four reactors connected in series.

According to Figure 8.9, there are three peaks for turbulent flow. The left peak corresponds to the effect of the viscous sublayer on the opposite side of the radiation source, while the right peak corresponds to the effect of the viscous sublayer near the radiation source. Finally, the middle peak corresponds to the effect of the fully turbulent region. Clearly, the fluence distribution for turbulent flow is superior to that for laminar flow, as most of the area in the distribution for turbulent flow is concentrated under a single relatively narrow peak.

8.2.2.1 Numerical Modeling of Turbulent Flow

The conservation equations of *Yersinia pseudotuberculosis* in axisymmetrical coordinates for the first-order model $k = k_1$ can be written as (Bird et al. 2002),

$$u_r \frac{\partial N}{\partial r} + u_z \frac{\partial N}{\partial z} = \frac{\mu_t}{\rho Sc_t}\left(\frac{1}{r}\frac{\partial}{\partial r}\left(r\frac{\partial N}{\partial r}\right) + \frac{\partial^2 N}{\partial z^2}\right) - kIN \tag{8.15}$$

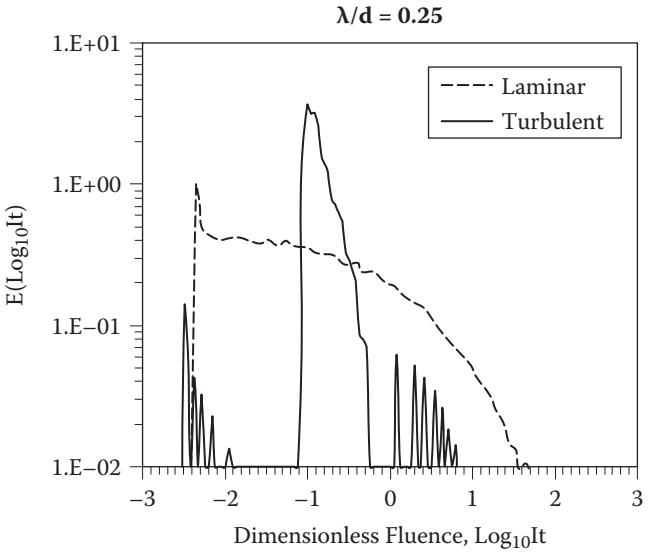

FIGURE 8.9 Fluence distribution for laminar and turbulent flow when $\lambda/d = 0.25$, absorption coefficient $A = 10\ \text{cm}^{-1}$, and gap width $d = 4$ mm.

where u_r and u_z are radial- and axial-velocity components and μ_t is turbulent viscosity. Equation (8.15) can be modified for the series-event model by substituting N_i for N and $kI(N_i - N_{i-1})$ for the source term where i is the event level and $k = k_{SE}$ is the rate constant. These three variables—u_r, u_z, and μ_t—can be obtained by solving time-averaged Navier–Stokes equations by means of the k-ε two-equation model (Launder and Spalding 1972). Sc_t is the turbulent Schmidt number, which relates the turbulent momentum transport to the turbulent transport of the *Y. pseudotuberculosis* concentration N. The recommended Sc_t for most cases is 0.8 (Fox 2003).

FLUENT (Fluent Inc.) software is used to determine the turbulent-flow field. Three k-ε models are provided: the standard k-ε model (Launder and Spalding 1972), the RNG k-ε model (Yakhot and Orszag 1986), and the realizable k-ε model (Shih et al. 1995). All of the three k-ε models were tested, and the differences among them are very small for this geometry. Therefore, the standard k-ε model is used here for modeling turbulence.

In FLUENT software, user-defined scalars (UDS) are provided to solve the conservation equations of *Y. pseudotuberculosis* concentrations given by equation (8.15). However, since the source terms in equation (8.15) are not standard forms, user-defined functions (UDF) are utilized to process the source terms in a special format. A UDF source C file is shown in Section 8.8.

8.2.3 UV Disinfection of *Y. pseudotuberculosis*

Figure 8.10 is the comparison of *Y. pseudotuberculosis* inactivation between experimental data and numerical simulation in turbulent flow with four reactors connected

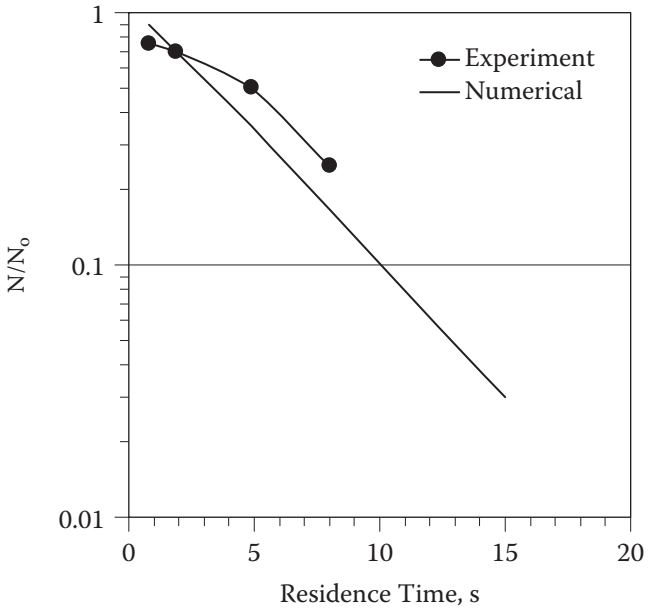

FIGURE 8.10 Comparison of *Y. pseudotuberculosis* inactivation between experimental data and numerical simulation in turbulent flow (A = 7.16 cm^{-1} and d = 5.15 mm).

in series. In Figure 8.10, the absorption coefficient of Ocean Spray (Ocean Spray, Lakeville-Middleboro, MA) apple juice is A = 7.155 cm^{-1} and the flow rate is Q = 120 mL/s (hydraulic Re_h = 2000). Each experimental data point in Figure 8.10 was taken at the outlet of each of the four reactors, and each data point is the average of three runs at the same conditions. The small deviation between experimental results and numerical simulations in Figure 8.10 was probably caused by the numerical assumption that perfect mixing occurs in the connection tubing between any two reactors in series.

8.2.4 Effect of Absorption Coefficient

Figure 8.11 shows the effect of the absorption coefficient upon the inactivation performance of UV turbulent reactors. The numerical calculations of turbulent flow assume a series-event model with a rate constant k_{SE} = 0.984 cm^2/mJ and an event level n = 3. The simulated UV reactor is 80 cm in length with an incident fluence rate of 60 mW/cm^2. Also shown in Figure 8.11 is the prediction of the inactivation N/N_0 for an ideal plug-flow reactor (PFR). The latter case assumes a uniform velocity distribution v = $Q/\pi(R_2^2 - R_1^2)$ and a uniform fluence rate I_{av} predicted by equation (8.6). The microbe inactivation N/N_0 for a PFR is therefore given by equation (8.10) with the substitution $It = I_{av}\tau$ and n = 3 where, from equation (8.6),

$$I_{av}\tau = \frac{I_0 R_1}{0.5\alpha\left(R_2^2 - R_1^2\right)}[L/v] \tag{8.16}$$

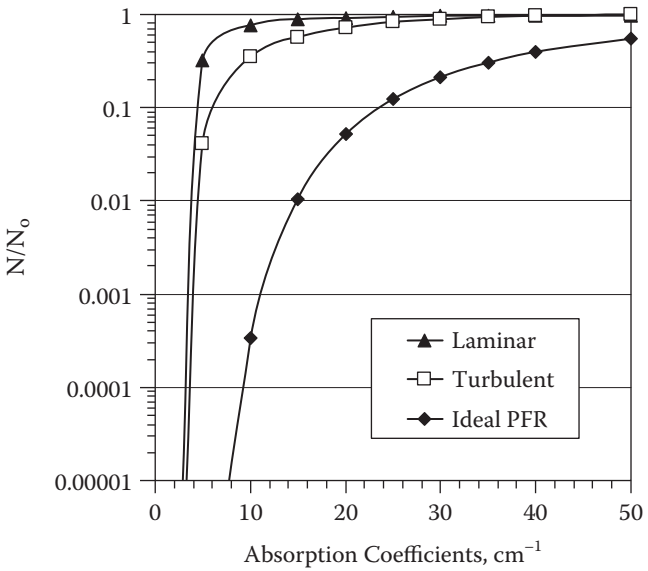

FIGURE 8.11 Effect of absorption coefficient upon the performance of UV laminar, turbulent, and PFT reactors. (From Ye 2007. With permission.)

In equation (8.16), one assumes a simplified version of equation (8.6), since $\exp[-\alpha(R_2 - R_1)] << 1$ for the normal product $\alpha(R_2 - R_1) > 3$. Finally, the laminar flow in Figure 8.11 is an imaginary status, where it is assumed that the flow rate is the same as the turbulent case, but with N/N_0 predicted by equation (8.14).

From Figure 8.11, when the absorption coefficients are low, turbulent flow provides superior inactivation levels compared with laminar flow because of the effect of turbulent mixing. However, when the absorption coefficients are high, e.g., more than 35 cm^{-1}, the microbe reductions in turbulent and laminar flows are similar. The main reason is the effect of the boundary layer.

Because the turbulent flow is almost laminar in what is called the *viscous sublayer* near a wall, turbulence plays a small role in mass transfer. According to the numerical simulations for Figure 8.11, the thickness of the viscous sublayer is $5(\nu/u_\tau) = 0.026$ cm, where ν is the kinematic viscosity and $u_\tau = \sqrt{\tau_w/\rho}$ is the friction velocity, where τ_w is the wall shear stress. When the absorption coefficient is 35 cm^{-1}, the penetration depth is about 0.029 cm, which is almost the same as the thickness of the viscous sublayer. In this case, disinfection is largely restricted in the viscous sublayer, and improved performance expected from the turbulent flow does not occur.

8.2.5 Effect of the Gap Width

When the juices to be processed have large absorption coefficients in turbulent flow, disinfection levels can be improved by decreasing the thickness of the viscous sublayer. This can be accomplished by decreasing the gap width, because the

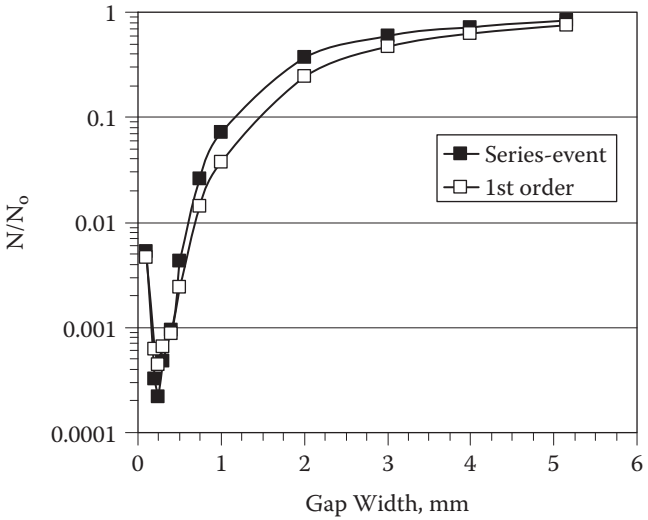

FIGURE 8.12 Disinfection of *Y. pseudotuberculosis* in apple juice processed by a UV reactor (29.2-cm lamp length) with an 800-mW/cm^2 incident fluence rate (Q = 120 mL/s, A = 37.2 cm^{-1}, d = 0.515 cm). (From Ye 2007. With permission.)

ratio of the thickness of the viscous sublayer to the gap width is almost constant. The effect of gap width on the inactivation of *Y. pseudotuberculosis* in UV turbulent reactors is investigated numerically in Figure 8.12, where all parameters are fixed except for the radius of the outer cylinder, which is decreased to decrease both the gap width and the thickness of the viscous sublayer. Figure 8.12 presents numerical results of apple juice processed by a reactor with a UV lamp length of L = 29.2 cm and with an 800-mW/cm^2 incident fluence rate. As in the case of laminar flow, the gap of the concentric cylinder turbulent reactor can be divided into three regions:

1. *Over-irradiated region in the viscous sublayer near the radiation source*: *Y. pseudotuberculosis* within this region is inactivated because of the large fluence rates and long residence times.
2. *Under-irradiated region in the viscous sublayer on the opposite side of the radiation source*: *Y. pseudotuberculosis* within this region survives because the UV is unable to penetrate juices with large absorption coefficients and reach the viscous sublayer on the opposite side of the radiation source.
3. *Uniform-irradiated region with fully turbulent flow*: Concentrations of *Y. pseudotuberculosis* are almost uniform because of turbulent mixing.

It should be noted in Figure 8.12 that a minimum in N/N_0 occurs at a gap width of d = 0.25 mm, where λ/d = 1.0 and the radiation penetration depth $\lambda = 1/A$. This result is discussed in Section 8.2.6.

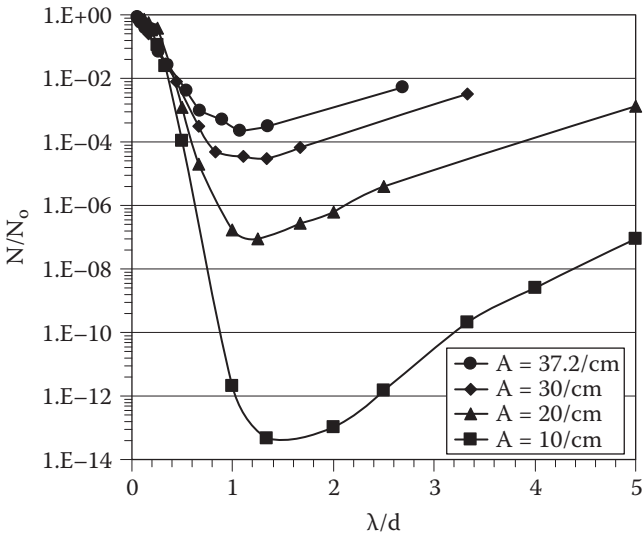

FIGURE 8.13 Disinfection of *Y. pseudotuberculosis* in apple juice processed by a UV reactor (29.2-cm lamp length) with an 800-mW/cm^2 incident fluence rate and in turbulent flow with Q = 120 mL/s. (From Ye 2007. With permission.)

8.2.6 Optimum Gap Width

There is an optimum gap width for each absorption coefficient in turbulent flow, as was the case for laminar flow. Figure 8.13 shows how *Y. pseudotuberculosis* microbe reductions change with gap width when the radius of the inner cylinder is constant at 1.225 cm while the radius of the outer cylinder is changed. In Figure 8.13, the series-event model is used with k_{SE} = 0.984 cm^2/mJ and n = 3, and radiation comes from the inner cylinder with a fluence rate of I_0 = 800 mW/cm^2 for a UV lamp length of L = 29.2 cm.

From Figure 8.13, it is shown that the optimum $\lambda/d \approx 1.0$ for turbulent flow, and this does not change dramatically for different absorption coefficients. As shown, the penetration depth equals the gap width for optimum disinfection in turbulent flow, or the radiation has to penetrate across the gap to obtain optimum disinfection. This requirement is caused by the under-irradiated region in the viscous sublayer on the opposite side of the radiation source. Though the under-irradiated region occupies only a small fraction of the gap, about 5% or less, surviving pathogens in the under-irradiated region contribute to the population of surviving pathogens within the gap. Because most of the pathogens in the under-irradiated region survive if $\lambda/d << 1$, the average concentration of the surviving pathogen at the outlet will be about 0.05 N_0. Because the normal absorption coefficients of juices are 10–40 cm^{-1}, the optimum gap width is in the range of 0.25–1.0 mm. Therefore, the gap width of laminar UV reactors used for juice disinfection should not be more than 1.5 mm.

One method to improve the performance of the turbulent UV reactor and to eliminate the viscous-sublayer problem is to irradiate from both of the cylinders.

Another method is to connect the UV reactors in series. In the latter case, pathogens in the viscous sublayer in the first UV reactor may enter the fully turbulent region in the next reactor. Moreover, the short residence time for turbulent-flow conditions may also require that one connect several reactors in series.

8.2.7 Correlation of UV Disinfection

In the attempt to model turbulent reactors, it is useful to begin the process with the concept of a plug-flow reactor. Assuming first-order kinetics or $k = k_1$, the log reduction of microbes within a PFR can be written in the form

$$\ln\left(\frac{N}{N_0}\right) = -kI_{\text{av}}\tau \tag{8.17}$$

With substitution of equation (8.16), one obtains

$$\ln\left(\frac{N}{N_0}\right) = \frac{-kI_0\tau R_1}{0.5\alpha\left(R_2^2 - R_1^2\right)} \tag{8.18}$$

It is convenient to simplify equation (8.18) by factoring the term $(R_2^2 - R_1^2)$, or

$$\ln\left(\frac{N}{N_0}\right) = -\frac{kI_0\tau \text{Rc}}{\alpha d} \tag{8.19}$$

where the gap width $d = R_2 - R_1$ and the dimensionless group Rc

$$\text{Rc} = \frac{2R_1}{R_2 + R_1} \tag{8.20}$$

To correct for differences between the experimental performance of real reactors and a PFR, it is useful to add the ratio c/δ to equation (8.19), where δ is the boundary layer thickness. Thus, equation (8.19) becomes

$$\ln\left(\frac{N}{N_0}\right) = -\frac{ckI_0\tau \text{Rc}}{\alpha d\delta} \tag{8.21}$$

Here, the boundary layer thickness δ is calculated according to equation (8.22) (Middleman 1998)

$$\delta = \frac{2\mu}{\rho \text{v} f} \tag{8.22}$$

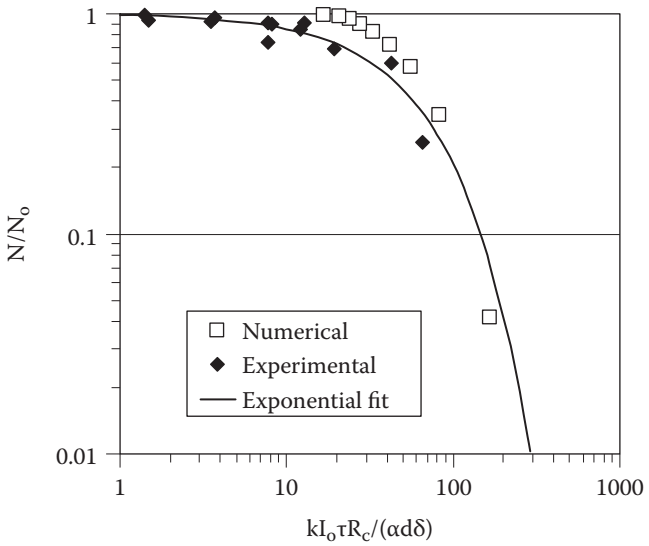

FIGURE 8.14 Correlation of UV disinfection of *Y. pseudotuberculosis* in turbulent reactors. Solid line is equation (8.21) with $c = 0.0158$. (From Ye 2007. With permission.)

where f is the dimensionless shear stress. According to boundary-layer theory (Schlichting 1979)

$$f = 0.079\,\mathrm{Re}_h^{-0.25} \tag{8.23}$$

The turbulent numerical results in Figure 8.11 and the experimental results for three commercial clarified apple juices with absorption coefficients of 7.2, 37.2, and 39.2 cm^{-1} are correlated in Figure 8.14, where the constant $c = 0.0158$ cm is obtained by the least-squares method with the experimental data. Figure 8.14 shows that the correlation in equation (8.21) agrees reasonably well with the experimental results. Unlike the log reductions in laminar reactors, which are proportional to $1/[\exp(dm)]^{\alpha}$, the log reductions in turbulent reactors are proportional to $1/\alpha$. Thus, the inactivation levels N/N_0 in the turbulent reactors decrease much more rapidly with an increase in the radiation penetration depth λ because of better turbulent mixing than would be the case with laminar reactors.

8.3 TAYLOR–COUETTE FLOW IN CONCENTRIC CYLINDERS

UV disinfection in laminar and turbulent reactors is discussed in Sections 8.1 and 8.2, respectively. In order to achieve good disinfection levels, the laminar reactors require very narrow gap widths when juices with high absorption coefficients are processed. Though turbulence can be introduced as a partial solution, unfortunately, the high flow rate to ensure turbulent flow is coupled with a reduced residence time. Achieving a 5-log reduction with turbulence requires either a very long lamp in a

thin-film annular reactor or many thin-film annular reactors connected in series. Furthermore, turbulent flow increases the pressure drop across the reactors, and the axial mixing resulting from turbulent flow broadens the fluence distribution.

Taylor–Couette flow between concentric cylinders provides the possibility to decouple mixing and the device flow rates. Recently, Forney et al. (2003a,b,c and 2004) investigated the possibility of applying laminar Taylor–Couette flow to the UV disinfection of juice. Their research showed that laminar Taylor–Couette flow largely eliminates the broad fluence distribution resulting from juices with high absorption coefficients compared with laminar Poiseuille flow. Moreover, Taylor–Couette flow decreases the momentum and concentration boundary-layer thickness, which improves the mass transfer of microbes to the UV-transmitting wall.

8.3.1 Thin-Film Annular Reactor

The schematic figure of the Taylor–Couette reactor is shown in Figure 8.15. The stator of the Taylor–Couette UV reactor is constructed with fused quartz (Vycor, Corning Inc., Corning, NY) with an internal diameter of $\Phi_2 = 4.577$ cm, while the Teflon rotor has an outer diameter of $\Phi_1 = 3.434$ cm. This geometry provides a gap width of $d = 0.5715$ cm. The radiation source consists of six medium-pressure mercury UVC lamps (MPML) with diameters of 0.95 cm and an effective length of $L = 5.34$ cm (Pen-Ray Lamps, UVP, Upland, CA) that are distributed evenly around the

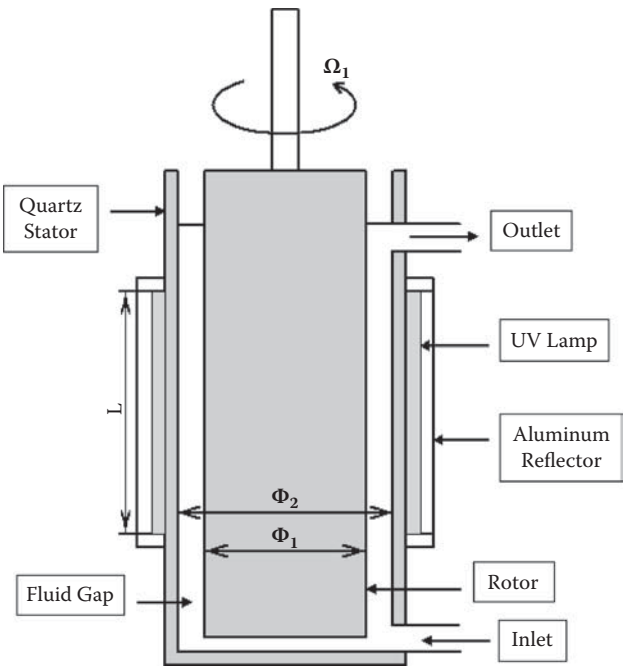

FIGURE 8.15 Schematic of a Taylor–Couette UV reactor. (From Ye 2007. With permission.)

quartz stator. The UV lamps are surrounded with an aluminum reflector to reduce radiation losses, as shown in Figure 8.15. The radiation fluence rate on the surface of quartz is assumed to be uniform and equals 25 mW/cm^2. The Taylor number used to characterize the flow is defined as

$$\mathrm{Ta} = \frac{R_1 \Omega_1 d}{\nu}\left(\frac{d}{R_1}\right)^{1/2} \tag{8.24}$$

where R_1 is the radius of the inner cylinder, $\Omega_1 = 2\pi f$ is the angular velocity of the inner cylinder, f is the frequency of rotation, d is the gap width, and ν is the kinematic viscosity.

8.3.2 UV Fluence Distribution

Figure 8.16 represents the UV fluence distribution for the Taylor–Couette reactor used in the experimental phase of this study. The fluence distribution $E(\log It)$ defined by equations (8.4) and (8.5) in Section 8.1.2 for Taylor–Couette flow has been plotted for five laminar Taylor numbers when $Q = 40$ mL/min, $A = 11$ cm^{-1}, $d = 0.572$ cm, and $\lambda/d = 0.16$. Here, the horizontal axis has the dimensionless units of $It/I_{av}\tau$, where I_{av} is defined by equation (8.6) for an ideal plug-flow reactor (PFR) and $\tau = L/\mathrm{v}$ is the average fluid residence time, where L is the total effective irradiated length for

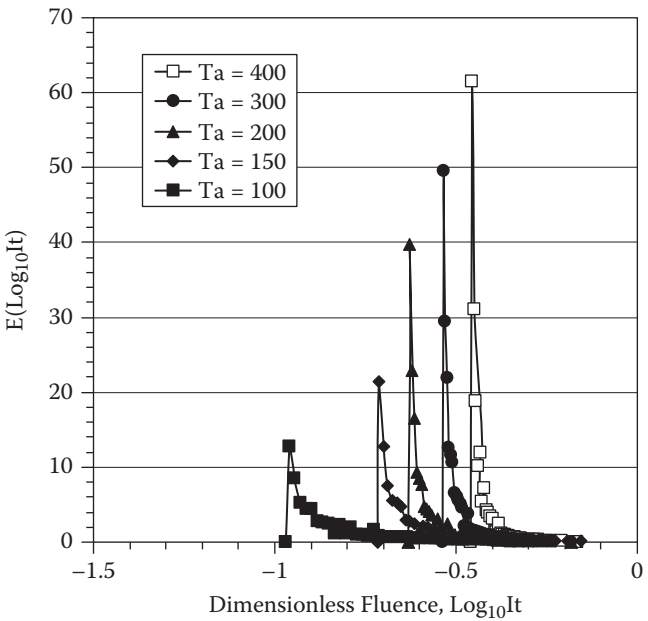

FIGURE 8.16 UV fluence distribution for different Taylor numbers ($Q = 40$ mL/min, $A = 11$ cm^{-1}, $d = 0.572$ cm, and $\lambda/d = 0.16$). (From Ye 2007. With permission.)

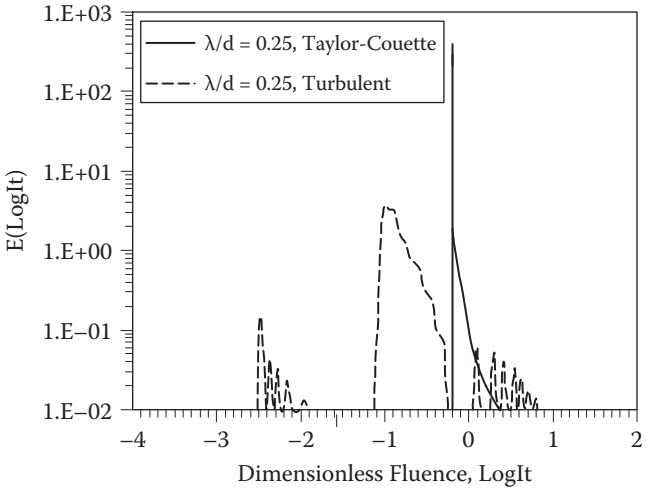

FIGURE 8.17 UV fluence distribution of Taylor–Couette (Ta = 200) and turbulent flow (d = 4 mm, A = 10 cm^{-1}, and λ/d = 0.25). (From Ye 2007. With permission).

the Taylor–Couette reactor and v is the average velocity. As indicated in Figure 8.16, the fluence distribution becomes narrower and higher with an increase in the laminar Taylor number, and in every case the distribution approaches the characteristics of ideal plug flow. It should be noted, however, that the flow will become turbulent at Taylor numbers exceeding roughly 600, where turbulent axial mixing broadens the fluence distribution and the response of the reactor approaches that of an inferior, continuously stirred tank reactor (CSTR).

Figure 8.17 represents a comparison between laminar Taylor–Couette flow (Ta = 200) and axial turbulent flow (axial hydraulic Reynolds number Re_h = 14) between two concentric cylinders. The UV fluence distribution for both flow patterns is plotted for a gap width of d = 4 mm, absorption coefficient A = 10 cm^{-1}, and λ/d = 0.25. Clearly, the fluence distribution for Taylor–Couette flow is superior to turbulent flow, and one observes that all microbes would receive an equal flux of photons when passing through the Taylor–Couette device.

8.3.2.1 Numerical Modeling of Taylor–Couette Flow

The steady-state governing equations for concentrations of *E. coli* K12 in axisymmetrical coordinates in laminar flow can be written as (Bird et al. 2002)

$$u_r \frac{\partial N}{\partial r} + u_z \frac{\partial N}{\partial z} = D_m \left(\frac{1}{r} \frac{\partial}{\partial r} \left(r \frac{\partial N}{\partial r} \right) + \frac{\partial^2 N}{\partial z^2} \right) - kIN \tag{8.25}$$

where u_r and u_z are radial and axial velocity components, respectively, and N is the concentration of viable microorganisms. Since the diffusion coefficient D_m is small, the diffusion term in equation (8.25) is neglected. Equation (8.25) can also

be modified for the series-event model by substituting N_i for N and $k_{SE}I(N_i - N_{i-1})$ for the source term, where i is the event level. The values for u_r and u_z can be obtained by solving the laminar Navier–Stokes equations using FLUENT software. The fluid inlet and outlet sections in Figure 8.15 are modified to a vertical position so that the axisymmetry assumption is valid. User-defined scalars (UDS) in FLUENT software are used to solve the governing equations of *E. coli* K12 concentrations. As in the case of turbulent reactors, user-defined functions (UDFs) are utilized to process the source terms in a special format. A UDF source C file is given in Section 8.8.

8.3.3 UV Disinfection of *E. coli*

Experiments were conducted to provide inactivation data for comparison with numerical predictions. Deionized water inoculated with *E. coli* K12 (ATCC 25253) was pumped into the reactor through the inlet by a positive-displacement pump. Caramel 050 (D.D. Williamson & Co., Inc., Louisville, KY) was added to adjust the absorption coefficient of the deionized water. Samples for microbial analysis were taken and place-plated before and after radiation exposure. The experimental data in Figure 8.18 demonstrate that large improvements in microbe inactivation levels occur with increasing Taylor numbers (Ta). As shown in Figure 8.18, the two-dimensional (2-D) numerical simulations generally agree with the experimental results. The numerical simulations show that the log reduction in viable microbes increases with Ta, caused by a decrease in the fluid boundary-layer thickness at large Ta.

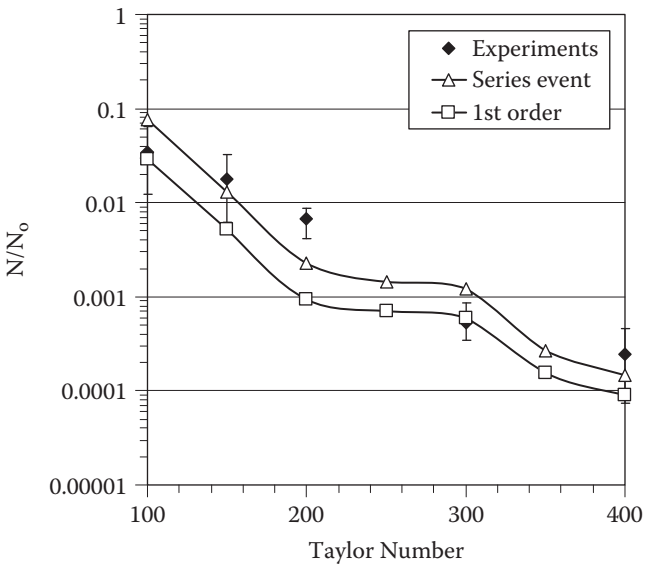

FIGURE 8.18 Comparison between experimental results and 2-D numerical simulations with different Taylor numbers (Q = 40 mL/min, A = 11 cm^{-1}, d = 0.572 cm, and λ/d = 0.16). (From Ye 2007. With permission.)

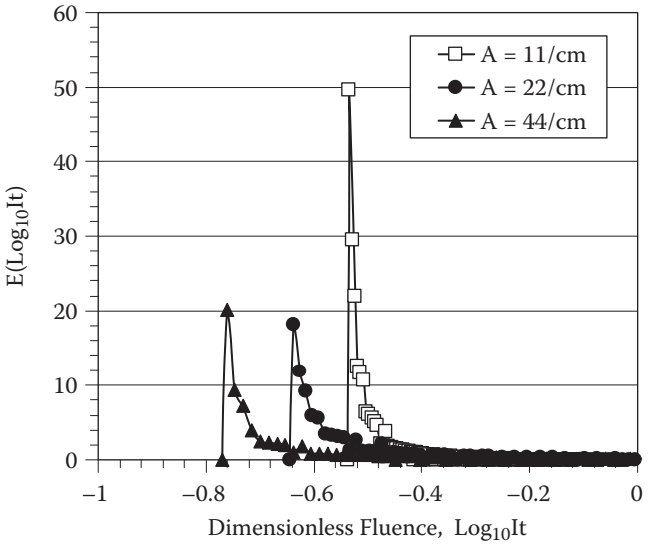

FIGURE 8.19 UV fluence distribution with Taylor–Couette flow for different absorption coefficients (Ta = 300, Q = 40 mL/min, and d = 0.572 cm). (From Ye 2007. With permission.)

8.3.4 Effect of Absorption Coefficient

Figure 8.19 shows the influence of the absorption coefficient on the UV fluence distribution in Taylor–Couette flow. The UV reactor is the experimental device operated with fixed Taylor number Ta = 300, flow rate Q = 40 mL/min, and gap width d = 0.572 cm. Figure 8.19 illustrates that one obtains superior performance when operating with small absorption coefficients such that radiation penetration $\lambda = 1/A$ extends across the fluid gap.

Figure 8.20 compares the numerical prediction of the inactivation of microbes with the dimensionless penetration depth. Also included are experimental data with *E. coli* K12. The two numerical models generated with FLUENT software and consisting of first-order or the series-event kinetics are compared. The first-order model with rate constant $k_1 = 0.32494$ cm^2/mJ and the series-event model with $k_{SE} = 0.67474$ cm^2/mJ and n = 4 are used for the numerical predictions. The latter values were found to be optimal with least-squares methods and using data from independent experiments (Ye 2007). As shown in Figure 8.20, the numerical results provide reasonable correlation of the data.

8.3.5 Optimum Gap Width

Taylor–Couette flow is characterized by nearly square Taylor vortices across the fluid gap, as shown by the streamlines on the left side of Figure 8.26. Microbes are carried by fluid streamlines that are parallel to the wall and then are transported across the gap on the same streamline in the symmetrical vortex pattern.

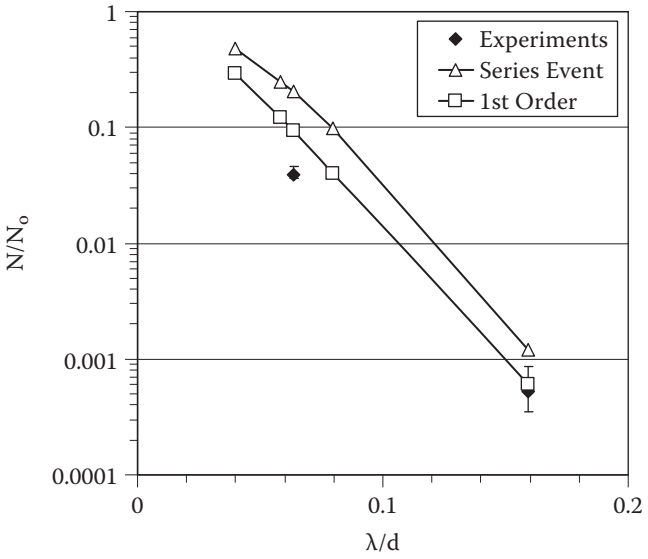

FIGURE 8.20 Comparison between experimental results and 2-D simulations with different absorption coefficients (Ta = 300, Q = 40 mL/min, and d = 0.572 cm). (From Ye 2007. With permission.)

Tracing a path across the fluid gap provides a profile of radiation intensity on the microbes that is shown in Figure 8.21. For example, microbes at the center of the gap are subjected to a small radiation intensity that is shown on a single curve at the center of Figure 8.21. Moreover, microbes near the wall experience a larger radiation intensity. Because the fluid velocity v is inversely proportional to the gap width, or v $\propto$ 1/d, contours at the top of Figure 8.21, where the gap width d is small, subject microbes to a large radiation intensity but short residence times. Conversely, if d is large, microbes across the gap are subject to a small radiation intensity representative of the bottom contour in Figure 8.21 but large residence times. Thus, the average dosage of photons $I_{av}\tau$ is low on both the top and bottom contours of Figure 8.21 but high for intermediate contours for both laminar, turbulent, and Taylor–Couette flows.

Figure 8.22 illustrates how the log reduction of microbes is affected by the absorbance $A = 1/\lambda$, in particular, the ratio of penetration depth to gap width λ/d. As shown, optimum inactivation occurs at a ratio of $\lambda/d = 0.5$ for all fluids in Taylor–Couette flow. For example, if one wishes to achieve a 5-log reduction ($N/N_0 = 10^{-5}$) in viable microbes with the Taylor–Couette device, the design would require a somewhat larger gap width with $\lambda/d < 0.5$. Because the normal absorption coefficients of juices are 10–40 cm^{-1}, the optimum gap width is in the range of 0.5–2.0 mm. Therefore, the gap width of laminar UV reactors used for juice disinfection should not be more than 3 mm.

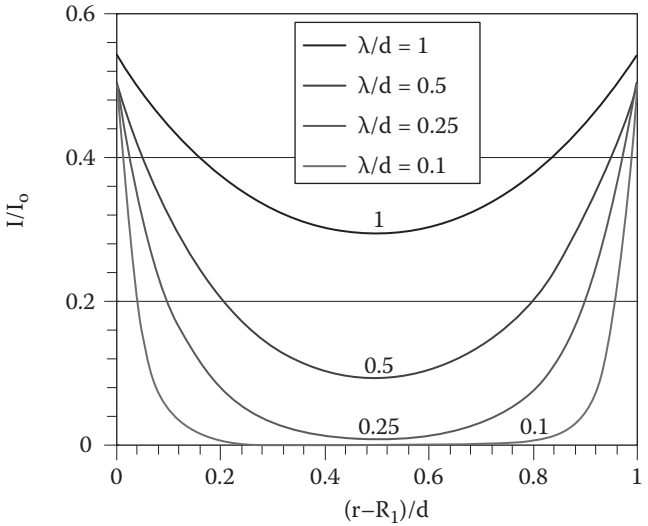

FIGURE 8.21 Profile of maximum radiation intensity across the gap in Taylor–Couette flow. (Order of λ/d values in legend is the same order as in graph.) (From Ye 2007. With permission.)

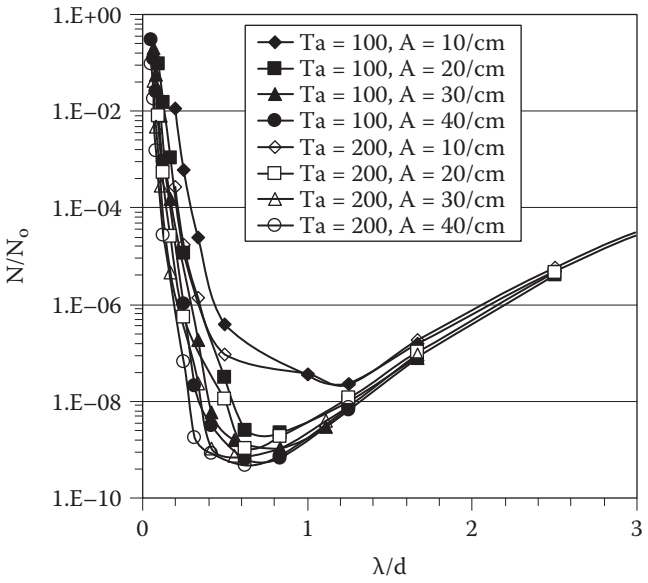

FIGURE 8.22 Inactivation with increasing radiation penetration depth λ/d in Taylor–Couette flow. Flow rate Q = 18 mL/min. (From Ye 2007. With permission.)

8.3.6 Correlation of UV Disinfection

A Taylor vortex reactor can be approximated as a plug-flow reactor (Kataoka et al. 1975), as is the case with both laminar and turbulent reactors. The correlation, which is similar to equation (8.19), can also be used to predict the log reduction in Taylor–Couette reactors, or

$$\ln\left(\frac{N}{N_0}\right)=-\frac{kI_0\tau}{\alpha d}\frac{2R_2}{R_2+R_1} \tag{8.26}$$

In equation (8.26), the dimensionless group Rc is redefined because radiation is introduced from the outside of the concentric cylinders, as shown in Figure 8.15, or

$$\mathrm{Rc}=\frac{2R_2}{R_2+R_1} \tag{8.27}$$

The boundary thickness δ in Taylor–Couette flow is proportional to $\mathrm{Ta}^{-1/2}$ (Baier et al. 1999; Forney and Pierson 2003b, c; Forney et al. 2003a), where

$$\delta=\frac{2d}{\sqrt{\mathrm{Ta}}} \tag{8.28}$$

A constant, c/δ, can be added to equation (8.26), as was done with turbulent flow in equation (8.21), to correct for the deviation between Taylor–Couette reactors and ideal PFRs, where one obtains

$$\ln\left(\frac{N}{N_0}\right)=-\frac{ckI_0\tau\mathrm{Rc}}{\alpha d\delta} \tag{8.29}$$

The experimental data are correlated according to equation (8.29) and shown in Figure 8.23, where the value $c = 0.0125$ cm is obtained by the least-squares method. Figure 8.23 shows that the correlation equation (8.29) agrees well with experimental results. These results confirm what is shown in equation (8.21) for turbulent flow, i.e., that the log reduction in Taylor–Couette flow is nearly proportional to the average residence time and the reciprocal of the absorption coefficient (or penetration depth).

The correlation equation (8.29) for UV disinfection in laminar Taylor vortex reactors has the same form as the correlation equation (8.21) for UV disinfection in turbulent reactors. The only differences are the definition for the boundary-layer thickness δ and the geometric ratio Rc. The experimental data for both turbulent reactors and laminar Taylor–Couette reactors are correlated with the same dimensionless group equation (8.29), characteristic of a plug-flow reactor (PFR), as shown in Figure 8.23.

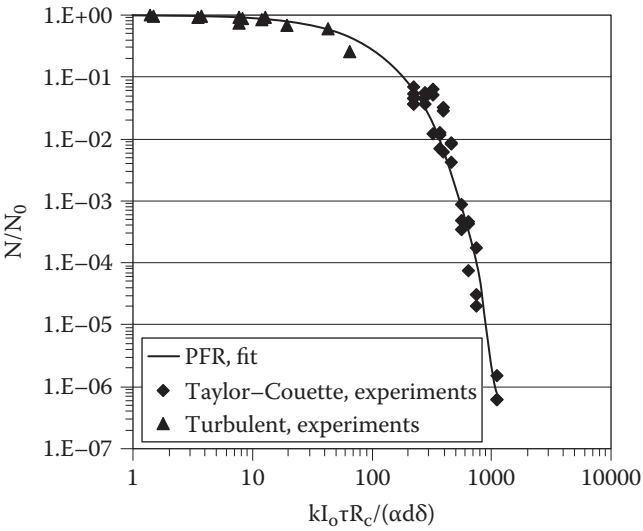

FIGURE 8.23 Correlation of experimental data for UV disinfection in laminar Taylor–Couette and turbulent reactors. The constant $c = 0.0125$ cm in the exponential PFR. (From Ye 2007. With permission.)

8.3.7 Turbulent Taylor–Couette Flow

The discussion above is restricted to laminar Taylor–Couette flow where the Taylor number is less than roughly 600. For larger values of Ta (>600), the flow becomes turbulent, and axial mixing will broaden the fluence distribution. Other problems also arise at large Ta, since the inactivation level of the reactor approaches that of an inferior, continuously stirred tank reactor (CSTR) (Resende et al. 2004). Figure 8.24 shows the log reductions, comparing both laminar and turbulent Taylor–Couette flow. In Figure 8.24 the axial hydraulic Reynolds numbers are $Re_h = 6.4$ and 12.8 for flow rates of 18 mL/min and 36 mL/min, respectively. The numerical calculations assume the radii of the inner and outer cylinders are 1.225 cm and 1.74 cm, respectively. The length of the UV lamp is 11.2 cm, with an intensity of $I_0 = 12$ mW/cm^2. The series-event inactivation model of *E. coli* is used, and the absorption coefficient is assumed to be $A = 20$ cm^{-1}.

From Figure 8.24, it is shown that inactivation levels (N/N_0) in turbulent Taylor–Couette flow do not decrease with larger Taylor numbers. The latter result is caused by axial turbulent mixing. Turbulent flow is a three-dimensional flow and intensifies mixing along all directions. Radial mixing is absolutely necessary to improve the performance of thin-film annular reactors. However, turbulent Taylor–Couette flow increases both the radial and axial mixing, where the latter should be avoided. Therefore, the Taylor vortex reactors should be operated in laminar Taylor–Couette flow and with Taylor numbers as high as possible.

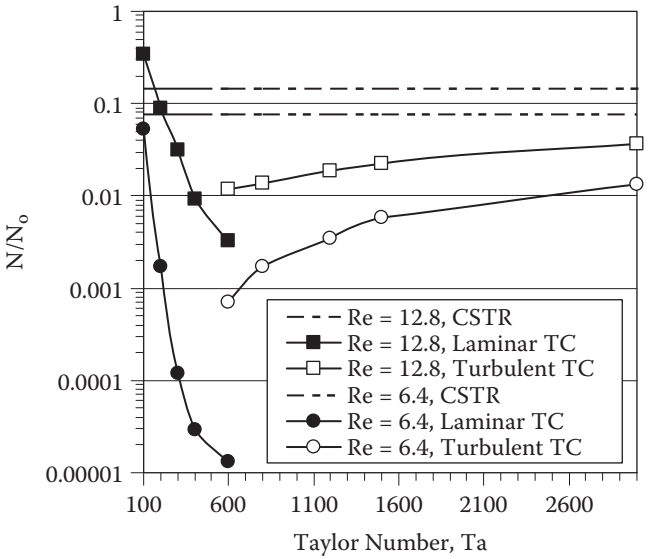

FIGURE 8.24 Microbe inactivation for laminar and turbulent Taylor–Couette flow (axial Re = Re_h, the hydraulic Reynolds number). (From Ye 2007. With permission.)

8.3.8 Modified Taylor–Couette Flow

Recently a number of modifications to classical Taylor–Couette reactors have been investigated in an effort to improve the yield with chemical reactions. These studies involve modification to the shape of the rotor (Rotz and Suh 1979; Ikeda and Maxworthy 1994; Wiener et al. 1997; Rafique and Lami 2001), for example, a V-grooved rotor, or a rotor with sinusoidal modulations. In this section, the wavy rotor as shown in Figure 8.25 is investigated. In Figure 8.25, the average radius of the

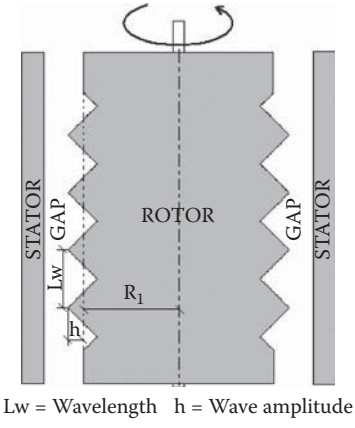

FIGURE 8.25 Schematic of a wavy-rotor UV reactor. (From Ye 2007. With permission.)

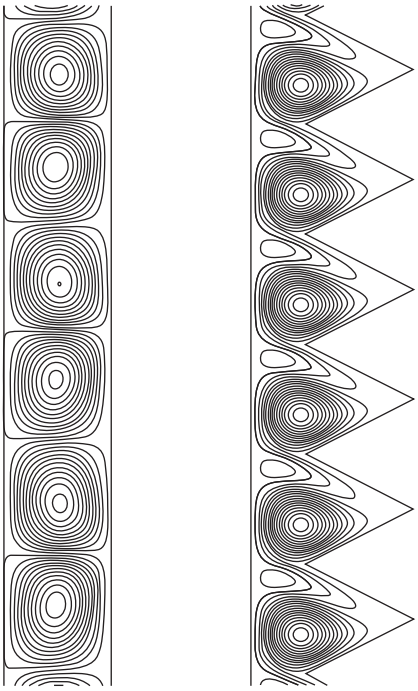

FIGURE 8.26 Fluid streamlines in Taylor–Couette flow. Flat rotor in left figure, $d = 2$ mm. Wavy rotor in right figure, wavelength $L_w = 2$ mm, wave amplitude $h = 1$ mm, and $d = 2$ mm. (From Ye 2007. With permission.)

rotor is used to calculate the Taylor number in equation (8.24). The distance between the highest point of the rotor and the average radius of the rotor is defined as the wave amplitude, h, and the distance between the two highest points as the wavelength of the rotor L_w.

Figure 8.26 is the stream function of a wavy rotor. The radius of the stator is 2.275 cm, and the average radius of the wavy rotor is 2.075 cm, corresponding to a gap width of $d = 2$ mm. The flow rate equals 13 mL/min. For flat rotors, vortices are nearly square and appear periodically in the form of counter-rotating pairs. The number of vortices within a radiation section for flat rotors is approximately the ratio of the UV lamp length to the gap width, namely L/d. When wavy rotors are used, vortices still appear periodically, as seen in Figure 8.26. However, unlike flat rotors, the number of vortices with wavy rotors within the radiation section is no longer determined by the ratio of the UV lamp length to the gap width. Instead, the number of vortices for a wavy rotor equals two times the ratio of the UV lamp length to the wavelength of the rotor, namely $2L/L_w$. Another interesting flow pattern is that there are two vortices within one rotor wavelength period: one is relatively large, another relatively small.

Figure 8.27 is the fluence distribution function with $A = 10$ cm^{-1}. Here, it is observed that more photons are incident on a microbe (larger fluence It) with either

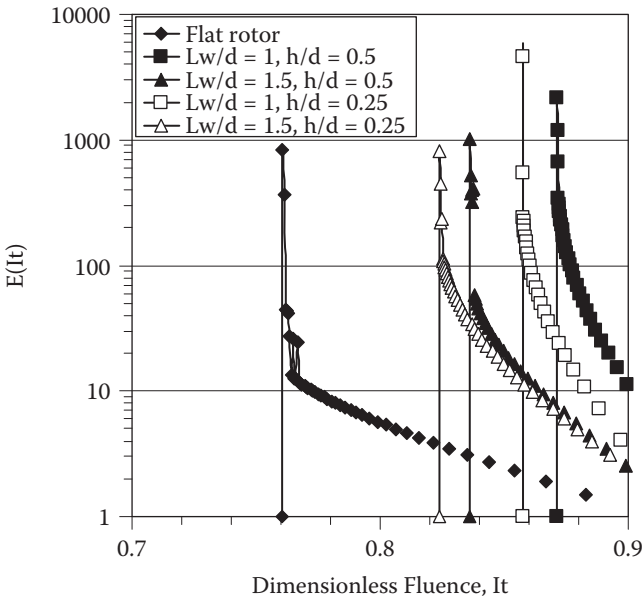

FIGURE 8.27 Fluence distribution for Taylor–Couette flow: Effect of wavy rotor with Ta = 100, $A = 10\ cm^{-1}$, $d = 2$ mm, and $\lambda/d = 0.5$. (From Ye 2007. With permission.)

the decrease in the wavelength or the increase in the wave amplitude. One also observes that decreasing the rotor wavelength is more effective than increasing the wave amplitude because the number of vortices with wavy rotors is proportional to the reciprocal of the wavelength. Decreasing the wavelength changes the flow pattern more dramatically than increasing the wave amplitude. Smaller wavelengths add more vortices and improve radial mixing.

Figure 8.28 shows the inactivation levels (N/N_0) of different wavy rotors (Forney et al. 2008). The straight horizontal line is the inactivation level with a flat rotor. The numerical computations in Figure 8.28 use an incidence radiation flux of $I_0 = 3\ mW/cm^2$ for a fluid with an absorption coefficient of $A = 10\ cm^{-1}$. Moreover, the fluid is irradiated from the outer cylinder, and the series-event inactivation model of *E. coli* is used. Other fixed parameters are a Taylor number Ta = 100 with an active UV lamp length of 5.7 cm.

Because Taylor vortices improve radial mixing, more vortices imply lower N/N_0 values. The number of vortices with a wavy rotor within the radiation section equals $2L/L_w$, while the number of the vortices with the flat rotor equals L/d. When $L_w/d = 2$, the number of vortices with the wavy rotor is identical to that with a flat rotor, since $2L/L_w = L/d$. This result is illustrated in Figure 8.28, where similar inactivation levels (N/N_0) are observed for both the wavy and flat rotors when $L_w/d = 2$. When $L_w/d > 2$, for example, Figure 8.28 shows that the inactivation levels N/N_0 for the wavy rotor are higher than values for the flat rotor because of fewer vortices. Therefore, $L_w/d < 2$ for the wavy rotor is required to achieve lower inactivation levels (N/N_0) compared with the flat rotor.

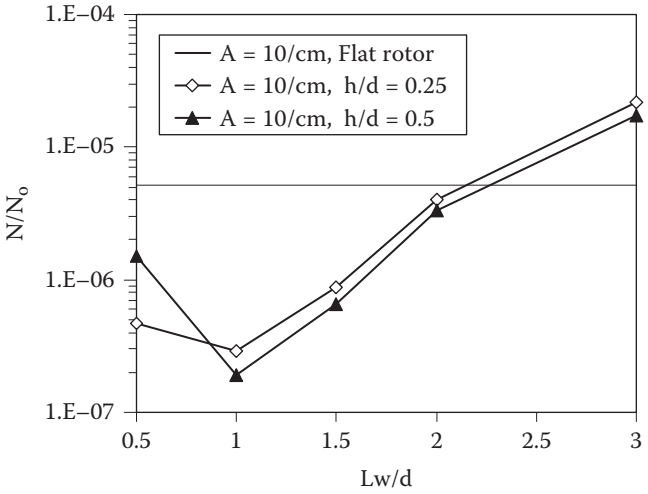

FIGURE 8.28 Comparison of inactivation with flat and wavy rotors. (From Ye 2007. With permission.)

However, decreasing the rotor wavelength cannot decrease inactivation levels N/N_0 indefinitely. For example, Figure 8.28 shows that the inactivation levels with $L_w/d = 0.5$ are greater than those with $L_w/d = 1$. Normally, there are two unequal vortices within one wavelength period, which is somewhat visible in Figure 8.26. However, when the wavelength decreases, the smaller vortex disappears. One observes in Figure 8.28 that decreasing rotor wavelengths and increasing wave amplitudes can improve the inactivation levels N/N_0 for Taylor–Couette reactors up to a factor of 40 for rotor wavelengths in the range $1 < L_w/d < 2$. Moreover, decreasing the rotor wavelength is more effective than increasing the wave amplitude for the Taylor–Couette reactor in the same range $1 < L_w/d < 2$.

8.4 COMPARISON OF DISINFECTION IN CONCENTRIC CYLINDERS

In the present discussion, inactivation data are compared for the three types of flow between concentric cylinders: laminar, turbulent, and Taylor–Couette flow. Comparisons are made for the predicted fluence distribution between the various flow patterns. The relative microbe concentrations and boundary-layer thicknesses for each flow pattern are also compared and discussed. Finally, useful correlation procedures derived from experimental data are suggested for plotting the inactivation data for all three devices on a single graph.

8.4.1 UV Fluence Distribution in Concentric Cylinders

One method of comparing the effects of different flow patterns within a plug-flow reactor is to determine the fluence distribution. The fluence distribution is computed

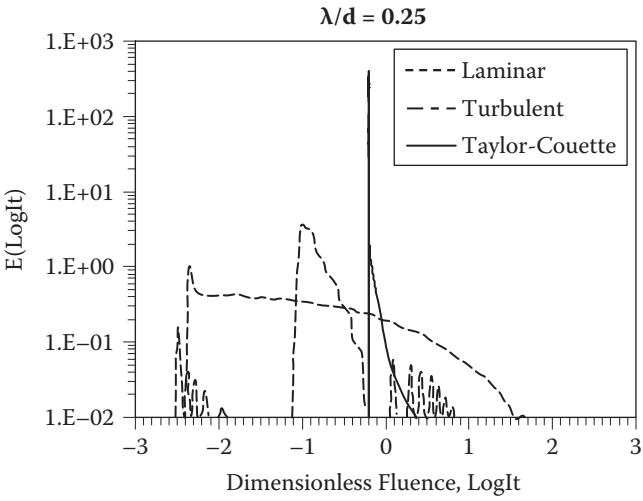

FIGURE 8.29 Fluence distribution for three flow patterns (Ta = 200 for Taylor–Couette flow, $A = 10\ \text{cm}^{-1}$, $d = 4$ mm). (From Ye 2007. With permission.)

by following a large number of microbes through the reactor while summing the number of photons incident on each microbe. According to Figure 8.29, Taylor–Couette reactors approach the superior characteristics of an ideal plug-flow reactor. In contrast, for turbulent flow there is a dominant peak corresponding to the central fully turbulent region and two subordinate peaks for the viscous boundary layers on both the inner and outer cylinders. Finally, the least-attractive design corresponds to laminar flow with a broad fluence distribution.

8.4.2 Optimum UV Inactivation in Concentric Cylinders

Figure 8.30 is the comparison of log reductions among the three flow patterns where the radius of the inner cylinder is 1.225 cm and a series-event inactivation model of *E. coli* is used. The radius of the outer cylinder is changed from 1.235 cm to 1.74 cm in order to create different gap widths. According to Figure 8.30, laminar Taylor–Couette flow achieves a higher log reduction than either laminar or turbulent flow with the same dosage $I_0\tau$ and absorption coefficient A. For example, when $A = 40\ \text{cm}^{-1}$ and $\lambda/d = 0.417$, the inactivation levels N/N_0 are 8.2×10^{-10}, 8.1×10^{-3}, and 0.27 for Taylor–Couette flow (Ta = 200), turbulent flow, and laminar flow, respectively.

Both turbulent and laminar flows achieve poor inactivation levels when the absorption coefficients of juices are high and λ/d is small. Moreover, the optimum λ/d for Taylor–Couette flow is reduced to $\lambda/d = 0.5$ compared with an optimum value of $\lambda/d = 1.0$ for turbulent and $\lambda/d = 1.5$ for laminar flow. Thus, for a given juice, Taylor–Couette flow is suitable for disinfecting juices with high absorption coefficients and with larger gap widths d, as shown in Figure 8.30.

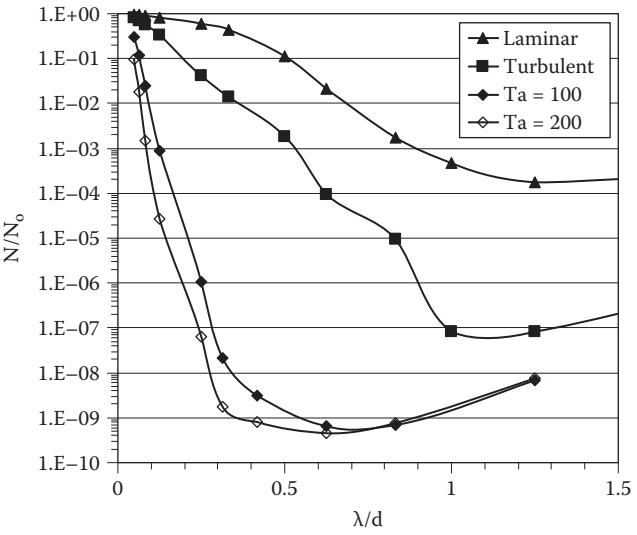

FIGURE 8.30 Comparison of inactivation for three flow patterns (dosage $I_0\tau = 2870$ mJ/cm^2 and absorption coefficient $A = 40$ cm^{-1}). (From Ye 2007. With permission.)

8.4.3 Microbe Mass Transfer

Microbe mass transfer to the radiation surface is rate limited by the relatively slow laminar diffusion across the surface-concentration boundary layer. The small concentration boundary-layer thickness δ_c varies, depending on the nature of the flow field from the three types considered: laminar, turbulent, and Taylor–Couette flow. In the previous sections treating both turbulent and Taylor–Couette flows, correlations for microbe inactivation were developed for simplicity in terms of the fluid boundary-layer thickness δ. In this section, correlations are developed for δ_c the concentration boundary layer thickness based on values developed in the literature from experimental data.

8.4.3.1 Laminar Flow

Laminar flow between concentric cylinders constitutes a parabolic velocity profile in the axial direction. Microbes must diffuse across the laminar channel. Considering bacterial motility of $Đ \approx 2 \times 10^{-5}$ cm^2 s^{-1} (Fenchel 2001), the bacterial Schmidt number Sc for *E. coli* in water is

$$Sc = \upsilon/Đ \approx 500 \tag{8.30}$$

In the present study, one considers the thin-film model for mass transfer where the mass-transfer coefficient

$$k_c = Đ/\delta_c \tag{8.31}$$

and δ_c is the microbe concentration boundary-layer thickness.

The Sherwood number for fully developed laminar flow in a circular tube annulus is defined by (Incropera and Dewitt 1996)

$$\mathrm{Sh} = 4.86 \tag{8.32}$$

where

$$\mathrm{Sh} = k_c(2d/Đ) \tag{8.33}$$

and d is the gap width between cylinders. Thus, substituting k_c from equation (8.31) into equation (8.33), one obtains

$$\delta_c/2d = \mathrm{Sh}^{-1} \tag{8.34}$$

From equation (8.32), the ratio of boundary thickness to gap width for laminar flow becomes

$$\delta_c/d = 0.41 \tag{8.35}$$

8.4.3.2 Turbulent Flow

Turbulent flow between concentric cylinders exists at large Reynolds numbers where

$$\mathrm{Re}_h = 2d\mathrm{v}/\upsilon \tag{8.36}$$

and $2d = D_h$ is the hydraulic diameter. The transition from laminar to turbulent flow occurs for values of $2000 < \mathrm{Re}_h < 4000$. The Sherwood number for fully developed turbulent flow in a circular tube annulus is defined by Welty et al. (2001) for $\mathrm{Sc} >> 1$

$$2d/\delta_c = \mathrm{Sh} = 0.023\ \mathrm{Re}_h^{0.8}\ \mathrm{Sc}^{0.33} \tag{8.37}$$

Values of the Sherwood number in turbulent flow for the transition Reynolds number over the range $2000 < \mathrm{Re}_h < 4000$ cover the range $80 < \mathrm{Sh} < 140$. Thus, the ratio of concentration boundary thickness to gap width for turbulent flow from equation (8.34) covers the range

$$0.0144 < \delta_c/d < 0.026 \tag{8.38}$$

where the lower limit could be reduced for $\mathrm{Re}_h > 4000$.

8.4.3.3 Taylor–Couette Flow

Laminar Taylor–Couette flow between concentric cylinders exists for a range of the dimensionless Taylor number defined by

$$\mathrm{Ta} = \frac{R_1\Omega_1 d}{\upsilon}\left(\frac{d}{R_1}\right)^{1/2} \tag{8.39}$$

where R_1 and Ω_1 are the radius and angular velocity of the inner cylinder, respectively. Numerical results for mass transfer in Taylor–Couette flow that are compatible with experiments provide a correlation of the Sherwood number of the form (Baier et al. 1999)

$$2d/\delta_c = \mathrm{Sh} = 1.1\ \mathrm{Ta}^{0.46}\ \mathrm{Sc}^{0.33} \tag{8.40}$$

Typical values of the Sherwood number in Taylor–Couette flow cover the range $72 < \mathrm{Sh} < 152$, corresponding to values of the laminar Ta from $100 < \mathrm{Ta} < 500$. Thus, the ratio of concentration boundary layer to gap width for Taylor–Couette flow from equation (8.34) covers the range

$$0.0123 < \delta_c/d < 0.0276 \tag{8.41}$$

8.4.4 Correlation of UV Inactivation in Concentric Cylinders

To simplify presentation of experimental data and to compare the results for laminar, turbulent, and Taylor–Couette flows, attempts have been made to correlate all of the inactivation results with a single dimensionless group. For the three flow patterns considered, a useful expression to predict microbe inactivation levels that accounts for both nonuniform (radial) radiation intensity and fluid velocity has been found in the form

$$\ln(N/N_0) = \frac{-ckI_0\tau\varphi\mathrm{Rc}}{\alpha d\delta_c} \tag{8.42}$$

for plug flow between concentric cylinders, where φ is defined for laminar flow in equation (8.44). Here,

$$\mathrm{Rc} = \frac{2R_1}{R_1 + \mathrm{R}_2} \tag{8.43}$$

corresponds to uniform UV radiation emitted from the inner cylinder. One can replace R_1 with R_2 in the numerator of equation (8.43) to predict a source of uniform radiation from the outer cylinder. Equation (8.42) is similar to the predictions of Severin et al. (1983, 1984), which account for nonuniform radiation levels within the fluid but assumed a uniform velocity in a plug-flow reactor. The quantity τ in equation (8.42) is the average fluid residence time V/Q, where V is the irradiated fluid volume and Q is the fluid flow rate. The parameter I_0 is the incident fluence rate at the reactor surface, $\alpha = 2.3A$, where A is the absorption coefficient (base 10) and k is the inactivation constant determined from separate laboratory procedures. The remaining constant $c = 8.7 \times 10^{-4}$ is an empirical value obtained by a least-squares method (Forney et al. 2008).

The experimental results for the inactivation of microbes are shown in Figure 8.31 with the correlation suggested by equation (8.42). Mass transport in both turbulent and Taylor–Couette flow occurs by the comparatively large fluid eddy transport in the bulk to the edge of the concentration boundary layer of thickness δ_c. The latter process is followed by the slow rate-limiting molecular diffusion step across a small laminar sublayer to the radiation surface. In contrast, for the laminar flow case within the reactor, microbes must diffuse across the entire laminar channel characterized by the slow molecular diffusion step. To account for laminar flow geometries, Ye (2007) has proposed a correction factor φ in equation (8.42) of the form

$$\varphi = \left(\frac{\alpha d\delta_c}{c}\right)\left[\frac{\exp(-\alpha dm)}{\mathrm{Rc}}\right] \tag{8.44}$$

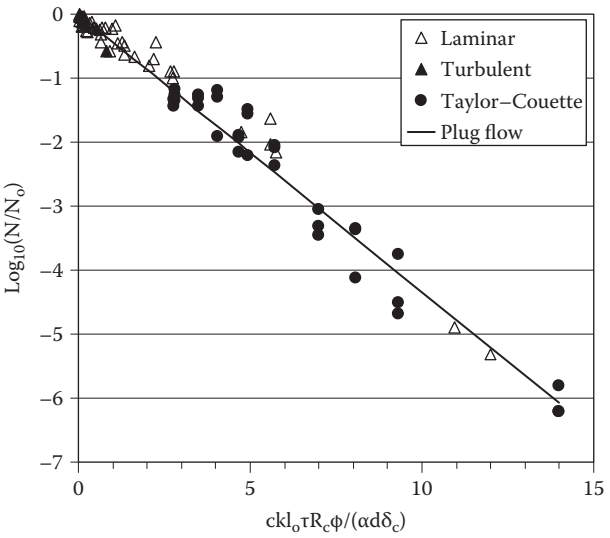

FIGURE 8.31 Correlation of microbe inactivation in concentric cylinders.

where $m = 0.92$. It should be noted that $\varphi = 1$ in the correlation given by equation (8.42) for both turbulent and Taylor–Couette flows.

8.5 TURBULENT CHANNEL FLOW

8.5.1 Turbulent Channel Reactor

In the Aquionics UV reactor (Hanovia Ltd., Slough, England), treatment is achieved by passing liquid through a cylindrical stainless steel chamber. The chamber contains 12 UV low-pressure arc tubes parallel to the flow, with each emitting 14.7 W of radiation per lamp. Each arc tube is mounted in a quartz sleeve that is 2.8 cm OD × 94 cm long and fitted within the flow chamber of diameter 18.2 cm, allowing the liquid to pass the sleeve on all sides. The latter geometry provides a radiation intensity of $I_0 = 25$ mW/cm^2 at the quartz surface of each lamp within the turbulent channel reactor shown in Figure 8.32. A sealed UV monitor fitted to the chamber detects the intensity of UV light being emitted from the arc tube. A temperature sensor is fitted on top of the chamber. Cider or model liquids are sampled before UV exposure and immediately after a single pass through the reactor. The reactor is also cleaned and sanitized before each pass through the reactor.

The reactor liquid volume is 14.7 L, with a flow rate range of 250–1300 mL/s. The liquid cross-sectional area $A_f = 186.2$ cm^2, which is the cross-sectional area of the reactor $A_t = 260$ cm^2 minus the cross-sectional area of the 12 lamps including quartz sleeves. The wetted perimeter of both the 12 lamp quartz sleeves plus the ID of the reactor is $P = 162.65$ cm. Thus, the hydraulic diameter ($D_h = 4\,A_f/P = 4.58$ cm) and the average fluid velocity ($v = Q/A_f$) are used to calculate the hydraulic Reynolds

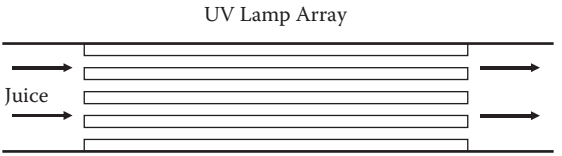

FIGURE 8.32 Schematic of cylindrical turbulent channel reactor.

number $Re_h = vD_h/\upsilon$. For the data presented below, the fluid flow rate is either $Q = 0.625$ or 1.25 L/s or the hydraulic Reynolds is either $Re_h = 1536$ or 3072 and is turbulent. It should be noted that the flow entering the reactor within a 2-cm pipe is fully turbulent with a Reynolds number $Re > 10^4$. The same flow is subjected to lamp support baffles within the reactor, so that one can assume turbulent conditions during microbe inactivation.

8.5.2 Effect of the Absorption Coefficient

The effect of the absorption coefficient on survival of *E. coli* K12 was studied for both a commercial apple juice and solutions containing clear malate buffer at pH = 3.75 with a range of 0.13–0.6% caramel solutions (Koutchma et al. 2004). Figure 8.33 is a plot of the inactivation rate defined as $-\log[N/N_0]/\tau$ at constant flow rate of 1.25 L/s (75 L/min) versus the absorption coefficient A (cm^{-1}), where τ is the total fluid residence time through the reactor. As observed in Figure 8.33, the inactivation rate varies as the inverse of the absorbance A, which is consistent with earlier observations of log reductions in concentric cylinders in Sections 8.1–8.4. The single data point at low absorbance $A = 2$ cm^{-1}, which is underpredicted by the theory in Figure 8.33, is a

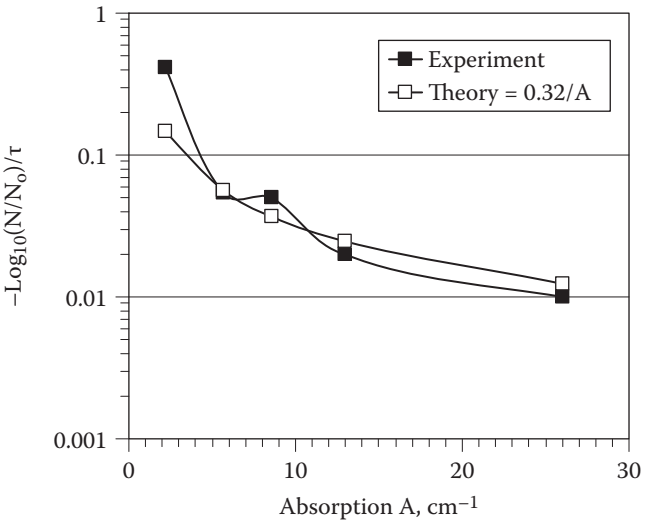

FIGURE 8.33 Inactivation rate versus absorbance.

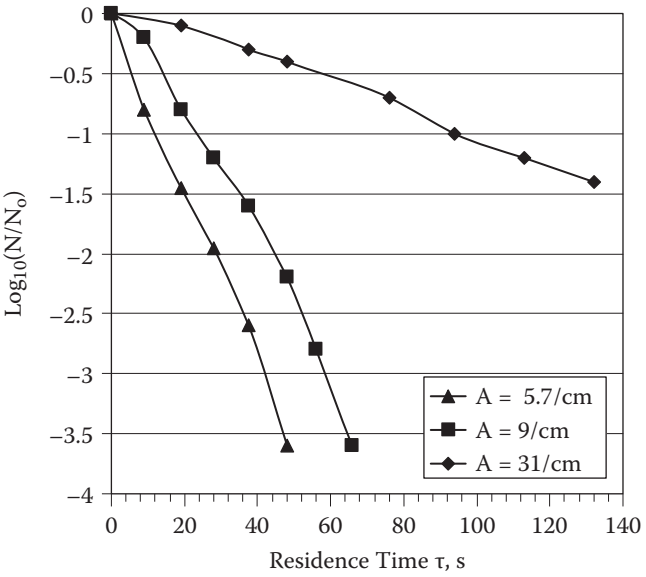

FIGURE 8.34 Inactivation of *E. coli* K12 in turbulent channel flow.

tailing effect that can occur with populations of microbes containing a few resistant microbes.

8.5.3 UV Disinfection of *E. coli*

The effect of the residence time and absorption coefficient on the survival of *E. coli* is studied with the same solutions and a flow rate of either 75 or 37.5 L/min, as described in Section 8.5.2. As observed in Figure 8.34, the inactivation of bacteria follows first-order kinetics. These results are similar to earlier data presented in Sections 8.1–8.4 obtained with concentric cylinder reactors. In Figure 8.34, each successive data point on a single curve represents one additional pass through the reactor. As shown in Figure 8.34, seven passes are required to approach a 4-log reduction for solutions with a small absorbance ($A < 10$ cm^{-1}).

8.5.4 Correlation of UV Disinfection

The turbulent channel reactor contains 12 UV lamps parallel to the direction of flow. The radius of each UV lamp with a quartz sleeve is $R_1 = 1.4$ cm. For the purpose of modeling microbe disinfection, it is assumed that each lamp irradiates an equal fraction of the total cross-sectional area of the reactor, or 260 cm^2/12 lamps = 21.7 cm^2 per lamp. Therefore, the radius of the irradiated area per lamp is $R_2 = 2.62$ cm with a gap width $d = R_2 - R_1 = 1.22$ cm. The remaining geometric parameters are the geometric ratio $\mathrm{Rc} = 2R_1/(R_1 + R_2) = 0.7$ and the hydraulic diameter calculated in Section 8.5.1, i.e., $D_h = 4.58$ cm.

The disinfection level for turbulent channel flow is calculated with the same expression used for turbulent flow within concentric cylinders described in Section 8.4. The disinfection level for turbulent plug flow is therefore

$$\log_{10}(N/N_0) = \frac{-ckI_0\tau \mathrm{Rc}}{2.3\alpha d\delta_c} \tag{8.45}$$

Here, $\alpha = 2.3A$, where A is the fluid absorbance; $I_0 = 25$ mW/cm^2 is the lamp quartz sleeve surface radiation flux; $k = k_{SE} = 0.675$ cm^2/mJ is the *E. coli* K12 series event rate constant, and δ_c is the microbe concentration boundary-layer thickness.

The concentration boundary-layer thickness δ_c is calculated from the empirical expression for the mass-transfer Sherwood number Sh, where (Welty et al. 2001)

$$2d/\delta_c = \mathrm{Sh} = 0.023\mathrm{Re}_h^{0.8}\mathrm{Sc}^{0.33} \tag{8.46}$$

Here, Re_h is the hydraulic Reynolds number, where $\mathrm{Re}_h = 3078$ for the fluid flow rate of 75 L/min and $\mathrm{Re}_h = 1535$ for the flow rate of 37.5 L/min. The Schmidt number is Sc = 500 for *E. coli* suspended in water or juice (Fenchel 2001).

Figure 8.35 is a plot of the dimensionless correlation for microbe disinfection in turbulent channel flow. The universal constant is found to be $c = 5.4 \times 10^{-3}$ cm for the turbulent channel reactor. As observed in Figure 8.35, all of the data from Figure 8.34 collapse into a single curve consistent with equation (8.45). The solid line in Figure 8.35 represents the yield from a plug-flow reactor (PFR).

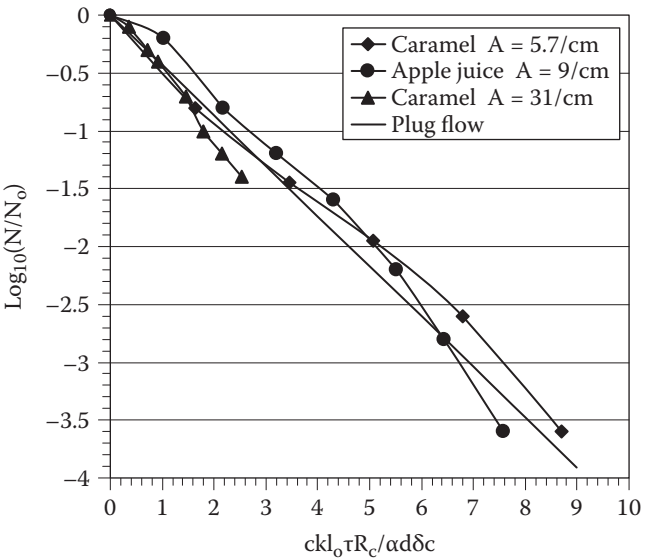

FIGURE 8.35 Dimensionless correlation for microbe disinfection in turbulent channel flow ($c = 5.4 \times 10^{-3}$ cm, Rc = 0.7).

8.6 DEAN FLOW REACTOR

The advantages of decreasing the laminar boundary layer and thus the microbe concentration boundary layer near the solid radiation surface has been discussed in previous sections. In particular, it is shown that turbulence both improves disinfection efficiency and provides a nearly uniform microbe radiation flux. Moreover, the secondary flow introduced by laminar Taylor–Couette vortices is shown to provide nearly ideal plug-flow conditions.

In the present section, the effects of a coiled-tube geometry are discussed. In particular, such geometries promote a secondary flow within the tube consisting of a pair of counter-rotating vortices called the Dean effect (Dean 1927, 1928; Fellouah et al. 2006). Experimental results are presented for the UV inactivation of *E. coli* K12 within Dean flow (Koutchma et al. 2007). A useful nondimensional plot is also developed to assist in the design of Dean flow reactors, including the effects of fluid properties, microbe inactivation constant, radiation levels, and device geometry.

8.6.1 Dean Flow Reactor

The Dean flow reactor in the present study is the ultraviolet module 420 (Salcor Inc., Fallbrook, CA) that contains a coiled fluorinated ethylene propylene (FEP) Teflon tube along with ultraviolet lamps and reflectors. The schematic diagram of the reactor is given in Figure 8.36. The UV lamps and reflectors are placed both inside and outside the coiled tube that can be seen from the side view of the reactor. The coiled tubing and lamps are housed in a stainless steel enclosure with the lamps mounted parallel to the axis of the tubing helix. The enclosure has 12 UV lamps mounted around the inside diameter of the tubing helix and 12 UV lamps mounted around the outside diameter. Each pair of lamps has a parabolic reflector to enhance the UV intensity at the tube surface. Juice or model fluids enter one side of the UV module through a stainless steel tube. The flux of UV radiation into the fluid from the inside tube surface is $I_0 = 15.2$ mW/cm^2 (Koutchma et al. 2007).

Within the UV module, fluid flows through 97.5 cm of diameter $D = 1.87$ cm ID tubing that has been wound into a 40 cm ID helix coil. The fluid flow rates are $Q = 3.5$, 5, and 7 gpm with, for example, a volume flow rate of 0.315 m^3/s (5 gpm)

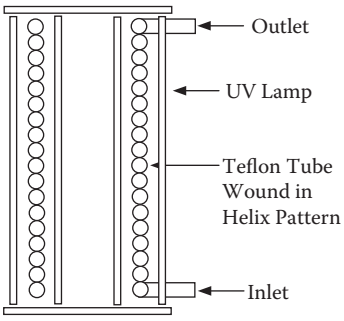

FIGURE 8.36 Schematic of Dean flow reactor. (From Koutchma et al. 2007. With permission.)

achieved with an average fluid velocity of 1.1 m/s. The tube Reynolds number Re = vD/υ is calculated to be Re = 20,570 and turbulent at a flow rate of 5 gpm with model caramel/water solutions but is calculated to be much lower with juices that have a viscosity that is at least a factor of five greater than water. For example, pineapple or orange juice would have a Reynolds number Re < 2000 and laminar flow for the fluid flow rates listed above (Koutchma et al. 2007).

An important feature of the helix coil geometry concerns the development of secondary vortices in the tube. It has been demonstrated by Dean (1927) that a secondary flow field develops in the fluid through a coiled tube because of the centrifugal forces acting on the fluid within the tube. The Dean number De is the similarity parameter governing fluid motion in such a flow configuration. The Dean number is calculated as De = Re $\sqrt{D/D_c}$, where D is the tube diameter, D_c is the coil diameter, and Re is the tube Reynolds number. Such secondary flows are promoted within the range of $0.03 < D/D_c < 0.10$. For the present device, the ratio of $D/D_c = 0.046$ indicates that secondary vortices developed for both laminar and turbulent flows.

8.6.2 Active Microbe Distribution

The active microbe distribution in the Dean reactor was studied by the pulse injection of an *E. coli* suspension as a tracer in model caramel solutions. The concentration of the bacteria was measured in the samples taken at the reactor outlet as a function of time when UV lamps were either "off" or "on." The level of inactivation of *E. coli* in each volume fraction was obtained by subtracting the $\log_{10}$ of the active bacterial concentrations in the corresponding UV-unirradiated and UV-irradiated model solutions at a given time after injection. Figure 8.37 shows the plots of concentration of viable bacteria versus time in a semi-log scale after injection into a 0.5% caramel solution with an absorbance of $A = 25.8$ cm^{-1} at $Q = 5$ gpm with UV lamps either "off" or "on." No survivors were detected at the outlet in model caramel solutions of 0.2% and 0.35%. The upper curve for the distribution of the concentration of unirradiated bacteria represents the residence time distribution (RTD) within the reactor.

The curve of the distribution of surviving UV irradiated bacteria (lamps on) reflects the combined effects of the flow distribution (RTD) and the UV-light irradiance distribution (LID) on the distribution of doses acting on any injected microorganism. It can also be seen in Figure 8.37 that the distribution of inactivated *E. coli* in 0.5% model caramel solution is close to uniform. The $\log_{10}$ concentration of inactivated microbes has an average of 1.86, with a maximum and minimum value of 2.1 and 1.6, respectively.

It is possible to estimate both the active and inactive microbe distributions from the RTD distribution (lamps-off data) from Figure 8.37. In the present discussion, the segregation model is used to estimate the active microbe distribution from the RTD (lamps-off data) represented by the upper curve in Figure 8.37 (Water Environment Federation 1996). Here, the distribution of active microbes (lamps-on data) is estimated from

$$\left(\frac{dN}{dt}\right)_{\text{lamps on}} = N_0(e^{-k_p t})E(t) \tag{8.47}$$

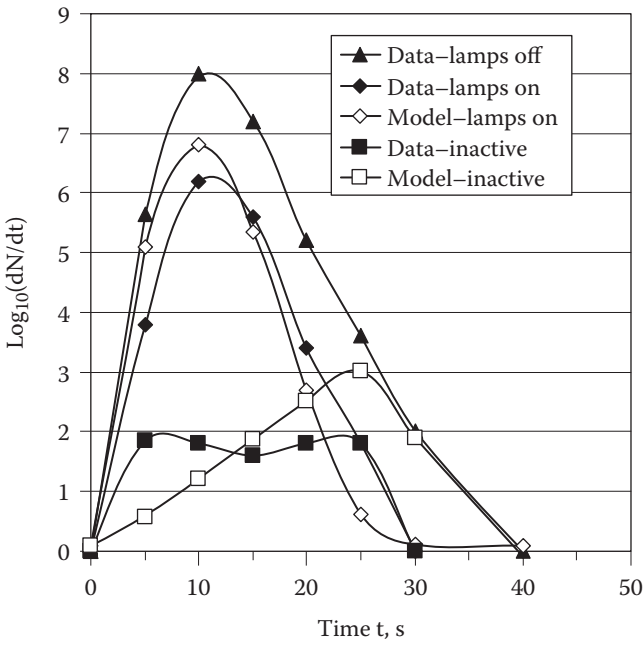

FIGURE 8.37 Microbe concentrations at the reactor outlet including both active and inactive components. Segregation model data are represented by the open symbols.

where the residence time distribution (RTD) is given by

$$E(t) = \left(\frac{dN}{dt}\right)_{\text{lamps off}} \left(\frac{1}{N_0}\right) \tag{8.48}$$

The constant $kp = 0.3\ s^{-1}$ in equation (8.47) is proportional to the product of the microbe rate constant k and the average radiation intensity within the reactor $I_{av} = I_0/(2.3Ad)$, where d is the tube radius. The total microbe concentration $N_0 = 4.82 \times 10^7$ CFU/mL is determined by estimating the total area under the upper curve or dimensional RTD for the (lamps off) data representing the concentration of unirradiated bacteria in Figure 8.37.

The experimental data (solid symbols) and model estimate (open symbols) representing the concentration of both active and inactive microbes are shown in Figure 8.37. The inactive data were determined by subtracting the active microbe distribution (lamps-on data) from the total microbe distribution (lamps-off data) for both the experimental and model results. As shown in Figure 8.37, the segregation model equation 8.47 represents a useful estimate of the active fraction of microbes. The parameter kp $\alpha\, kI_0/2.3Ad = 0.1\ s^{-1}$ for the segregation model in Figure 8.37. The value of $kp = 0.3\ s^{-1}$, however, provides a reasonable estimate of the active fraction of microbes. The latter value of kp is chosen such that the area under the model active distribution (open symbols) is equal to the area under the experimental active distribution (solid diamonds).

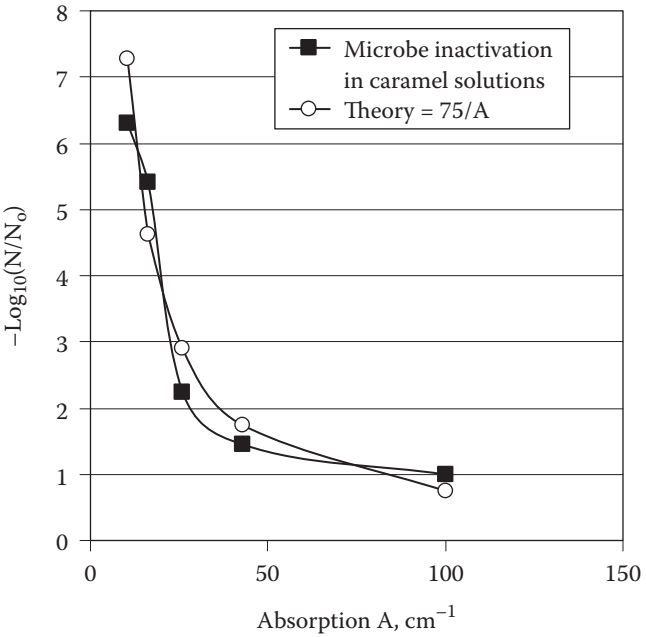

FIGURE 8.38 Inactivation of *E. coli* versus absorbance.

8.6.3 Effect of the Absorption Coefficient

The effect of the absorption coefficient on survival of *E. coli* K12 was studied for both a variety of commercial juices and solutions containing a clear malate buffer at pH = 3.75 with a range of 0.13–0.6% caramel/water solutions (Koutchma et al. 2007). Figure 8.38 is a plot of the inactivation defined as $-\log[N/N_0]$ at a constant flow rate of 0.315 m^3/s (5 gpm) versus the absorption coefficient A (cm^{-1}). As observed in Figure 8.38, the inactivation rate varies as the inverse of the absorbance A, which is consistent with earlier observations of log reductions in both concentric cylinders and turbulent channel reactors (e.g., Figure 8.33).

8.6.4 UV Inactivation of *E. coli*

The effect of the residence time and absorption coefficient on the survival of *E. coli* was studied. Survival curves of *E. coli* K12 in model caramel solutions with concentrations from 0.2% to 2% are shown in Figure 8.39. As observed in Figure 8.39, the inactivation of bacteria follows first-order kinetics. These results are similar to earlier data presented in Sections 8.1–8.4 obtained with concentric cylinder reactors. In Figure 8.39, each successive data point on a single curve represents one additional pass through the reactor. As shown in Figure 8.39, three passes are required to approach a 5-log reduction for solutions with a large absorbance of $A = 25.7\ cm^{-1}$, while only one pass is required for an absorbance of 10.3 cm^{-1}.

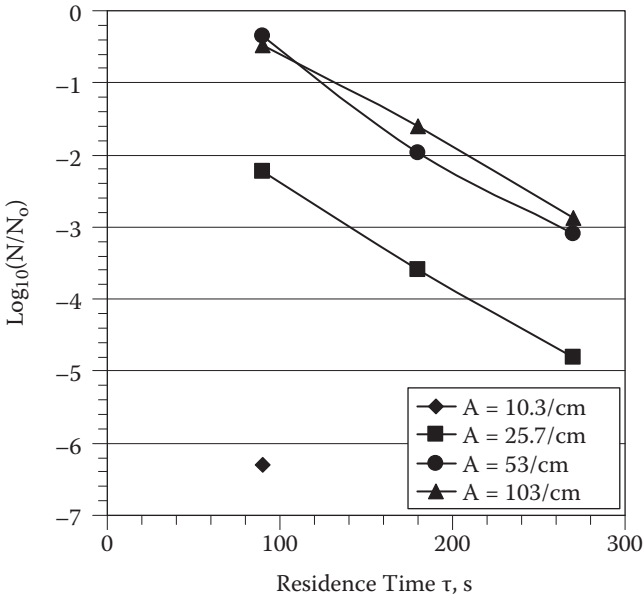

FIGURE 8.39 Inactivation of *E. coli* in caramel solutions with up to three passes through the Dean reactor. The residence time for a single pass through the reactor is 90 s.

8.6.5 Correlation of UV Disinfection

The Dean flow reactor contains 24 UV lamps parallel to the axis of the helix tube coil. With 12 lamps evenly distributed both inside and outside the helix, the irradiance into the fluid is $I_0 = 15.2$ mW/cm^2 from the inside surface of the Teflon tube. For the purpose of modeling microbe disinfection, the radius (gap width) of the irradiated area within the Teflon tube is $d = R_2 = 0.935$ cm. The remaining geometric parameters are the geometric ratio $\mathrm{Rc} = 2R_2/(R_1 + R_2) = 2.0$ because $R_1 = 0$ and the tube diameter $2d = D = 1.87$ cm.

The disinfection level for Dean flow is calculated with the same expression used for turbulent flow within concentric cylinders described in Section 8.4. The disinfection level for plug flow in a Dean flow reactor is therefore

$$\log_{10}(N/N_0) = \frac{-ckI_0\tau \mathrm{Rc}}{2.3\alpha d\delta_c} \tag{8.49}$$

Here, $\alpha = 2.3A$, where A is the fluid absorbance; $I_0 = 15.2$ mW/cm^2 is the Teflon tube inside surface radiation flux; $k = 0.675$ cm^2/mJ is the *E. coli* K12 series event rate constant k_E; and δ_c is the microbe concentration boundary-layer thickness.

The concentration boundary-layer thickness δ_c is calculated from the empirical expression for the mass-transfer Sherwood number Sh, where (Welty et al. 2001)

$$D/\delta_c = \mathrm{Sh} = 0.023 f_D\, \mathrm{Re}^{0.8}\, \mathrm{Sc}^{0.33} \tag{8.50}$$

Here, Re is the tube Reynolds number Re = vD/υ, where Re = 20,570 for the water fluid flow rate of 0.315×10^{-3} m^3/s (5 gpm). The Schmidt number is Sc = 500 for *E. coli* suspended in water or juice (Fenchel 2001).

The secondary pair of vortices along the tube axis, called Dean flow, increase the friction factor and decrease the momentum and concentration boundary-layer thickness. To account for these effects, a correction factor f_D shown in equation (8.50) must be included. The empirical correction factor for turbulent Dean flow is defined as (Schlichting 1979)

$$f_D = \left[\mathrm{Re}\left(\frac{D}{D_c} \right)^2 \right]^{0.05} \tag{8.51}$$

for values of $\mathrm{Re}(D/D_c)^2 > 6$, where D is the tube diameter and D_c is the tube helix diameter. For the geometry considered with water flowing at 5 gpm, the parameter $\mathrm{Re}(D/D_c)^2 = 45.5$ so that equation (8.51) applies. It should be noted that a somewhat different expression for both f_D and the Sherwood number Sh must be used for laminar Dean flow.

Figure 8.40 is a plot of the dimensionless correlation for microbe disinfection in turbulent Dean flow. The universal constant is found to be $c = 4.42 \times 10^{-4}$ cm for Dean flow. As observed in Figure 8.40, all of the data from Figure 8.39 collapse into

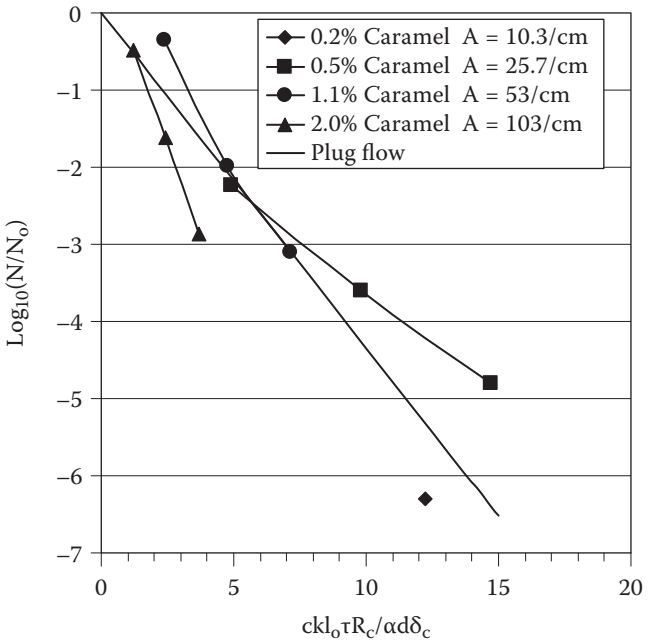

FIGURE 8.40 Dimensionless correlation for microbe disinfection in Dean flow ($c = 4.42 \times 10^{-4}$ cm, Rc = 2.0).

a single curve consistent with equation (8.49). The solid line in Figure 8.40 of the form given by equation (8.49) represents the yield from a plug-flow reactor (PFR), similar to earlier concentric cylinder and turbulent channel geometries.

8.7 EVALUATION OF UV REACTOR DESIGN

Most continuous disinfection units do not provide ideal flow conditions characteristic of an ideal plug-flow reactor. The flow patterns in many disinfection units exhibit hydraulic short-circuiting, back-mixing, and stagnation problems. In fact, viscous fluids flowing between concentric cylinders and in pipes are subject to a boundary condition of zero velocity at the walls, contributing to a residence time distribution. These nonideal reactors complicate attempts to predict the disinfection efficiency.

8.7.1 Segregation Model

The segregation model assumes that all fluid elements pass through the reactor without mixing. Moreover, one assumes that microbes in each fluid element are subject to the UV dose-response curve as determined by independent experiments with a collimated UV beam directed at the same microbe/fluid combination and evaluated at the mean radiation flux for the reactor.

Because the population of fluid elements experience a residence time distribution within the reactor corresponding to a measured RTD or E curve, it is now possible to estimate the reactor efficiency. Thus, by multiplying the E curve by the UV dose response, one obtains a reactor distribution efficiency in the form (Water Environment Federation 1996),

$$\frac{N}{N_0} = \sum_{0}^{\infty} E_i e^{-k_p t_i} \Delta t_i \tag{8.52}$$

where

$$E_i = \frac{\Delta N_i}{\Delta t_i}\left(\frac{1}{N_0}\right) \tag{8.53}$$

Here, $kp = kI_{AV}$, where k is the microbe inactivation constant, I_{AV} is the mean radiation flux within the reactor, and ΔN_i is the number of active microbes with residence time t_i in the time interval Δt_i.

To illustrate the active microbe distributions in a Dean flow reactor, the distributions are studied by the pulse injection of an *E. coli* suspension as a tracer in model caramel solutions. The concentration of the bacteria is measured in the samples taken at the reactor outlet as a function of time when UV lamps were either "off" or "on." The level of inactivation of *E. coli* in each volume fraction is obtained by subtracting the active bacterial concentrations in the corresponding UV-unirradiated and UV-irradiated model solutions at a given time after injection. The plots of

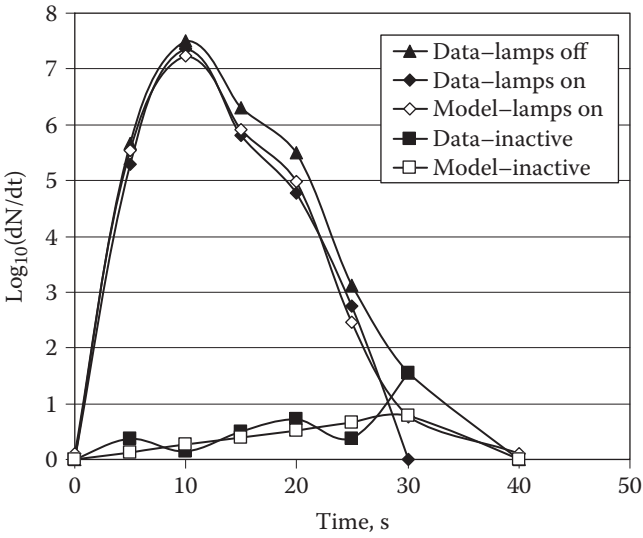

FIGURE 8.41 Microbe concentrations at the reactor outlet, including both active and inactive components. Segregation model data are represented by the open symbols.

concentration of viable bacteria versus time in a semi-log scale after injection into a 1% caramel solution with an absorbance of $A = 51.6$ cm^{-1} at $Q = 5$ gpm with UV lamps either "off" or "on" are shown in Figure 8.41. The upper curve for the distribution of the concentration of unirradiated bacteria represents the residence time distribution (RTD) within the reactor.

The experimental data (solid symbols) and model estimate (open symbols) representing the concentration of both active and inactive microbes are shown in Figure 8.41. The inactive data were determined by subtracting the active microbe distribution (lamps-on data) from the total microbe distribution (lamps-off data) for both the experimental and model results. As shown in Figure 8.41, the segregation model in equation 8.52 represents a useful estimate of the active fraction of microbes. The parameter $kp = kI_0/2.3Ad = 0.052$ s^{-1} for the segregation model in Figure 8.41, where the factor $I_{AV} = I_0/2.3Ad$ represents the mean radiation intensity within the reactor, with $I_0 = 15.2$ mW/cm^2 and $d = 0.935$ cm. The value of $kp = 0.06$ s^{-1}, however, provides a reasonable estimate of the active fraction of microbes. The latter value of kp is chosen such that the area under the model active distribution (open symbols) is equal to the area under the experimental active distribution (solid diamonds).

Finally, the total microbe concentration $N_0 = 3.4 \times 10^7$ CFU/mL is determined in Figure 8.41 by estimating the total area under the upper curve or dimensional RTD for the (lamps off) data representing the concentration of unirradiated bacteria. It is observed in Figure 8.41 that the microbial inactivation is broadly distributed from 0.2-log$_{10}$ to 0.8-log$_{10}$ reduction in the sample volumes, with an average inactivation of 0.34 log$_{10}$ in the 1.0% model caramel solution with an absorbance of $A = 51.5$ cm^{-1}. The latter reflects the higher gradient of UV-light irradiance near the lamp surface and reduced penetration of radiation into the fluid.

8.7.2 Dosage Distribution Model

The previous geometries considered in Sections 8.2–8.6 assume uniform flow conditions along the UV reactor axis. For example, fluid mixing in the radial direction due to either turbulence or secondary flow within either Taylor–Couette or Dean flow reactors is uniform along the direction of flow. These geometries also provide a uniform boundary-layer thickness and microbe mass transfer rate along the flow direction. Moreover, these geometries provide a uniform radial radiation distribution in the axial flow direction.

Under these circumstances, scale-up issues are minimized, since universal curves are provided in Sections 8.2–8.6 to predict distribution levels of N/N_0. Such predictions can also be verified with relatively simple CFD calculations or just two data points taken with a bench-scale reactor and plotted on a semi-log graph (see Figs. 8.35 and 8.40).

In contrast to the geometries described above, a number of medium- to large-scale commercial UV reactor designs contain both nonuniform flow conditions and radiation fields. In this case, UV dose distributions can be determined by introducing radiation-sensitive microspheres that record an integrated radiation dose along individual fluid streamlines (Blatchley et al. 2006). CFD methods that include complex radiation fields can also be used to compute UV dose distributions (Levy et al. 2007).

The microbe inactivation levels for a UV reactor can be determined by integrating the product of the reactor dose distribution and the exponential survival curve of the test organism (Cabaj et al. 1996). The exponential survival curve is determined with a separate collimated-beam apparatus for a specific microbe. The number of active microbes N can now be determined with the expression

$$\frac{N(D_{eq})}{N_0} = \int_{D_{min}}^{D_{max}} E(D) e^{\frac{-aD}{D_{1log}}} dD \tag{8.54}$$

Here, the continuous dosage distribution $E(D)$ in units of cm^2/mJ is defined as

$$E(D) = \frac{dN}{dD}\left(\frac{1}{N_0}\right) \tag{8.55}$$

The dosage $D = D_{1log}$ is the dose required for a 1-log inactivation of the specified microbe in a collimated beam, and $a = \ln(10) = 2.3$.

It is now possible to predict the number of active microbes that have traversed the disinfection system by the expression

$$\frac{N(D_{eq})}{N_0} = e^{-aD_{eq}/D_{1log}} \tag{8.56}$$

where the equivalent dose D_{eq} is often called the RED (reduction equivalent dose). Equation (8.56) can be solved for D_{eq}, or

$$\text{RED} \equiv D_{eq} = -D_{1log} \log_{10}[N(D_{eq})/N_0] \tag{8.57}$$

Here, the microbe rate constant k can be defined as the slope of the linear part of the semi-$\log_{10}$ survival curve from equation (8.57)

$$k = \frac{\Delta \log_{10}[N(D_{eq})/N_0]}{\Delta D_{eq}} \tag{8.58}$$

The experimental procedures to determine the dose distribution in a UV reactor provide discrete values for the integrated dosage along a finite number of streamlines. These values provide a discrete dosage distribution

$$E(D_i) = \left(\frac{\Delta N_i}{N_0}\right)\left(\frac{1}{\Delta D_i}\right) \tag{8.59}$$

where ΔN_i represents the number of streamlines with a dosage in the range $D_i - \Delta D_i/2 < D_i < D_i + \Delta D_i/2$.

It is now possible to determine the active microbe fraction

$$\frac{N(D_{eq})}{N_0} = \sum_{1}^{n} E(D_i)[e^{-aD_i/D_{1\log}}]\Delta D_i \tag{8.60}$$

where the number of discrete values for the dosage n is defined by

$$n = (D_{max} - D_{min})/\Delta D_i \tag{8.61}$$

The RED or equivalent dose can now be computed as defined in equation (8.57).

An example of a discrete dose distribution is shown in Figure 8.42, where ΔD_i = 30 mJ/cm^2. Also shown is a two-parameter log-normal distribution that compares

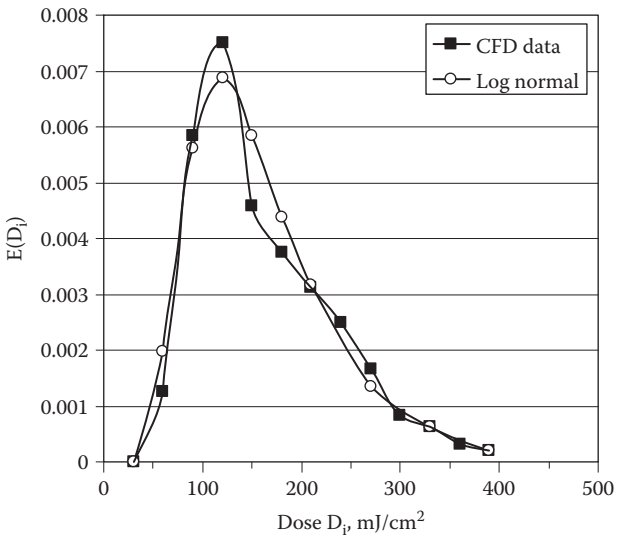

FIGURE 8.42 Comparison of CFD and log-normal dose distributions.

well with the numerical data (Wright 2007). The form of the log-normal distribution is a density function

$$E(D;\mu,\sigma)=\frac{e^{-(\ln D-\mu)^2/2\sigma^2}}{D\sigma\sqrt{2\pi}} \tag{8.62}$$

where μ and σ are the mean and standard deviation of ln(D). Another popular density function to predict UV dose distributions is the Weibull distribution in the form

$$E(D;c,b)=\frac{c}{b}\left(\frac{D-D_0}{b}\right)^{c-1}e^{-\left(\frac{D-D_0}{b}\right)^c} \tag{8.63}$$

where D_0 is the minimum UV dose for which $E(D) = 0$ (Cabaj et al. 2007).

Attempts have been made recently to correlate RED values with empirical expressions of the form (Rennecker et al. 2005)

$$\text{RED}=10^A(\text{UVA})^{B(\text{UVA})}\left(\frac{S/S_0}{Q}\right)^C \tag{8.64}$$

Here, the parameters A, B, and C are predicted with a regression analysis from either numerical predictions or from experimental data where UVA is the absorbance, S is the product of the average light intensity and reactor residence time, and Q is the reactor volume flow rate.

8.7.3 Comparison of Reactor Design Performance

In this section, the reactor performance is compared, including the three types of flow between concentric cylinders plus the turbulent-channel and Dean-flow designs. All of the five designs compared have uniform flow and radiation distributions along the reactor axis. The constraints for Table 8.1 are that the reactor axial length should not

TABLE 8.1
Components of Nondimensional Group

	Microbe/ Fluid Optics (cm^3/mJ)	Dose (mJ/cm^2)	Geometry (cm^{-1})	Boundary Layer (Sherwood number)	Inactivation
Concentric cylinder:	k/A	$I_0\tau$	$c\text{Rc}/2d^2$	$2d/\delta_c$	$\log_{10}(N/N_0)$
Laminar	0.113	870	2.7×10^{-3}	4.8	–0.6
Turbulent	0.137	116	2.7×10^{-3}	143	–0.61
Taylor–Couette	0.061	1265	1.53×10^{-3}	121	–6.0
Turbulent channel	0.075	225	1.26×10^{-3}	142	–0.2
Dean flow	0.066	1370	5.1×10^{-4}	621	–6.3

exceed roughly 1 m. The only exceptions are reactors that provide a 6-$\log_{10}$ reduction of active microbes in a shorter reactor length.

The inactivation levels for all of the designs are predicted by the expression

$$\ln\left(\frac{N}{N_0}\right) = -\frac{ckI_0\tau \mathrm{Rc}}{\alpha d\delta_c} \tag{8.65}$$

It is possible to factor the right-hand side of equation (8.65) into terms with different physical interpretations. Thus, factoring equation (8.65), one obtains four terms as shown by

$$\ln\left(\frac{N}{N_0}\right) \propto = -\left(\frac{k}{A}\right)\left(I_0\tau\right)\left(\frac{c\mathrm{Rc}}{2d^2}\right)\left(\frac{2d}{\delta_c}\right) \tag{8.66}$$

The terms grouped on the right-hand side of equation (8.66) are described by the interpretation below

$$\ln\left(\frac{N}{N_0}\right) \propto -(\text{microbe/optics})(\text{dosage})(\text{geometry})(\text{boundary layer}) \tag{8.67}$$

For example, the microbe/optics term refers to the ratio of the microbe rate constant to the fluid absorbance or k/A. This ratio is independent of the reactor design. The second term ($I_0\tau$) defines the radiation dosage, while the third term represents a collection of geometrical properties. Finally, the last term on the right-hand side of equation (8.67) is the inverse of the nondimensional boundary layer thickness, called the Sherwood number Sh.

Focusing on the microbe inactivation levels in the right-hand column of Table 8.1, one observes that only the Taylor–Couette and Dean flow designs achieve a 6-$\log_{10}$ reduction. This is the result of secondary flow in the form of vortices within the fluid gap for both designs. In contrast to the laminar reactor, the laminar boundary-layer thickness is large or the inverse boundary-layer term $\mathrm{Sh} = 2d/\delta_c$ in Table 8.1 is small, yielding less than a 1-$\log_{10}$ microbe reduction. The remaining two reactor designs with less than 1-$\log_{10}$ reduction are the turbulent flow between concentric cylinders and the turbulent channel flow. The latter turbulent designs have small inactivation levels because the fluid residence times are small due to the large fluid velocities necessary for turbulence.

It is interesting to note that the product of the geometry and Sherwood terms in Table 8.1 or $c\mathrm{Rc}/d\delta_c$ is within the range of 0.15–0.30 for all reactors except the laminar design. This result simplifies reactor design, leaving only the dosage term $I_0\tau$ as a variable. The laminar reactor is excluded from this discussion because the microbe mass transfer rate in laminar flow in the absence of secondary flow is limited by a diffusivity that is similar in magnitude to molecular diffusion.

Finally, the magnitude of the constant c that appears as the first term on the right of equation (8.65) is provided in Table 8.2 for all geometries with the exception of

TABLE 8.2
Constant *c* in Dimensionless Group

UV Reactor Geometry	Constant *c* in Dimensionless Group (Eq. 8.65)
Concentric cylinder:	
Turbulent Laminar Taylor–Couette	8.7×10^{-4}
Turbulent channel	5.4×10^{-3}
Dean flow	4.4×10^{-4}

the concentric laminar flow case. For the remaining laminar concentric cylinder geometry, one obtains inactivation levels in the form

$$\ln\left(\frac{N}{N_0}\right) = -\frac{kI_0\tau}{1+m(R_2/R_1-1)}\exp(-\alpha dm) \tag{8.68}$$

where the term $[1 + m(R_2/R_1 - 1)] \approx 1$ and $m = 0.92$ and is approximately a constant for thin-film reactor geometries, or $d/R_1 << 1$.

8.8 UDF SOURCE C CODES

8.8.1 Turbulent Flow between Concentric Cylinders

The user-defined function to determine the inactivation of microbes in turbulent flow between concentric cylinders and used with a CFD FLUENT code is shown below. (From Ye, Z., PhD thesis, 2007. With permission.)

```
UDF for UV Inactivation in Turbulent Reactors
/*********************************************************
*******/
/* Implementation of the Y. pseudotuberculosis model
using user-defined scalars */
/*********************************************************
*******/
#include "udf.h"
#include "math.h"
#define R1 0.01225 /* radius of inner cylinder, rotating*/
#define R2 0.0174 /* radius of outer cylinder,
stationary*/
#define alpha (3716*log(10)) /* absorbance coefficient
1/m */
```

```
/* I/I0=0.1 @3/4 gap distance when absorbance
coefficient alpha=768 */
/* I/I0=0.1 @1/2 gap distance when absorbance
coefficient alpha=1152 */
/* I/I0=0.1 @1/5 gap distance when absorbance
coefficient alpha=2878 */
#define I0 (16.0E+01) /* Initial radition intensity, W/
m2 */
      /* I/I0= R1/y*exp(-alpha*(y-R1)) */
#define keff1 0.572836E-01 /* first order inactiviation
constant, m2/(W S) */
#define keffSE 0.983663E-01 /* Series Event
inactiviation constant, m2/(W S) */
#define ScT 0.8 /* Turbulent Schmit number */
DEFINE_SOURCE(UDS_1stOrder, cell, thread, dS, eqn)
{
double x,y,source;
double coor[ND_ND];
 C_CENTROID(coor,cell,thread);
 x=coor[0];
 y=coor[1];
 if(x>0.0)
       {
             dS[eqn]=-keff1*I0*R1/y*exp(-alpha*(y-
R1))*C_R(cell,thread);
             source=-keff1*I0*R1/y*exp(-alpha*(y-R1))*C_
UDSI(cell,thread,0)*C_R(cell,thread);
       }
 else
       { dS[eqn]=0.0; source=0.0;}
       return source;
}
DEFINE_SOURCE(SE_N0, cell, thread, dS, eqn)
{
double x,y,source;
double coor[ND_ND];
 C_CENTROID(coor,cell,thread);
 x=coor[0];
 y=coor[1];
 if(x>0.0)
       {
             dS[eqn]=-keffSE*I0*R1/y*exp(-alpha*(y-
R1))*C_R(cell,thread);
             source=-keffSE*I0*R1/y*exp(-alpha*(y-
R1))*C_UDSI(cell,thread,1)*C_R(cell,thread);
       }
```

```
 else
       { dS[eqn]=0.0; source=0.0;}
       return source;
}
DEFINE_SOURCE(SE_N1, cell, thread, dS, eqn)
{
double x,y,source;
double coor[ND_ND];
 C_CENTROID(coor,cell,thread);
 x=coor[0];
 y=coor[1];
 if(x>0.0)
       {
             dS[eqn]=-keffSE*I0*R1/y*exp(-alpha*(y-
R1))*C_R(cell,thread);
             source=keffSE*I0*R1/y*exp(-alpha*(y-
R1))*C_R(cell,thread)*(C_UDSI(cell,thread,1)-C_
UDSI(cell,thread,2));
       }
 else
       { dS[eqn]=0.0; source=0.0;}
       return source;
}
DEFINE_SOURCE(SE_N2, cell, thread, dS, eqn)
{
double x,y,source;
double coor[ND_ND];
 C_CENTROID(coor,cell,thread);
 x=coor[0];
 y=coor[1];
 if(x>0.0)
       {
             dS[eqn]=-keffSE*I0*R1/y*exp(-alpha*(y-
R1))*C_R(cell,thread);
             source=keffSE*I0*R1/y*exp(-alpha*(y-
R1))*C_R(cell,thread)*(C_UDSI(cell,thread,2)-C_
UDSI(cell,thread,3));
       }
 else
       { dS[eqn]=0.0; source=0.0;}
       return source;
}
DEFINE_DIFFUSIVITY(diff,cell,thread,i)
{
double x,y,coor[ND_ND],wall_distance;
/* Yplus=0.293306@y=0.0122652 and R1=0.01225*/
```

```
/* Yplus=0.293306/(0.0122652-0.01225)*wall_
distance=19296*wall_distance*/
 C_CENTROID(coor,cell,thread);
 x=coor[0];
 y=coor[1];
       if((y-R1)<(R2-y))
       {wall_distance=y-R1;}
       else{wall_distance=R2-y;}
 if(x>0.0)
       {
             if((19296*wall_distance)>5.0)
             {return (C_MU_T(cell,thread)/ScT);}
             else{return 0.0;}
       }
 else {return 0.0;}
}
```

8.8.2 Taylor–Couette Flow between Concentric Cylinders

The user-defined function to determine the inactivation of microbes in Taylor–Couette flow between concentric cylinders and used with a CFD FLUENT code is shown below. (From Ye, Z., PhD thesis, 2007. With permission.)

```
UDF for UV Inactivation in Taylor Vortex Reactors
/*****************************************************
*******/
/* Implementation of the E-Coli model using user-defined
scalars */
/*****************************************************
*******/
#include “udf.h”
#include “math.h”
#define R1 0.01717 /* radius of inner cylinder,
rotating, m*/
#define R2 0.022885 /* radius of outer cylinder,
stationary, m*/
#define Q 40 /* Flow rate, mL/min */
#define alpha (1100*log(10)) /* absorbance coefficient
1/m */
#define I0 25.0E+01 /* Initial radition intensity, W/m2 */
      /* I/I0=R2/y*exp(-alpha*(R2-y)), radiation from
outer cylinder */
#define L0 5.34E-02 /* Length of UV lamp, m */
#define keff1 0.32494E-01 /* first order inactiviation
constant, m2/(W S) */
```

```
#define keffSE 0.674742E-01 /* Series Event
inactiviation constant, m2/(W S) */
DEFINE_PROFILE(velocity_profile,thread,position)
{
 double coor[ND_ND];          /* this will hold the
position vector */
 double y,kappa,temp,Uav;
 face_t f;
 Uav=Q*1.0E-6/60/(3.1416*(R2*R2-R1*R1));
 kappa=R1/R2;
 temp=2.0*Uav/((1-pow(kappa,4))/(1-kappa*kappa)-(1-
kappa*kappa)/log(1.0/kappa));
 begin_f_loop(f, thread)
 {
 F_CENTROID(coor,f,thread);
 y = coor[1];
 F_PROFILE(f,thread,position)=temp*(1.0-(y/R2)*(y/
R2)+(1.0-kappa*kappa)/log(1.0/kappa)*log(y/R2));
 }
 end_f_loop(f, thread)
}
DEFINE_SOURCE(UDS_1stOrder, cell, thread, dS, eqn)
{
double x,y,source;
double coor[ND_ND];
 C_CENTROID(coor,cell,thread);
 x=coor[0];
 y=coor[1];
 if(x>0.0&&x<L0)
       {
             dS[eqn]=-keff1*I0*R2/y*exp(-alpha*(R2-
y))*C_R(cell,thread);
             source=-keff1*I0*R2/y*exp(-alpha*(R2-y))*C_
UDSI(cell,thread,0)*C_R(cell,thread);
       }
 else
       { dS[eqn]=0.0; source=0.0;}
       return source;
}
DEFINE_SOURCE(SE_N0, cell, thread, dS, eqn)
{
double x,y,source;
double coor[ND_ND];
 C_CENTROID(coor,cell,thread);
 x=coor[0];
 y=coor[1];
```

```
 if(x>0.0&&x<L0)
       {
             dS[eqn]=-keffSE*I0*R2/y*exp(-alpha*(R2-
y))*C_R(cell,thread);
             source=-keffSE*I0*R2/y*exp(-alpha*(R2-y))*
C_UDSI(cell,thread,1)*C_R(cell,thread);
       }
 else
       { dS[eqn]=0.0; source=0.0;}
       return source;
}
DEFINE_SOURCE(SE_N1, cell, thread, dS, eqn)
{
double x,y,source;
double coor[ND_ND];
 C_CENTROID(coor,cell,thread);
 x=coor[0];
 y=coor[1];
 if(x>0.0&&x<L0)
       {
             dS[eqn]=-keffSE*I0*R2/y*exp(-alpha*(R2-
y))*C_R(cell,thread);
             source=keffSE*I0*R2/y*exp(-alpha*(R2-
y))*C_R(cell,thread)*(C_UDSI(cell,thread,1)-C_
UDSI(cell,thread,2));
       }
 else
       { dS[eqn]=0.0; source=0.0;}
       return source;
}
DEFINE_SOURCE(SE_N2, cell, thread, dS, eqn)
{
double x,y,source;
double coor[ND_ND];
 C_CENTROID(coor,cell,thread);
 x=coor[0];
 y=coor[1];
 if(x>0.0&&x<L0)
       {
             dS[eqn]=-keffSE*I0*R2/y*exp(-alpha*(R2-
y))*C_R(cell,thread);
             source=keffSE*I0*R2/y*exp(-alpha*(R2-
y))*C_R(cell,thread)*(C_UDSI(cell,thread,2)-C_
UDSI(cell,thread,3));
       }
 else
```

```
        { dS[eqn]=0.0; source=0.0;}
        return source;
}
DEFINE_SOURCE(SE_N3, cell, thread, dS, eqn)
{
double x,y,source;
double coor[ND_ND];
 C_CENTROID(coor,cell,thread);
 x=coor[0];
 y=coor[1];
 if(x>0.0&&x<L0)
        {
              dS[eqn]=-keffSE*I0*R2/y*exp(-alpha*(R2-
y))*C_R(cell,thread);
              source=keffSE*I0*R2/y*exp(-alpha*(R2-
y))*C_R(cell,thread)*(C_UDSI(cell,thread,3)-C_
UDSI(cell,thread,4));
        }
 else
        { dS[eqn]=0.0; source=0.0;}
        return source;
}
```

REFERENCES

Baier, G., T. M. Grateful, M. D. Graham, and E. N. Lightfoot. 1999. Prediction of mass transfer in spatially periodic systems. *Chem. Eng. Sci.* 54: 343–355.

Bird, R. B., W. E. Stewart, and E. N. Lightfoot. 2002. *Transport Phenomena*. New York: Wiley.

Blatchley III, E. R., C. Shen, Z. Naunovic, L. Lin, D. A. Lyn, J. P. Robinson, K. Ragheb, G. Gregori, D. E. Bergstrom, S. Fang, Y. Guan, K. Jennings, and N. Gunaratna. 2006. Dyed microspheres for quantification of UV dose distributions: Photochemical reactor characterization by Lagrangian actinometry. *J. Environ. Eng. (ASCE)* 132: 1390–1403.

Cabaj, A., R. Sommer, and G. Hirschmann. 2007. Multiple use of water in biodosimetry of UV-disinfection plants. Paper No. WedAM3-3, presented at 2007 World Congress on Ozone and Ultraviolet Technologies, Los Angeles.

Cabaj, A., R. Sommer, and D. Schonen. 1996. Biodosimetry: Model calculations for UV water disinfection devices with regard to dose distributions. *Water Res.* 30: 1003–1009.

Dean, W. R. 1927. Note on the motion of fluid in a curved pipe. *Philos. Mag.* 4: 208–223.

Dean, W. R. 1928. The stream-line motion of fluid in a curved pipe. *Philos. Mag.* 5: 673–695.

Fenchel, T. 2001. Eppur si muove: Many water column bacteria are motile. *Aquatic Microbial Ecol.* 24: 197–201.

Forney, L. J., C. F. Goodridge, and J. A. Pierson. 2003a. Ultraviolet disinfection: Similitude in Taylor-Couette and channel flow. *Environ. Sci. Technol.* **3**7: 5015–5020.

Forney, L. J., and J. A. Pierson. 2003b. Optimum photolysis in Taylor-Couette flow. *AIChE J.* 49: 727–733.

Forney, L. J., and J. A. Pierson. 2003c. Photolytic reactors: Similitude in Taylor-Couette and channel flows. *AIChE J.* 49: 1285–1292.

Forney, L. J., J. A. Pierson, and Z. Ye. 2004. Juice irradiation with Taylor-Couette flow: UV inactivation of *Escherichia coli*. *J. Food Prot.* 67: 2410–2415.

Forney, L. J., Z. Ye and T. Koutchma. 2008. UV disinfection of *E. coli* between concentric cylinders: effects of the boundary layer and a wavy wall. *Ozone: Science & Engineering* (in press).

Fox, R. O. 2003. *Computational models for turbulent reacting flows*. Cambridge, UK: Cambridge University Press.

Fellouah, H., C. Castelain, A. Quld El Moctar and H. Peerhossaini. 2006. A criterion for detection of the onset of Dean instability in Newtonian fluids. *European Journal of Mechanics–B/Fluids*. 25:505–531.

Froment, G. F., and K. B. Bischoff. 1990. *Chemical reactor analysis and design*. New York: John Wiley & Sons.

Hanes, D. E., P. A. Orlandi, D. H. Burr, M. D. Miliotis, M. G. Robi, J. W. Bier, G. J. Jackson, M. J. Arrowood, J. J. Churey, and R. W. Worobo. 2002. Inactivation of *Cryptosporidium parvum* oocysts in fresh apple cider using ultraviolet irradiation. *Appl. Environ. Microbiol*. 68: 4168–4172.

Ikeda, E., and T. Maxworthy. 1994. Spatially forced corotating Taylor-Couette flow. *Physical Rev. E* 49: 5218–5224.

Incropera, F. P., and D. P. Dewitt. 1996. *Introduction to heat transfer*. 3rd ed. New York: John Wiley & Sons.

Kataoka, K., H. Doi, T. Hongo, and M. Futagawa. 1975. Ideal plug-flow properties of Taylor vortex flow. *J. Chem. Eng. Japan* 8: 472–476.

Koutchma, T., and B. Parisi. 2004. Biodosimetry of *Escherichia coli* UV inactivation in model juices with regard to dose distribution in annular UV reactors. *J. Food Sci.* 69: E14–E22.

Koutchma, T., S. Keller, S. Chirtel, and B. Parisi. 2004. Ultraviolet disinfection of juice products in laminar and turbulent flow reactors. *Innovative Food Sci. Emerging Technol.* 5: 179–189.

Koutchma, T., B. Parisi, and E. Patazca. 2007. Validation of a UV coiled tube reactor for fresh fruit juices. *J. Environ. Eng. Sci.* 6: 319–328.

Launder, B. E., and D. B. Spalding. 1972. *Lectures in mathematical models of turbulence*. London: Academic Press.

Levy, U., Y. Rosenberg, and M. Kertser. 2007. Calculating system-defined reduction equivalent dose and deriving analytical system-control expressions. Paper No. WedPM3a-1, presented at 2007 World Congress on Ozone and Ultraviolet Technologies, Los Angeles.

Middleman, S. 1998. *An introduction to mass and heat transfer: Principles of analysis and design*. New York: John Wiley & Sons.

Rafique, M., and S. S. Lami. 2001. Flow regimes and vortex competition in modified Taylor-Couette system: Inner rotating wavy cylinder coaxial with a smooth stationary outer cylinder. Paper presented at 12th International Couette-Taylor Workshop, Evanston, IL.

Rennecker, J., D. Gaithuma, H. Wright, P. White, K. Bircher, and M. Matuszewski. 2005. A semiempirical approach for analyzing UV disinfection system validation data. Paper presented at Disinfection 2005, Mesa, AZ.

Resende, M. M., P. G. Vieira, R. Sousa, R. L. C. Giordano, and R. C. Giordano. 2004. Estimation of mass transfer parameters in a Taylor-Couette-Poiseuille heterogeneous reactor. *Brazilian J. Chem. Eng.* 21: 175–184.

Rotz, C. A., and N. P. Suh. 1979. Vortex motion induced by V-grooved rotating cylinders and their effect on mixing performance. *J. Fluid Mech.* 101: 186–192.

Schlichting, H. 1979. *Boundary-layer theory*. 7th ed. New York: McGraw-Hill.

Severin, B. F., M. T. Suidan, and R. S. Engelbrecht. 1983. Kinetic modeling of UV disinfection of water. *Water Res.* 17: 1669–1678.

Severin, B. F., M. T. Suidan, B. E. Rittmann, and R. S. Engelbrecht. 1984. Inactivation kinetics in a flow-through UV reactor. *J. WPCF* 56: 164–169.

Shih, T.-H., W. W. Liou, A. Shabbir, Z. Yang, and J. Zhu. 1995. A new k-ε eddy-viscosity model for high Reynolds number turbulent flows: Model development and validation. *Computers Fluids* 24: 227–238.

Unluturk, S. K., H. Arastoopour, and T. Koutchma. 2004. Modeling of UV dose distribution in a thin-film UV reactor for processing of apple cider. *J. Food Eng.* 65: 125–136.

Water Environment Federation. 1996. *Wastewater disinfection manual of practice FD-10*. Alexandria, VA: WEF.

Welty, J. R., C. E. Wicks, R. E. Wilson, and G. L. Rorrer. 2001. *Fundamentals of momentum, heat and mass transfer*. 4th ed. New York: John Wiley & Sons.

Wiener, R. J., G. L. Snyder, M. P. Prange, D. Frediani, and P. R. Diaz. 1997. Periodic-doubling cascade to chaotic phase dynamics in Taylor vortex flow with hourglass geometry. *Phys. Rev. E* 55: 5489–5497.

Wright, H. 2007. MS2 biodosimetry predicts UV dose distributions. Paper No. WedAM3-2, presented at 2007 World Congress on Ozone and Ultraviolet Technology, Los Angeles.

Wright, J. R., S. S. Sumner, C. R. Hackney, M. D. Pierson, and B. W. Zoecklein. 2000. Efficacy of ultraviolet light for reducing *Escherichia coli* O157:H7 in unpasteurized apple cider. *J. Food Prot.* 63: 563–567.

Yakhot, V., and S. A. Orszag. 1986. Renormalization group analysis of turbulence: I, Basic theory. *J. Scientific Computing* 1: 1–51.

Ye, Z. 2007. UV disinfection between concentric cylinders. PhD thesis, School of Chemical & Biomolecular Engineering, Georgia Institute of Technology, Atlanta.

Ye, Z., L. J. Forney, T. Koutchma, A. Giorges, and J. A. Pierson. 2008. Optimum UV disinfection between concentric cylinders. *Ind. Eng. Chem. Res*. 47: 3444–3452.

Ye, Z., T. Koutchma, B. Parisi, J. Larkin, and L. J. Forney. 2007. Ultraviolet inactivation kinetics of *E. coli* and *Y. pseudotuberculosis* in annular reactors. *J. Food Sci.* 72: E271–E278.

9 Principles of Validation of UV-Light Pasteurization

Process validation plays a key role in the use of novel technology for the production of safe food products. This chapter identifies the structure and key components of the validation process for the use of new UV-light technology as a technique for pasteurization of fresh juices. The topics addressed include microbiological safety, quality validation, and equipment validation, along with the associated elements of cleaning, calibration of analytical parts, and validation of facilities. The general guidelines for each key component of the validation process are demonstrated by describing the steps required to validate a UV reactor for processing fresh juices as an FDA-approved UV treatment in the food industry. The chapter also provides a basic outline for the objectives and critical procedures of process and equipment validation that are relevant to those involved in commercialization of new food-processing technologies, including juice processors, technology developers, equipment manufacturers, regulatory inspectors, and extension specialists. The importance and steps of the scale-up process are also discussed in the chapter.

9.1 VALIDATION CONCEPT

According to the U.S. FDA (U.S. FDA 1987), process validation involves establishing documented evidence that provides a high degree of assurance that a specific process will consistently produce a product meeting its predetermined specifications and quality attributes. Documented evidence includes a validation protocol of the performance of the UV reactor. The validation protocol comprises the scope of the validation study as well as a detailed description of the procedures, acceptance criteria, and responsibilities. Acceptance criteria are governed by the predetermined specifications of safety and quality attributes, and they should be closely related to the risk of the process steps. For instance, as a result of disease outbreaks across North America associated with the consumption of unpasteurized juices and cider, the U.S. Food and Drug Administration (U.S. FDA) published a juice Hazard Analysis and Critical Control Point (HACCP) regulation designed to improve the safety of juice products (U.S. FDA 2000; U.S. FDA 2001). Under the rule, juice processors are required to produce juice under the HACCP system and achieve a 5-log reduction for the most resistant microorganism of public health significance that is likely to occur in the juice.

The primary objective of validation is to demonstrate product and specific process consistency over time across scales in R&D and manufacture with various raw materials and operating ranges. *Process consistency* shows that the process, when operated according to manufacturing procedures, yields a product that consistently meets specifications. This type of validation usually is not required during early

development. *Validation of operating ranges* illustrates that the process, when operated within established ranges for critical operating parameters, yields a product that meets released specifications.

Key aspects of the validation of a UV-light reactor for treatment of liquid food include:

- Documentation describing all aspects of the UV reactor that impact the relationship between delivered UV dose and microbial inactivation
- Information on the range and variation of flow rates, lamp power, and the absorptive and physicochemical properties of the food being treated
- Data relating inactivation of a challenge microorganism and/or its surrogate and the associated delivered dose
- Interpretation of validation results to ensure that the UV reactor meets performance requirements

UV systems undergoing validation must comply with this documentation. Dose delivery by the reactor during validation is assessed using biodosimetry. With biodosimetry, inactivation of a challenge microorganism is measured and related to a decimal reduction dose using the known UV dose-response of that challenge microorganism. Inactivation of the challenge microorganism is measured over a range of flow, product UV absorbance, and other physical properties and lamp power to challenge the UV reactor's dose-monitoring system under conditions expected during normal operation of the reactor at the food plant.

9.2 VALIDATION AT DIFFERENT PHASES OF PROCESS DEVELOPMENT—SCALE-UP PROCESS

A critical component of process validation is the selection and qualification of scale-up models. Three important aspects of the scale-up models—design, performance, and quality—must be considered during qualification before process validation experiments are begun. *Design* refers to the use of scientifically valid principles in specifying conditions for the scale-up process. For example, all the materials that are used for the equipment must meet the U.S. FDA Food Equipment Contact Surface Requirements. *Performance* of the various scale-up models must be comparable and the differences among the models have to be quantified. For UV reactors, the characteristics of the UV-light source and flow pattern need to be considered as critical in the scale-up process. The models must have sufficient sensitivity to detect changes when input variables are manipulated. Finally, the *quality* aspect calls for identical quality among the various scale-up models where any differences among the models must be quantified.

Four phases of validation activity are common during the scale-up process of new technology. R&D of a process goes through the four phases of benchtop development, pilot model, prototype skid, to the commercial system (Table 9.1). The probability of success has to be evaluated step by step during the whole validation process.

Benchtop development in the laboratory includes the development of the principal process scheme, the definition and validation of process operating parameters,

TABLE 9.1
Activity on Different Phases of Scale-Up Process

	Process Validation				
Phase	**Microbial**	**Quality**	**Equipment**	**Analytical**	**Cleaning**
Benchtop	X	X	…	…	…
Pilot	X	X	X	X	…
Prototype	X	X	X	X	X
Commercial	X	X	X	X	X

the inactivation kinetics studies, the establishment of the processing parameters for required log reduction on the pertinent pathogen, and the determination of shelf-life and packaging requirements. At the end of this phase, a process has to be defined for the production of a high-quality product by the benchtop model.

The *pilot model* is an important step during the scale-up of a production process. It requires formal qualification of the equipment and the appropriate calibration of instruments. Process validation usually concentrates on the scalability and reproducibility of the process. If necessary, process modifications should be made to optimize the production process for full-scale manufacturing. Product derived from pilot and prototype production processes should possess high quality attributes and be safe (hazard free).

On-site validation is preferred in the juice industry. Equipment that will be used for *commercial-scale* production has to be qualified according to U.S. FDA good manufacturing practices (GMPs) and current industrial standards, and appropriate calibration of the instrument is required. Process validation should demonstrate that the product produced by the commercial unit would be comparable to that produced by the pilot/prototype models, and that the commercial unit can be operated within the predetermined process parameters and specifications.

The first criterion is to measure and document the performance of the commercial unit at established processing parameters: X [gpm], Y [s, processing time], and Z [UV dose]. The production efficiency must be calculated based on the time for production, clean-in-place (CIP) sanitation, and inspection. The second criterion is to meet the required inactivation at 95% confidence levels. Variances associated with measurements made during validation are quantified at the 90% confidence level. The third criterion is to demonstrate a consistent performance over four consecutive weeks of 24 hr/day, 5 days/week operation.

In addition, a well-designed cleaning program and analytical methods established for in-process control have to be fully validated. The juice processors should follow 3-A sanitary standards and 3-A accepted practices (3-A Sanitary Standards, Inc., McLean, VA) or Canadian dairy standards for their equipment. Equipment manufacturers, fabricators, users, and sanitarians universally accept 3-A criteria. The 3-A SSI organization formulates standards and practices for the sanitary design, fabrication, installation, and cleanability of dairy and food equipment or systems used to

handle, process, and package consumable products where a high degree of sanitation is required. Individual standards are now available in downloadable electronic format at http://www.3-a.org/.

9.3 KEY COMPONENTS OF VALIDATION PROCEDURES

The key components for the validation procedures of any new technology include validation of microbiological safety, product quality, equipment and calibration, facility, cleaning, and analytical elements, as shown in Figure 9.1. Each element has its own objectives and procedures.

Process validation can be accomplished by microbiological and/or physical methods and includes evaluation of product quality. *Physical validation* means that the critical process parameters must be measured within the processing range. For instance, the least UV dose delivered to the product must be determined.

9.3.1 Microbiological Validation

9.3.1.1 Pertinent Pathogen Selection

In any process validation study, the target pathogen of concern must be identified. According to the juice HACCP regulation (21CFR120), this microorganism is called the "pertinent pathogen." There is guidance in the Juice HACCP Alliance's standardized training curriculum and FDA's Hazards and Controls Guide to aid in this process. Once the pertinent pathogen(s) are identified, a thorough search of the literature or discussions with experts will identify gaps in knowledge with respect to the level of treatment to yield the required 5-log inactivation of the microorganism using any particular processing technology. At this stage, various laboratory studies may be designed and performed to generate new data to close the gaps in knowledge.

In challenge studies such as this, a "cocktail" of at least three strains of the pertinent pathogen would be selected, based on previous association with the product or process in question (e.g., outbreak strains associated with a particular product). Use of a cocktail in this way gives assurance that the strain most resistant to the challenge would be the one that survives to be evaluated, and hence would present the most conservative picture, at least experimentally, of the efficacy of the process. Clearly, for any particular process, there may be more-resistant strains yet to be discovered in the environment. There may even be more-resistant spoilage (i.e., not safety related) organisms that have to be considered as a final process is established. The use of target pathogen strains in studies such as these is a conventional approach that, in a properly designed and executed study, will meet the need to demonstrate the efficacy of the process through inactivation of a target level of the pertinent pathogen according to the requirements of the juice HACCP regulation.

Good experimental design will consider the number of replicate studies needed to provide data that can be analyzed for statistical validity, the number of variables to consider in such a design (i.e., the number of multiple treatment parameters), and the choice of adequate controls. Based on the most appropriate design, the ability to effectively provide a statistical evaluation of data, e.g., to determine statistical

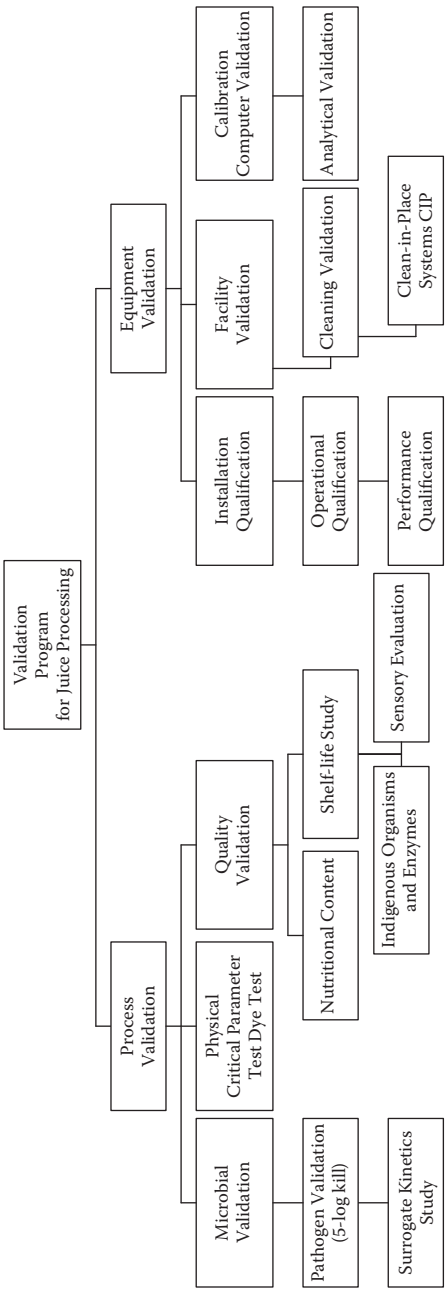

FIGURE 9.1 Chart of validation procedures of new technologies for juices. (From Koutchma et al. 2005. With permission.)

significance of results with respect to first-order or linear inactivation, is determined. This relates to integrated lethal processes applied to apple juice and the cumulative reductions that are part of the stepwise interventions allowed in the juice HACCP rule applied to whole citrus fruits.

9.3.1.2 Microbiological Methods

One important consideration regarding the choice and application of challenge strains is the need to "adapt" them to their most resistant level. Obviously, in the wild or in the manufacturing environment, the would-be microorganisms of concern most likely would not exist in ideal conditions. Very often they survive, but they may be "stressed" and very close to death under adverse conditions such as low environmental pH or near-starvation conditions. So it is important to "stress-adapt" the strains used in inoculation studies under conditions that simulate as much as possible the conditions imposed in the future challenge. Prior culture, for example, in nutrient-limiting (starvation) conditions or other nonoptimal growth conditions such as low pH, high or low temperatures, reduced a_W, or others, either alone or in combination with other adverse pretreatments, is often done. The exact inoculation method is critical. Of course, to the best of available knowledge, this should effectively resemble the most likely route of contamination or ingress of the pathogen into the product. This is most important with respect to surface inoculation of fresh fruit before pressing or extraction of the juice. This particular consideration is presently an area of considerable research activity, although some information regarding optimization of the inoculation process is currently available.

9.3.1.3 Inoculum Levels

Generally, the extremes of contamination levels are explored (i.e., high versus low inoculation levels). Although generally artificial with respect to the "normal" levels seen on fruit or in juice processing operations, the use of the former (e.g., $>10^6$/mL or g) can be applied under appropriate treatment conditions to give a measurable level of survivors that facilitates comparison of the effects of different process variables.

Since high bacterial concentration levels can influence absorbance of the sample solution, the appropriate maximum initial inoculation level for the inactivation studies needs to be determined. The absorbance coefficient needs to be measured, and the rates of inactivation at various bacterial inoculation levels need to be compared. It was found that initial inoculation levels of colony-forming units (CFU) up to 10^7 CFU/mL had no effect on the absorbance of the sample solution. However, the absorption coefficient of the sample tended to increase when the initial count was higher than 10^8.

The lower inoculum levels, while reflective of more "typical" anticipated levels found in the process, will provide lower levels of survivors under equivalent processing conditions. In these instances, specialized techniques (e.g., evaluation of large volumes of product combined with most probable number (MPN) or other sensitive techniques) must be used to enumerate survivors. A comparison of studies performed with high and low levels of inoculum will determine if uncontrolled process effects produce key differences in predicted levels of inactivation. For routine enumeration of survivors, it is traditional to recover survivors on both selective and nonselective

media. The difference in numbers counted between the two media will give a measure of the number of sublethally injured microorganisms surviving the process. The total count from the nonselective medium will provide the basis to evaluate process performance criteria.

9.3.2 Model Systems

Usually, inactivation models can be developed in media designed to simulate the natural product as closely as possible, since the use of such media is very often much easier to work with than the natural product. The models are then validated in the actual food, usually using a smaller number of experimental variables, which is another benefit that the simulated modeling route often permits. With juices, which are generally easy and inexpensive products to work with, the need to develop models in simulated product media may not be a paramount consideration; i.e., inoculated studies very often are performed using the product in question directly. Finally, it is usually customary to monitor the viability and potential for growth of surviving microorganisms throughout the anticipated shelf life of the product. It is conceivable, but highly unlikely given the low pH of most juice products, that sublethally injured microorganisms may repair to full viability and that fully viable survivors may actually increase in numbers with time.

However, in order to reduce the effects of variation of fresh juice properties, juice simulants can be used in the initial stages of validation of UV-light processes. Koutchma et al. (2007) used model caramel solutions to simulate absorption properties of exotic tropical juices and to study the effect of absorbance on UV inactivation, as the cost of shipping the required volumes of juices from Hawaii was very high. The base for the model system was a 0.025 M sodium malate buffer at pH 3.5, and sucrose was added to 10°Brix. Caramel (Pepsi Cola Co., NY) was added in the range of concentration from 0.2% to 2.0% to approximate tropical juices. The calibration plot of absorption coefficient vs. caramel concentration is given in Figure 9.2.

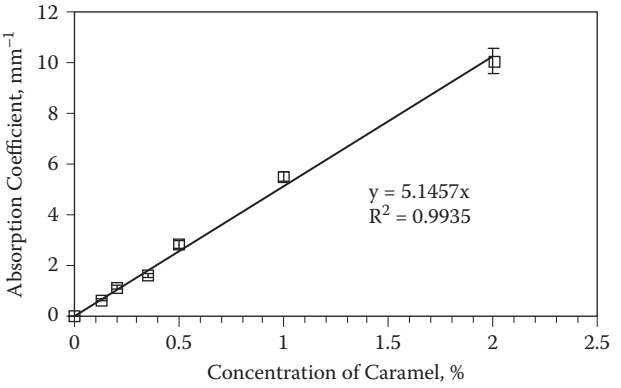

FIGURE 9.2 Absorption coefficients of model caramel solutions at 254 nm. (From Koutchma et al. 2007. With permission.)

TABLE 9.2
Model Juice Solutions for UV Inactivation Studies

Juice	Absorption Coefficient (cm^{-1})	Caramel Juice Model (%)
Lilikoi	12	0.2
Apple	26	0.5
Orange	48	1.0
Carrot	53	1.1
Guava	46	1.0
Pineapple	73	2.0

According to the data in Table 9.2, absorbance of a 0.2% model caramel solution was comparable with the absorbance of a clarified lilikoi juice. Absorbance of a 0.5% model caramel solution matched that of unfiltered apple juice. Model caramel solutions of between 1% to 1.1% were similar in absorbance to commercial orange, guava, and carrot juices, and 2.0% model caramel solution was used to mimic the absorbance of pineapple juice.

9.3.3 Microbial Validation in Scale-Up Process

Once processing parameters to inactivate the target level of pertinent pathogen have been established in laboratory studies, the process is usually scaled-up through pilot plant development and then through prototype equipment/process development, and commercial roll-out and commissioning of the system. Obviously, unless working in a controlled environment (e.g., a Biosafety level, or BSL, 2/3 pilot-scale containment facility), pathogens should not be used in an open processing environment where there is potential for contamination of equipment and facilities. In these situations nonpathogenic "surrogate" organisms or challenge microorganisms are selected for use in further studies in lieu of the pertinent pathogen. Obviously, such challenge strains must have resistance traits that have been predetermined in controlled studies to match as closely as possible those of the pertinent pathogen. Moreover, many will have a marker (e.g., natural antibiotic resistance) that will facilitate their identification as process survivors separate from any number of similar strains found as indigenous flora in the natural product. Other characteristics desirable of chosen challenge strains have been described by the Institute of Food Technologists (2000). Very importantly, it is highly desirable that the chosen surrogate (challenge) strain, if it survives the process, should not itself become a product spoilage organism, and will not persist as a hard-to-remove nuisance organism in the processing facility or the process waste stream. Suggested levels of microbial validation at four phases of process scale-up are summarized in Table 9.3.

9.3.4 Generation of UV Dose Requirements for Test Microorganism

The UV dose requirements to achieve various levels of pathogen inactivation are determined using data from laboratory-scale studies in which suspensions of the

TABLE 9.3
Levels of Microbial and Quality Validation at Different Phases of Scale-Up

	Pathogen	Surrogate	Spoilage	Quality
Concept/Lab	X	…	…	X
Pilot	X	…	…	X
Prototype	X	X	X	X
Commercial	X	X	X	…

Source: Koutchma et al. (2005).

pathogens are exposed to UV light under controlled conditions. The UV light is generated from a UV source that will be used in prototype and commercial units. Detailed descriptions of some batch or continuous-flow systems and principles that should be used in their design and testing can be found in the literature (Kuo et al. 2003; Koutchma and Parisi 2004; Ye at al. 2007). By measuring exposure time, UV intensity at the surface of the test product sample, product depth, and UV absorbance of the sample food, the UV dose delivered to the test food can be accurately determined. By plotting pathogen inactivation achieved versus the UV dose delivered, as shown in Figure 9.3, UV dose-response curves are developed and used to identify dose requirements.

9.3.5 Dose Delivery and Microbial Inactivation by UV Reactors

Dose delivery by a UV reactor is a function of the hydraulic flow through the reactor, or residence time distribution (RTD), and the UV fluence rate field generated by the lamps.

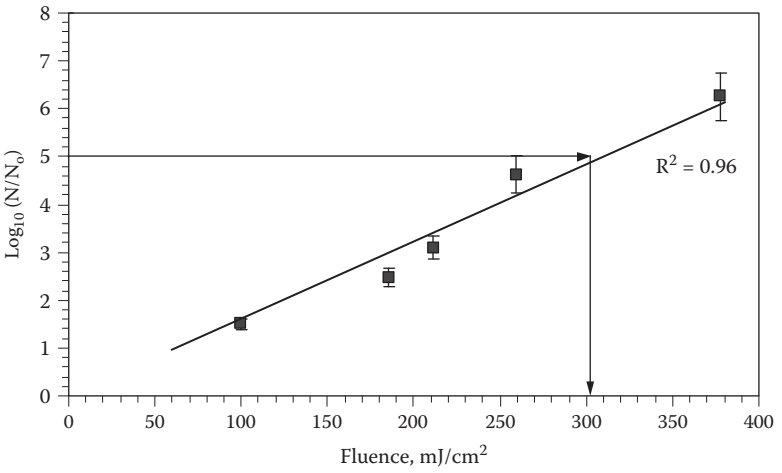

FIGURE 9.3 UV dose-response relationship.

Microorganisms passing through a UV reactor may travel close to the lamps and be exposed to relatively high UV fluence, or they may travel along the reactor walls or between lamps and be exposed to lower UV fluences. Microorganisms may pass through the reactor relatively quickly or be caught in dead zones. As such, microorganisms leaving a UV reactor receive different UV doses, and dose delivery by the reactor is thus best described using a dose distribution.

Bioassay or biodosimetry is a practical method to measure the dose delivery by a UV reactor. A bioassay involves passing a challenge microorganism through the UV reactor, measuring the average log inactivation achieved, and relating that inactivation to a single decimal reduction dose value based on the known UV dose-response of that microorganism. This measured dose value is termed the reduction equivalent dose (RED). The measured RED will have a value lying between the minimum and average in the dose distribution. The inactivation of a pathogen cannot be precisely determined using bioassay data unless the reactor's dose distribution is known or the challenge microorganism has the same UV dose-response curve as the pathogen. The range of inactivation is bounded by the inactivation expected with an ideal and worst-case reactor (Figure 9.4).

With an ideal reactor delivering a single dose, the bioassay is a measure of the dose delivered to all microorganisms. The log reduction of any given microorganism

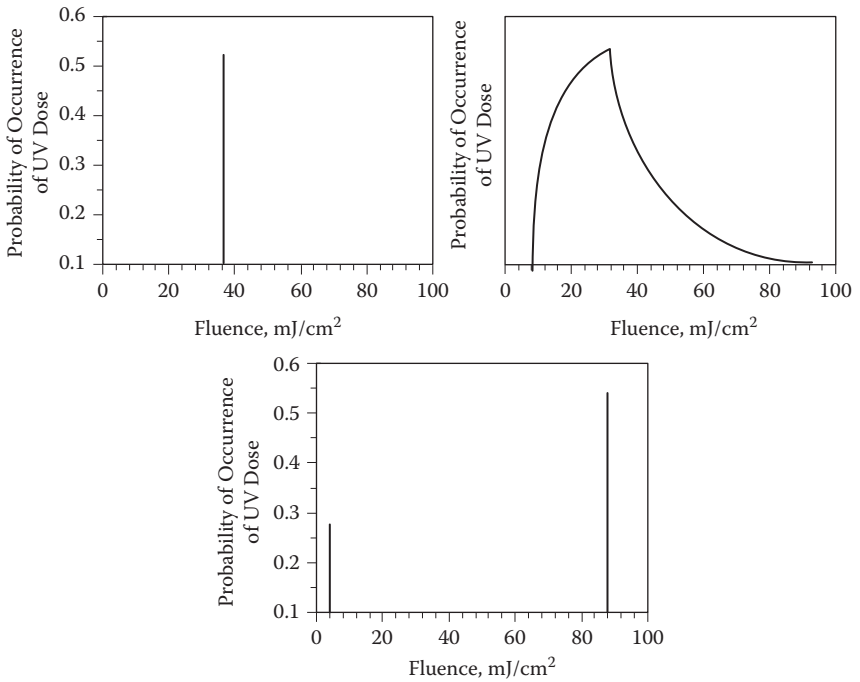

FIGURE 9.4 Performance of UV reactor bounded between the ideal and worst-case reactors.

can be calculated using equation (9.1).

$$\log(S_p) = \frac{\log(S_c) \times D_c}{D_p} = \frac{\text{RED}}{D_p} \tag{9.1}$$

where

$\log(S_p)$ = log reduction of the pathogen
$\log(S_c)$ = log reduction observed with the challenge microorganism
D_p = UV sensitivity of the pathogen expressed as the dose required per log reduction or decimal reduction dose (DRD)
D_c = UV sensitivity of the challenge microorganisms expressed as the dose required per log reduction or decimal reduction dose (DRD)
RED = dose equivalent of the challenge microorganism calculated

Equation (9.1) can be used to calculate a specific log reduction in terms of spoilage microorganisms such as yeasts and molds that can be achieved by the designed process. Ideally, the UV reactor's performance should be challenged using a surrogate microorganism whose UV sensitivity matches that of the target pathogen as defined by regulations.

9.3.6 Hydraulic Considerations

Flow dynamics must be evaluated for all tested liquid products. Velocity (v) is calculated as ($v = Q/A$), where Q is a volumetric flow rate and A is the cross-sectional area of the tube. Reynolds numbers (Re) are then calculated as ($\text{Re} = vd\rho/\mu$), where d is characteristic dimension, ρ is density of fluid, and μ is dynamic viscosity. The Reynolds number must be calculated for the range of flow rates and for each product if viscosity differs. For instance, as reported by Koutchma et al. (2007), the Re numbers were calculated for all tested groups of tropical juices whose viscosities varied in a wide range. It was found that the magnitude of Re for pineapple and orange juice was less than 2000, indicating that at the selected flow rates, the hydraulic regime was laminar. However, for juices characterized as Newtonian liquids (lilikoi, guava, apple, and watermelon) at the flow range from 3.5 to 7 gpm used in the experiments, the flow dynamics could be characterized as a turbulent flow with $\text{Re} > 2000$. Figure 9.5 illustrates the areas of laminar and turbulent flow behavior for juices with varied viscosity.

Another important feature of coil-geometry reactors concerns the development of secondary flow in the tube. It has been demonstrated by Dean (1927) that a secondary flow field accompanies laminar flow of fluid through a coiled tube. The curvature radius that exists between the inner and outer boundary layer causes the phenomenon called the Dean effect. The Dean number, De, is the unique similarity parameter governing fluid motion in such a flow configuration. The Dean number is calculated as $\text{De} = \text{Re}\sqrt{D/D_c}$, where D is the tube diameter and D_c is the coil diameter. Secondary flow eddies are highly promoted within the range of D/D_c of 0.03–0.10. The magnitude of Dean numbers from 65 to 132 for pineapple and orange juices, and from 573 to 1145 for apple and lilikoi, and the ratio of $D/D_c = 0.046$ indicated that

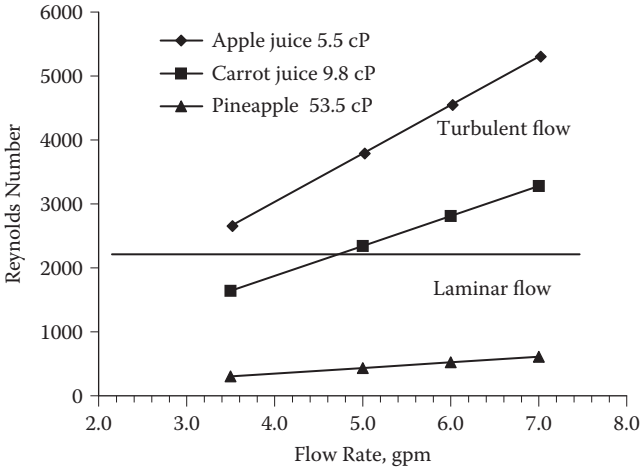

FIGURE 9.5 Flow regimes of Newtonian and non-Newtonian juices in the Salcor UV unit. (From Koutchma et al. 2007. With permission.)

secondary flows developed in juices provide additional mixing in the case of both laminar and turbulent flow regimes. Dean flow and another example of secondary flow occurring in Taylor–Couette reactors are also discussed in Chapter 8.

A stimulus-response technique can be used for experimental determination of RTD in the UV reactor. Koutchma et al. (2007) used a 50% caramel solution as a stimulus, or tracer, in the validation studies of the coiled-tube UV reactor. The special loop in the inlet tube of the reactor containing an inlet port and two-way valves was built up in order to inject the tracer into the reactor tube. A 50% caramel model solution was injected into the center of the loop assembly when the valves were closed. When flow achieved a steady-state condition, the valves were opened and the caramel solution mixed with the water stream in the tube. The change in the caramel concentration was measured with time at the output. The distribution of caramel concentration or $c(t)$ curve reflected the RTD in the UV reactor (Figure 9.6). The normalized curve $E(t)$, which represents the fraction of fluid leaving the system at each time or RTD function (Figure 9.6b), can be constructed from the $c(t)$ curve using the summation technique (equation 9.2)

$$E(t) = \frac{c(t)}{\int_0^t c(t)dt} \tag{9.2}$$

The mean residence time of the flow $\bar{t}$ is calculated from the function $E(t)$ and time t using the summation technique (equation 9.3)

$$\bar{t} = \int_0^t tE(t)dt \tag{9.3}$$

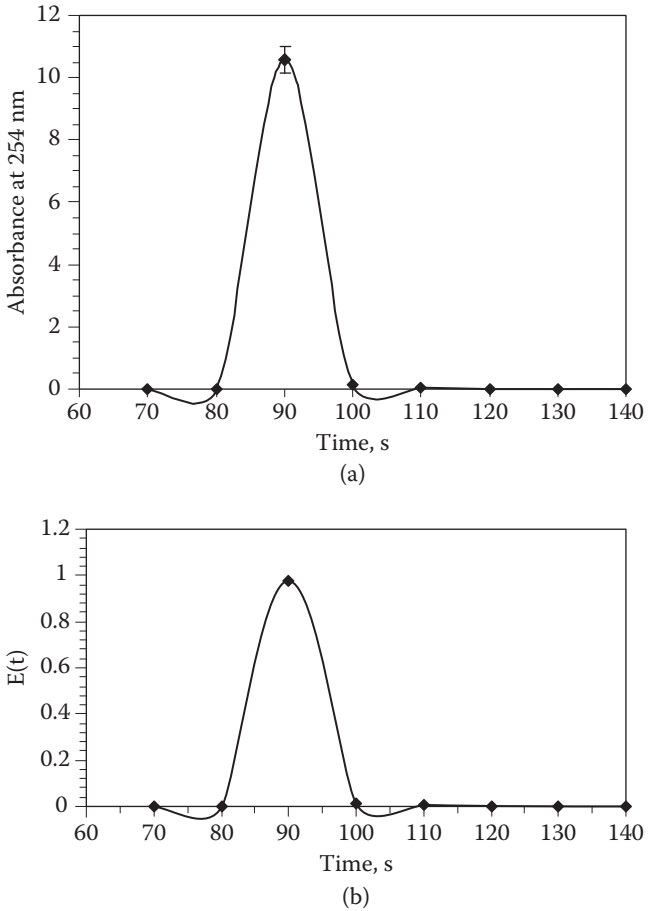

FIGURE 9.6 (a) Absorbance of a caramel solution at the exit, $c(t)$ function. (b) RTD $E(t)$ function of caramel solution after pumping through the coiled UV reactor. (From Koutchma et al. 2007. With permission.)

The theoretical residence time ($t = V/Q$) can be also calculated from the fill volume of the reactor V and volumetric flow rate Q. The ratio of $\overline{t}/t$ indicates whether full use is made of the reactor volume. If the value is <1, it indicates that the effective volume is much less than the actual volume of the reactor (Downey et al. 1998).

Because there was a distribution of UV fluence (UV dose) in the model system, consequently, there was a distribution of doses that any injected bacteria were exposed to. The arithmetic mean of the decimal UV dose distribution was calculated in all fractional volumes of liquid elements by dividing the volume-averaged UV fluence by the logarithm of bacterial inactivation in fractional volumes and comparing with the volume-averaged decimal reduction dose (DRD). The value of the volume-averaged decimal reduction dose (DRD) was determined from the volume-averaged

UV fluence absorbed by a 0.5% model caramel solution divided by the mean of the $\log_{10}$ inactivation of *E. coli* obtained from the same microbial tracer experiments (average of three replicates). In 0.5% model caramel solution, the decimal UV dose that the bacteria received varied from 12.9 to 17.5 mJ/cm^2, with a DRD of 13.8 mJ/cm^2. A rather broad overall range of decimal UV dose was observed in 0.1% model caramel solution, ranging from 91.1 to 12.0 mJ/cm^2 with a DRD value of 32.2 mJ/cm^2, indicating poor fluid mixing and low UV-light penetration. However, the variations of UV dose could be decreased at the higher flow rates due to the additional mixing. In absorptive liquids, portions of the solution that have a radial position further from the UV source and a minimum reactor path length due to insufficient mixing would receive a minimal UV dose and thus represent the insufficiently irradiated portions. That means that UV process calculations based on the maximum decimal dose will deliver a safe process.

9.3.7 UV Lamp Output

The effect of the lamps' output power on inactivation performance of the UV reactor must be tested in case of possible lamp failure. In the coiled-tube UV reactor, the UV lamps and reflectors are placed both inside and outside the coiled tube, which can be seen from the cross section of the reactor shown in Figure 9.7. The tubing is housed in a stainless steel enclosure. The enclosure has 12 UV lamps mounted around the inside diameter of the tubing and 12 UV lamps mounted around the

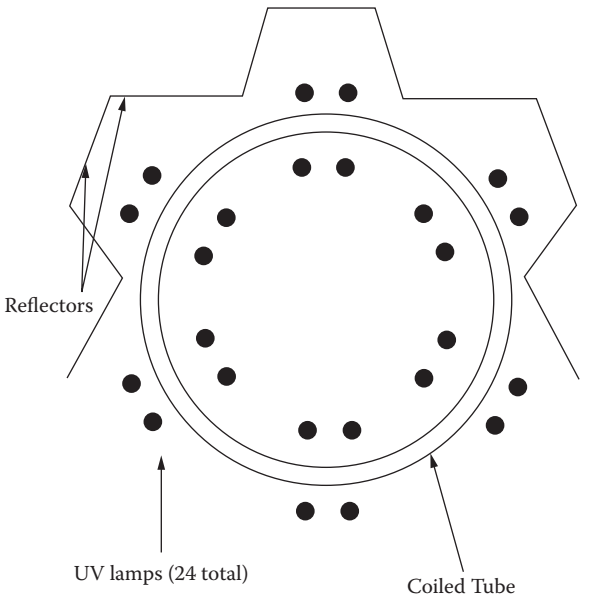

FIGURE 9.7 Schematic diagram and cross section of coiled UV reactor.

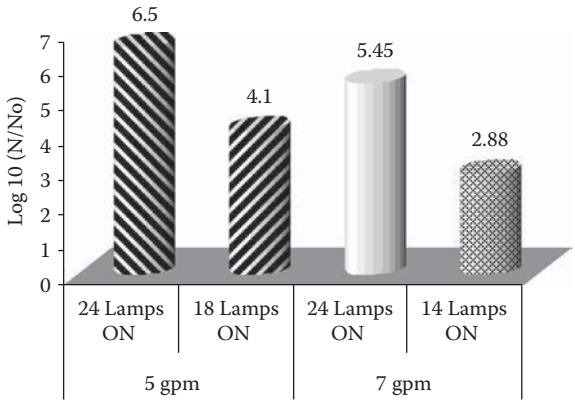

FIGURE 9.8 Effect of output power (24, 18, and 14 UV lamps "on") and flow rate on inactivation of *E. coli* K12 in 0.2% model caramel solution. (From Koutchma et al. 2007. With permission.)

outside diameter. Each pair of lamps has a parabolic reflector to enhance the UV intensity at the tube surface.

The effects of the UV output power was studied using 0.2% model caramel solution when six UV lamps located outside and inside the coil were "off," but the UV lamps were not removed from the reactor, so the geometry of the flow pattern was not affected. It can be seen from Figure 9.8 that approximately a 4-$\log_{10}$ reduction of *E. coli* was found in this case. When 10 UV lamps were "off" at a flow rate of 7 gpm, even two passes through the reactor were not sufficient to achieve a 5-$\log_{10}$ inactivation.

9.3.8 Chemical and Physical Safety

During process validation, the production of toxic by-products, for example, and the use of unapproved additives and inadvertent introduction of potential allergens must be avoided by proper process design and evaluation. As there is uncertainty about the production of potentially toxic substances such as free radicals or new compounds by the new process, it is essential to confirm the absence of these unwanted by-products as part of the validation program. Likewise, introduction of physical hazards such as contamination of product by introduction of foreign objects during processing must be prevented. Examples include introduction of glass fragments from bottles as a result of cracking through inappropriate temperature cycling, or the inclusion of metal shards from lids as a result of exceeding tolerance in filling operations. Again, properly designed and executed process-validation studies will effectively consider the likelihood of such occurrences and lead to measures for their prevention, elimination, or reduction to acceptable levels.

9.3.9 Quality Validation

Besides ensuring the absence of pathogenic microorganisms, inactivating indigenous microorganisms and enzymes that are responsible for spoilage and quality

deterioration is another critical goal in food processing. For example, the quality of juice is defined by the indigenous microbial populations, indigenous enzyme activities, physical attributes (pH, °Brix, color, viscosity, and cloud), chemical attributes (sugar profile, acid profile, minerals, and titratable acidity), nutritional content (ascorbic acid, folic acid, and beta-carotene), and organoleptic properties (aroma profile, flavor profile, and texture).

Shelf-life studies are commonly performed to assess the consistency of the treated juice quality throughout its targeted shelf life. During the shelf-life study, samples are periodically tested for indigenous microorganisms, indigenous enzymes, and the evaluation of other quality attributes. In addition, factors such as types of packaging materials (glass, PET, HDPE, paper carton, and pouch), storage temperature (abused and normal cold-chain-distribution refrigeration temperature), and transportation should also be included in the study. Standard plate-counting techniques are generally used to estimate the total number of viable cells in the treated juice. The yeast and mold populations and lactic acid bacteria counts are determined, as these are microorganisms that are important in juice spoilage.

Pectins are a group of colloidal carbohydrates naturally present in fruit juices. They act as natural stabilizers and give the fruit juice a consistency that is generally referred to as "body" by the fruit juice industry. Pectinesterase is the indigenous enzyme that degrades the pectin colloid and decreases the cloud stability of the juice. The titration method using a pH stat system or the colorimetric method developed by Rouse and Atkins (1955) can be used to measure the activity of pectinesterase in citrus juice. Standard tests such as the official methods from AOAC or the Department of Citrus, Florida, must be employed to analyze the physical, chemical, and nutritional attributes of the juice. Sensory evaluation by expert and consumer panels is used to document changes in sensory profile and consumer acceptance. Analysis of the aroma profile by gas chromatography is employed to supplement the organoleptic information collected from sensory evaluation.

Prior to commercialization, open dialogue among regulatory agencies, food processors, and technology developers must be initiated to address the labeling and grading issues for new categories of foods. Last but not least, variations due to the properties of raw materials (e.g., beginning/end-of-season fruit, varieties of fruit, amount of pulp) should also be analyzed and established.

9.3.10 Equipment Validation

The key elements of equipment validation include initial inspection, installation and operational qualification, performance qualification, and commissioning. Prior to the installation of the equipment**,** a description of the equipment, checklist of the software, and accurate supporting documentation must be provided. The manufacturer of UV reactors must provide information on the proper installation and operation of the reactor. This includes performance characteristics such as nominal pressure, flow rates, head loss, pressure rating of the sleeve, UV-intensity sensor and monitoring window used, assembly and installation instructions, electrical requirements, and operation and maintenance manuals. During installation and operational qualification, sensors need to be calibrated

against standards (e.g., National Institute of Standards, NIST) and control loops have to be tuned.

9.3.11 UV-Intensity Sensors

UV reactors are equipped with at least one on-line UV-intensity sensor that measures the UV intensity at some point within the UV reactor. Measurements made by the on-line UV-intensity sensors are used to ensure that the reactor is delivering a UV dose that meets the regulatory requirement. For example, the CiderSure 1500 UV reactor is equipped with two sensors. Based on sensor readings at two points within the flow path, an "auto" setting can adjust flow using an algorithm based on the transmittance of the UV light through the treated fluid.

The UV-intensity sensor should detect germicidal UV radiation and produce a standardized output signal (4–20 mA) proportional to the UV intensity incident on the sensor. UV-intensity sensors must be calibrated to an absolute intensity standard and have a suitable measurement range, angular response, wavelength response, linearity, and stability for monitoring and controlling UV dose delivery by the UV reactor. An ideal UV-intensity sensor has the following characteristics:

1. Responds linearly as the UV intensity within the reactor changes over the measurement range of the UV-intensity sensor
2. Responds independent of product temperature
3. Is stable over time
4. Has a fixed acceptance angle
5. Responds only to germicidal UV ranges

The manufacturer of the UV reactor must provide documentation on the UV-intensity sensor and monitoring window that is separate from the UV sensor. A separate monitoring window provides reproducible measurements of UV intensity by the on-line and reference UV-intensity sensor.

The measurement uncertainty of a UV sensor is due to the uncertainty in UV-intensity sensor calibration, linearity over the working range, and stability over time and temperature. In addition, UV-sensor degradation will occur due to exposure to UV light. The reference UV-intensity sensor should not be exposed to UV light longer than it takes to make the measurement. Alarms, interlocks, equipment communication protocols, utility cleaning, and consumable requirement should also be verified at the installation stage. Analytical methods for in-process controls and release testing have to be fully validated according to GMPs and current standards.

The *performance* of the system must be validated over the operating range of processing conditions for each specific product. The following approaches can be used to estimate performance qualification for the "worst-case scenario approach" or the "process-steps approach." Inoculated pack studies can be run for the selection of the appropriate microorganism. The worst-case approach is attractive, since the validation can be accomplished in only a few experiments if they are successful. For efficient analysis, the sampling plan and statistics must be used along with optimal experimental design. The process-steps approach requires the establishment of the

processing steps prior to the validation of the system performance. The set-point values of process variables should be determined from process development studies. In practice, the exact control of a variable at the set point is seldom achieved, and the variable is typically maintained within a specified range of values, or normal operating range (NOR). The magnitude of the NOR can be ascertained during a production trial and set at two or three standard deviations. To cover occasional excursions outside the NOR, it is desirable to establish a wider range known as the maximum operating range (MOR) within which product quality attributes have been shown to be acceptable. Any performance outside the MOR is at the edge of failure.

The objective of process validation is not to determine the edge of failure but to demonstrate acceptable process operation. In juice validation studies, processing parameters must be varied to get (+)/(–) vs. microbial inactivation. To ensure that all system components are functioning, they need to be challenged on process deviations as well. Another key element of the system performance evaluation is to demonstrate the uniformity of the process. Supporting documentation should describe all aspects of the system that impact performance parameters.

At the *commissioning phase*, an equipment validation System Acceptance Test should be run. First, normal CIP and sanitization steps on the system should be performed, then environmental air samples are collected and swabs in the critical areas should be taken. The product is passed through the system using the designed process. The samples are collected according to a statistical sampling plan at the beginning, middle, and end of the production for microbiological counting. It is highly desirable to repeat the test three times and to collect samples from each trial. In order to accept the system for production, the defective rate must be less than 1%.

9.3.12 Cleaning Validation

Cleaning strategies adopted in multiuse facilities play a major part in the prevention of cross-contamination of food products. Government-approved chemicals must be used for cleaning and sanitation. Cleaning different pieces of equipment has to be evaluated on a case-by-case basis and justified according to performance qualification studies. Cleaning routines must be defined, validated, and set. The three main parameters that are used for the evaluation of equipment cleanliness are analysis of final rinse water samples at the end of cleaning, analysis of surface swab samples, and visual inspection. The buildup of biofilms has to be considered in cleaning validation. In order to pass an equipment sanitation test, the validation test must be performed three times. In the case of fresh juices, juice is inoculated with mold spores and circulated through the system for 30 min. Then the system is drained, dried, and cleaned with normal CIP and sanitation cycles. After cleaning, the machine is disassembled and swabbed in preselected sites. Microbiological testing is then performed on the swabbed samples using standard procedures. Dye tests can also be used for determining cleaning effectiveness.

Automated clean-in-place (CIP) can be used and validated against established cleaning regimes. The juice processors can consider two options for CIP validation. The first method includes circulation of buttermilk in the system overnight, drying of the system for 4 hours, running of normal CIP cycles at proper conditions, adding

erythrosin dye during the final rinse, and at the end disassembling the machine for the diagnosis of dye residue. The second option involves circulating riboflavin in the system, drying the system for 4 hours, running the normal CIP cycles, and disassembling the machine for the diagnosis of fluorescent residue. The European Hygienic Equipment Design Group (EHEDG) may have other methods for CIP validation to assist industry in complying with European hygienic machinery directives.

9.3.13 Testing Facility Requirements

Manufacturing facilities require key operational strategies to be in place. Facility safety and worker safety do not need to be part of food safety validation, but could be considered as a part of the overall plant validation program. Some of the basic requirements for a manufacturing facility include well-designed facilities and equipment; appropriate personnel; safe product, raw materials, and waste flows; and training programs for personnel with regard to cleaning. A cleaning validation program specifically for facilities and equipment is required for all GMP-regulated food facilities.

9.4 CONCLUSIONS

Not all of the issues of validation of UV technology for juices and other liquid foods were discussed in this chapter, but a step forward was made in understanding the needs and important steps for the future. For example, little is currently known about the impact of UV lamp aging, the degree of fouling, and choice of cleaning technique. It is important to recognize that each process will be unique, and the presented information can be considered only as recommendations. Each unique process suggests that validation studies are process and product specific. It is the responsibility of the juice or food processors to demonstrate the ability of their process to achieve the specific (required) log reduction of the pertinent microorganism in each portion of the product produced. In addition, process validation should lead consistently to high-quality products with significant commercial benefits for the manufacturer and reduced risk of process failures.

REFERENCES

Dean, W. R. 1927. *Phil. Mag. J. Science*, 4: 208–223.

Downey, D., D. Giles, and M. Delwiche. 1998. Finite element analysis of particle and liquid flow through an ultraviolet reactor. *Comput. Electron. Agric.* 21: 81–105.

Institute of Food Technologists. 2000. Kinetics of microbial inactivation for alternative food processing technologies. *J. Food Sci. Suppl*. http://vm.cfsan.fda.gov/~comm/ift-pref.html.

Koutchma, T., H. Grace, and P. J. Slade. 2005. Roadmap to validation of processing technologies for juices. *Food Prot. Trends* 2: 114–119.

Koutchma, T., and B. Parisi. 2004. Biodosimetry of *E. coli* UV inactivation in model juices with regard to dose and RTD distribution in annular UV reactor. *J. Food Sci*. 69: 14–22.

Koutchma, T., B. Parisi, and E. Patazca. 2007. Validation of UV coiled tube reactor for fresh fruit juices. *J. Environ. Sci. Eng*. 6: 319–328.

Kuo, J., C. Chen, and M. Nellor. 2003. Standardized collimated beam testing protocol for water, wastewater disinfection. *J. Env. Eng*. 8: 773–779.

Rouse, A. H., and C. D. Atkins. 1955. Pectinesterase and pectin in commercial orange juice as determined by methods used at the Citrus Experiment Station. *Univ. of Florida Agricultural Experiment Station Bulletin*. 570: 1–19.

U.S. FDA. 1987. Center for Drugs and Biologics and Center for Devices and Radiological Health. Guideline on General Principles of Process Validation. May 1987.

U.S. FDA. 2000. 21 CFR Part 179. Irradiation in the production, processing and handling of food. *Federal Register* 65: 71056–71058.

U.S. FDA. 2001. Hazard analysis and critical control point (HACCP): Procedures for the safe and sanitary processing and importing of juice. Final rule. *Federal Register* 66 (13). U.S. Food and Drug Administration, Washington, DC.

Ye, Z., T. Koutchma, B. Parisi, J. Larkin, and L. Forney. 2007. Ultraviolet inactivation kinetics of *E. coli* and *Y. pseudotuberculosis* in annular reactors. *J. Food Sci*. 72: E271–E278.

10 Pulsed-Light Treatment *Principles and Applications*

Carmen I. Moraru and Aaron R. Uesugi

10.1 DESCRIPTION OF PULSED-LIGHT TREATMENT

10.1.1 General Aspects of Pulsed-Light Treatment

Pulsed-light technology has emerged in recent years as a feasible alternative to thermal treatment for killing pathogenic and spoilage microorganisms in foods. Pulsed light has been proven effective in reducing the microbial populations on the surfaces of foods, food-contact materials, and medical devices (Dunn et al. 1995, 1997; MacGregor et al. 1998; USFDA/CFSAN 2000; Ozen and Floros 2001; McDonald et al. 2002). In the United States, the FDA has already approved the use of pulsed light for the decontamination of food or food-contact surfaces, provided that the treatment uses a xenon lamp with emission of wavelengths between 200 and 1000 nm, with a pulse width not exceeding 2 ms, and the cumulative level of the treatment not exceeding 12 J/cm^2 (Food and Drug Administration 1996).

Pulsed-light treatment consists of applying a series of very short, high-power pulses of broad-spectrum light in order to kill bacteria, yeasts, molds, and viruses. The key element of a pulsed-light unit is a flash lamp filled with an inert gas, such as xenon. A high-voltage, high-current electrical pulse is applied to the inert gas in the lamp, and the strong collisions between electrons and gas molecules cause excitation of the latter, which then emit an intense, very short light pulse. Pulsed-light treatment consists of applying a variable number of light pulses to the treated material, each pulse having a duration between 1 μs to 0.1 s. Typically, the light source is a xenon lamp, which emits broadband radiation that ranges from ultraviolet (UV) to near-infrared (NIR) (Fig. 10.1).

The pulsed-light treatment dose is quantified by its "fluence," which represents the total radiant energy of all wavelengths passing from all directions through an infinitesimally small sphere of cross-sectional area dA, divided by dA. It represents the light exposure of a substrate and is typically expressed in units of J/cm^2 (Bolton 2000). Although the number of pulses and pulse characteristics (width, fluence per pulse) are very useful, ideally the total fluence should also be reported to allow direct comparisons of different treatments, regardless of the experimental setup. A complete guide of radiometric quantities and units that apply to pulsed-light treatment is given in Table 10.1.

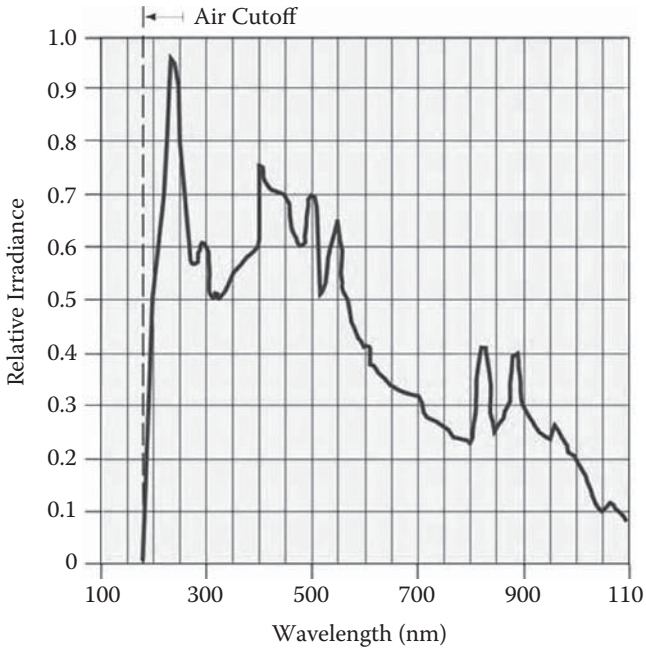

FIGURE 10.1 Spectral range of xenon pulsed lamps. (Courtesy Xenon Corp. 2005.)

10.1.2 Pulsed-Light Equipment

10.1.2.1 Flash Lamps: Design and Pulsed-Light Generation

The key element of any pulsed-light system is the flash lamp, whose main structural elements are the envelope, the seals, and the electrodes.

10.1.2.1.1 Lamp Envelope

The envelope represents the jacket that surrounds the electrodes and physically contains the filling gas. The material used to build the envelope must be transparent to the radiation emitted by the lamp, must be impervious to air and the filling gas, withstand high temperatures and thermal shocks, and also be mechanically strong (Perkin Elmer Optoelectronics 2008). Based on these considerations, the material used for envelopes of flash lamps is transparent fused quartz, which meets all of these requirements and can be easily processed in various shapes and sizes. Quartz tubing with 1-mm wall thickness is the most frequently specified for flash lamps. Thicker quartz (2.5–3 mm) is not desirable, as high thermal gradients can form in the quartz envelope during lamp operation, which can lead to the formation of stress cracks (Perkin Elmer Optoelectronics 2008).

Three different types of quartz can be used in flash lamp construction: clear fused quartz, doped quartz, and synthetic quartz. The main difference between these materials is their transmittance in the UV region of the emitted light spectrum. Clear fused quartz is used for the building of most flash lamps. It can operate up to

TABLE 10.1
Radiometric Quantities and Units

Quantity	Symbol	Unit	Definition
Radiant energy	Q	joule (J)	Total energy in a radiation field or the total energy delivered by such a radiation field
Radiant power, radiant flux	P	watt (W)	Rate at which radiant energy is transferred from one region to another by the radiation field; $P = dQ/dt$, where t is time
Radiant exposure	H	$J \times m^{-2}$	Energy per unit area received by a real or imaginary surface element; $H = dQ/dA$, where A is area
Radiant energy density	w	$J \times m^{-3}$	Radiant energy per unit volume of the radiation field; $w = dQ/dV$, where V is volume
Radiant energy fluence rate, spherical irradiance	φ	$W \times m^{-2}$	At a given point in space, the radiant power incident on a small sphere divided by the cross-sectional area of that sphere
Radiant excitance	M	$W \times m^{-2}$	The flux per unit area leaving the surface of a source of radiation; $M = dP/dA$, where dA is the area of the source element
Irradiance	E	$W \times m^{-2}$	Flux per unit area received by a real or imaginary surface element; $E = dP/dA$, where dA is the area of the surface element
Radiant intensity	I	$W \times sr^{-1}$	Flux per unit solid angle emitted by a source in a given direction; $I = dP/d\Omega$, where Ω is the solid angle
Radiance	L	$W \times m^{-2} \times sr^{-1}$	Flux per unit projected area per unit solid angle leaving a source or reference surface; $L = d^2P/dA_{proj}d\Omega$; projected area is given by $dA_{proj} = dA\cos\theta$, where θ is the angle between the outward surface normal of the area element dA and the direction of observation

Source: Moseley and Sliney (1997).

temperatures of about 600°C, and its UV cutoff is at about 220 nm. Another important property of quartz is the softening point, which is defined as the temperature at which glass deforms under its own weight. The softening point of fused quartz is generally reported in the range 1500°C to 1670°C, the different values resulting from differing conditions of measurement.

Malitson (1965) offers detailed information about the optical properties of fused quartz. The main problem associated with clear fused quartz is solarization, a phenomenon that leads to the appearance of a purplish discoloration with time. This occurs mostly during high-energy operation of flash lamps, and can result in a broadband reduction of light transmittance.

The UV transmission properties of quartz can be modified by the incorporation of a dopant such as cerium or titanium oxides. Doped quartz still has a clear

appearance, but its UV transmission is modified. The UV cutoff of fused quartz doped with cerium oxide is about 380 nm. Fused quartz doped with titanium oxide is available in different grades, each having a different UV cutoff profile. It has similar characteristics to cerium-doped quartz, but is greatly affected by solarization.

Synthetic quartz is a high-purity, man-made quartz that allows transmission down to 160 nm. It has excellent optical properties and does not exhibit solarization. It is the most expensive of all the quartz materials and the least readily available.

10.1.2.1.2 Seals

Flash lamps must be hermetic, which means that the quartz envelope and the electrode assembly must have a gas-tight seal. The seals commonly used in flash lamp construction belong to three categories: ribbon seals, solder seals, and rod seals. When *ribbon seals* are used, the quartz is bonded directly to a thin strip of molybdenum foil to prevent cracking of the seal that could be caused by the unequal expansion and contraction between quartz and molybdenum. This seal is considered to be very robust and strong. A significant advantage of the ribbon seal is that it minimizes the dead volume of the lamps. Ribbon seals are extensively employed in the manufacture of high-pressure xenon compact arc lamps, but cannot be used for pulsed flash lamps. *Solder seals,* also known as end-cap seals, allow lamps to have very small dead volumes. These seals have higher mechanical strength than the other seals and arguably the highest peak current capability of all the seal types. They have however a low service temperature, typically 100°C, which is a disadvantage both during the operation of the lamp and during its manufacture. *Rod seals,* also known as graded or bright seals, allow physical bonding of quartz to metal by means of a transition glass. These seals withstand high temperature and high vacuum and are extensively used in flash lamps for solid-state laser pumping. Solder seals do not have a long shelf life, while ribbon and rod seals have a virtually unlimited shelf life (Perkin Elmer Optoelectronics 2008).

10.1.2.1.3 Electrodes

The metallic electrodes protrude into each end of the envelope and are connected to a capacitor that is charged to a high voltage. They are only responsible for delivering the electric current into the gas. The electrodes are very important, as they limit the lifetime of the lamp (Flesch and Neiger 2005). The most important component of a flash lamp is the cathode, since it can determine the lifetime of the lamp, while the anode is of minor importance in flash-lamp lifetime. The materials used for making electrodes for flash lamps are selected carefully. At the anode, the main concern is power loading due to electron bombardment from the arc, while the cathode must be able to supply an adequate amount of electrons without damage to its surface, a phenomenon called *sputtering* (Perkin Elmer Optoelectronics 2008).

Cathodes are commonly manufactured using the dispenser method. Pulsed xenon flash lamps generally use cathodes with a flattened radius. An important design consideration for pulsed flash lamps is to prevent the formation of hot spots that could result in sputtering of the cathode material during operation, which can strip off large amounts of material, drastically reducing the lifetime of the lamp. Generally, little heating occurs at the electrodes during low-average-power operation, while at peak power, heating effects can be very high. Anodes are made from either pure

tungsten or lanthanated tungsten. For anodes, the most important consideration is that they have sufficient mass or surface area to satisfy the expected power level (Perkin Elmer Optoelectronics 2008).

10.1.2.1.4 Lamp Cooling

When operated at low input energies and/or low flash rates, flash lamps do not generally require special cooling, as heat from the quartz envelope and electrodes is lost by natural radiation. At high power and flash rates, additional cooling of the lamp is required to ensure reliable operation and long lamp lifetime. Typical cooling solutions include convection, forced air, or liquid. Most commercial pulsed lasers, for instance, require liquid cooling. For liquid cooling, deionized water is generally the liquid of choice. When forced air is used to cool flash lamps, the air should be filtered, and the air blast must reach the ends of the lamp as well as the seals and connectors (Perkin Elmer Optoelectronics, 2008).

Envelope materials have a maximum power loading, expressed in units of W/cm^2, which depends both on the material and the type of cooling system. According to Perkin Elmer Optoelectronics (2008), convection cooling is sufficient for power loading that does not exceed 15 W/cm^2, forced-air cooling is recommended for loads of 15–30 W/cm^2, while liquid cooling must be used at loads of 30–320 W/cm^2. The approximate upper limits for various envelope materials and wall thicknesses are shown in Table 10.2.

10.1.2.1.5 Filling Gas

Xenon and krypton are typically chosen as the filling gases for pulsed flash lamps. Xenon is more commonly used because of its higher conversion efficiency; xenon is also the gas of choice for most microbial-inactivation applications. A critical parameter of the filling gas is the fill pressure. For pulsed lamps, the highest practical pressure is about 3000 torr. Above this, problems with lamp triggering may be encountered. Fill pressure can be altered to modify the electrical parameters of the lamp. Lower pressures allow for lower trigger voltages, but at pressures below 100 torr, cathode sputtering can become significant. Typical values for gas fill pressures used in flash and arc lamps are: 450 torr for general-purpose xenon flash lamps, 700

TABLE 10.2
Maximum Power Loading for Various Lamp Envelopes

Envelope Material	Envelope Wall Thickness (mm)	Max. Power Loading (W/cm^2)
Doped quartz (UV absorbing)	1.0	160
Clear fused quartz	1.0	200
Clear fused quartz	0.5	320
Synthetic quartz	1.0	240

Source: Data adapted from Perkin Elmer Optoelectronics (2008).

torr for pulsed krypton flash lamps, and 1–3 atm for xenon compact arc flash lamps (Perkin Elmer Optoelectronics 2008).

10.1.2.1.6 Dead Volume of the Lamp

Dead volume is defined as the inactive internal area of the lamp, i.e., the internal volume from the electrode tip to the seal. Lamps are manufactured with a certain cold fill pressure, but during operation the pressure rises as current density increases. A large dead volume leads to a lower pressure during operation, while a small dead volume leads to a higher pressure during operation and a higher efficiency, as discussed later. This is why small dead volumes are desirable in the manufacture of high-average-power pulsed lamps (Perkin Elmer Optoelectronics 2008).

10.1.2.1.7 Generation of Pulsed Light

Figure 10.2 is a schematic representation of a gas-discharge flash lamp. In a few words, generation of light using xenon flash lamps can be described as follows: A flash is initiated by ionizing the xenon gas that fills the lamp envelope. A very large pulse of current is then sent through the ionized gas, which excites the electrons surrounding the xenon atoms, causing them to jump to higher energy levels. The electrons release this energy and drop back to a lower orbit by producing photons.

The pulsed operation of xenon discharge lamps is characterized by two stages. During the first stage, direct ionization of the xenon gas takes place, and plasma is formed near the anode by the electrons traveling toward it. After accumulation of a sufficient number of metastable species, a transition from direct to stepwise ionization occurs. This is accompanied by a sharp increase in the growth rate of electron density, which results in a current peak. After plasma is formed near the anode, an ionization wave propagates from the anode to the cathode, and the plasma region expands along the lamp toward the cathode. When the ionization wave arrives at the cathode, the plasma current reaches its maximum value. The further deposition of surface charges at the anode side of the dielectric leads to cessation of the discharge (Perkin Elmer Optoelectronics 2008).

During the current pulse, electron-induced chemical reactions take place. Table 10.3 lists some of the most important plasma–chemical processes that can occur in xenon (Bogdanov et al. 2004). Detailed information about the transitions that occur in atomic xenon and the corresponding energy-level diagrams have been

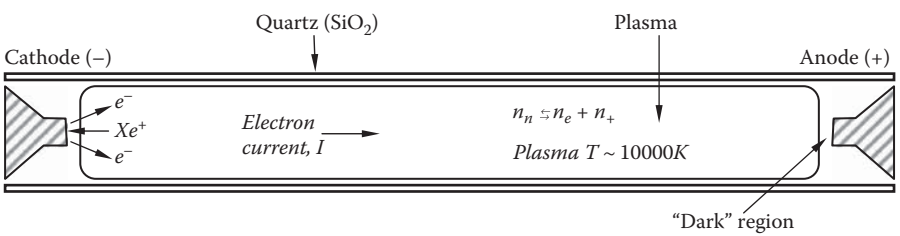

FIGURE 10.2 Schematic representation of a xenon-filled flash lamp (n_n = number of neutral atoms; n_e = number of electrons; n_+ = number of ionized xenon atoms).

TABLE 10.3
Plasma-Chemical Processes in Xenon

No.	Reaction	Comment
1	$e + Xe \rightarrow e + Xe$	Momentum transfer
2	$e + Xe \leftrightarrow e + Xe^{*}$	Xe^{*} excitation–deexcitation
3	$e + Xe \leftrightarrow e + Xe^{**}$	Xe^{**} excitation–deexcitation
4	$e + Xe \leftrightarrow e + Xe^{***}$	Xe^{***} excitation–deexcitation
5	$e + Xe \rightarrow 2e + Xe^{+}$	Direct ionization
6	$e + Xe^{*} \rightarrow 2e + Xe^{+}$	Stepwise ionization
7	$e + Xe^{**} \rightarrow 2e + Xe^{+}$	Stepwise ionization
8	$e + Xe^{***} \rightarrow 2e + Xe^{+}$	Stepwise ionization
9	$e + Xe^{**}_{2} \rightarrow 2e + Xe^{+}_{2}$	Stepwise ionization
10	$e + Xe^{**}_{2} \rightarrow 2e + Xe^{+}_{2}$	Stepwise ionization
11	$e + Xe^{*} \leftrightarrow e + Xe^{**}$	$Xe^{*} - Xe^{**}$ transitions
12	$e + Xe^{**} \leftrightarrow e + Xe^{***}$	$Xe^{**} - Xe^{***}$ transitions
13	$e + Xe^{**}_{2} \leftrightarrow e + Xe^{***}_{2}$	$Xe^{**}_{2} - XE^{***}_{2}$ transitions
14	$e + Xe^{+}_{2} \rightarrow Xe + Xe^{***}$	Dissociative recombination
15	$e + Xe^{+}_{3} \rightarrow 2Xe + Xe^{***}$	Dissociative recombination
16	$2Xe + Xe^{+} \rightarrow Xe + Xe^{+}_{2}$	Ion conversion
17	$2Xe + Xe^{+}_{2} \rightarrow Xe + Xe^{+}_{3}$	Ion conversion
18	$Xe + Xe^{+}_{3} \rightarrow 2Xe + Xe^{+}_{2}$	Thermal dissociation
19	$Xe + Xe^{***} \rightarrow Xe + Xe^{**}$	Deexcitation by atoms
20	$Xe + Xe^{**} \rightarrow Xe + Xe^{*}$	Deexcitation by atoms
21	$Xe^{**}_{2} \rightarrow Xe + Xe^{*}$	Dissociation
22	$Xe + Xe^{**}_{2} \rightarrow 2Xe + Xe^{*}$	Thermal dissociation
23	$Xe^{*}_{2} \rightarrow 2Xe$	Radiation
24	$2Xe^{*} \rightarrow Xe + Xe^{+} + e$	Penning ionization[a]
25	$2Xe^{**} \rightarrow Xe + Xe^{+} + e$	Penning ionization[a]
26	$Xe^{*} + Xe^{**} \rightarrow Xe + Xe^{+} + e$	Penning ionization[a]
27	$Xe^{*} + Xe^{*}_{2} \rightarrow 2Xe + Xe^{+} + e$	Penning ionization[a]
28	$Xe^{**} + Xe^{*}_{2} \rightarrow 2Xe + Xe^{+} + e$	Penning ionization[a]
29	$2Xe^{*}_{2} \rightarrow 2Xe + Xe^{+}_{2} + e$	Penning ionization[a]
30	$Xe^{*} + 2Xe \rightarrow Xe^{*}_{2} + Xe$	Conversion into excimers[b]

Source: Adapted from Bogdanov et al. (2004).

[a] Penning ionization: a form of chemi-ionization that involves reactions between neutral atoms and/or molecules; it occurs when the target molecule has an ionization potential lower than the internal energy of the excited-state atom or molecule.

[b] Excimer: a short-lived (lifetime on the order of nanoseconds) dimeric or heterodimeric molecule formed from two species, at least one of which is in an electronic excited state.

reported by various authors (Horiguchi et al. 1981; McCown et al. 1982; Ledru et al. 2006). Electron kinetics, collisions, and transport processes of xenon atoms in the metastable and resonance levels have been analyzed extensively by modeling and laser absorption spectroscopy (Bussiahn et al. 2007).

During lamp operation, ions travel from the anode to the cathode, while electrons travel from the cathode to the anode (Figure 10.2). Electrons have a higher mobility than ions; they have oscillation frequencies in the GHz range, while ion oscillations are in the MHz range. Since electrons have higher mobility than the positively charged Xe ions, they will be found in large concentrations near the inside surface of the quartz envelope, making this surface electronegative. The attraction by this negative charge causes ions to migrate toward this surface, which allows electron–ion recombinations to occur. This leads to the formation of a large population of neutral Xe atoms near the inner wall, which have a much lower temperature than the ionized particles, thus leading to a lower temperature at the envelope wall as compared with the central axis of the lamp. During the operation of xenon pulsed lamps, temperatures as high as 10,000 K can be reached at the center of the lamp axis. Temperature drops rapidly in the radial direction because of the formation of neutral xenon atoms described above, and it reaches about 1200 to 1500 K near the surface of the envelope. This temperature is below the softening point of quartz, which allows the lamp to maintain its integrity.

When the current pulse ends, the plasma decay stage starts. This is a slow process during which the electron temperature quickly drops down to gas temperature. Excited and ionized species generated by electron impact during the short current pulse participate in chemical reactions among heavy particles, which results in active radicals and species capable of emitting light. The concentration of ionized atoms is less than 1% and accounts for all the emitted light energy (Perkin Elmer Optoelectronics 2008).

10.1.2.1.8 Spectral Output of Xenon Flash Lamps

Xenon flash lamps emit an optical spectrum that covers a range of wavelengths that range from the UV cutoff of the envelope material (160–380 nm, depending on the type of quartz used), to the IR cutoff (around 2500 nm). The energy level at the extremes of this spectral range is quite small.

The spectral profile of the electromagnetic radiation produced by xenon flash lamps depends primarily on current density. At low current density, atomic line radiation corresponding to bound–bound energy state transitions occurs. At higher current density, continuum radiation resulting from free–bound and free–free transitions predominates. By changing the amplitude of the applied voltage and the rise time, one can modify the electron energy spectrum, which allows optimization of the spectral output.

According to lamp manufacturers, the conversion of electrical power into radiated optical power for xenon flash lamps is approximately 50%. Generally, the efficiency improves with increasing current density and gas fill pressure (Perkin Elmer Optoelectronics, 2008; Xenon Corp. 2005).

10.1.2.1.9 Triggering of Flash Lamps

Flash lamps exhibit extremely high resistance in their nonconducting state. Therefore, in order for the lamp to conduct, a spark streamer is formed between the electrodes. This is achieved by the application of a high-voltage trigger pulse. The trigger process occurs in several stages. Initially, a spark streamer is formed between one or

both electrodes and the inside wall of the lamp. This spark then propagates along the inside wall of the lamp to the other electrode. The lamp will conduct when the voltage drop between the electrodes formed by the trigger streamer is lower than the capacitor voltage. The process depends on the presence of a reference plane on or near the lamp's surface, which can be represented by a nickel wire wrapped around the lamp (external trigger) (Perkin Elmer Optoelectronics 2008).

10.1.2.1.10 Lifetime Estimation of Flash Lamps

For commercial applications of pulsed-light technology, the lifetime of the flash lamp is a critical economic consideration. The main reasons for lamp failure are electrode erosion, gas fill contamination, glass-to-metal seal failure, and envelope aging (Ghasemi et al. 2003). It is generally agreed, however, that the lifetime depends primarily on the operating conditions of the lamp. In a high-energy regime, the method typically used to estimate flash lamp lifetime is based on the operating energy (E_o) as a percentage of lamp single-pulse explosion energy (E_x). The following calculations are recommended (Perkin Elmer Optoelectronics 2008):

$$\text{Life} = (E_o/E_x)^{-8.5} \text{ (pulses)} \tag{10.1}$$

where

E_o = operating energy (J)
E_x = explosion energy for the lamp (J)

For a given lamp that operates under a known set of operating conditions, E_x can be calculated based on the single-pulse explosion constant (K_e) and the pulse width (T)

$$E_x = K_e\,(T)^{0.5} \text{ (J)} \tag{10.2}$$

where

K_e = lamp single-pulse explosion constant
T = 1/3 pulse width (s)

The explosion constant K_e is available either from data sheets or it can be estimated as

$$K_e = Q \times l \times d \tag{10.3}$$

where

Q = quartz tubing coefficient (typical values for Q: 24,600 for tubing of 8-mm diameter, 21,000 for diameters of 10–12 mm, and 20,000 for 13-mm diameter)
l = arc length (cm)
d = bore diameter (cm)

Table 10.4 gives examples of lifetime estimations for lamps operated under high-energy conditions.

In a low-energy regime, at $E_o/E_x < 0.197\%$ or lifetimes greater than 10^6 pulses, lifetime is determined by electrode effects and erosion of the quartz envelope. Accurate estimations of lamp lifetime are difficult and are often based on testing under the known operating conditions (Perkin Elmer Optoelectronics 2008).

TABLE 10.4
Lifetime Estimations for Lamps Operated under High Energy

Lamp Life (pulses)	E_0/E_x (%)
10^2	0.58
10^3	0.44
10^4	0.33
10^5	0.26
10^6	0.197

Source: Adapted from Perkin Elmer Optoelectronics (2008).

10.1.2.2 Design of Pulsed-Light Systems

Pulsed-light equipment may vary from manufacturer to manufacturer, but pulsed-light systems consist of several common components (Figure 10.3). A high-voltage power supply (1) provides electrical power to the storage capacitor (2), which stores electrical energy for the flash lamp (4). The pulse-forming network (3) determines the pulse shape and spectrum characteristics. A trigger signal (5) initiates discharging of the electrical energy to the flash lamp. The xenon gas discharge flash lamp then converts 45% to 50% of the input electrical energy to pulsed radiant energy (Xenon Corp. 2005). The flash lamps used to generate the broad-spectrum light are available in a variety of shapes, such as linear or circular, which allows them to uniformly treat substrates of different shapes and sizes. The lamps are typically enclosed in a lamp housing, which usually includes a quartz panel to protect the lamp. Pulsed-light units

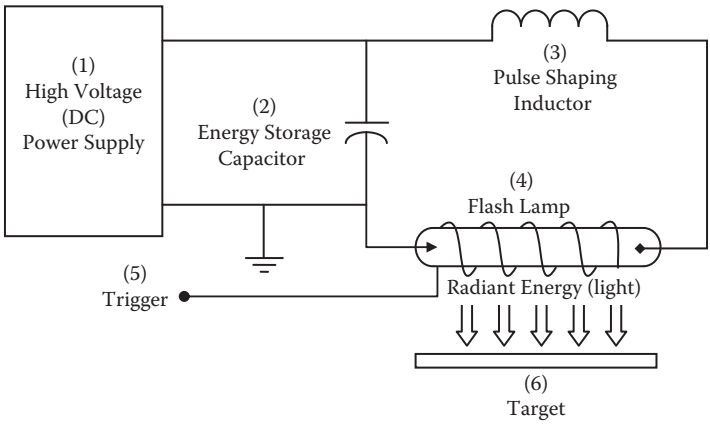

FIGURE 10.3 Functional diagram of a high-intensity pulsed-light system. (Adapted from Xenon Corp. 2005. With permission.)

also have a cooling system to reduce any heat buildup in the treatment area. Reflectors are often incorporated in the treatment chamber to redirect light to the sample.

Pulsed-light systems can be designed for batch or continuous treatments. In batch configurations, such as those developed by Xenon Corp. (Waltham, MA), samples are placed within a chamber with lamps located along the walls of the chambers. The simplest designs include a single lamp located above the sample and an adjustable tray to hold the samples. More complex designs may incorporate up to eight lamps within a chamber along with a quartz stand to hold the sample and allow a 360° exposure and treatment. The French company Claranor has developed a wide range of pulsed-light equipment for the food-processing and pharmaceutical industries, including static equipment for laboratories and technical centers (Tecum system); treatment units for unwrapped or packaged products on flat conveyor belts (Gratia system), on spool-bars (Plena system), or in tunnels (Dominus system); as well as in-line treatment units for caps, preformed packaging, films, or jars (Ventris system). In these systems, a flash lamp or a number of flash lamps are located above a moving conveyor belt. Other components of the equipment include a hood to contain the lamp, reflectors to redirect light to the sample, and a quartz panel that has the role of protecting both the flash lamp and the workers from being exposed to the treatment. The same company also built a reactor for in-line treatment of clear liquids and water (Maria system), in which liquids are moved through a cylindrical reactor that is equipped with a lamp that is placed in the center of the reactor. The system can be integrated into the manufacturing line as a single treatment reactor, or several reactors could be coupled in series to increase the pulsed-light exposure and thus treatment efficiency.

In addition to equipment for use in food processing, pulsed-light equipment has been developed for other applications. Pulsed-light equipment could be installed within the heating, ventilating, and air-conditioning air ducts to reduce airborne microorganisms. These air-purification systems use pulsed light to reduce and destroy biological agents that might be introduced in a bioterrorism attack upon a facility through the building's ventilation system. Other facilities that may require cleaned air include hospital operating and isolation rooms, clean rooms in manufacturing or pharmaceutical production, or for general air-quality improvement. Pulsed-light treatment units have also been developed for the treatment of medical prosthetics and implants (such as the Mulieribus system from Claranor). Xenon Corp. is commercializing equipment for pulsed UV curing processes such as optical disc coatings, wood coatings, plastic bonding, or medical electrodes.

For all existing pulsed-light systems, a control system is used to automate the process and control the rate of pulsing. Optical sensors can be installed to record the output of the entire unit. The newest generation of SteriPulse-XL® systems sold by Xenon Corp. are equipped with a LiteMark light monitor. This system contains a photoelectric detector module installed in the treatment chamber that senses the light intensity from each flash, which is scattered sideways in the lamp housing window, and relates it to the side-scattered intensity produced by a new lamp. This enables the operator to monitor in real time the performance of a lamp system and to make decisions regarding the lamp replacements prior to the lamp output reaching a predetermined minimal level.

10.1.3 Alternative Technologies to Generate Pulsed Light

10.1.3.1 Static-Discharge Lamps

Static-discharge lamps are produced using a technology patented by Phoenix Science & Technology, Inc. (Schaefer 2004). According to the manufacturer, these lamps are capable of higher UV efficiency and higher energy per pulse than the xenon flash lamps and can operate at stress levels well above the explosion limit of the xenon flash lamps described previously (Schaefer 2004; Grapperhaus and Schaefer 2006; Schaefer et al. 2007). Static-discharge lamps consist of two electrodes connected to a substrate such as a fused silica tube. The electrodes and tube are encased in a larger quartz tube filled with xenon gas. A fast high-voltage pulse generates plasma around the center tube. The xenon gas between the substrate and outer tube is not involved in the generation of the plasma, which occurs along the surface of the substrate. In a comparison of various UV-producing lamps, Schaefer et al. (2007) noted that the UV efficiency of a flash lamp was about 9.0%, with efficiency increasing as the pulse width decreased. The surface-discharge lamp UV efficiency varied between 12.2% and 17.2% based on various operating conditions. Spectral maps of the flash lamp and static-discharge lamp showed similar output shapes.

Static-discharge lamps, like flash lamps, have been used to treat water and have also been used to remove lead paint (Grapperhaus and Schaefer 2006). To remove lead paint, surfaces were treated with pulsed light generated by static-discharge lamps followed by application of rotating brushes to help remove residual paint products. The lamp and brushes were encased in a system that included a vacuum and filter system to capture the paint products.

10.1.3.2 Sparkers

Sparker technology has also been developed by Phoenix Science & Technology, Inc. Sparkers are pulsed electrical discharges that can be generated in water or in the air. A pulsed discharge is generated between two electrodes, which generate plasma that emits light and a sonic-wave sound pulse. High voltage is needed to efficiently generate the pulse, and the resulting light and sound are influenced by the air in the environment. A wire is placed between the electrodes to initiate the discharge in water. The wire is vaporized during the plasma generation and is replaced between pulses by a wire feed. A wire control can also be used in air applications to eliminate the environmental influence. A parabolic reflector can be used to give directional focus to the generated light and sound.

Underwater sparker systems can be used to prevent organic growth, such as zebra mussels, on underwater surfaces. Additionally, sparkers can be used for nonlethal crowd control and for security of ports, harbors, and ships. Antimicrobial applications of this technology have not yet been reported. All information about this technology is available from the manufacturer, and to date there is very little data available.

10.1.3.3 Other Pulsed-Light Technologies

Although the technologies described above are the only ones commercially available at the moment, there are reports in the literature referring to incremental

improvements of existing pulsed-light technology. For instance, Ghasemi et al. (2003) reported the use of a solid-state Marx generator for pulsing a UV lamp in microbial-inactivation applications. One of the advantages of this technology is that it features a low-voltage power supply for charging and does not require a pulse transformer for the generation of the high voltage. Voltage multiplication is achieved by charging several capacitors in parallel, through charging resistors, and then discharging them in series. The limitation of Marx generators is that they tend to have a limited lifetime.

Researchers at the University of Missouri–Columbia have developed pulsed-UV photon sources capable of enhanced UV inactivation of microorganisms. Pulsed xenon flash lamps have been optimized to produce a high UV photon yield in the lethal 180 to 320 nm range.

10.2 INACTIVATION OF MICROORGANISMS BY PULSED-LIGHT TREATMENT

10.2.1 Mechanisms of Inactivation

Despite the increasing efforts of scientists to fully elucidate the mechanisms of microbial inactivation by pulsed light, the specific mechanisms by which pulsed light causes cellular inactivation are not yet fully understood. Since a significant portion of the pulsed-light spectrum includes UV light, it is generally accepted that UV plays an important role in the inactivation of microorganisms by pulsed light. The antimicrobial effects of UV light on bacteria are attributed to the absorption of radiation by conjugated carbon–carbon double bonds in proteins and nucleic acids and subsequent DNA structural changes (Tyrrell 1973; Rosenstein and Ducore 1983; Farkas 1997; Bintsis et al. 2000; Jay 2000), as well as abnormal ion flow, increased cell membrane permeability, and depolarization of the cell membrane (Wuytack et al. 2003).

The UV portion of the electromagnetic spectrum includes long-wave UV-A (320–400 nm), medium-wave UV-B (280–320 nm), and short-wave UV-C (200–280 nm) (Bintsis et al. 2000). While the overall lethal effects of UV light on microorganisms are known, the effect of each of these ranges is not fully elucidated. UV-C, the shortest wavelength range that also contains the wavelength 254 nm, is often credited as carrying most of the bactericidal effects (Jay 2000). The 250 to 260 nm range is capable of destroying most microorganisms due to the alteration of the cellular DNA via pyrimidine dimer formation (Bintsis et al. 2000). The longer-wavelength UV portions (UV-A and UV-B) are believed to impart lethal effects as a result of membrane damage and the formation of peroxides (Bintsis et al. 2000). Davies-Colley et al. (1997) reported an approximate 2-log reduction of enterococci in wastewater ponds after exposure to wavelengths (λ) above 340 nm, and an approximate 1-log reduction after exposure to $\lambda > 400$ nm. No significant reduction was seen for *Escherichia coli*, however, unless the light range included light of $\lambda < 340$ nm (Davies-Colley et al. 1997). Another study that examined the lethality of the UV-A and UV-B range was performed by Fargues et al. (1997). Using *Paecilomyces fumosoroseus* conidia at initial inoculums of 10^6–10^7 colony-forming units (CFU)/cm^2, they observed more

than a 3-log reduction in spores after applying a dose of up to 800 J/m^2 of UV-B light at an irradiance of 1.98 W/m^2. A similar reduction in the viability of spores was observed after exposure to up to 600 kJ/m^2 of UV-A light at an irradiance of 45 W/m^2 (Fargues et al. 1997). The report by Bintsis et al. (2000) also suggested that UV-A has a low lethal effect on microorganisms, cautioning that UV-A treatment is efficient only when paired with other means of destruction.

A study on the effect of different laser sources on the DNA of lymphoblasts revealed that DNA damage occurred after exposure to the wavelength range 750–1064 nm, with a peak at around 760 nm (Mohanty et al. 2002). The extent of DNA damage depended significantly on the wavelength, with the level of DNA damage inflicted by λ of 750–780 nm being twice as large as that inflicted by λ of 800–1064 nm. The authors also reported that higher-energy doses were required to inflict the same amount of DNA damage at higher wavelengths compared with the lower wavelengths.

To identify which region of the broad spectrum of light is responsible for cell death in pulsed-light treatment, Woodling and Moraru (2007) treated stainless steel coupons inoculated with ca. 10^8 CFU/mL of *Listeria innocua* with pulsed light in different spectral ranges: full spectrum (λ = 180–1100 nm), ultraviolet (UV), visible (VIS), and near-infrared (NIR). The authors reported that at a fluence of about 6 J/cm^2, the full-spectrum treatment resulted in a 4.08-log reduction of *L. innocua* on a stainless steel surface with a mill finish. The removal of $\lambda < 200$ nm diminished the reduction to only 1.64 log, while the treatments performed utilizing a UV-blocking filter, with elimination of $\lambda < 400$ nm, did not have any lethal or sublethal effects on *L. innocua*. These data demonstrated that the portions of the pulsed-light spectrum responsible for bacterial inactivation were located in the range $\lambda < 300$ nm (the UV-B and UV-C spectral ranges), with some death taking place as a result of exposure in the range of λ = 300–400 nm (UV-A). No lethal effects were observed for $\lambda > 400$ nm (VIS and NIR).

Several studies also indicated observable injurious effects on microbial cells following exposure to pulsed light. Wekhof (2003) reported the physical destruction of *Aspergillus niger* spores as a result of structural collapse, while Takeshita et al. (2003) reported enlarged vacuoles in *Saccharomyces cerevisiae* yeast cells as a result of pulsed-light treatment. These effects were attributed to intracellular heating that occurred as a result of the pulsed-light exposure. Takeshita et al. (2003) reported that continuous UV treatment resulted in a larger amount of DNA damage in *S. cerevisiae* than pulsed light, but pulsed light induced a greater level of structural damage (i.e., greatly expanded vacuoles and compromised cell membranes). In another study, Rowan et al. (2000) found only minimal heat damage after treating a variety of food-related microorganisms with two light sources of slightly different emission spectra: high UV content vs. low UV content. Similarly, Woodling and Moraru (2005) observed a temperature increase of 3ºC when treating rough stainless steel surfaces with nine pulses of light, corresponding to a fluence of about 10 J/cm^2. However, since the thermal effects were observed on the substrate level, they do not necessarily offer a prediction of what might be happening at a cellular level. Further investigations are therefore required to elucidate whether or not heating plays any role in microbial inactivation by pulsed-light treatment.

10.2.2 Factors that Influence the Efficiency of Pulsed-Light Treatment

The microbicidal efficiency of pulsed-light treatment depends on a range of factors, including pulsed-light dose and spectral distribution, type of microorganism, interaction between light and the microorganism, as well as the interaction between light and the treated substrate. The effect of pulsed-light dose on microbial inactivation is typically shown in the form of survivor curves, such as the one in Figure 10.4. As observed in Figure 10.4, the survivor curves show a rapid decrease in survivors with increasing fluence, after which the curve reaches a plateau, depending on the microorganism treated. For the treatment of *L. innocua*, the plateau is reached at fluence levels of about 6 J/cm^2 (Woodling and Moraru 2005; Uesugi et al. 2007). The effect of spectral characteristics on the outcome of the pulsed-light treatment has been discussed in previous sections.

The interaction between light and the treated substrate and between light and the microbial cells is of paramount importance for the efficiency of pulsed-light treatment. When reaching a medium, incident light can be reflected, refracted, scattered, or absorbed in varying degrees, depending on the composition and structure of the substrate and the wavelength of the light. In the case of biological tissues, absorption and scattering are the most relevant types of light–substrate interaction (Cheong et al. 1990). When an incident beam of light enters a material, refraction occurs due to the difference in the optical density between the substrate and the surrounding air. Refraction is particularly relevant for transparent and colored materials. When reaching an opaque material, light can be reflected. For smooth surfaces, the incident light bounces on the surface and comes out at the same angle as the incident beam, with the same spectral distribution of energy, which is termed *specular reflection*. For rough surfaces, light travels through the outer layers of the material, where the incident light is partly absorbed, a phenomenon called *diffuse reflection*. Since absorption is uneven at different wavelengths, the spectral distribution of the incident light

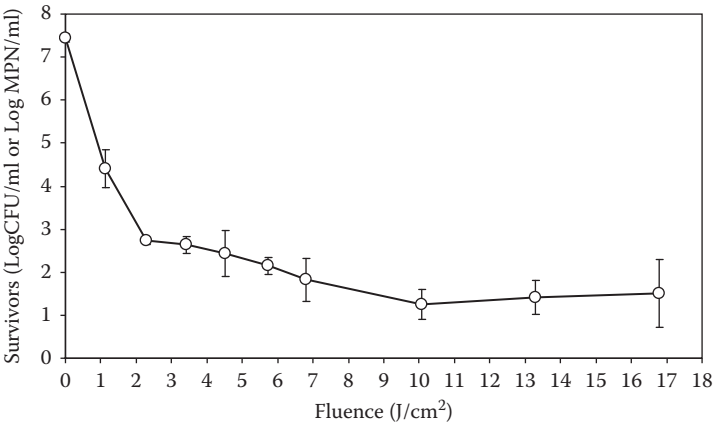

FIGURE 10.4 Survivor curve for the inactivation of *L. innocua* in Butterfield's phosphate buffer.

changes, and the diffused light comes out in all directions (Durán and Calvo 2002). This effect is very important for pulsed-light treatment, as reflection by the substrate could significantly decrease the efficiency of the treatment.

For translucent materials, a portion of the incident light interacts with the internal structure and undergoes multiple internal reflections and redirections, resulting in scattering. As a result of structural heterogeneity and relative refractive index mismatch at the boundaries between cell membranes or intracellular structures, light propagation in biologic tissues thicker than several tens of micrometers is typically characterized by multiple scattering events (Flock et al. 1987; Hollis 2002). Tissues that manifest strong scattering cause light to be backscattered toward the tissue surface and increase the delivered irradiance, resulting in a higher fluence rate and greater penetration (Xie et al. 2003). This can be particularly relevant in the pulsed-light treatment of tissue foods, as it can affect the actual fluence delivered to microbial cells present in their internal structure or on their surface. Scattering can also occur in opaque substrates that have surface irregularities. When surface roughness size is larger than the wavelength (λ) of the incident light, it has negligible scattering effects; however, when roughness is comparable with λ, it can cause substantial scattering (Guenther et al. 1993). This effect is particularly important for the UV region of the pulsed-light spectrum, as it could affect the UV dose available for microorganism inactivation.

The reduction in the intensity of the light traversing the substrate due to light absorption is very important in pulsed-light treatment, since it can diminish significantly the amount of light that reaches the microbial cells. Absorption of photons by the molecules in the substrate results in an increase in the energy content of those molecules, which causes an increased level of vibration or rotation (Sakai and Hanzawa 1994). If significant, such motions could lead to quantifiable heating effects, which could affect the outcome of the pulsed-light treatment.

Light absorption by the substrate depends both on the substrate composition and on the wavelength of the radiation. For biological systems, including foods, absorption of UV is mainly due to proteins that contain the amino acids tyrosine, phenylalanine, and tryptophan, and to nucleic acids, since purine and pyrimidine bases absorb strongly in the near-UV. In VIS, the absorption is due to tissue chromophores, such as hemoglobin, deoxyhemoglobin, myoglobin, melanin, and cytochrome C oxidase from meat (Marquez et al. 1998; Hollis 2002), or carotene, chlorophyll, and xanthophyll from vegetal tissues. In the NIR range, most of the absorption by food substrates is due to water, which has an absorption peak at 970 nm (Cooper et al. 1996), but also to fat (Frank 1981; Conway et al. 1984). In milk, absorption in the NIR is also caused by casein (Frank 1981).

Besides chemical composition, surface topography has a significant effect in any light-based treatment, including pulsed light. Shading effects by the surface details could greatly limit the efficiency of the treatment as well as its reproducibility. Woodling and Moraru (2005) investigated the effect of surface topography of pulsed-light inactivation using stainless steel of four different surface finishes—from a highly polished surface with a near mirror finish (electropolished finish) to a relatively rough and irregular surface (aluminum oxide finish). The total roughness (R_t) for these surfaces varied from 1.95 μm for the electropolished finish to 17.45 μm

for the aluminum oxide finish, while the cell size of the challenge organism (*L. innocua*) was in the 1–2-μm range (Woodling and Moraru 2005). The rough surfaces are expected to provide location for the bacterial cells to "hide" or form layers of cells that may possibly limit their exposure to pulsed light and reduce the efficacy of the treatment. The four different substrates were inoculated with $\approx 10^8$ CFU/coupon and treated with varying doses of pulsed light. Maximum "raw losses," which designate inactivation levels calculated without taking into consideration cell losses that occurred during inoculation and recovery, were around 5-log cycles. The reduction levels for the two smoothest surfaces were not statistically different from each other, but were significantly lower than for the two roughest surfaces.

Based on the surface topography and the potential hiding effects discussed above, it would have been expected that the rough surfaces should yield a lower level of reduction than the smooth surfaces. The experimental data suggested, however, that topography was not the only surface property that affected microbial inactivation. For the electropolished finish, the liquid inoculum was particularly difficult to spread on the surface, due to surface hydrophobicity. Measurement of contact angles indicated a significant increase in surface hydrophobicity as surface roughness decreased. The smoothest surface was the most hydrophobic of all, with an average contact angle (θ) of 91.2°. The mill finish and the bead-blasted surface had an average θ of 73.9° and 69.8°, respectively, while the aluminum oxide-treated surface (the roughest) was the least hydrophobic of all, with an average contact angle of 45°. Another factor that could have affected the distribution of bacteria on the metal surfaces was the hydrophobicity of the bacterial cells themselves. *Listeria* cells exhibit rather hydrophilic properties and low values of the water contact angles. This led to the hypothesis that, in a system comprising stainless steel/*L. innocua* cells/watery media, the bacteria would be preferentially located between the metal and the watery media, since the latter has a more pronounced tendency to "run away" from the hydrophobic metal surface and a higher affinity for the bacteria. This was possibly the most significant for the highly hydrophobic electropolished finish, for which the watery inoculum beaded up during inoculation and drying, creating a protective, relatively thick layer of medium that covered the cells, shielding them from the direct effect of pulsed light (PL). A visual confirmation of this layer was provided in this study. In the same study, a significant role was also attributed to the optical properties of the surfaces. A high degree of reflectivity could potentially result in less light being absorbed by the microbial cells, which could have also contributed to the lower-than-expected inactivation levels found for the smooth, electropolished surface (Woodling and Moraru 2005).

An additional factor of influence in surface treatment by pulsed light was found to be the level of surface contamination, i.e., the inoculum concentration for controlled studies (Uesugi et al. 2007). For clear liquid substrates, the initial inoculum level did not influence the reduction when the same pulsed-light treatment was applied. For treatments conducted on the surfaces of stainless steel, the profiles of survivor curves were similar to those conducted in clear liquid, but a higher level of inactivation was observed with the use of higher initial inoculum levels. This difference is likely due to the distribution of cells on the stainless steel surface. Cells directly exposed to pulsed light are more likely to be damaged and die than those that may

be hidden by imperfections on the surface or by the layering of cells on top of each other that may shield other cells. As the level of inoculum increases, the number of cells that are directly exposed to treatments increases, leading to greater levels of inactivation.

In practical applications it is very important to be able to quantify the overall effect of the substrate on the light dose received by the microorganisms. The optical property that describes quantitatively the distribution of light dose inside a substrate is *optical penetration depth* (δ), which represents the distance over which light decreases in fluence rate to 1/*e* or 37% of its initial value. It is important to note that optical penetration varies with wavelength, with shorter wavelengths providing deeper penetration into the food than longer wavelengths (Dagerskog and Österström 1979). This means that the spectral distribution of light changes from the surface into the internal structure of the material, which can change the outcome of the treatment as a function of substrate depth. Sauer and Moraru (2007) and Uesugi and Moraru (2007) examined several substrates to determine the optical penetration depth of pulsed light. For Butterfield's phosphate buffer, apple juice, and apple cider, the optical penetration depth of pulsed light was calculated as 166.7, 41.7, and 15.9 mm, respectively. For the pulsed-light treatment of Vienna sausages, the optical penetration depth was calculated to be 2.3 mm. This clearly demonstrates that light treatments, such as PL, will only be effective as a surface treatment for this type of solid substrate, but it may be an effective treatment for liquids if the proper depth is selected.

Knowledge about the optical properties of microbial cells themselves is also important in understanding the microbicidal effects of pulsed-light treatment. Waltham et al. (1994) measured light scattering and absorption from a population of *E. coli* in water and observed a significant decrease in these two properties from UV to VIS. Similar results were reported by Arakawa et al. (2003) for *Erwinia herbicola*. Tuminello et al. (1997) performed spectral reflectance and transmittance measurements of *Bacillus subtilis* spores from 200 to 2500 nm and found an increase in the transmission of *Bacillus* spores from UV to NIR. Such findings also support the idea that, during pulsed-light treatment, it is the UV radiation that affects the microbial cells mostly, since this component of the electromagnetic spectrum is absorbed the most. Similar to biological substrates, UV absorption by microbial cells is predominantly due to proteins and nucleic bases.

10.2.3 Inactivation Kinetics in Pulsed-Light Treatment

An important aspect in the commercial application of any microbial-inactivation technique, including pulsed light, is the quantitative characterization of inactivation kinetics, in order to allow for accurate process calculations. Since inactivation curves in pulsed-light treatment show an obvious non-log-linear decline, evidence of tailing, and a concave upward shape (Woodling and Moraru 2005, 2007; Uesugi et al. 2007), the traditional first-order-kinetics approach is not applicable. Due to its ability to successfully model nonlinear inactivation, the Weibull model has been used to describe the survival of *L. innocua* after exposure to pulsed light (Uesugi et al. 2007). The Weibull model is a nonmechanistic model that uses a power function to describe the variation of survivor ratio as a function of treatment intensity

(van Boekel and Martinus 2002). For microbial inactivation by pulsed light, the Weibull function can be written as

$$\log\left(\frac{N}{N_0}\right) = -\frac{1}{2.303}\left(\frac{F}{\alpha}\right)^{\beta} \tag{10.4}$$

where

N = survivors after treatment
N_0 = initial number of microorganisms
α = the scale parameter
β = the shape factor, which describes the shape of the survivor curve
F = pulsed-light fluence (J/cm^2)

When $\beta > 1$, a concave down curve is described, while a shape parameter $\beta < 1$ indicates a concave up curve; if $\beta = 1$, the survivor curve will assume a linear form (Peleg and Cole 1998; van Boekel and Martinus 2002).

Uesugi et al. (2007) demonstrated that the Weibull model can be used successfully to predict pulsed-light inactivation of *L. innocua* in clear liquid substrates, and calculated shape and scale parameters of 0.33 and 3.01, respectively (Figure 10.5). Regardless of initial inoculum level, the predicted and experimental data difference was within 0.1 log. The modeling was far less accurate for stainless steel surfaces, for which the model significantly overestimated the level of pulsed-light inactivation due to differences in surface properties and initial inoculum levels. This demonstrated that, as substrates become more complex, it is very difficult to use a modeling approach to accurately predict the level of inactivation, mainly due to the various influences of substrate properties on inactivation.

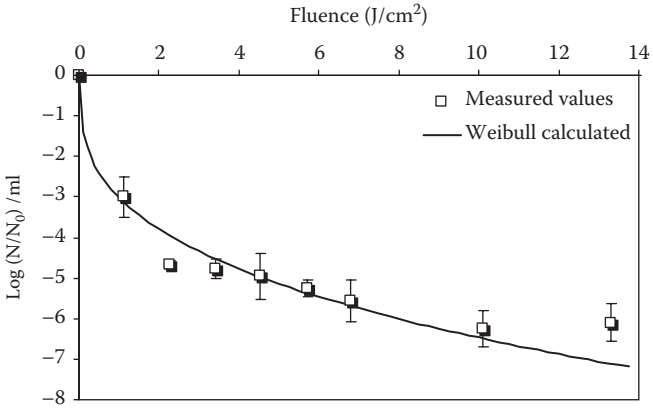

FIGURE 10.5 Experimental and Weibull-calculated survival ratios ($S = N/N_0$) for *L. innocua* treated with pulsed light in Butterfield's phosphate buffer at an initial inoculum of 7.45 log CFU/mL. (From Uesugi et al. 2007. With permission.)

10.3 APPLICATIONS OF PULSED-LIGHT TREATMENT

10.3.1 Microbial Inactivation in Water and Other Liquids

The ability of pulsed light to reduce microbial counts in liquids is dependent on the distance of the lamp to the sample, the treatment time or fluence exposure, the turbidity of the liquid, and the depth of the liquid. Huffman et al. (2000) examined the inactivation of bacteria, viruses, and parasites suspended in water and treated with pulsed light at 0.25 J/cm^2 using a PureBright water treatment unit. For the bacteria *Klebsiella terrigena,* two pulses resulted in a reduction of >7.4 log CFU/mL. For viruses (Poliovirus type 1 and Rotavirus SA11), human viral surrogates (bacteriophages MS-2 and PRD-1), and a parasite (*Cryptosporidium parvum*), two pulses achieved an inactivation of >4-log reduction.

Bacteria and yeast suspensions in buffers can also be greatly reduced by pulsed light. Takeshita et al. (2003) noted a decrease of 5.8 log CFU/mL of *Saccharomyces cerevisiae* when cells were suspended in potassium phosphate buffer in a 110 mm diameter watch glass treated with a total of 3.5 J/cm^2 from a flash lamp and reflector positioned above the sample. The SteriPulse-XL 3000 benchtop unit with a pulse width of 360 μs, 3800-V input power, and a pulse rate of three flashes per second from Xenon Corp. was used in a large number of pulsed-light inactivation studies. Krishnamurthy et al. (2004) suspended *Staphylococcus aureus* in phosphate buffer and treated the suspension with pulsed light for 5 s at a distance of 80 mm from the lamp. They reported an inactivation level of 7.5 log CFU/mL. *Listeria innocua* in Butterfield's phosphate buffer in thin layer (about 1.2 mm) was reduced by 6.04 log CFU/mL after exposure to 13.3 J/cm^2 by Uesugi et al. (2007) at a distance of 50 mm from the quartz face of the lamp. *Escherichia coli* suspended in apple cider and apple juice was reduced by 5.5 log CFU/mL and over 7 log CFU/mL, respectively, when samples were subjected to agitation and treated with pulsed light at a distance of 50 mm from the lamp, at fluence levels below 12 J/cm^2 (Sauer and Moraru 2007). Milk samples treated with 25.1 J/cm^2 of pulsed UV light from a UV laser showed reductions of >2 log CFU/mL of *Serratia marcescens* (Smith et al. 2002). Further plating of treated milk samples did not show signs of growth after 21 days of storage. Table 10.5 includes a comprehensive set of data on pulsed-light inactivation of microorganisms in liquids available in the literature to date.

10.3.2 Microbial Inactivation in Food Systems

10.3.2.1 Pulsed-Light Treatment of Meat Products

As seen in Table 10.6, only a few studies have looked at the potential of pulsed light to inactivate microorganisms on the surface of meat products. The inactivation of *L. innocua* on the surface of Vienna sausages by 9.4 J/cm^2 pulsed light was investigated by Uesugi and Moraru (2007) using a SteriPulse-XL 3000 lamp at a distance of 50 mm. A reduction of 1.39 log CFU was observed after PL treatment, and significant growth did not occur until after 8 days of storage at 4°C. When pulsed light was used in combination with a nisin dip, a reduction of *L. innocua* between 4–5 log CFU/sausage was observed. The number of survivors on the sausage did not change

TABLE 10.5
Published Data for the Inactivation of Microorganisms in Liquid Substrates by Pulsed Light

Treated Substrate	Microorganism	Dose (fluence) (J/cm^2)	Fluence/ pulse (J/cm^2)	No. Pulses	Distance to Lamp (mm)	Inoculum (log CFU/ mL)	Reduction (log CFU/ mL)	Source
Apple cider	*Escherichia coli*	11.7	n.d.	n.d.	50.8	n.d.	5.5	Sauer and Moraru (2007)
Apple juice	*Escherichia coli*	8.8	n.d.	n.d.	50.8	n.d.	>7	Sauer and Moraru (2007)
Butterfield phosphate buffer	*Listeria innocua*	13.3	n.d.	12	50.8	7.45	6.04	Uesugi et al. (2007)
Milk	*Serratia marcescens*	25.1	n.d.	n.d.	n.d.	4.4	>2.0	Smith et al. (2002)
Phosphate buffer	*Staphylococcus aureus*	84	5.6	15	80	7–8	7.5	Krishnamurthy et al. (2004)
Potassium phosphate buffer	*Saccharomyces cerevisiae*	n.d.	0.7	5	n.d.	6.8	5.8	Takeshita et al. (2003)
Water	Bacteriophage MS-2	n.d.	0.25	2	n.d.	4.3	>4.3	Huffman et al. (2000)
Water	Bacteriophage PRD-1	n.d.	0.25	2	n.d.	5.8	4.8	Huffman et al. (2000)
Water	*Cryptosporidium parvum*	n.d.	0.25	2	n.d.	5.6	4.2	Huffman et al. (2000)
Water	*Klebsiella terrigena*	n.d.	0.25	2	n.d.	5.5	>7.4	Huffman et al. (2000)
Water	Poliovirus type 1	n.d.	0.25	2	n.d.	4.6	4.1	Huffman et al. (2000)
Water	Rotavirus SA11	n.d.	0.25	2	n.d.	5.1	4.1	Huffman et al. (2000)

Note: n.d. = no data available.

TABLE 10.6
Published Data for the Inactivation of Microorganisms in Meat Products by Pulsed Light

Treated Food	Microorganism	Dose (fluence) (J/cm²)	Fluence/ pulse (J/cm²)	No. Pulses	Distance to Lamp (mm)	Inoculum (log CFU/mL)	Reduction (log CFU/mL)	Source
Raw salmon fillet	*Escherichia coli* 0157:H7	n.d.	5.6	180	80	6	0.30–1.09	Ozer and Demirci (2006)
Raw salmon fillet	*Listeria monocytogenes*	n.d.	5.6	180	80	6	0.74–1.02	Ozer and Demirci (2006)
Vienna sausages	*Listeria innocua*	9.4	n.d.	9	50.8	6.5	1.39	Uesugi and Moraru (2007)

Note: n.d. = no data available.

after the initial reduction until after 28 days of refrigerated storage. The survivors did not reach the initial level of inoculum until 40 days of storage.

Ozer and Demirci (2005) examined the reduction of *L. monocytogenes* and *E. coli* O157:H7 on the muscle and skin side of raw salmon fillets using a SteriPulse-XL 3000. For *E. coli* O157:H7, a reduction of 0.30 and 1.09 log CFU/g was seen on the muscle and skin side, respectively when treated at a distance of 80 mm with 180 pulses. For *L. monocytogenes* on the salmon muscle and skin, reductions of 0.74 and 1.02 log CFU/g, respectively, were reached after 180 pulses at a distance of 80 mm. Surface temperatures increased after 60 s of pulsed-light treatment from a distance of 80 mm by 28°C and 51°C on the muscle and skin side, respectively. For treatments of less than 5 s, the muscle and skin surface temperatures did not increase. These differences in temperature change are due to the differences in color between the darker skin side and the lighter muscle side. The increased temperature may have contributed to the greater reduction observed on the skin side of the fish.

10.3.2.2 Pulsed-Light Treatment of Fruits and Vegetables

A variety of minimally processed vegetables were examined to see the effect of pulsed light on mesophilic aerobic counts (Table 10.7). Gomez-Lopez et al. (2005) examined celeriac, green bell peppers, iceberg lettuce, radicchio, soybean sprouts, spinach, and white cabbage treated with up to 2700 pulses with a xenon flash lamp with a pulse duration of 30 μs and an intensity of 7 J at a distance of 128 mm from the lamp, with samples spread over a sterile 14 × 21-cm tray. Microbial reductions ranged from 0.56 log to 2.04 log for the variety of produce examined. The tested vegetables were naturally contaminated and not inoculated with a known microorganism, so the variability between the samples was hypothesized by the author to be due to different resistances of the natural microbial population, the location of the microorganisms, shadow

TABLE 10.7
Published Data for the Inactivation of Microorganisms on Fruits and Vegetables by Pulsed Light

Treated Food	Microorganism	Dose (fluence) (J/cm²)	Fluence/ pulse (J/cm²)	No. Pulses	Distance to Lamp (mm)	Inoculum (log CFU/ mL)	Reduction (log CFU/ mL)	Source
Alfalfa seeds	*Escherichia coli* O157:H7	n.d.	5.6		80	5	0.17–4.89	Sharma and Demirci (2003)
Blueberries	*Escherichia coli* O157:H7	22.6	n.d.	180	80	6	4.3	Bialka and Demirci (2007)
Blueberries	*Salmonella enterica*	22.6	n.d.	180	80	6	2.9	Bialka and Demirci (2007)
Carrot slices	*Saccharomyces cerevisiae*	n.d.	0.7	24	n.d.	5.28	4.93	Kaack and Lyager (2007)
Celeriac	Mesophilic aerobic counts	7	n.d.	675	128	n.d.	0.21	Gomez-Lopez et al. (2005)
Green bell pepper	Mesophilic aerobic counts	7	n.d.	2700	128	n.d.	0.56	Gomez-Lopez et al. (2005)
Iceberg lettuce	Mesophilic aerobic counts	7	n.d.	2700	128	≈6.5	2.04	Gomez-Lopez et al. (2005)
Radicchio	Mesophilic aerobic counts	7	n.d.	2700	128	n.d.	0.79	Gomez-Lopez et al. (2005)
Soybean sprouts	Mesophilic aerobic counts	7	n.d.	2700	128	n.d.	0.65	Gomez-Lopez et al. (2005)
Spinach	Mesophilic aerobic counts	7	n.d.	2700	128	n.d.	0.90	Gomez-Lopez et al. (2005)
Strawberries	*Botrytis cinerea*	n.d.	7	3750	n.d.	5.7	<1	Marquenie et al. (2003b)
White cabbage	Mesophilic aerobic counts	7	n.d.	2700	128	≈3.5	1.64	Gomez-Lopez et al. (2005)

Note: n.d. = no data available.

effects, or protective substances found in the vegetables. The processing (shredded, grated, chopped, or whole) shape or sample size did not produce any observable patterns in reduction. While the initial microbial load was reduced on the minimally processed vegetables, shelf life was not increased compared with untreated controls, as both sets of samples became poor for overall visual quality.

Kaack and Lyager (2007) inoculated carrot slices with *S. cerevisiae* prior to treatment with pulsed light from two flash lamps, located above and below the sample, that emitted a total energy flux of 0.7 J/cm^2. After the first two pulses, with each pulse delivering 0.7 J/cm^2, there was a reduction of 3.07 log CFU/g. After exposure to 24 pulses, reduction increased to 4.93 log CFU/g. The authors hypothesized that, in combination with washing, pulsed light may reduce the level of yeast on sliced carrots by up to 6-log cycles.

Strawberries inoculated with *Botrytis cinerea* and treated with pulsed light from a xenon lamp with pulse duration of 30 μs and an intensity of 7 J (within a treatment chamber with reflective inner walls to enhance distribution of the light) showed no effect for surface decontamination to reduce storage rot (Marquenie et al. 2003b). Fruit firmness of the treated strawberries decreased during 10 days of storage for a variety of treatment durations, but there was no significant difference between treated and untreated fruit. Combining pulsed-light treatments with additional UV-C exposure of $\lambda = 254$ nm at 1.0 kJ/m^2 for 120 s delayed observation of fungal mycelium by 1 day. Previous studies had shown that similar treatment of *B. cinerea* conidia in phosphate buffer had resulted in a reduction or 3–4 log units (Marquenie et al. 2003a), but the in vitro reductions did not occur on the strawberry fruit surface.

Alfalfa seeds inoculated with 5 log CFU/g of *E. coli* O157:H7 were reduced log 4.89 at a distance of 80 mm and 270 pulses from a SteriPulse-XL 3000 lamp (Sharma and Demirci 2003). The same treatment performed at a distance of 130 mm resulted in a log reduction of 1.42. A short distance between seeds and the lamp and longer treatment times were the most effective in decontaminating the seeds. The distance from the lamp, 30–130 mm, did not significantly change the germination percentage of the seeds but did result in an *E. coli* O157:H7 reduction ranging between 0.07 log and 4.89 log. The limited penetration depth of the pulsed light made seed layer thickness a critical variable in the reduction of *E. coli* O157:H7.

Bialka and Demirci (2007) noted a reduction of 1.1 and 4.3 log CFU/g of *E. coli* O157:H7 with 1.9 and 22.6 J/cm^2, respectively, on blueberries treated with a SteriPulse-XL 3000 lamp at a distance of 80 mm from the lamp. No significant differences were seen at other fluence doses between 1.9 and 22.6 J/cm^2. Treatments at a distance of 30 mm resulted in slightly greater reductions but resulted in damaged fruit. For treatments of *Salmonella enterica* on blueberries, the differences in fluence did not create significantly greater reductions at 30 and 80 mm from the lamp. At 130 mm treatment distance, however, the reduction of *Salmonella enterica* increased significantly with fluence. Treated and untreated blueberries were not significantly different after examination by *L*a*b** color analysis and a sensory panel.

10.3.2.3 Pulsed-Light Treatment of Other Foods

Fine and Gervais (2004) achieved log reductions of 2.93 and 0.7, respectively, for pulsed-light-treated black pepper and wheat flour inoculated with *S. cerevisiae*.

TABLE 10.8
Published Data for the Inactivation of Microorganisms of Other Foods by Pulsed Light

Treated Food	Microorganism	Dose (fluence) (J/cm²)	Fluence/ pulse (J/cm²)	No. Pulses	Distance to Lamp (mm)	Inoculum (log CFU/ mL)	Reduction (log CFU/mL)	Source
Honey	*Clostridium sporogenes* spores	n.d.	5.6	135	80–200	6.24	0.0–5.65	Hillegas and Demirci (2003)
Black pepper	*Saccharomyces cerevisiae*	31.12	n.d.	64	20	6.6	2.93	Fine and Gervais (2004)
Corn meal	*Aspergillus niger*	n.d.	5.6	300	80	5	4.95	Jun et al. (2003)
Wheat flour	*Saccharomyces cerevisiae*	31.12	n.d.	64	20	7.0	0.7	Fine and Gervais (2004)

Note: n.d. = no data available.

The difference in inactivation between the two samples, both exposed to 31.12 J/cm² at a distance of 20 mm from the lamp, was assumed to be due to the difference in color between the black pepper and the wheat flour. A fluidized-bed treatment unit was used to mix samples and to increase exposure. The visual flavor qualities of the black pepper and the wheat flour decreased prior to reaching an acceptable yeast reduction, as both products became progressively burned with increased exposure. *Aspergillus niger* spores were greatly inactivated in corn meal (Jun et al. 2003). A log reduction of 4.95, when starting with an initial inoculum of 5 log CFU/g on the corn meal, was reached after 100 s of treatment at a distance of 8 cm. The reduction changed to 3.26 and 2.95 log CFU/g when the distance from the lamp was 30 and 130 mm, respectively. A sample temperature greater than 120°C was noted at the maximum treatment parameters, leading to changes in quality and food properties. Clover honey was inoculated with *Clostridium sporogenes* spores to a level of 6.25 log/g (Hillegas and Demirci 2003). Spore reductions ranged from 0.0 to 5.65 log/g when treated with pulsed light from a SteriPulse-XL 3000 lamp at different honey depths, treatment times, or distances from the lamp. When the three parameters were modified, no combination could completely reduce all the spores present in the honey. Table 10.8 presents a summary of the published data for the inactivation of microorganisms in foods other than meat and fruit and vegetable products.

10.3.3 Pulsed-Light Treatment of Packaging Materials

Pulsed light can be used to inactivate microorganisms on the surface of food packaging materials, and potentially on the surface of products packaged in "UV transparent"

materials. The use of pulsed light could lead to a reduction in the need for preservatives or chemical sterilizing agents. Chemical surface sterilizers such as hydrogen peroxide, propylene oxide, or peracetic acid may leave a residue or require time to reduce to an acceptable level, but pulsed light has the advantage of not leaving undesirable residue after treatment. When mold spores of *Cladosporium harbarum* were placed onto paper coated with polyethylene, a 2.7-log reduction was noted after 30 pulses at a distance of 70 mm from the lamp (Turtoi and Nicolau 2007). One aspect that needs to be accounted for when using pulsed light to treat packaged products is that the treatment is limited to the surface of the product and is restricted by the ability of light to penetrate opaque and irregular surfaces. Additionally, undesirable chemical effects may be encountered. UV-treated low-density polyethylene and polyethylene terephthalate have shown increased levels of surface oxidation products when compared with untreated samples, which indicated that UV may accelerate the oxidation of the plastic film surfaces (Ozen and Floros 2001). Such phenomena could also occur in pulsed-light treatments, and therefore any successful microbial-inactivation study should be followed by an investigation of the potential side effects of the treatment.

10.3.4 Other Applications of Pulsed-Light Treatment

Pulsed light is also used in a number of nonfood applications. Of particular importance is the use of pulsed UV light in curing processes, which involve the use of UV light to harden a liquid film by inducing polymerization in its structure. A wide variety of products and industrial processes involve a UV curing step, including inks, paints, metal coatings, adhesives, building materials, or textiles. More recently, pulsed light has found uses in the manufacturing of optical discs, including DVDs, CDs, and high-definition discs such as Blu-Ray discs. In these applications, high peak UV energy is delivered in short pulses that penetrate the polycarbonate substrate layer and cure the adhesive sandwiched in between them (Xenon Corp. 2005). The CoolCureXL-DVD® model RC-801 system produced by Xenon Corp., which can deliver 207 J/pulse, at a rate of 10 pulses per second, is able to achieve effective curing after 500 ms and a total energy of 1242 J, delivered with six pulses. At 15 pulses per second, the PS-813 model can achieve the same curing effect in only 333 ms (Xenon Corp. 2005).

In addition to curing, pulsed light has been used in several medical applications to treat skin ailments. In these treatments, a water-based gel is applied in a thin layer to help cool the treated skin as well as evenly disperse the light. A broad spectrum of light is used, but the range is usually between 500 to 1200 nm, with low-end cutoff filters to remove the UV portions of the spectrum. The fluence applied ranges from 3 to 90 J/cm^2. Melasma, or hyperpigmented patches that occur on sun-exposed areas of the body, was treated in Chinese patients with intense pulsed light (Li et al. 2008). Dermatologists determined that 69 of 89 patients, or 78%, had improvements between 51% and 100%. Rusciani et al. (2008) used pulsed light to treat a reddish-brown pattern of pigmentations on sun-exposed areas, called *poikiloderma of Civatte*. A reduction between 75% to 100% of poikiloderma was seen in 81% of the 175 patients in the study. A group of 25 Korean women was treated with pulsed light to treat dyspigmentation, a common skin lesion of concern with Asians. After treatments with pulsed light, 19 of the 25 subjects reported a good to excellent

response to treatments (Park et al. 2008). In all of these studies, no adverse effects were reported, but Sorg et al. (2007) showed that the exposure of human skin to VIS-NIR does not lead to the formation of thymine dimers, but that oxidative stresses and lipid peroxides can be generated at levels six times higher than in the case of skin exposed to solar radiation. This could raise some general concerns related to the use of pulsed-light technology, particularly worker safety concerns. Yet, when considering such effects, it is important to remember that the fluence levels used for medical applications are much higher than those used for microbial inactivation, and that the treatment is applied directly to the patient's skin.

10.4 FUTURE PROSPECTS OF PULSED-LIGHT TREATMENT IN THE FOOD INDUSTRY

The research data available in the scientific literature and discussed in this chapter clearly demonstrate the potential of pulsed-light technology to inactivate pathogenic and spoilage microorganisms in food products or in food-contact materials. The fact that the effectiveness of the treatment is strongly influenced by substrate characteristics, particularly optical properties and topography, suggests that there are also significant limitations that need to be taken into consideration when using pulsed light to treat complex substrates such as foods. Based on the experience of the food industry with other emerging technologies, probably the best approach is to channel pulsed-light technology toward niche applications, i.e., situations in which no other treatment can be used. For instance, pulsed light could be used as a terminal, postprocess treatment for surface decontamination of fresh fruits and vegetables or ready-to-eat products such as meats. Although uniform exposure of the substrate poses challenges, the use of "UV-transparent" packaging materials, which are commercially available, combined with a 360° exposure of the treated foods could represent a solution to this problem.

Overall, it is our opinion that pulsed-light technology brings new and exciting opportunities to the food industry, which might be able to use this treatment as a new means to increase the safety and shelf life of certain food products. Although pulsed light is attracting increasing attention from scientists and the industry, it remains one of the least-studied emerging technologies, and much work still needs to be done in this area. Besides microbial-inactivation studies, systematic work is also necessary to investigate the impact of microbicidally effective pulsed-light treatments on the nutritional and sensory properties of the treated foods. Issues related to generation of ozone, economic feasibility, and worker safety also need to be addressed in the near future.

REFERENCES

Arakawa E. T., P. S. Tuminello, B. N. Khare, and M. E. Milham. 2003. Optical properties of *Erwinia herbicola* bacteria at 0.190–2.50 μm. *Biopolymers (Biospectroscopy)* 72: 391–398.

Bialka, K. L., and A. Demirci. 2007. Decontamination of *Escherichia coli* O157:H7 and *Salmonella enterica* on blueberries using ozone and pulsed UV-light. *J. Food Sci*. 72: M391–M396.

Bintsis, T., E. Litopoulou-Tzanetaki, and R. K. Robinson. 2000. Existing and potential application of ultraviolet light in the food industry: A critical review. *J. Sci. Food Agr.* 80: 637–645.

Bogdanov, E. A., A. A. Kudryavtsev, R. R. Arslanbekov, and V. I. Kolobov. 2004. Simulation of pulsed dielectric barrier discharge xenon excimer lamp. *J. Phys. D: Appl. Phys*. 37: 2987–2995.

Bolton, J. R. 2000. Calculation of ultraviolet fluence rate distributions in an annular reactor: Significance of refraction and reflection. *Water Res.* 34: 3315–3324.

Bussiahn, R., S. Gorchakov, H. Lange, D. Loffhagen, and D. Uhrlandt. 2007. AC operation of low-pressure He–Xe lamp discharges. *J. Phys. D: Appl. Phys*. 40: 3882–3888.

Cheong, W., S. A. Prahl, and A. J. Welch. 1990. A review of the optical properties of biological tissues. *IEEE J. Quant. Elec*. 26: 2166–2185.

Conway, J. M., K. H. Norris, and C. E. Bodwell. 1984. A new approach for the estimation of body composition: Infrared interactance. *Am. J. Clin. Nutri*. 40: 1123–1130.

Cooper, C. E., E. E. Elwell, J. H. Meek, S. J. Matcher, J. S. Wyatt, M. Cope, and D. T. Delpy. 1996. The noninvasive measurement of absolute cerebral deoxyhaemoglobin concentration and mean optical path length in the neonatal brain by second derivative near infrared spectroscopy. *Pediat. Res.* 39: 32–38.

Dagerskog, M., and L. Österström. 1979. Infra-red radiation for food processing: I, A study of the fundamental properties of infra-red radiation. *Lebensm. Wiss. Technol*. 12: 237–242.

Davies-Colley, R. J., A. M. Donnison, and D. J. Speed. 1997. Sunlight wavelengths inactivating faecal indicator micro-organisms in waste stabilisation ponds. *Water Sci. Technol.* 35: 219–225.

Dunn, J., W. Clark, and T. Ott. 1995. Pulsed-light treatment of food and packaging. *Food Technol.* 49 (9): 95–98.

Dunn, J. E., T. M. Ott, and R. W. Clark. 1997. Prolongation of shelf life in perishable pod products. U.S. Patent 5,489,442.

Durán, L., and C. Calvo. 2002. Optical properties of foods. In: *Encyclopedia of life support systems*. http://www.eolss.net.

Fargues, J., M. Rougier, R. Goujet, N. Smits, C. Coustere, and B. Itier. 1997. Inactivation of conidia of *Paecilomyces fumosoroseus* by near-ultraviolet (UVB and UVA) and visible radiation. *J. Invertebr. Pathol.* 69: 70–78.

Farkas, J. 1997. Physical methods of food preservation. In *Food microbiology: Fundamentals and frontiers*, ed. M. P. Doyle, L. R. Beauchat, and T. J. Montville, 497–519. Washington, DC: ASM Press.

Fine, F., and P. Gervais. 2004. Efficiency of pulsed UV light for microbial decontamination of food powders. *J. Food Prot.* 67: 787–792.

Flesch, P., and M. Neiger. 2005. Understanding anode and cathode behaviour in high-pressure discharge lamps. *J. Phys. D: Appl. Phys.* 38: 3098–3111.

Flock, S. T., B. C. Wilson, and M. S. Patterson. 1987. Total attenuation coefficients and scattering phase functions of tissues and phantom materials at 633 nm. *Med. Phys*. 14: 835–841.

Food and Drug Administration. 1996. *Code of Federal Regulations* 21 CFR, part 179.41.

Frank, J. F. 1981. Potential for rapid determination of cheese composition using reflectance spectroscopy. Paper presented at Marschall Italian & Specialty Cheese Seminars 3, 1981-1. http://www.marschall.com.

Ghasemi, Z., S. Macgregor, J. Anderson, and Y. Lamont. 2003. Development of an integrated solid-state generator for light inactivation of food-related pathogenic bacteria. *Meas. Sci. Technol.* 14 (6): N26–N32.

Gomez-Lopez, V. M., F. Devileghere, V. Bonduelle, and J. Debevere. 2005. Intense light pulses decontamination of minimally processed vegetables and their shelf-life. *Int. J. Food Microbiol*. 103: 79–89.

Grapperhaus, M. J., and R. B. Schaefer. 2006. Lead paint removal with high-intensity light pulses. *Environ. Sci. Technol*. 40: 7925–7929.

Guenther, K. H., J. A. McCandless, and F. D. Orazio, Jr. 1993. Correlation of light-scattering measurements and visual ranking of optical surfaces. *Appl. Opt.* 32: 3425–3432.

Hillegas, S. L., and A. Demirci. 2003. Inactivation of *Clostridium sporogenes* in clover honey by pulsed UV-light treatment. *Agric. Eng. Int.: CIGR J. Sci. Res. Dev.* 5: FP03-009.

Hollis, V. 2002. *Non-invasive monitoring of brain tissue temperature by near-infrared spectroscopy.* PhD thesis, University College London. http://www.medphys.ucl.ac.uk/.

Horiguchi, H., R. Chang, and W. Setser. 1981. Radiative lifetimes and two-body collisional deactivation rate constants in argon for xenon (5p 56p), xenon (5p 56p), and xenon (5p 57p) states. *J. Chem. Phys*. 75: 1207.

Huffman, D. E., T. R. Slifko, K. Salisbury, and J. B. Rose. 2000. Inactivation of bacteria, virus and *Cryptosporidium* by a point-of-use device using pulsed broad spectrum white light. *Water Res*. 34: 2491–2498.

Jay, J. M. 2000. *Modern food microbiology*. Gaithersburg, MD: Aspen.

Jun, S., J. Irudayaraj, A. Demirci, and D. Geiser. 2003. Pulsed UV-light treatment of corn meal for inactivation of *Aspergillus niger* spores. *Int. J. Food Sci. Technol*. 38: 883–888.

Kaack, K., and B. Lyager. 2007. Treatment of slices from carrot (*Daucus carota*) using high intensity white pulsed light. *Eur. Food Res. Technol*. 224: 561–566.

Krishnamurthy, K., A. Demirci, and J. Irudayaraj. 2004. Inactivation of *Staphylococcus aureus* by pulsed UV-light sterilization. *J. Food Prot*. 67: 1027–1030.

Ledru G., F. Marchal, N. Sewraj, Y. Salamero, and P. Millet. 2006. Comparative study of the formation and decay of xenon excimers following selective excitation of the $5p^5 6s$ states: Spectroscopic and kinetic analysis. *J. Phys. B: At. Mol. Opt. Phys.* 39: 2031–2057.

Li, Y. H., J. Z. S. Chen, H. C. Wei, Y. Wu, M. Liu, Y. Y. Xu, G. H. Dong, and H. D. Chen. 2008. Efficacy and safety of intense pulsed light in treatment of melasma in Chinese patients. *Dermatol. Surg.* 34: 693–701.

MacGregor, S. J., J. G. Anderson, R. A. Fouracre, O. Farish, L. McIlvaney, and N. J. Rowan. 1998. Light inactivation of food-related pathogenic bacteria using a pulsed power source. *Lett. Appl. Microbiol.* 27 (2): 67–70.

Malitson, I. H. 1965. Interspecimen comparison of the refractive index of fused silica. *J. Opt. Soc. Am.* 55: 1205–1209.

Marquenie, D., A. H. Geeraerd, J. Lammertyn, C. Soontjens, J. F. Van Impe, C. W. Michiels, and B. M. Nicolai. 2003a. Combinations of pulsed white light and UV-C or mild heat treatment to inactivate conidia of *Botrytis cinerea* and *Monilia fructigena. Int. J. Food Microbiol*. 85: 185–196.

Marquenie, D., C. W. Michiels, J. F. Van Impe, E. Schrevens, and B. M. Nicolai. 2003b. Pulsed white light in combination with UV-C and heat to reduce storage rot of strawberry. *Postharvest Biol. Technol*. 28: 455–461.

Marquez, G., L. V. Wang, S. Lin, J. A. Schwartz, and S. L. Thomsen. 1998. Anisotropy in the absorption and scattering spectra of chicken breast tissue. *Appl. Opt.* 37: 798–804.

McCown, A. W., M. N. Ediger, and J. G. Eden. 1982. Resonantly enhanced, three-photon ionization of Xe: Optically pumped rare-gas laser. *Phys. Rev. A* 26: 2281–2284.

McDonald, K., R. Curry, and P. Hancock. 2002. Comparison on pulsed and CW ultraviolet light sources to inactivate bacterial spores on surfaces. *IEEE Trans. Plasma Sci.* 30: 1986–1989.

Mohanty, S. K., A. Rapp, S. Monajembashi, P. K.. Gupta, and K. O. Greulich. 2002. Comet assay measurements of DNA damage in cells by laser microbeams and trapping beams with wavelengths spanning a range of 308 nm to 1064 nm. *Radiation Research.* 157 (4): 378–385.

Moseley, H., and D. H. Sliney. 1997. Radiometric quantities and units. *Phys. Med. Biol.* 42 (5): 762.

Ozen, B. F., and J. D. Floros. 2001. Effects of emerging food processing techniques on the packaging materials. *Trends Food Sci. Technol*. 12: 60–67.

Ozer, N. P., and A. Demirci. 2006. Inactivation of *Escherichia coli* O157:H7 and *Listeria monocytogenes* inoculated on raw salmon fillets by pulsed UV-light treatment. *Int. J. Food Sci. Technol*. 41: 354–360.

Park, J. M., H. Tsao, and S. Tsao. 2008. Combined use of intense pulsed light and Q-switched ruby laser for complex dyspigmentation among Asian patients. *Lasers Surg. Med*. 40: 128–133.

Peleg, M., and M. B. Cole. 1998. Reinterpretation of microbial survival curves. *Crit. Rev. Food Sci.* 38: 353–380.

Perkin Elmer Optoelectronics. 2008. High performance flash and arc lamps. http://www.optoelectronics.perkinelmer.com.

Rosenstein, B. S., and Ducore, J. M. 1983. Induction of DNA strand breaks in normal human fibroblasts exposed to monochromatic ultraviolet and visible wavelengths in the 240–546 nm range. *Photochem. Photobiol.* 38: 51– 55.

Rowan, N. J., J. G. Anderson, S. J. MacGregor, and R. A. Fouracre. 2000. Inactivation of food-borne enteropathogenic bacteria and spoilage fungi using pulsed light. *IEEE Trans. Plasma Sci.* 28: 83–88.

Rusciani, A., A. Motta, P. Fino, and G. Menichini. 2008. Treatment of poikiloderma of Civatte using intense pulsed light source: 7 years of experience. *Dermatol. Surg.* 34: 314–319.

Sakai, N., and T. Hanzawa. 1994. Applications and advances in far-infrared heating in Japan. *Trends Food Sci. Technol*. 5: 357–362.

Sauer, A., and C. I. Moraru. 2007. Inactivation of *E. coli* in apple cider using pulsed light treatment. Paper presented at Institute of Food Technologists Annual Meeting, Chicago. http://www.ift.org.

Schaefer, R. B. 2004. Surface discharge lamp and system. U.S. Patent 6,724,134. http://www.freepatentsonline.com/6724134.html.

Schaefer, R., M. Grapperhaus, I. Schaefer, and K. Linden. 2007. Pulsed UV lamp performance and comparison with UV mercury lamps. *J. Environ. Eng. Sci*. 6: 303–310.

Sharma, R. R., and A. Demirci. 2003. Inactivation of *Escherichia coli* O157:H7 on inoculated alfalfa seeds with pulsed ultraviolet light and response surface modeling. *J. Food Sci*. 68: 1448–1453.

Smith, W. L., M. C. Lagunas-Solar, and J. S. Cullor. 2002. Use of pulsed ultraviolet laser light for the cold pasteurization of bovine milk. *J. Food Prot*. 65: 1480–1482.

Sorg, O., V. Janer, C. Antille, P. Carraux, E. Leemans, E. Masgrau, J. H. Saurat, and D. Salomon. 2007. Effect of intense pulsed-light exposure on lipid peroxides and thymine dimers in human skin in vivo. *Arch. Dermatol*. 143: 363–366.

Takeshita, K., J. Shibato, T. Sameshima, S. Fukunaga, S. Isobe, K. Arihara, and M. Itoh. 2003. Damage of yeast cells induced by pulsed light irradiation. *Int. J. Food Microbiol*. 85: 151–158.

Tuminello, P. S., E. T. Arakawa, B. N. Khare, J. M. Wrobel, M. R. Querry, and M. E. Milham. 1997. Optical properties of *Bacillus subtilis* spores from 0.2 to 2.5 μm. *Appl. Opt.* 36: 2818–2824.

Turtoi, M., and A. Nicolau. 2007. Intense light pulse treatment as alternative method for mould spores destruction on paper-polyethylene packaging material. *J. Food Eng*. 83: 47–53.

Tyrrell, R. M. 1973. Induction of pyrimidine dimers in bacterial DNA by 365 nm radiation. *Photochem. Photobiol*. 17: 69–73.

Uesugi, A. R., and C. I. Moraru. 2007. Reduction of *L. innocua* on cooked sausages after exposure to a combination of pulsed light and nisin. Paper presented at Institute of Food Technologists Annual Meeting, Chicago. Abstract available at http://www.ift.org.

Uesugi, A. R., S. E. Woodling, and C. I. Moraru. 2007. Inactivation kinetics and factors of variability in the pulsed light treatment of *Listeria innocua* cells. *J. Food Prot.* 70: 2518–2525.

USFDA/CFSAN. 2002. Kinetics of microbial inactivation for alternative food processing technologies: Pulsed light technology. USFDA Center for Food Safety and Applied Nutrition. http://www.cfsan.fda.gov/~comm/ift-puls.html.

van Boekel, M. A. J. S., and A. J. S. Martinus. 2002. On the use of the Weibull model to describe thermal inactivation of microbial vegetative cells. *Int. J. Food Microbiol.* 74: 139–159.

Waltham**,** C., J. Boyle, B. Ramey, and J. Smit. 1994. Light scattering and absorption caused by bacterial activity in water. *Appl. Opt*. 33: 7536–7540.

Wekhof, A. 2003. Sterilization of packaged pharmaceutical solutions, packaging and surgical tools with pulsed UV light. Paper presented at Second International Congress on UV Technologies, Vienna, July 9–11, 2003. http://www.steribeam.com/articles/UV-Congr-2.pdf.

Woodling, S. E., and C. I. Moraru. 2005. Influence of surface topography on the effectiveness of pulsed light treatment for the inactivation of *Listeria innocua* on stainless steel surfaces. *J. Food Sci*. 70: 345–351.

Woodling, S. E., and C. I. Moraru. 2007. Effect of spectral range in surface inactivation of *Listeria innocua* using broad spectrum pulsed light. *J. Food Prot.* 70: 906–916.

Wuytack, E. Y., L. D. Phuong, A. Aertsen, K. M. Reyns, D. Marquenie, B. De Ketelaere, B. Masschalck, I. Van Opstal, A. M. Diels, and C. W. Michiels. 2003. Comparison of sublethal injury induced in *Salmonella enterica* serovar *Typhimurium* by heat and by different nonthermal treatments. *J. Food Prot.* 66: 31–37.

Xenon Corp. 2005. AN-104 application note. Achieving faster cure time with pulsed UV. http://www.globalspec.com.

Xie, S., H. Li, and B. Li. 2003. Measurement of optical penetration depth and refractive index of human tissue. *Chin. Opt. Lett.* 1 (1): 44–46.

Index

A

B

C

D

E

F

G

H

I

J

K

L

M

N

O

P

Q

R

S

T

U

V

W

X

Y

Food Science and Technology

Ultraviolet Light in Food Technology
Principles and Applications

Exploring a novel alternative for food processing, **Ultraviolet Light in Food Technology: Principles and Applications** incorporates the fundamentals of continuous and pulsed UV light generation and propagation; current food regulations; recommendations for optimal UV reactor design, selection, and validation; information on both commercially available and under-development UV sources; and the outlook for future food applications.

After reviewing essential terms, definitions, and current applications, the book emphasizes the need to properly assess the physical and chemical properties in foods that influence the effectiveness of UV treatment and impact inactivation kinetics. It also addresses the effects of UV processing on food quality, before considering the engineering aspects of UV light treatment. The book then describes the principles of validating UV reactors as well as the principles and applications of UV pulsed light.

For anyone working in food research, development, and operations, this resource provides broad, accessible information on the science and applications of UV light technology. It shows how UV light irradiation can be used as a physical preservation method in food processing.

Features

- Summarizes the findings of published studies that investigate the UV treatment of foods, including international, US FDA, and USDA regulations
- Discusses the efficacy of using UV light to disinfect liquid foods and beverages, such as juice, milk, liquid egg products, and sweeteners, as well as the surfaces of solid foods, including fresh produce, fresh-cut fruits, meats, eggs, and bakery items
- Presents fundamental knowledge of UV light generation and propagation
- Analyzes the concerns and challenges associated with the application of continuous and pulsed UV light in food
- Evaluates UV system performance
- Provides practical recommendations for the design of UV reactors and the selection of commercial UV sources
- Explores the future of successful food applications

CRC Press
Taylor & Francis Group
an informa business
www.crcpress.com

6000 Broken Sound Parkway, NW
Suite 300, Boca Raton, FL 33487
270 Madison Avenue
New York, NY 10016
2 Park Square, Milton Park
Abingdon, Oxon OX14 4RN, UK

59505
ISBN: 978-1-4200-5950-2
90000
9 781420 059502